

Doctoral Thesis

For a doctoral degree at the Graduate School of Life Sciences

Julius-Maximilians-Universität Würzburg

Section – Biomedicine

Modelling of Mesenchymal Stromal Cells Interactions within the Skeletal Niche

Modellierung der Interaktionen von Mesenchymalen Stromazellen
in der skelettalen Nische

Submitted by
Ana Rita Oliveira Alves Pereira
born in Ovar, Portugal

Wuerzburg, 2021



Submitted on:

Members of the Thesis Committee

Chairperson: Prof. Dr. Georg Gasteiger

Primary Supervisor: Dr. Marietta Herrmann

Supervisor (Second): Prof. Dr. Franz Jakob

Supervisor (Third): Prof. Dr. Jürgen Groll

Supervisor (Fourth): Dr. Yuval Rinkevich

Date of Public Defence:

Date of Receipt of Certificates:

This work was conducted at the IZKF research group of Tissue Regeneration in Musculoskeletal Diseases (Project 361) at the University of Wuerzburg from August 2017 until November 2021 under the supervision of Dr. Marietta Herrmann.

Summary

Mesenchymal stem/stromal cells (MSCs) are a rare subpopulation of cells first identified in bone marrow with the potential to proliferate in plastic-adherent colonies and to generate *de novo* bone marrow stroma and its environment upon serial transplantation to heterotopic anatomical sites. Given their multipotency and self-renewal competence, MSCs are prime prospective candidates for most modern musculoskeletal-tissue engineering and regenerative medicine approaches. Still, their envisioned therapeutic use is being questioned with concerns regarding their definition, characterization and integrative functions *in vivo*.

It is well established that microenvironmental cues such as the extracellular matrix (ECM)-chemistry, the mechanical environment and local cellular and/or paracrine interactions critically control MSCs behavior. Yet, most of the scientific knowledge regarding the biology and therapeutic effect of MSCs originates from mechanistic *in vitro* studies where microenvironmental cues are hardly addressed. Therefore, manifestable changes in cell proliferation behavior and multilineage differentiation potential might be triggered that eventually compromise the translation of results to clinics.

This thesis aims to address the complexity of MSCs interactions within the skeletal niche microenvironment in order to provide alternative methods to bypass the current MSCs *in vitro* culture limitations.

Firstly, the influence of ECM-chemistry on MSCs behavior *in vitro* was explored by means of decellularized human bone models here established. Basal or osteogenic tailored cell-derived decellularized 2D matrices (dECM), proved to be suitable culture substrates for MSCs expansion by providing close-to-native cell-ECM interactions. Moreover, quantified morphological shape changes suggested a material osteo-supportive potential, further functionally validated by observable spontaneous mineralization of MSCs. Aiming to identify novel intrinsic ECM regulatory features specific to the skeletal niche, 3D decellularized human trabecular bone scaffolds (dBone) were additionally developed and comprehensively characterized. Remarkably, the MSCs cultured on dBone scaffolds exhibit upregulation of genes associated with stemness as well as niche-related protein expression advocating for the conservation of the naïve MSCs phenotype.

On the other hand, the effect of biomimetic mineralization on MSCs osteogenic lineage differentiation potential was further addressed by hydroxyapatite-functionalization of type-I collagen in presence of magnesium. Mineralized scaffolds exhibited higher cell viability and a clear trend of osteogenic genes upregulation comparing with non-mineralized scaffolds.

Lastly, in order to mimic the complexity of the native MSCs environment, a dynamic culture system was applied to the 3D decellularized bone constructs, previously studied in single static conditions. Mechanical stimuli generated by (1) continuous perfusion of cell culture medium at 1.7 mL/min and (2) compressive stress from 10% uniaxial load at 1 Hz, resulted in an improved cell repopulation within the scaffold and boosting of *de novo* ECM production. The stress-induced gene expression pattern suggested early MSCs commitment towards the osteogenic lineage mediated by integrin-matrix adhesion, therefore further corroborating the recapitulation of a reliable *in vitro* bone niche model in dBone scaffolds.

To conclude, the here developed *in vitro* models provide a progressive increased biomimicking complexity through which significant insights regarding MSC interactions with microenvironmental features in the skeletal niche can be obtained, thus surely paving the way for a better understanding of the role of MSCs in bone homeostasis and regeneration.

Zusammenfassung

Mesenchymale Stamm-/Stromazellen (MSZ) sind eine seltene Subpopulation von Zellen, die erstmals im Knochenmark identifiziert wurden und die das Potenzial haben, sich in plastikadhärenten Kolonien zu vermehren und bei serieller Transplantation an heterotopen anatomischen Stellen *de novo* das Knochenmarkstroma und seine Umgebung zu bilden. Aufgrund ihrer Multipotenz und ihrer Fähigkeit zur Selbsterneuerung sind MSZ erstklassige Kandidaten für moderne Ansätze des muskuloskelettalem Gewebe-Engineering und der regenerativen Medizin. Dennoch wird ihr therapeutischer Einsatz aufgrund von Bedenken hinsichtlich ihrer Definition, Charakterisierung und *in vivo* Integration in Frage gestellt.

Es ist hinlänglich bekannt, dass die Mikroumgebung wie die Komposition der extrazellulären Matrix (EZM), die mechanische Umgebung und die lokalen zellulären und/oder parakrinen Interaktionen das Verhalten der MSZ entscheidend beeinflussen. Die meisten wissenschaftlichen Erkenntnisse über die Biologie und die therapeutische Wirkung von MSZ stammen jedoch aus mechanistischen *In-vitro*-Studien, in denen Faktoren aus der naiven Mikroumgebung von MSZ kaum berücksichtigt wurden. Dies kann zu offensichtlichen Veränderungen des Zellproliferationsverhaltens und des Differenzierungspotenzials der Zellen führen, was die Übertragung der Ergebnisse in die klinische Praxis beeinträchtigt.

Diese Arbeit zielt darauf ab, die Komplexität der Interaktionen von MSZ in der Mikroumgebung der skelettalen Nische zu untersuchen, um Methoden zur Umgehung der derzeitigen Limitationen bei der *In-vitro*-Kultur von MSZ zu etablieren.

Zunächst wurde der Einfluss der EZM auf das Verhalten von MSZ *in vitro* mit Hilfe von dezellularisierten menschlichen Knochenmodellen untersucht. Basale oder dezellularisierte 2D-Matrizen (dECM) osteogen differenzierter Zellen erwiesen sich als geeignete Zellkultursubstrate für die MSZ-Expansion, da sie nahezu native Zell-EZM-Interaktionen ermöglichen. Darüber hinaus deutet die quantifizierten morphologischen Formveränderungen in MSZ auf ein osteoinduktives Potenzial des Materials hin, was durch eine beobachtete spontane Mineralisierung der MSZ funktionell bestätigt wurde. Mit dem Ziel, neue intrinsische EZM-Faktoren zu identifizieren, die für die skelettale Nische spezifisch sind, wurden zusätzlich dezellularisierte 3D-Gerüste aus menschlichem

trabekulärem Knochen (dBone) entwickelt und umfassend charakterisiert. Bemerkenswerterweise zeigen die auf dBone-Gerüsten kultivierten MSZ eine Hochregulierung von typischen Stammzell-assoziierten Genen, sowie die Expression von charakteristischen Nischenproteinen, was für die Erhaltung des Phänotyps naiver MSZ spricht.

Andererseits wurde die Auswirkung einer biomimetischen Mineralisierung auf das osteogene Potenzial von MSZ durch Hydroxyapatit-Funktionalisierung von Typ-I-Kollagen Trägermaterialien in Gegenwart von Magnesium untersucht. Mineralisierte Gerüste zeigten eine höhere Zellviabilität und einen klaren Trend zur Hochregulierung osteogener Gene im Vergleich zu nicht-mineralisierten Gerüsten.

Um die Komplexität der nativen MSZ-Umgebung zu imitieren, wurde schließlich ein dynamisches Kultursystem auf die dezellularisierten 3D-Knochenkonstrukte angewandt, die zuvor unter statischen Bedingungen untersucht worden waren. Mechanische Stimuli, die durch (1) kontinuierliche Perfusion des Zellkulturmediums bei 1,7 ml/min und (2) Druckbelastung durch eine einachsige Last von 10 % bei 1 Hz erzeugt wurden, führten nachweislich zu einer verbesserten Zellrepopulation innerhalb des Gerüsts und zu einer Steigerung der *de novo* EZM-Produktion. Das stressinduzierte Genexpressionsmuster deutet darauf hin, dass es schon früh durch Integrin-Matrix-Adhäsion zu einer Festlegung der MSZ auf die osteogene Linie kommt, was die Rekapitulation eines Zuverlässigen *in vitro*-Knochenmodells in dBone-Konstrukten weiter bestätigt.

Zusammenfassend lässt sich sagen, dass die hier entwickelten *in vitro*-Modelle eine zunehmende Komplexität der zellulären Mikroumgebung darstellen, durch die wichtige Erkenntnisse über die Interaktionen von MSZ mit der Mikroumgebung in der Knochenhülle gewonnen werden können, was sicherlich den Weg für ein besseres Verständnis der Rolle von MSZ in der Knochenhomöostase und -regeneration ebnet.

Acknowledgements

To many wonderful and inspirational people without whom this thesis would not have been completed.

First and foremost, I would like to thank my supervisor and mentor *Dr. Marietta Herrmann* for believing in me, all the way back since Switzerland, and offering me the opportunity to join her freshly founded junior research group in the beautiful city of Wuerzburg. I am tremendously glad to witness the growth of the team over these last years, which all comes from your evident hard and very competent work. Needless to say, you played a major role in guiding me during this journey, which I am proud to say was our journey. You were and will always be a true inspiration for me for your positive insights, determination, trust and creativity – I am extremely fulfilled with your support as a leader and foremost an ally.

Extensive acknowledgements to *Prof. Dr. med. Franz Jakob, Prof. Dr. Jürgen Groll and Dr. Yuval Rinkevich* (Helmholtz Zentrum München) for being part of my thesis committee and providing me with their valuable multidisciplinary guidance upon the project progression.

Many thanks also to my colleagues in IZKF group for creating such a pleasant work environment. I really enjoyed working with you, and specially share with you so many wine tastings and Christmas markets visits. In this regard I would like to thank *Jovana Ilić, Sebastian Haeusner, Katharina Marnet, Janek Harder, Maximilian Leucht, Noah Volkmann, Annika Schiminski, Magdalena Stoeckl, Kim Koschitzki, Sofia Paulus, Jana Schiffmaier, Christoph Koelbl* and *Alexandra Maag* for a great time over the last past 4 years. Special thanks to *Dr. Drenka Trivanović*, with whom I worked closely and who regularly supported me with regard to various scientific and personal concerns since the very beginning – your perseverance is truly an inspiration for me.

I am glad for the opportunity to supervise numerous students. I learned a lot from you, and I hope I was able to create a positive mark in your life as well. To bachelor students *Jasmin Batani* and *Lea Schroeter*, master student *Mert Ergin* (and adopted ones: *Franziska Sennfelder* and *Louisa Belz*), I wish you all the best in your future bright career.

A special thank you to *Theresa Kreuzahler, Bianca Schlierf* and *Andrea Knorz*, who always supported me in various technical situations.

Furthermore, I want to thank all my collaborators, who allow me to extend my research towards several multidisciplinary forefront techniques:

To *Dr. Eng. Gloria Belén Ramírez-Rodríguez* (University of Granada, Spain) for the collagen-based scaffold synthesis and the very pleasant and rewarding collaboration.

To *Andreas Lipphaus* (Ruhr-University Bochum) for the fluid computer simulations.

To *Prof. Eng. Jan Hansmann* and his *engineering team* (Fraunhofer Translational Center for Regenerative Therapy) for the bioreactor setup and other technical aspects.

To all members of Tissue Engineering and Regenerative Medicine department, particularly to *Dr. Marco Metzger, Dr. Joachim Nickel, Dr. Gudrun Dandekar, Dr. Sarah Nietzer, Dr. Franziska Ehlicke, Dr. Claudia Siverino, Dr. Constantin Berger, Dr. David Kessie, Sanjana Mathew, Jiyoung Choi, Rinu Sivaraj and Thomas Daeullary* for the extremely supportive collaboration of resources and friendships.

To all members of the department for Functional Materials in Medicine and Dentistry, particularly to *Dr. Andrea Ewald, Prof. Dr. Uwe Gbureck, Dr. Biranche Tandon, Christoph Boehm, Leonard Forster, Viktoria Niklaus, Philipp Stahlhut and Anton Hofmann*. A heartfelt special mention to *Ezgi Bakirci* for sharing some of the wildest and deepest memories along these incredible years, from the German classes adventures to all the selfies with your happy face in the big plan. Thank you for sharing my craziness and let me be who I am – you are forever in my heart.

To *Dr. Regina Elbert* and *her research team* for the initial sheltering in her facilities and for all the valuable discussions during literature seminars. Equally, extended thanks to *Prof. Dr. med. Norbert Schuetze* and *his team*.

To the orthopedic surgery team from Clinic Koenig-Ludwig-Haus, particularly to *Prof. Dr. med. Maximilian Rudert, Dr. med. Manuel Weissenberger* and *Dr. med. Konstantin Horas* for gently providing fundamental fresh human material, without which this project would not be possible.

To *Dr. Sahar Salehi* (University of Bayreuth) for sharing the co-mentoring of Mert Ergin's master thesis, and further support with scan electron microscopy techniques.

To *Dr. Dominik Gehweiler* (AO Research Institute Davos, Switzerland) for performing micro-CT scans of high precision.

Apart from that, I am grateful for the opportunity to exchange beliefs and thoughts with colleagues around the world during international conferences in Germany, Spain, Greece, (virtually in Turkey and Netherlands).

Furthermore, I would like to thank the Interdisciplinary Center for Clinical Research (IZKF Wuerzburg) and orthopedic clinic Koenig-Ludwig-Haus for financial support and excellent equipment and infrastructures.

Additionally, a special mention of honor to Graduate School of Life Sciences team, for all the gentle support and visible effort to provide the students with a fulfilling scientific career, but also a socially enjoyable journey.

It has been a period of intense learning for me, not only in the scientific field but also on a personal level. I would like to share this moment also with my oldest friends: my water polo girls that shown me 15 years ago what really means to be part of a team. I learned that is ok to feel homesick sometimes – it means we come from a happy place. Thank you for making me feel like nothing changed with every visit back home. I cannot wait to witness all your successes in life and be there for you as well in every step.

Last but not least, to Pieter who makes me believe everyday in true honest love and proves to me that home is not a place. Thank you for rescuing me so many times from my own mind and bringing me back to a world where I can be my happiest self. Thank you for being so patient and loving me for my flaws as well.

To my dear family: I cannot be grateful enough for all the support you gave me all my life. I truly feel how much you love me as the person I am, and how proud you are of me – that makes me extremely happy and fulfilled. Distance only made us to grow stronger. People say that children belong to the world, but I promise to always remember where my roots are.

*It is not the strongest species that survive, nor the most intelligent,
but the ones most responsive to change.*

— Charles Darwin

Table of Contents

Summary.....	v
Zusammenfassung.....	vii
Acknowledgements.....	ix
Table of Contents.....	xiii
Chapter 1. Introduction.....	1
Bone microenvironment: tissue structure and functions.....	3
MSCs skeletal niche.....	4
<i>In vitro</i> modelling: novel research tools	4
Motivations and aims of work.....	5
Review article: Eur. Cells Mater. 2019, Vol.37.....	7
Chapter 2. Methods: Development of a decellularized bone scaffold.....	33
Protocol article: Methods in Cell Biology. 2020, Vol.157.....	35
Chapter 3. Results: Decellularized bone ECM for MSC culture.....	55
Original research article: J. Tissue Eng. (in revision).....	57
Chapter 4. Results: Role of mineral nucleation on osteogenesis.....	83
Original research article: Int. J. Mol. Sci. 2021, Vol.22.....	85
Chapter 5. Results: Effect of mechanical stimuli on osteogenesis.....	101
Original research article: Materials. 2021, Vol.14.....	103
Chapter 6. Conclusion remarks.....	125
Future perspectives.....	129
References.....	133

APPENDIX A. Affidavit.....	A-1
APPENDIX B. List of publications and authors contributions.....	B-1
Statement of individual author contributions to figures/tables/chapters.....	B-5
APPENDIX C. Curriculum Vitae.....	C-1

Chapter 1.

Introduction

In this introductory chapter the bone tissue structure, the MSCs identity and their interactions with the native environment are firstly addressed. It follows a comprehensive description of the motivation and aims for this thesis. Lastly, the most recent and relevant bioengineering approaches to model the MSCs-niche complexity *in vitro* are extensively reviewed, with special focus on their potentials and limitations.

Parts of this chapter were published as a review-article in the European Cells and Materials journal (Volume 37). Reprint permission was obtained from all co-authors and from the publisher under Creative Commons license (CC BY-SA).

Reference: Pereira AR, Trivanović D and Herrmann M. Approaches to mimic the complexity of the skeletal mesenchymal stem/stromal cell niche in vitro. Eur. Cell. Mater., 2019, 37, pp.88–112.

Bone microenvironment: tissue structure and functions

Bone is a complex, highly organized tissue capable of adapting its structure to mechanical or biochemical stimuli, therefore providing support and protective functions to the body [1]. Elastic collagen type-I fibers constitute approximately 95% of the bone organic matrix, equipping the tissue with appropriated flexibility [2, 3]. On another hand, its inorganic mineral phase is mainly composed of highly organized intrafibrillar calcium phosphate ions, known as hydroxyapatite, providing the bone with rigidity, thus creating the right mechanical balance to handle resistance to fractures [4, 5]. Anatomically, long bones are composed of two different compartments: cortical and trabecular/cancellous bone. Differences in the structural arrangements of the two bone types are related to their primary functions: robust calcified and mineralized structure of cortical bone provides mechanical and protective functions, while porous honeycomb-like network of cancellous bone permit allocation of bone marrow, facilitating rather metabolic functions [6].

The major cellular elements that constitute the bone remodeling unit include matrix-forming osteoblasts, matrix-resorption osteoclasts, and mature matrix-supporting osteocytes, along with MSCs as the precursors of specialized osteoblasts [7]. Disturbances in the balance between these complementary processes might result in metabolic bone diseases, such as osteoblastic or osteolytic lesions [8].

Furthermore, the bone lacuna-cunicular network is particularly sensible to physical signals, where mechanical energy is converted to electrical/biochemical signals by mechanical sensing cells, hence guiding precursor cell-fate decisions, and ultimately dictating the function of the tissue [9]. Multiple physical stimuli have been identified that actively affect and guide MSCs interactions and fate, namely: (1) the trabeculae interconnective porosity [10], (2) the surface rough-nanotopography [11], (3) the matrix stiffness [12] and external mechanical signals, such as (4) shear stress as a result of interstitial fluid movement [13] and (5) strain caused by tension or compression [14].

As such, understanding the complex structure of bone tissue and biomechanical aspects of bone homeostasis and regeneration in detail is essential for better comprehending the integration of stimuli to which cells are subjected to either physiologically or pathologically.

MSCs skeletal niche

MSCs were first identified by Friedenstein in 1974 from bone marrow fragments' outgrowths in culture, due to their competence to rapidly form adherent colony units with fibroblast-like appearance [15]. Since their first discovery in bone marrow, similar cell populations with proliferative competence, undifferentiated phenotype and the ability to differentiate into osteoblastic, adipogenic and chondrogenic lineages *in vitro*, have been identified and reported in many adult [16-20] and fetal tissues [21-23].

In native tissues, MSCs are sheltered in specific microenvironments, also known as stem cell niches [24, 25]. Stem cell niches constitute a basic unit of tissue physiology, with not only well-defined anatomical as well as functional dimensions, where cell stemness is protected, yet tissue-adjacent cells, endocrine signals or external forces may trigger their activation and mobilization [26-28]. Recent studies suggested that at least three different osteoblastic niches for skeletal progenitor cells exist in bone marrow, in particular at endosteal, perivascular and stromal regions [29].

The primary function of ECM is providing anchorage to the tissue-resident cells by exposing pro-adhesive integrin-mediated RGD-peptide motifs, present in fibronectin and other ECM proteins [30]. Additionally, ECM also acts like a reservoir of growth factors, e.g., bone morphogenetic proteins, transforming growth factor-beta, etc., which are released by proteases in a time- and dose-dependent way during ECM remodeling [31, 32]. It is therefore reasonable to assume that the inherent chemistry, mechanical structure, and function of different tissues may have a major influence the single MSCs entity, albeit their influence is not fully understood.

In vitro modelling: novel research tools

To date, the simplest models for examining biological behavior of MSCs in response to microenvironmental factors are conducted by direct exposition to soluble factors [33, 34] or by cultivating monolayer cells on protein-coated engineering substrates [35, 36].

Although very convenient and effective for mechanistic purposes, the results from 2D cell culture models do not represent the essential and complex features of native

microenvironments. A main limitation of *in vitro* studies in 2D monolayer cultures is the lack of spatial and temporal control of multiple signals [37, 38].

Progress in the development of biomimetic materials have lately been chasing the complexity of the mechanical and 3D physical-chemistry arrangement of the biomaterial itself, such as hydrogels or scaffolds, commonly used for tissue engineering applications [39, 40]. A wide variety of material alternatives have been developed to recreate the tissue-specific ECM composition, albeit a single *in vitro* model that reproduces the *in vivo* microenvironment homeostasis remains a bioengineering challenge. Commonly used synthetic biodegradable polymers, mostly -lactic and -glycolic based, are widely used due to their reproducible large-scale production, with controlled properties of strength, degradation rate, and microstructure [41]. On the other hand, natural polymers such as collagen, fibrin, alginate, silk, hyaluronic acid, and chitosan, provide high biological integration, yet often lack mechanical structure [42].

Aiming to address this issue, decellularization of cell-derived ECM, tissues and organs emerged with a reverse-engineering concept able to faithfully mimic the native tissue complexity [43, 44]. Through physical, chemical and/or enzymatic treatments, the central goal of decellularization protocols is to preserve the above-mentioned biochemical complexity and mechanical integrity of the tissue, while efficiently removing all cellular elements to prevent any immunological reaction [45, 46].

The future holds great potential for combined *in vitro* models towards tissue engineering and regenerative medicine applications. Progress in engineering, technology, chemistry and imaging will surely be at the forefront of MSCs niche modelling revolution.

Motivation and aims of work

As aforementioned, MSCs have a vast prospective value for most modern musculoskeletal-tissue engineering and regenerative medicine approaches due to their multipotency and self-renewing competence [47]. Contrariwise, their envisioned therapeutic use is being questioned by the scientific community in spite of decades of extensive research in the field with concerns regarding their identification, characterization and integrative functions *in vivo* [48, 49], therefore harshening their prospective value.

Due to the lack of distinct surface markers that identify these cells *in vivo*, the location and identification of MSCs in adult tissues is a subject of controversy [50-52].

In fact, most of the MSCs biology knowledge derives from *in vitro* studies, evidently exposing cells to highly artificial situations that do not recapitulate the complexity of the naïve environment [53]. As a result, an ambiguous distinction between the physiological function of isolated MSCs in culture and their presumed *in vivo* counterpart often leads to a translation gap of results towards the clinics.

Although several major progresses have been made to mimic the complexity of the MSCs niche *in vitro*, a major challenge is still to understand how the chemical composition and mechanical properties of the ECM can functionally influence tissue homeostasis under physiological and pathological conditions. Therefore, this thesis is structured in two main aims that sequentially address unique niche properties:

Aim 1. Addressing the bone matrix composition

In here, unique human bone ECM models (2D and 3D) based on decellularization techniques are developed, aiming to identify intrinsic ECM regulatory factors that may be responsible for the maintenance of MSCs stem-cell competence *in vitro* and their response to homeostatic and extrinsic signals. Additionally, the effect of bone biomimetic mineralization on MSCs osteogenic lineage differentiation potential is further addressed through a type I collagen-functionalized scaffold.

Aim 2. Addressing the bone biomechanics

Biomaterial design often targets the recapitulation of individual features of the natural bone ECM network [54]. As well, several dynamic experimental setups have been reported to mimic the above-mentioned mechanical stimuli with observable bone-forming augmentation effect [55, 56]. Yet, in this thesis the bidirectional influence of combined biochemical and biophysical cues are addressed for the first-time in a step-wise holistic approach, by means of a laminar flow perfusion bioreactor with integration of cyclic compression, thus opening new opportunities to validate bone development, remodeling and pathologies studies.



APPROACHES TO MIMIC THE COMPLEXITY OF THE SKELETAL MESENCHYMAL STEM/STROMAL CELL NICHE *IN VITRO*

A.R. Pereira^{1,2}, D. Trivanović^{1,2} and M. Herrmann^{1,2,*}

¹IZKF Group Tissue Regeneration in Musculoskeletal Diseases, University Clinics, Würzburg, Germany

²Orthopedic Center for Musculoskeletal Research, University of Würzburg, Würzburg, Germany

Abstract

Mesenchymal stem/stromal cells (MSCs) are an essential element of most modern tissue engineering and regenerative medicine approaches due to their multipotency and immunoregulatory functions. Despite the prospective value of MSCs for the clinics, the stem cells community is questioning their developmental origin, *in vivo* localization, identification, and regenerative potential after several years of far-reaching research in the field. Although several major progresses have been made in mimicking the complexity of the MSC niche *in vitro*, there is need for comprehensive studies of fundamental mechanisms triggered by microenvironmental cues before moving to regenerative medicine cell therapy applications. The present comprehensive review extensively discusses the microenvironmental cues that influence MSC phenotype and function in health and disease – including cellular, chemical and physical interactions. The most recent and relevant illustrative examples of novel bioengineering approaches to mimic biological, chemical, and mechanical microenvironmental signals present in the native MSC niche are summarized, with special emphasis on the forefront techniques to achieve bio-chemical complexity and dynamic cultures. In particular, the skeletal MSC niche and applications focusing on the bone regenerative potential of MSC are addressed. The aim of the review was to recognize the limitations of the current MSC niche *in vitro* models and to identify potential opportunities to fill the bridge between fundamental science and clinical application of MSCs.

Keywords: Mesenchymal stem/stromal cells, skeletal progenitor cells, niche, *in vitro* models, bone, tissue engineering.

***Address for correspondence:** Marietta Herrmann, IZKF Group Tissue Regeneration in Musculoskeletal Diseases, Orthopedic Center for Musculoskeletal Research, Friedrich-Bergius-Ring 15, 97076 Würzburg, Germany.

Telephone number: +49 9318031587 Email: m-herrmann.klh@uni-wuerzburg.de

Copyright policy: This article is distributed in accordance with Creative Commons Attribution Licence (<http://creativecommons.org/licenses/by-sa/4.0/>).

List of abbreviations			
2D	two dimensional	FasL	Fas ligand
3D	three dimensional	FDA	Food and Drug Administration
4D	four dimensional	Flt3	fms like tyrosine kinase 3
ALP	alkaline phosphatase	HCs	hematopoietic cells
BM	bone marrow	HLA	human leucocyte antigene
BMP	bone morphogenetic protein	HSCs	hematopoietic stem cells
CFU-Fs	colony-forming unit fibroblasts	HSPCs	hematopoietic stem and progenitor cells
CXCL12	C-X-C motif chemokine ligand 12	IL	interleukin
CXCR4	C-X-C chemokine receptor type 4	iNOS	inducible nitric oxide synthase
DCCs	disseminated cancer cells	MAPK	mitogen-activated protein kinases
DKK1	Dickkopf-related protein 1	MCP-1	monocyte chemoattractant protein-1
ECs	endothelial cells	M-CSF	macrophage-colony-stimulating factor
ECM	extracellular matrix	miRNA	microRNA

MMPs	matrix metalloproteinases
MSCs	mesenchymal stem/stromal cells
M ϕ	macrophages
NG2	neural/glial antigen 2
OC	osteoclasts
OPG	osteoprotegerin
PDGFR β	platelet-derived growth factor receptor beta
piRNA	piwi-interacting RNA
PCL	polycaprolactone
PGA	poly(glycolic acid)
PLA	poly(lactic acid)
PLGA	poly(lactic-co-glycolic acid)
PMMA	polymethylmethacrylate
RANKL	receptor activator of NF- κ B ligand
RGD	arginylglycylaspartic acid
RNAi	RNA interference
ROS	reactive oxygen species
Runx2	Runt-related transcription factor 2
SCF	stem cell factor
SCID	severe combined immunodeficiency
SDF-1	stromal cell-derived factor-1
STAT3	signal transduces and activator of transcription 3
TRP	transient receptor potential
VEGF	vascular endothelial growth factor

Introduction

Friedenstein and co-workers originally identified a rare sub-population of cells in the BM with the potential to proliferate in plastic-adherent colonies with a fibroblastic appearance, first designated as CFU-Fs (Friedenstein *et al.*, 1974). Later *in vivo* experiments have revealed the potential of BM-isolated adherent cells to generate *de novo* the BM stroma and its environment upon serial transplantation to heterotopic anatomical sites (Caplan, 1991; Owen, 1988), leading to the current concept of BM-derived MSCs.

Although the BM is the most widely recognized source of MSCs, further research has suggested the presence of MSC-like cells in other tissues, including adipose tissue (Zuk *et al.*, 2002), peripheral blood (Tondreau *et al.*, 2005), dental pulp (Gronthos *et al.*, 2000), pancreatic islets (Carlotti *et al.*, 2010), synovial membrane (Hermida-Gómez *et al.*, 2011), periodontal ligament (Seo *et al.*, 2004), anterior cruciate ligament (Prager *et al.*, 2018), endometrium (Schwab *et al.*, 2008), *bursa subacromialis* (Steinert *et al.*, 2015), placenta (Fukuchi *et al.*, 2004), umbilical cord (Baksh *et al.*, 2007), and umbilical cord blood (Sarugaser *et al.*, 2005). It has been further proposed that MSCs may be present in any vascularized tissue at perivascular sites (Crisan *et al.*, 2008).

Due to their multipotency and wide dispersion in the body, MSCs are an essential element of most modern tissue engineering and regenerative medicine approaches. There are extensive reviews

on the biology of the MSCs, elucidating their nature and unique properties (Bronckaers *et al.*, 2014; Méndez-Ferrer *et al.*, 2010; Phinney and Prockop, 2007; Prockop and Oh, 2012). In the present review, the different microenvironmental cues influencing the MSC phenotype and function either in health and disease – including cellular, chemical, and physical interactions – are discussed. In addition, the most recent *in vitro* culture strategies addressing the complexity of the *in vivo* MSC environment are summarized.

The MSC identity relies on their localization

The characterization of MSCs either *ex vivo* or *in vivo* remains difficult since there is neither a distinct definition nor a robust assay to identify MSCs in a mixed population of cells. However, the International Society of Cellular Therapy has established three main criteria that should be fulfilled by genuine MSCs *in vitro*. These cells should (1) exhibit plastic adherence; (2) express a set of surface markers – *i.e.*, CD73, CD90, CD105, and lack the expression of CD45, CD34, CD14 or CD11b, CD79 α or CD19, and HLA-DR; (3) have the ability to differentiate *in vitro* into mesenchymal lineages, namely adipocyte, chondrocyte, and osteoblast (Dominici *et al.*, 2006). These criteria are applied for the *in vitro* characterization and validation of putative MSCs isolated from different tissue sources; however, differences exist in MSCs isolated from various tissue origins for what concerns the clonogenicity level, proliferation rate, differentiation potential, cell surface marker expression, and, most importantly, their regenerative potential *in vivo* (Bianco *et al.*, 2008; Hass *et al.*, 2011; Raicevic *et al.*, 2011). In fact, only cells isolated from the BM reestablish the marrow stroma upon serial transplantation in mice (Méndez-Ferrer *et al.*, 2010; Sacchetti *et al.*, 2007). CD146⁺ pericytes, firstly isolated from the BM (Bianco *et al.*, 2008) and later from multiple vascularized human organs (Crisan *et al.*, 2008), exhibit long-term proliferation and trilineage differentiation potential in *in vitro* cultures. However, pericytes, identified by the expression of the transcription factor Tbx18, maintain their identity during aging and diverse pathological *in vivo* settings and do not contribute to tissue regeneration (Guimarães-Camboa *et al.*, 2017), suggesting that the plasticity of these cells observed *in vitro* can be in fact the result of artificial cell manipulations. Regardless of the controversy, these findings provide evidence that MSCs should not be classified as a uniform population of theoretically multipotent cells, but rather a super-family of tissue-specific committed progenitors, possibly even with a distinct developmental origin, as proposed by Robey (2017) and Sacchetti *et al.* (2016). Noteworthy, isolated MSCs seem to reflect an organ-specific potency and a mechanical memory from past physical

environments, which can influence cell fate – *e.g.*, MSCs originated from the BM are more predisposed to give rise to the skeleton, MSCs from adipose tissue to adipocytes and those from other organs to the respective native connective tissues (Sacchetti *et al.*, 2016; Yang *et al.*, 2014).

The nomenclature debate

Due to already identified functional and anatomical diversity of putative MSCs and the lack of robust assays, the nomenclature of these cells has been extensively debated in the field since their discovery. First named as ‘colony-forming-unit fibroblasts’ by Friedenstein in 1974 (Friedenstein *et al.*, 1974), quickly their name was changed to ‘marrow stromal cells’ when their *in vivo* potential to generate *de novo* the complete BM structural components was proven (Owen, 1988). Caplan (Caplan, 1991) has proposed to introduce the term ‘mesenchymal stem cells’ due to their clonability and multilineage potential as well as their loose architecture of randomly organized cells surrounded by large amounts of ECM, which is a characteristic of mesenchymal tissues. However, the International Society for Cellular Therapy (Horwitz *et al.*, 2005) has decided to change the term back to ‘mesenchymal stromal cell’, due to the inappropriate and misleading use of the term ‘stem’, especially in the context of cell therapy applications. Also, the term ‘mesenchymal’ has been lately involved in controversy since it can be easily misinterpreted with the differentiated lineages derived from the mesoderm germinal layer – *i.e.*, skeletal muscle, bone, connective tissue, heart, and urogenital system – which do not have the same MSC differentiation potential. Given that, the scientific community has widely accepted that, for terms of clarity, the tissue of origin of the isolated MSCs should always be stated in their name (Robey, 2017; Sipp *et al.*, 2018). Other suggested terminologies have emerged, not based on the cell’s anatomical location nor their differentiation potential but on their function and application for clinics – *e.g.*, Caplan proposal to change the name to ‘medicinal signaling cells’ because of their *in vivo* secretory function (Caplan, 2017).

The dynamics of the MSC niche

There is abundant evidence suggesting that the MSC ability to maintain themselves or to give rise to differentiated progeny is strictly governed by complex interactions within their close environment – first proposed for HSCs as stem cell niche (Schofield, 1978). The concept of a stem cell niche has later been established as an interactive structural unit, organized to facilitate cell-fate decisions in a proper spatiotemporal manner, comprising the structural and functional components of the ECM, the cellular signaling with stem adjacent cells and other environmental cues, such as gradients of hypoxia (Fig. 1) (Li and Xie, 2005; Scadden,

2006). *In vivo* remodeling of the stem cell niche occurs constantly during development, *e.g.*, during skeletal development and epithelial branching morphogenesis (Rozario and DeSimone, 2010) or in adults during wound healing (Schultz and Wysocki, 2009), where both inflammatory, angiogenic, and morphogenetic factors are present, culminating in an adjustment of the mechanochemistry and cellular composition of the tissue.

Age and diseases

The dynamics of the BM niche vary strongly with age and disorder phenotypes. During aging, a quiescence-to-senescence transition occurs in niche-residing MSCs, which strongly impairs the interactive signaling network of all niche-residing cells and ultimately the complete regenerative activity (Herrmann *et al.*, 2019). This phenomenon is driven either by the age-associated BM fat tissue expansion (Ambrosi *et al.*, 2017) and/or by the inherent modulation of number and type of vessels in bone and BM (Watson and Adams, 2017; Zimmermann *et al.*, 2011). The signature and proliferation capacity of MSCs is also compromised in ECM-related disorders, such as tissue fibrosis – where an excessive deposition of ECM is observed (Usunier *et al.*, 2014) – or osteoarthritis (Maldonado and Nam, 2013) – which is linked to a resilient ECM degradation mediated primarily by MMPs and to an over-activation of osteoclast activity (Maldonado and Nam, 2013). Disruption of such control mechanisms generates aberrant ECM, both structurally and mechanically altered, leading to abnormal behaviors of cells residing in the niche and, ultimately, to enormous repercussions on the overall tissue homeostasis and functionality (Bonnans *et al.*, 2014; Cox and Erler, 2011).

BM niches can also be targeted by metastasizing cancer cells (discussed in more detail below), where a malignant vicious cycle between niche and tumor cells is created, adapting the ECM dynamics to each step of tumor progression (Herrmann *et al.*, 2019; Lu *et al.*, 2012).

Cellular interactions

MSCs gather in niches in distinct location within the BM – namely endosteal (Nakamura *et al.*, 2010), stromal (Herrmann *et al.*, 2019; Pereira *et al.*, 1998), and perivascular (Winkler *et al.*, 2010). The phenotypical similarities of MSCs within their respective niches are currently not completely known. However, the interplay with cells of different maturation and activation states from each niche must surely play a pivotal role in adult tissue dynamics.

MSC communication with ECs and HCs in the BM, which drives the BM niche integrity and bone tissue homeostasis and repair, is discussed in this section. The proper reproduction of these interactions in experimental approaches is mandatory for revealing fundamental properties of the regenerative process and creating rational cell-based therapeutic

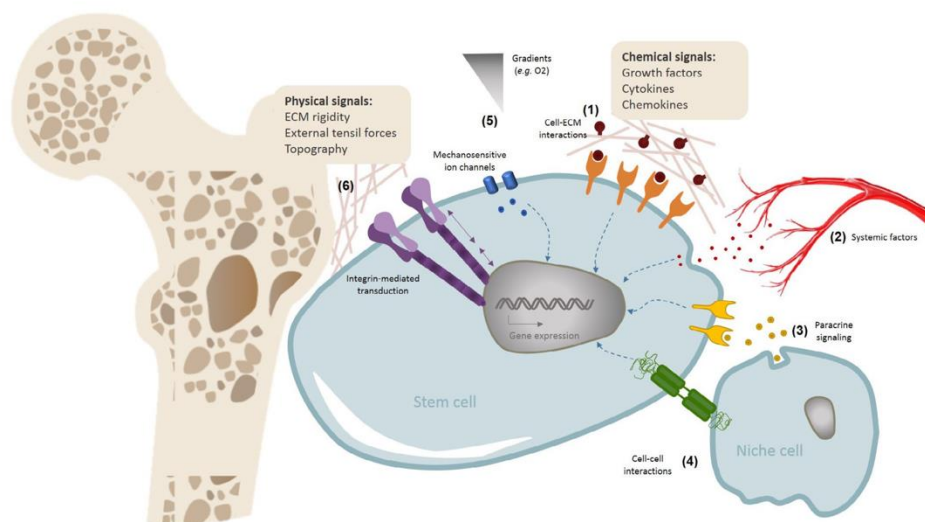


Fig. 1. MSCs' biochemical and physical interactions within the BM niche. A bidirectional synergetic cross-talk is present in the MSC niche, which is ultimately responsible for the modulation of the dynamic state of multicellular tissues – *e.g.*, external signals can change cell DNA transcription, while, in turn, signal transduction from the interior of the cell can modify the extracellular chemistry and mechanics (Bottaro *et al.*, 2002). These interactions may comprise: (1) receptor recognition of insoluble and soluble ECM components – such as cytokines, growth factors, morphogenetic proteins, collagenous proteins, proteoglycans; (2) systemic factors through the vascular system; (3) paracrine and endocrine signals from local or distant sources, *e.g.*, small-molecule agonists, steroid hormones, cytokines, peptides, ions; (4) cell-cell interactions with the neighbor cells, such as niche-supporting cells, immune cells, ECs, or nerve cells; (5) environmental cues, including shear forces, pH effects, oxygen tension; (6) ECM mechanotransduction based on matrix elasticity and geometry.

strategies. The understanding of the relationships between these cells is loaded by difficult definitions of certain cell phenotypes and functionalities, as they might share cell origin, *i.e.*, mesenchyoblast and hemangioblasts, where progenies possess endothelial and hematopoietic signatures (Angelos *et al.*, 2018; Breitbach *et al.*, 2018; Guibentif *et al.*, 2017). By protecting the primitive stem cells from exhaustion and, on the other side, supporting extensive progenitor activation and differentiation when needed (Ramasamy *et al.*, 2016), the spatial arrangement of the BM hubs is responsible for governing heterogeneity within cell populations (Crisan and Dzierzak, 2016). Cell-to-cell communication includes interaction between membrane and cytoplasm and production of growth factors and cytokines. Extracellular vesicles containing proteins, lipids, miRNA, piRNA (De Luca *et al.*, 2016), or mitochondria transfer (Mahrouf-Yorgov *et al.*, 2017) are important mechanisms of cell communication between MSCs and HCs (De Luca *et al.*, 2016), as well as ECs (Gong *et al.*, 2017; Qin and Zhang, 2017) and cancer cells (Lin *et al.*, 2016), regulating their differentiation, migration, and survival. MSCs provide an instructive environment

for angiogenesis, hematopoiesis, and osteopoiesis but also functional assistance to local and disseminated unhealthy or malignant cells (Dhawan *et al.*, 2016; Lee *et al.*, 2012; Roccaro *et al.*, 2014; Xu *et al.*, 2018).

MSCs and ECs

Stem cell behavior, tissue formation and regeneration as well as survival of bone grafts are under the control of the blood vessels, which supply oxygen and nutrients to the cells (Böhrnsen and Schliephake, 2016; Ramasamy *et al.*, 2016). Controlled diffusion of ROS, BM blood-vessel-forming ECs and vascular integrity determine and regulate HSPC as well as MSC localization and functionality (Fehrer *et al.*, 2007; Gomariz *et al.*, 2018; Langen *et al.*, 2014; Xu *et al.*, 2018). Low permeable endosteal vessels with high integrity (H-type) differ from sinusoidal vessels with low integrity (L-type) and provide a poor ROS microenvironment, favoring HSPC maintenance, while fenestrated L-type vessels allow for HSPC respiration and mobilization (Itkin *et al.*, 2016). Sca-1⁺ and Nestin⁺ MSCs are likewise associated with H-type vessels and sensitivity to ROS with HSPCs (Itkin *et al.*, 2016). During aging, reduction of H-type vessels

results in decreased levels of SCF and PDGFR β ⁺ or NG2⁺ perivascular stromal cells, which is associated with a decrease in the HSPC population in the BM (Kusumbe *et al.*, 2016). Endothelial to mesenchymal transition, an example of cell plasticity, generating pro-inflammatory ECs (Al-Soudi *et al.*, 2017; Chen *et al.*, 2015), is often observed in adult pathologies (Erba *et al.*, 2017; Medici and Olsen, 2012), musculoskeletal injury (Agarwal *et al.*, 2016), and heterotopic bone ossification (Sun *et al.*, 2016), but is also recognized as a developmental process connecting maturation and fate of MSCs and ECs.

MSC-EC cross-talk leads to the modulation of the angiogenic response, with MSCs behaving as pericyte-like cells in the stabilization of newly formed blood vessels (Duttenhoefer *et al.*, 2013; Herrmann *et al.*, 2014; Loibl *et al.*, 2014). However, current data are conflicting. MSCs attenuate activation, proliferation and angiogenesis of ECs, through the production of MMP-1 (Zanotti *et al.*, 2016) and ROS, leading to EC apoptosis, capillary degeneration (Marfy-Smith and Clarkin, 2017; Otsu *et al.*, 2009), and, finally, disease (Cipriani *et al.*, 2007). In contrast, MSC-EC crosstalk stimulates proliferation and osteogenesis in MSCs and angiogenesis in ECs (Bidarra *et al.*, 2011; Böhrnsen and Schliephake, 2016). While BM endothelial progenitors, considered to be CD34⁺ or CD133⁺ cells, downregulate osteogenesis in MSCs (Duttenhoefer *et al.*, 2015), EC progenitor-derived growth factors are of critical importance for MSC engraftment, stemness, and repopulation in secondary grafts and osteogenesis (Lin *et al.*, 2014).

MSCs and HCs

Crosstalk of MSCs and HSPCs is one of the most studied issues in physiological homeostasis and adult tissue regeneration (Chan *et al.*, 2015; Raggatt *et al.*, 2014), where progenies of these cells are major participants in immune response, inflammation resolution, and tissue repair. Coherency of the skeletal system and hematopoiesis maintenance (Visnjic *et al.*, 2004) contributes to the BM as stem cell niche environment, as described above. Many mechanisms of HSPC activation by infections or various cytokines have been revealed, while the major pathways involved in steady state and emergency hematopoiesis, generating the full repertoire of immune cells, are still not understood (Boulais and Frenette, 2015; Crisan and Dzierzak, 2016). In case of an altered MSC contribution to osteoblast or adipocyte pool in the BM, biased hematopoiesis occurs through disbalanced myelo-/lymphopoiesis. Distinct stromal cell factors – such as SCF, CXCL12, Flt3 ligand, Wnt3a, angiopoietin-like proteins, thrombopoietin, and fibroblast growth factor 1 – control HSPC quiescence, survival, proliferation, self-renewal, and mobilization or retention in their niche (Crisan and Dzierzak, 2016; Wohrer *et al.*, 2014). Deletion of CXCL12 from perivascular stromal cells or osteoblasts depletes HSPCs and early lymphoid

progenitors, respectively (Ding and Morrison, 2013). Leptin receptor⁺ perivascular stromal cells are the main source of SCF and CXCL12 in the BM (Ding and Morrison, 2013; Zhou *et al.*, 2014) and conditional deletion of SCF leads to the depletion of quiescent HSPCs (Zhou *et al.*, 2014), while deletion of CXCL12 leads to HSPC mobilization (Ding and Morrison, 2013). Since the fast onset of HSPC differentiation in culture complicates the *ex vivo* amplification of HSPCs for their clinical application, development of improved HSPC-amplifying strategies where HSPCs retain their stem cell capacity are still in progress. MSCs support the proliferation of *ex-vivo*-expanded committed hematopoietic progenitors (Hammoud *et al.*, 2012) and their co-culture in 3D macroporous hydrogel scaffolds, mimicking the spongy architecture of trabecular bone, results in higher CD34⁺ frequency (Raic *et al.*, 2014). However, the impact of MSCs on HSPC stemness during different *in vitro* cultivation and repopulating activity in SCID remains unclear. MSC effects on mature or differentiated HCs are widely studied, particularly in order to reveal the immunobiology of MSCs, where their immunosuppressive capacity is attempted to be harnessed in clinical settings (Galleu *et al.*, 2017; Simonson *et al.*, 2015; Trento *et al.*, 2018). On the contrary, functional adjustment of MSCs in hematologic malignancies, including acute lymphoblastic or myeloid leukemia, multiple myeloma, lymphomas, chronic myeloid leukemia, and myelodysplastic syndromes are described (Civini *et al.*, 2013; de la Guardia *et al.*, 2017), while it is still unknown whether malignant hematopoietic progenitors modify MSCs or if leukemia-triggering changes occur first in MSCs and the healthy marrow niche (Schroeder *et al.*, 2016).

The murine Lin⁻Sca-1⁺cKit⁺ population, referred to as HSPCs, controls MSC differentiation, stimulating osteogenesis through the production of BMP-2 and -6, while, in aged and osteoporotic mice, HSPCs fail to generate BMPs (Jung *et al.*, 2008). Also, *in vitro* co-culturing demonstrates that murine HSPCs impact clonogenicity and favor an osteogenic gene expression profile in MSCs (Jung *et al.*, 2008). On the other hand, differentiated HCs may also affect MSC features, directly through the modulation of their properties as constitutive cells of the mutual niche or indirectly through paracrine activity and feedback effects (Vasandan *et al.*, 2016).

Increased megakaryocyte numbers in the BM are associated with elevated BMP-2, -4, and -6 in mice and are followed by stimulation of MSC osteogenesis (Garimella *et al.*, 2007). While osteoblast maturation and skeletal homeostasis might be supported by megakaryocyte (Alvarez *et al.*, 2018; Kacena *et al.*, 2006), data regarding the effects on osteoclastogenesis suggest inhibitory effects of megakaryocyte on osteoclast development and functions (Beeton *et al.*, 2006; Ciovacco *et al.*, 2010; Kim *et al.*, 2018). *In vitro* studies show that

monocytes can induce osteogenesis in MSCs through cell contact, which leads to the activation of STAT3 signaling followed by upregulation of Runx2, ALP, and Oncostatin M and downregulation of DKK1 in MSCs (Nicolaidou *et al.*, 2012). From these data, it is clear that bidirectional interactions of MSCs and HCs at different developmental stages regulate local tissue functionality and their elucidation particularly contributes to the understanding of normal as well as malignant stem cell biology.

MSCs and M ϕ

M ϕ are phagocytic myeloid cells involved in inflammatory processes through dead cell and foreign material degradation. M ϕ pool contains self-renewable embryonic M ϕ , which are established before the emergence of adult M ϕ which derive from marrow immature myeloid progenitors or circulating monocytes (Gomez Perdiguero *et al.*, 2015; Yona *et al.*, 2014). M ϕ are functionally specialized in lung, liver (Kupffer cells), or bone, where multinucleated OC near the bone surface participate in physiologic or pathologic bone resorption (Kim *et al.*, 2014; Park *et al.*, 2014; Wu *et al.*, 2015). OC dissolve crystalline hydroxyapatite (Wenisch *et al.*, 2003) and degrade the collagen-rich organic bone matrix (Henriksen *et al.*, 2006). Due to their plasticity, M ϕ may have an anti-inflammatory (M2) or pro-inflammatory (M1) profile as well as many intermediate activation states. MSCs can facilitate monocyte to macrophage transition, but attenuate (Vasandan *et al.*, 2016) or favor their pro-inflammatory and osteoclastic activities (Gamblin *et al.*, 2014). MSCs induce a M2 phenotype in BM-M ϕ , increasing their expression of arginase-1, IL-10, IL-4, and CD206 and decreasing the expression of IL-6, MCP-1, and iNOS (Cho *et al.*, 2014; Takizawa *et al.*, 2017). Through the production of major osteoclastogenic [e.g., RANKL (Biswas *et al.*, 2018) and M-CSF (Cappellen *et al.*, 2002)] and anti-osteoclastogenic factors [e.g., OPG (Oshita *et al.*, 2011)], MSCs control bone resorption and remodeling (Sharaf-Eldin *et al.*, 2016). By producing OPG and/or FasL protein, MSCs exert a suppressive effect on osteoclastogenesis (Shao *et al.*, 2015; Varin *et al.*, 2013) and are proposed to be suitable cell candidates for controlling inflammation-associated bone destruction, such as rheumatoid arthritis (Oshita *et al.*, 2011). However, the absence of osteoclastogenesis may be associated with reduced osteoblastic commitment of MSCs, endosteal osteoblast loss, and impaired homing (Mansour *et al.*, 2012) or clonogenicity of HSPCs (Lymeri *et al.*, 2011).

MSCs and DCCs

MSC and their progeny may facilitate neoplastic growth (Doron *et al.*, 2018). Communication between MSCs and bone-metastatic DCCs is unclear, but it is possible that MSCs control DCC settlement in the BM as competition for niche space may exist (Dhawan *et al.*, 2016; Gordon *et al.*, 2014; Rosnagl *et al.*, 2018; Shiozawa *et al.*, 2015). Prostate cancer cells induce

an osteoblastic-type lesion, while breast cancer and myeloma cells form osteolytic-type of bone lesions (Hashimoto *et al.*, 2018). Human BM biopsies show higher CD271⁺ MSCs and CD31⁺ frequencies in the absence of DCCs in the BM of prostate cancer patients in comparison with breast cancer (Rosnagl *et al.*, 2018). SDF-1 chemokine gradient is one of the most described explanations for tumor-to-BM homing and MSC-derived osteoblasts produce SDF-1, creating a chemo-attractant gradient for CXCR4-expressing cancer cells (Amend *et al.*, 2016; Devignes *et al.*, 2018). *In vitro* and *in vivo* migration assays have revealed that MSCs have tropism toward multiple myeloma cells, where MSCs promote multiple myeloma progression (Xu *et al.*, 2012). Although tumor-homing ability of MSCs suggests their utilization in anti-tumor strategies, it is still unknown how MSCs in the metastatic niche of the BM contribute to graft *versus* tumor reaction, one of the currently most investigated anti-tumor approaches. Exosomal transfer of miRNAs from MSCs to breast DCCs (Ono *et al.*, 2014) induces MSCs dormancy in the BM niche. Moreover, multiple-myeloma-cell-derived exosome miRNA promotes a phenotype switch of MSCs towards a cancer-associated fibroblast state (Cheng *et al.*, 2017). Concerning tumor persistence, there is a complex bidirectional crosstalk of MSCs and cancer cells involving various mechanisms which are still unclear but important for the understanding of peculiarities of normal and stem cell niche in tumors.

ECM dynamics

Although the crucial importance of cellular interactions with surrounding elements is recognized, a major challenge is still to understand how the chemical composition and mechanical properties of the ECM can functionally influence tissue homeostasis under physiological and pathological conditions.

Particularly, a better understanding on how disruption of ECM dynamics, *i.e.*, both biochemical signaling and physical cues, contributes to progression of complex diseases will be important towards the development of new therapeutic targets in regenerative medicine.

Biochemical interactions

Microenvironmental cues, such as cellular interactions, the paracrine environment and ECM-associated proteins, critically influence MSC behavior *via* biochemical pathways. This is suggested by plenty of studies demonstrating that MSCs acquire tissue-specific characteristics when co-cultured with mature cells types (Csaki *et al.*, 2009; Deng *et al.*, 2008; Plotnikov *et al.*, 2008; Schneider *et al.*, 2011; Strassburg *et al.*, 2010) or in complex biological substrates *in vitro* (Bosnakovski *et al.*, 2006; Datta *et al.*, 2005; Hoch *et al.*, 2016; Suzuki *et al.*, 2010).

The oxygen tension applied to the *in vitro* culture also significantly influences both MSC proliferation and differentiation potential in a lineage-specific matter.

Although the published literature is quite diverse and occasionally contradictory, some studies have reported that reduced oxygen tension attenuates the MSC differentiation capacity into the osteogenic lineage (D'Ippolito *et al.*, 2006) whilst promoting adipogenic (Fink *et al.*, 2004) and chondrogenic differentiation (Kanichai *et al.*, 2008; Robins *et al.*, 2005). This correlates with the *in vivo* situation where chondrocytes and adipocytes reside in more hypoxic environments. Low oxygen tension also regulates MSC paracrine activity. An induced hypoxic *in vitro* culture stimulates an upregulation of angiogenic genes, such as VEGF and IL-6 (Hu *et al.*, 2008). Furthermore, in hypoxia, large amounts of SDF-1, along with its receptor CXCR4, are expressed and secreted by MSCs, stimulating their mobilization and, thus, promoting MSC-homing toward damaged tissue (Liu *et al.*, 2012; Rosenkranz *et al.*, 2010). Likewise, tissue-specific ECM proteins have an important role as a supportive scaffold, exposing binding sites for growth factors, cell receptors ligands, proteases, *etc.*. In the context of bone, a type I collagen-rich ECM is required to regulate local availability of BMPs in a spatio-temporal manner and, therefore, controls osteoblast lineage progression. Specifically, integrin binding of ECM-released BMPs to osteoblastic precursor cells initiates a MAPK-dependent signaling cascade that leads to the phosphorylation and activation of Runx2 (Yang *et al.*, 2003), the master transcriptional regulator of the osteoblastic differentiation. Noteworthy, the ECM-MSD dynamic is rather a bidirectional system, where the lineage commitment process of MSCs also induces a remodeling of the microenvironment's chemical and mechanical characteristics. Manduca *et al.* (2009) have investigated the role of MMPs in osteogenic differentiation, demonstrating that preosteoblastic cells sense the microenvironment through binding of $\beta 1$ integrins to fibronectin and collagen type I in the ECM, resulting in the formation of a complex with MMP-1. This complex initiates the expression of proMMP-2, required for type-I collagen and ALP proteolysis, which is involved in mineral deposition during osteogenic differentiation.

These studies emphasize the crucial role of cell-matrix interactions as highly instructive elements for stem cell biologic functions including growth, differentiation, apoptosis, and, ultimately, tissue remodeling.

The importance of the environmental mechanical properties



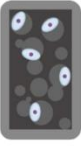



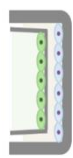
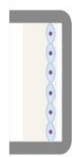
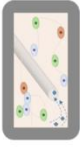

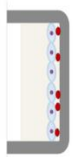




In the context of bone, collagen fibrils comprise binding sites for mineral deposition while still keeping the structural flexibility for a tissue that would otherwise be overly rigid. Alongside, there is evidence showing that ECM physical cues not only provide support and anchorage for the cells but strongly elicit changes in gene expression and, ultimately, affect cell fate and tissue development (Chen, 2008; Engler *et al.*, 2006; Lutolf and Hubbell, 2005). Biologically, osteocytes trapped within the

matrix are the principal sensors of mechanical forces applied to the bone, with a crucial role in local mineral deposition regulation (Klein-Nulend *et al.*, 2013). Likewise, for tissue engineering approaches, MSCs are sensitive to their substrate stiffness and able to detect its nano- and micro-topography or porosity (reviewed by Sun *et al.*, 2012a). The transduction of these mechanical stimuli into cellular processes, otherwise known as a mechanotransduction, is accomplished through direct or indirect processes (described in detail by Sun *et al.*, 2012a; Yim and Sheetz, 2012). Briefly, direct mechanotransduction occurs when forces applied to integrins, which are linked to the nucleus through focal adhesion interactions with the cytoskeletal protein filaments (*e.g.*, actin and vimentin), lead to changes in gene expression through chromatin remodeling. Indirect mechanotransduction occurs either through mechanosensitive ion channels, mainly from TRP family (Ranade *et al.*, 2015), or through integrin-mediated signal pathways (Jalali *et al.*, 2001; Schwartz, 2010), which internally couple with other growth factor pathways to regulate stem cell fate. Even with all the recent discoveries on how MSC behavior can be tailored by artificial mechanic features (refer to the next section for MSC environment modelling applications), there is still a poor understanding of the underlying mechanisms of biophysically-induced stem cell differentiation and how these dynamic complex feedbacks can be manipulated towards a therapeutic application.

Modelling MSC niche complexity

The extensive presence of MSC-like progenitor cells throughout the vascularized organs raises a wide range of possible therapeutic strategies intending to accelerate the tissue regenerative capacity following injury. The up-to-date therapeutic applications, either based on the stem-properties or on the paracrine and immunomodulatory competence of these cells, are highlighted in recent reviews (Matsumoto *et al.*, 2016; Park *et al.*, 2011; Peired *et al.*, 2016; Yousefi *et al.*, 2016). Nevertheless, in most cases, MSC-based clinical trials occur in an early phase (phase I or II) according to FDA guidelines, where the long-term safety and treatment efficacy is not yet conclusively established (Squillaro *et al.*, 2016). Regardless of the extensive effort and advances made in MSC identity and experimental handling, there are still substantial ambiguities about their integrative functions *in vivo* and long-term safety, which continues to pose a major limitation on their envisioned therapeutic use. An extensive scientific knowledge of each MSC subpopulation and their interaction with the environment is still necessary to successfully translate them to the clinic. The more recent and relevant illustrative examples of novel bioengineering approaches to mimic biological, chemical, and mechanical microenvironmental signals present in

Table 1. Research models to study MSC behavior and their interactions with the surrounding biochemical and physical cues.

Model	Features and relevance	Model	Features and relevance	Model	Features and relevance
<p>Soluble factors</p> 	<p>Low cost</p> <p>Simple output analysis</p>	<p>Spheroids culture</p> 	<p>Low cost</p> <p>Simple output analysis</p> <p>Cell-cell adhesion</p> <p>Three-dimensionality</p> <p>Diffusion gradients</p>	<p>3D scaffolds</p> 	<p>Cell-ECM interactions</p> <p>Tunable chemistry</p> <p>Tunable mechanical properties</p> <p>Three-dimensionality</p> <p>Diffusion gradients</p>
<p>Conditioned media</p> 	<p>Low cost</p> <p>Simple output analysis</p> <p>Biochemical complexity</p>	<p>Topography-patterning</p> 	<p>Simple output analysis</p> <p>Spatial control</p> <p>Cell-ECM interactions</p> <p>Pseudo-3D arrangement</p>	<p>Decellularized tissue</p> 	<p>Native ECM arrangement</p> <p>Cell-ECM interactions</p> <p>Three-dimensionality</p> <p>Diffusion gradients</p>
<p>Indirect co-culture</p> 	<p>Low cost</p> <p>Simple output analysis</p> <p>Biochemical complexity</p>	<p>Substrate stiffness</p> 	<p>Simple output analysis</p> <p>Cell-ECM interactions</p> <p>Tunable chemistry</p> <p>Tunable mechanical properties</p>	<p>Dynamic bioreactors</p> 	<p>Continuous perfusion</p> <p>Tunable chemistry</p> <p>Tunable mechanical properties</p> <p>Biochemical complexity</p> <p>Cell-cell and cell-ECM interactions</p> <p>Three-dimensionality</p>
<p>Direct co-culture</p> 	<p>Low cost</p> <p>Biochemical complexity</p> <p>Cell-cell adhesion</p>	<p>Surface protein-immobilization</p> 	<p>Spatial control</p> <p>Simple output analysis</p> <p>Cell-ECM interactions</p> <p>Pseudo-3D arrangement</p> <p>Tunable chemistry</p>	<p>Microfluidic chips</p> 	<p>Spatial-temporal control</p> <p>Continuous perfusion</p> <p>Accessible live tracking</p> <p>Highly customizable</p>
<p>Protein coating</p> 	<p>Low cost</p> <p>Simple output analysis</p> <p>Tunable chemistry</p> <p>Cell-ECM interactions</p>	<p>3D gel matrices</p> 	<p>Tunable chemistry</p> <p>Tunable mechanical properties</p> <p>Cell-ECM interactions</p> <p>Diffusion gradients</p> <p>Three-dimensionality</p>	<p>In vivo models</p> 	<p>Native environment</p>

the MSC niche are summarized in this section (see Table 1). Furthermore, the current limitations are highlighted and potential opportunities to fill the bridge between fundamental science and clinical application discussed.

Monolayer culture: an *in vitro* mechanistic tool

Culture of an adherent cell monolayer on flat and rigid 2D substrates is a well-established straightforward technique by which cells of interest can be maintained outside the body and observed over time with a good viability of cells in culture.

Paracrine factors

To date, the simplest models for examining biological behavior of MSCs in response to microenvironmental factors are conducted by direct exposition to soluble factors (Celil and Campbell, 2005; Indrawattana *et al.*, 2004; Kratchmarova *et al.*, 2005; Luo *et al.*, 2010) and conditioned media from either other cell type cultures (Chowdhury *et al.*, 2015; Menon *et al.*, 2007; Siciliano *et al.*, 2015) or from tissue extracts (Chen *et al.*, 2002). In the strictest sense, the conditioned medium refers to the cell secretome, which encompasses proteins shed from the cell surface and intracellular proteins released through non-classical secretion pathway or exosomes, including numerous enzymes, growth factors, cytokines and hormones, or other soluble mediators (Veronesi *et al.*, 2017). Therefore, conditioned medium approaches offer the possibility of studying the paracrine interactions of complex combinations of factors, in a specific physiological or pathological environment.

Co-cultures

Co-culture techniques find countless applications in biology for studying interactions between cell populations. Overall, the co-culture systems can be set-up either by direct co-culture of both cell types or

using compartmented systems, such as trans-wells or microfluidic chambers, to study solely the paracrine crosstalk and not the cell-cell signaling pathways that may occur. Many studies have explored this approach by co-culturing MSCs with mature cells in direct (Aguirre *et al.*, 2010; Ball *et al.*, 2004; Csaki *et al.*, 2009; Deng *et al.*, 2008; Strassburg *et al.*, 2010; Takigawa *et al.*, 2017; Wang *et al.*, 2007) and indirect contact (Li *et al.*, 2011; Luo *et al.*, 2009; Wei *et al.*, 2010). When comparing cultures of MSCs and osteoblasts alone with MSC/osteoblast co-cultures, for example, an increase in calcification over time is observed in co-culture. These results suggest the idea of a positive augmentation of the MSC differentiation process by osteoblast-secreted factors (Glueck *et al.*, 2015).

Protein-coating

The native ECM is essentially a 3D network of fibrillar and non-fibrillar proteins, such as collagens, fibronectin, elastin, laminin, vitronectin, glycosaminoglycans, such as hyaluronan or heparin, and proteoglycans (Bason *et al.*, 2018). Many of these ECM components are commercially available, either as complex mixtures (*e.g.*, matrigel) or as purified proteins and are extensively applied to guide MSC differentiation *in vitro* (Curran *et al.*, 2006; Phillips *et al.*, 2010; Qian and Saltzman, 2004; Rojo *et al.*, 2016). To achieve a high chemical complexity, MSCs are also cultured on decellularized extracellular 2D coatings, *i.e.*, matrix produced by cells *in vitro*, resulting in a composition of cell-secreted components without the potentially antigenic cellular structures or contaminating DNA after collection and processing (Hoshiba *et al.*, 2010). The enhancement of proliferation and stemness maintenance of naïve MSCs is verified in cells cultured on a basal-cultured MSC-derived decellularized ECM; while, when cultured on decellularized ECM deposited by MSCs under osteogenic differentiation, an osteogenic

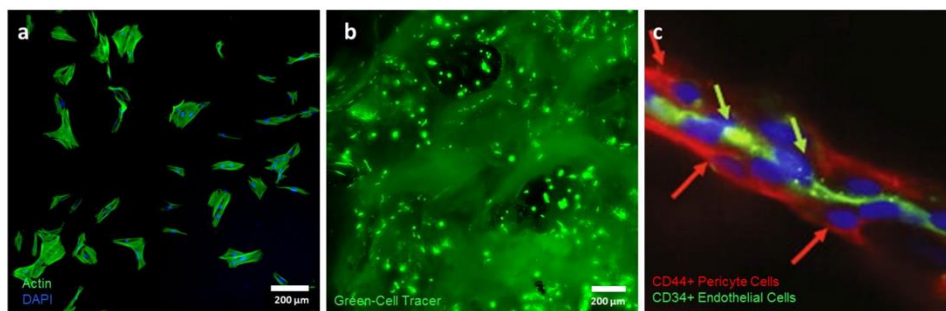


Fig. 2. Comparison of morphology and spatial organization of MSC *in vitro* cultures with the MSC perivascular niche *in vivo*. When cultured on a 2D monolayer culture of standard tissue culture polystyrene (a) MSCs acquire a stretched and flattened morphology. On the other hand, when a 3D decellularized bone scaffold is used to physically support MSC culture, (b) the cell-matrix interactions induce a different cellular distribution and arrangement which closely mimics the niche organization observed in (c) an *in vivo* perivascular niche [600× magnification (with permission of Crisan *et al.*, 2008)].

lineage differentiation is observed in seeded MSCs cultured in the absence of dexamethasone (Rao *et al.*, 2014).

Limitations

Although very convenient and effective for mechanistic purposes, the results from 2D cell culture models may not be representative of essential and complex features of native microenvironments. A main limitation of *in vitro* studies in 2D monolayer cultures is the lack of spatial and temporal control of multiple signals, similar to what happens in a native 3D context. Furthermore, a significant limitation of 2D cell cultures is that diffusion and transport conditions do not reflect the *in vivo* situation – cells grown in monolayers are exposed to a uniform environment with constant supply of oxygen, nutrients or metabolic products, which can lead to significant deviations in cellular function and response (Baker *et al.*, 2012).

Paradigm shift: mimicking MSC niche environment through third dimension

Due to the lack of structural architecture, 2D cell culture models are substantially diverging from the *in vivo* state (Fig. 2). Accordingly, many research groups apply a 3D culture environment that aims to better resemble the native tissue organization.

Spheroids culture

Since the observation that chondrocytes lose their phenotype quickly in monolayer culture (Caron *et al.*, 2012; Thompson *et al.*, 2017), micromasses and pellet *in vitro* cultures have been established, allowing cells to aggregate in high densities and create their own 3D cartilaginous matrix (Cottrill *et al.*, 1987; Johnstone *et al.*, 1998). In addition, using a simple 3D scaffold-free spheroid culture system, Wang *et al.* (2009) have demonstrated that MSC multipotency can be significantly increased for both osteogenic and adipogenic lineage when compared with the conventional 2D monolayer culture. Moreover, using a perivascular-like *in vitro* 3D spheroid co-culture system, Saleh *et al.* (2011) have shown that endothelial cells regulate MSC activity by maintaining quiescence and facilitating niche exit by osteogenic differentiation through activation of endogenous Wnt and BMP signaling. Other studies have reported enhanced anti-inflammatory properties after a short period of spheroid culture by increased expression of genes, such as CXCR4, which promotes adhesion, or IL-24, with tumor-suppressing properties (Bartosh *et al.*, 2010; Potapova *et al.*, 2008; Ylöstalo *et al.*, 2012).

Micropatterning

A different approach being adopted is the creation of a pseudo-3D environment for MSCs using soft lithography techniques to imprint a topography-patterning in the culture substrates. This is rather a bottom-up organization approach, with cells being instructed at the molecular level. Several studies have

shown increased mineralization during osteogenesis induction on micro- and/or nano-patterning growth surfaces (McNamara *et al.*, 2010; Oh *et al.*, 2009; Yim *et al.*, 2007; Zhao *et al.*, 2012). Differences in groove size as well as their geometric arrangement dictate the matrix alignment and cell morphology, resulting in a strong effect on cell proliferation and gene expression and eventually induction of bone nodules formation. Dalby *et al.* (2007) have shown that MSC osteogenic differentiation can be initiated with a nanopitted topographical pattern in a square geometry with a moderate level of disorder embossed into PMMA surfaces; while, on the other hand, an ordered square nanopit-pattern is proposed to mediate retention of MSC stemness (McMurray, 2011). Also, Stanciuc *et al.* (2018) have shown an accelerated maturation of human osteoblast maturation on micro-rough surfaces of zirconia-toughened alumina with nanoporosity obtained by selective chemical etching.

Substrate stiffness

Engler *et al.* (2006) have demonstrated for the first time that the substrate stiffness itself can direct MSC lineage fate. Subsequently, Pek *et al.* (2010) have optimized a 3D hydrogel system to guide MSC differentiation either to neural, myogenic, or osteogenic phenotypes depending on whether they are cultured in gels of elastic moduli in the lower (7 Pa), intermediate (25 Pa), or higher range (75 Pa), respectively. Interestingly, the matrix that optimally drives MSC differentiation to specific lineages corresponds to the stiffness of the relevant target tissue. Accordingly, tuning the elasticity of the culture material is a common strategy, adopted to control MSC fate (Du *et al.*, 2016; Huebsch *et al.*, 2015; Kuboki and Kidoaki, 2016; Seib *et al.*, 2009; Wingate *et al.*, 2012).

The influence of the chemical and physical biomaterial properties

Progress in the development of biomimetic materials have lately been chasing the complexity of the mechanical and physical-chemistry arrangement of the biomaterial itself, such as a scaffold, commonly used for tissue engineering applications. Such tissue-engineered constructs not only represent potential therapeutic options for the treatment of bone defects but may also serve as a model system of the MSC naïve environment in the bone and facilitate our understanding of the interactions within the niche.

3D gel matrices/scaffolds

For tissue engineering applications, the culture substrate should not only provide physical support but also present a functional surface chemistry compliant with the biological purpose. Noteworthy, the chemical composition as well as the fabrication process itself determine the final geometry, porosity, and roughness of the bulk material (Akbarzadeh and Yousefi, 2014; Loh and Choong, 2013; Pina *et al.*, 2016). The macroporosity (pores > 50 µm) of a scaffold

contributes to osteogenesis by facilitating cell and ion transport (Bignon *et al.*, 2003), while microporosity (pores < 20 μm) augments bone growth by providing attachment points for osteoblasts (Bignon *et al.*, 2003) and increasing growth factors retention upon which bone formation depends in ectopic sites (Hing *et al.*, 2005; Woodard *et al.*, 2007).

Commonly used natural polymers for bone tissue engineering are collagen, fibrin, alginate, silk, hyaluronic acid, and chitosan. They provide high biological recognition that may positively support cell adhesion and function, yet often lack the mechanical strength required by bone (reviewed by O'Brien, 2011). Synthetic biodegradable polymers, such as PLA, PGA, and PCL are widely used due to their reproducible large-scale production, with controlled properties of strength, degradation rate, and microstructure (reviewed by O'Brien, 2011). Calcium-phosphate-based materials, such as hydroxyapatite and beta-tricalcium phosphate, are widely used ceramics that often shape the inorganic-phase of bone graft substitutes. Their non-toxic, non-inflammatory, non-immunogenic properties and their biological affinity (*i.e.*, ability to form direct chemical bonds with the surrounding environment) direct tissue integration when implanted in bone defects (Ambar and Mueninghoff, 2006; Venkatesan and Kim, 2014). Besides, extensive studies of organic modifications of hydroxyapatite-based composites show the enhancement of the osteoconductive properties of the material (review by Swetha *et al.*, 2010). For example, Zhao *et al.* (2006) have investigated two types of biomimetic composite materials, chitosan-gelatin and hydroxyapatite/chitosan-gelatin. They have shown that hydroxyapatite enhances protein and calcium ion adsorption – which in turn improves i) initial cell-adhesion and long-term growth, ii) maintains MSC stemness and iii) upon induction enhances osteogenic differentiation (Zhao *et al.*, 2006).

Engineered substrates

The tissue engineering field provides valuable knowledge for modeling the MSC niche *in vitro*. Moreover, advances in protein engineering and synthetic chemistry of peptide-conjugated polymers allow the fabrication of the so-called artificial ECM constructs, which can respond to cell-secreted signals and enable proteolytic matrix remodeling (Lutolf and Hubbell, 2005). These synthetic networks are typically achieved by crosslinking of specific bioactive components in a structural mesh – *e.g.*, (1) cell-adhesive ligands, such as integrin-binding peptides of the prototypical RGD family, resulting in an increased cell growth efficiency (Chang *et al.*, 2009; Maia *et al.*, 2014); (2) domains with susceptibility to degradation by cell-secreted proteases to facilitate bidirectional cell-matrix interactions (Lutolf *et al.*, 2003); (3) binding sites for growth factor matching the pretended application (Madl *et al.*, 2014; Park *et al.*, 2009). Thevenot *et al.* (2010) have developed a PLGA

scaffold with incorporated SDF-1 to enhance the recruitment of endogenous MSCs to the injury site. Likewise, Phillippi *et al.* (2008) have created spatially defined patterns of immobilized BMP-2 using inkjet bioprinting technology to modulate the cell organization and, consequently, their differentiation toward the osteogenic lineage.

As another powerful element, synthetic biology has recently been applied to tissue engineering modeling. Encapsulated modified cells with sophisticated tunable modular genetic switches that couple repressor proteins with an RNAi can be controlled by an external factor or specific microenvironment changes (Saxena *et al.*, 2016; Weber and Fussenegger, 2012).

3D biofabrication

Combined knowledge of material science and 3D fabrication principles results in the advent of additive manufacturing techniques as a complex innovative approach to generate complex 3D environments with a designed and controlled arrangement of tissue morphology features and spatial distribution of cells (Bose *et al.*, 2013; Malda *et al.*, 2013). 3D biofabrication is becoming popular due to the ability to directly print porous scaffolds with designed shape, controlled chemistry, and interconnected porosity. Apart from inorganic scaffold manufacturing, additive manufacturing approaches are also used to explore the possibilities in fabricating scaffolds with live cells and tissues. Levato *et al.* (2014) have shown a combined method where MSC-laden polylactic acid microcarriers are printed by encapsulation in gelatin methacrylamide-gellan. This combined bioprinting approach allows for the improvement of the elastic modulus of the hydrogel construct, facilitating cell adhesion and survival, while supporting osteogenic differentiation and bone matrix deposition (Levato *et al.*, 2014). Alternatively, Gurkan *et al.* (2014) have used another interesting approach where MSCs are encapsulated in a gelatin-based methacrylated hydrogel with addition of BMP-2 and TGF- β 1 mimicking the fibrocartilage phase of the bone. Incorporating bioprinting technology with a nanoliter gel droplet system, this model can induce the upregulation of osteogenesis and chondrogenesis, thus making this approach a functional tissue model system (Gurkan *et al.*, 2014).

Decellularized tissue

Although a variety of different materials and composites are available, to achieve a physiologically relevant protein and structural complexity, whole organ or tissue decellularization techniques are investigated. These natural scaffolds preserve the complex biochemical and biomechanical ultrastructure of the native tissue and can be recellularized to generate a new functional tissue or organ (Crapo *et al.*, 2011; Lund *et al.*, 2017). Particularly, decellularized bone is used as a scaffold for bone

tissue engineering or bone *in vitro* modelling due to its 3D porous structure and its natural biochemical component arrangement, providing osteoinductive properties that are not fully resembled by synthetic polymers or hydrogels (Nyberg *et al.*, 2017). However, the current challenge of working with decellularized matrices and their translation to clinics is to balance the decellularization methods in order to maintain the specific epitopes that will have a positive impact on cell functions but eliminate any component that could cause an immunogenic response (Gilpin and Yang, 2017; Keane *et al.*, 2016).

The dynamic dimension

Biomechanical stimuli caused by physical deformation and fluid shear stress generated by interstitial fluid movement through bone lacunae are recognized as a significant part of *in vivo* bone remodeling (Carter, 1984; Duncan and Turner, 1995). Therefore, to better reassemble the *in vivo* counterpart, *in vitro* models for skeletal progenitors may likewise be integrated in an intrinsic dynamic environment.

Dynamic bioreactors

Dynamic culture of MSCs has expanded greatly in the last 15 years and dynamic optimized bioreactors are now widely used to provide the technological means to achieve both improved nutrient transportation and mechanical stimulation. A variety of dynamic 3D bioreactor concepts mimicking the native microenvironment of bone tissues have been developed – e.g., perfusion chambers (Dahlin *et al.*, 2012; Hosseinkhani *et al.*, 2006; Kleinhans *et al.*, 2015; Porter *et al.*, 2005; Yeatts and Fisher, 2010), stirred tanks (Eibes *et al.*, 2010; King and Miller, 2007), rotating wall vessels (Nishi *et al.*, 2013; Song *et al.*, 2008), mechanical loading chambers (Altman *et al.*, 2002; Baker *et al.*, 2011; Pelaez *et al.*, 2012; Sittichokechaiwut *et al.*, 2009), and, more recently, nanovibrational reactors (Tsimbouri *et al.*, 2017). MSCs cultured under those dynamic cultures are subjected to mechanical shear created by fluid flow, which promotes osteogenesis *via* the ERK1/2 pathway through upregulation of Runx2 (Yeatts *et al.*, 2013) and, therefore, provides the right microenvironmental setup to augment bone formation (David *et al.*, 2007; McCoy and O'Brien, 2010; Stiehler *et al.*, 2009).

Microfluidic chips

The advances in microfluidic technology brought great progresses in the field of dynamic *in vitro* models, mainly regarding the spatiotemporal control of gradients and the introduction of individual or combination of factors with low volumes and low cell suspension density requirements (Sart *et al.*, 2016; Sun *et al.*, 2012b; Tatárová *et al.*, 2016). Recently, Marturano-Kruik *et al.* (2018) have developed a perivascular model containing ECs and MSCs seeded on a bone matrix, forming a bone perivascular niche-on-a-chip, which allows following slow-cycling metastatic cancer cells in a BM niche.

Smart materials

Meanwhile, advances in the material science field have been made with the development of the so-called 'smart' materials – i.e., biomaterials specifically designed to allow dynamic changes in their structure in response to an external stimulus (Kaliva *et al.*, 2017). These materials can be metals or polymers sensitive either to temperature (Dessi *et al.*, 2013; Roy *et al.*, 2013), pH (Wang *et al.*, 2004), magnetic (Ribeiro *et al.*, 2016) or electrical fields (Balint *et al.*, 2014), light (Muraoka *et al.*, 2009; Zhao, 2012), or lytic-enzymes (Hu *et al.*, 2012; Todd *et al.*, 2007). The concept of a dynamic 4th dimension is also being explored in 3D printing approaches for tissue engineering (reviewed by Gladman *et al.*, 2016; Khoo *et al.*, 2015). The development of new tailored inks capable of adapting their shape or functionalities to external stimuli will surely be a pivotal milestone in achieving reliable and close to *in vivo* MSC niche models.

In vivo models

Animal models are a vital part of MSC biology research and MSC-based therapeutic approaches, enabling investigations at the systemic level in a physiological environment. Nevertheless, the prediction of effectiveness of a therapeutic approach in preclinical models can be highly inaccurate, resulting in hurdles upon translation of results in clinics. This frequent discrepancy happens mainly due to (1) intrinsic divergence of molecular mechanisms between species and the non-human stromal component of the ECM, or (2) anatomic discrepancies particularly in orthopedic applications. These facts, along with high costs of maintenance, need for qualified expertise, limited output analysis, and ethical concerns about animal experimentation are motivating governments and regulatory organizations to limit their use and support the implementation of alternative methods following the 3R's principles – firstly established by Russell in 1959 (Russell *et al.*, 1959). Yet, improvements in modeling the complex bone environment (as discussed in the present review) present promising options to provide tissue grafts for regenerative medicine in large bone fractures and, also, to screen with precision therapeutic agents that may facilitate bone repair.

Final remarks

In vitro models should not be confined to single stationary conditions; i.e., an individual architecture or a particular chemical functionalization with a specific biological function. Instead, it is desirable that the emerging constructs should comprise complex combinatorial signals with tunable cues, to support stemness maintenance or direct stem cell differentiation with spatiotemporal control. Nevertheless, successes in various aspects of the tissue engineering assure a bright future for the development of models that mimic the relevant properties of naïve tissues. The progressive increase in complexity of *in vitro* models that is been

witnessed is surely paving the way towards a better understanding of the detailed biological events involved in tissue homeostasis and related disorders *in vivo*.

Further perspectives

The localization, identification, and regenerative potential of MSCs is under controversial discussion in the stem cell community. This is mainly attributed to the lack of distinct surface markers for the identification and prospective isolation of naïve MSC/tissue-specific progenitor cells *in vivo* in mouse and human, resulting in inconsistencies of the studied cell population, and the restriction of many studies to the assessment of the cell regenerative potential *in vitro*. The *in vitro* MSC characterization methods are highly artificial and do not proof the function of MSC/tissue-specific progenitor cells *in vivo*. Indeed, there is an ambiguous distinction between the physiological function of isolated MSCs in culture and their presumed *in vivo* counterpart – *i.e.*, MSCs isolated from the BM give rise to all the mesenchymal cell lineages (Pittenger *et al.*, 1999) and even transdifferentiate into cells from the central nervous system (Wislet-Gendebien *et al.*, 2005), the skeletal muscle system (Ferrari *et al.*, 1998), the hepatic system (Lee *et al.*, 2004), and the cardiac system (Toma *et al.*, 2002) when exogenously stimulated; whereas naïve non-stimulated BM-MSCs do not share the same phenotypic plasticity (Bara *et al.*, 2014). In fact, robust *in vivo* assays of progenitor cells from other tissues, all sharing the *in vitro* characteristics attributed to MSCs (Dominici *et al.*, 2006), suggest that distinct tissue-specific stem/progenitor cells with distinct regenerative capacity exist throughout the body (Robey, 2017; Sipp *et al.*, 2018), specifically settled in a specific environment which control either the maintenance of their stemness or the orchestration of tissue modulation activities. This, along with the increasing amount of data showing a microenvironmental-dependent behavior of MSCs, as reviewed in the present article, highlights the importance of considering and implementing microenvironmental cues upon assessment of the MSC regenerative potential.

Although substantial advances have already been made in the field, the recapitulation of the complex biological recognition and signaling functions, *e.g.*, between cells and ECM, is still crucial and controlling the dynamics and spatial organization of multiple signals remains a current challenge. Substantial testing and optimization is still required to ensure that the 3D constructs realistically mimic the native tissue counterparts. Accordingly, despite the unquestionable value of MSCs for clinical applications, comprehensive studies of fundamental mechanisms triggered by microenvironmental cues

are critical before moving to regenerative medicine cell therapy applications.

The future holds great potential for 3D/4D models for studying tissue dynamics in health and disease as well as for tissue engineering applications. Progress in engineering, technology, biomaterials, and imaging will surely be at the forefront of the MSC niche model revolution.

Acknowledgements

This work was supported by the Interdisciplinary Center for Clinical Research (IZKF) at the University of Wuerzburg (Project D-361). The authors have no conflict of interest to declare.

References

- Agarwal S, Loder S, Cholok D, Peterson J, Li J, Fireman D, Breuler C, Hsieh HS, Ranganathan K, Hwang C (2016) Local and circulating endothelial cells undergo endothelial to mesenchymal transition (EndMT) in response to musculoskeletal injury. *Sci Rep* 6: 32514. DOI: 10.1038/srep32514.
- Aguirre A, Planell J, Engel E (2010) Dynamics of bone marrow-derived endothelial progenitor cell/mesenchymal stem cell interaction in co-culture and its implications in angiogenesis. *Biochem Biophys Res Commun* 400: 284-291.
- Akbarzadeh R, Yousefi AM (2014) Effects of processing parameters in thermally induced phase separation technique on porous architecture of scaffolds for bone tissue engineering. *J Biomed Mater Res B* 102: 1304-1315.
- Al-Soudi A, Kaajj M, Tas S (2017) Endothelial cells: from innocent bystanders to active participants in immune responses. *Autoimmun Rev* 16: 951-962.
- Altman GH, Lu HH, Horan RL, Calabro T, Ryder D, Kaplan DL, Stark P, Martin I, Richmond JC, Vunjak-Novakovic G (2002) Advanced bioreactor with controlled application of multi-dimensional strain for tissue engineering. *J Biomech Eng* 124: 742-749.
- Alvarez MB, Xu L, Childress PJ, Maupin KA, Mohamad SF, Chitteti BR, Himes E, Olivos III DJ, Cheng Y-H, Conway SJ (2018) Megakaryocyte and osteoblast interactions modulate bone mass and hematopoiesis. *Stem Cells Dev* 27: 671-682.
- Ambard AJ, Mueninghoff L (2006) Calcium phosphate cement: review of mechanical and biological properties. *J Prosthodontics* 15: 321-328.
- Ambrosi TH, Scialdone A, Graja A, Gohlke S, Jank A-M, Bocian C, Woelk L, Fan H, Logan DW, Schürmann A (2017) Adipocyte accumulation in the bone marrow during obesity and aging impairs stem cell-based hematopoietic and bone regeneration. *Cell Stem Cell* 20: 771-784.

- Amend SR, Roy S, Brown JS, Pienta KJ (2016) Ecological paradigms to understand the dynamics of metastasis. *Cancer Lett* **380**: 237-242.
- Angelos MG, Abrahante JE, Blum RH, Kaufman DS (2018) Single cell resolution of human hematoendothelial cells defines transcriptional signatures of hemogenic endothelium. *Stem Cells* **36**: 206-217.
- Baker BM, Chen CS (2012) Deconstructing the third dimension: how 3D culture microenvironments alter cellular cues. *J Cell Sci* **125**(Pt 13): 3015-3024.
- Baker BM, Shah RP, Huang AH, Mauck RL (2011) Dynamic tensile loading improves the functional properties of mesenchymal stem cell-laden nanofiber-based fibrocartilage. *Tissue Eng Part A* **17**: 1445-1455.
- Baksh D, Yao R, Tuan RS (2007) Comparison of proliferative and multilineage differentiation potential of human mesenchymal stem cells derived from umbilical cord and bone marrow. *Stem Cells* **25**: 1384-1392.
- Balint R, Cassidy NJ, Cartmell SH (2014) Conductive polymers: towards a smart biomaterial for tissue engineering. *Acta Biomater* **10**: 2341-2353.
- Ball SG, Shuttleworth AC, Kielty CM (2004) Direct cell contact influences bone marrow mesenchymal stem cell fate. *Int J Biochem Cell Biol* **36**: 714-727.
- Bara JJ, Richards RG, Alini M, Stoddart MJ (2014) Concise review: bone marrow-derived mesenchymal stem cells change phenotype following *in vitro* culture: implications for basic research and the clinic. *Stem Cells* **32**: 1713-1723.
- Bartosh TJ, Ylöstalo JH, Mohammadipoor A, Bazhanov N, Coble K, Claypool K, Lee RH, Choi H, Prockop DJ (2010) Aggregation of human mesenchymal stromal cells (MSCs) into 3D spheroids enhances their antiinflammatory properties. *Proc Natl Acad Sci U S A* **107**: 13724-13729.
- Bason C, Gallorini M, Berardi AC (2018) The Extracellular matrix, growth factors and morphogens in biomaterial design and tissue engineering. In: *Extracellular matrix for tissue engineering and biomaterials*. Editor Berardi AC, Springer Nature Switzerland AG, pp: 3-26.
- Beeton C, Bord S, Ireland D, Compston J (2006) Osteoclast formation and bone resorption are inhibited by megakaryocytes. *Bone* **39**: 985-990.
- Bianco P, Robey PG, Simmons PJ (2008) Mesenchymal stem cells: revisiting history, concepts, and assays. *Cell Stem Cell* **2**: 313-319.
- Bidarra SJ, Barrias CC, Barbosa MA, Soares R, Amédée J, Granja PL (2011) Phenotypic and proliferative modulation of human mesenchymal stem cells *via* crosstalk with endothelial cells. *Stem Cell Res* **7**: 186-197.
- Bignon A, Chouteau J, Chevalier J, Fantozzi G, Carret J-P, Chavassieux P, Boivin G, Melin M, Hartmann D (2003) Effect of micro- and macroporosity of bone substitutes on their mechanical properties and cellular response. *J Mater Sci Mater Med* **14**: 1089-1097.
- Biswas S, Li P, Wu H, Shafiquzzaman M, Murakami S, Schneider MD, Mishina Y, Li B, Li J (2018) BMPRIA is required for osteogenic differentiation and RANKL expression in adult bone marrow mesenchymal stromal cells. *Sci Rep* **8**: 8475. DOI: 10.1038/s41598-018-26820-8.
- Böhrnsen F, Schliephake H (2016) Supportive angiogenic and osteogenic differentiation of mesenchymal stromal cells and endothelial cells in monolayer and co-cultures. *Int J Oral Sci* **8**: 223-230.
- Bonnans C, Chou J, Werb Z (2014) Remodelling the extracellular matrix in development and disease. *Nat Rev Mol Cell Biol* **15**: 786-801.
- Bose S, Vahabzadeh S, Bandyopadhyay A (2013) Bone tissue engineering using 3D printing. *Mater Today* **16**: 496-504.
- Bosnakovski D, Mizuno M, Kim G, Takagi S, Okumura M, Fujinaga T (2006) Chondrogenic differentiation of bovine bone marrow mesenchymal stem cells (MSCs) in different hydrogels: influence of collagen type II extracellular matrix on MSC chondrogenesis. *Biotechnol Bioeng* **93**: 1152-1163.
- Bottaro DP, Liebmann-Vinson A, Heideran MA (2002) Molecular signaling in bioengineered tissue microenvironments. *Ann N Y Acad Sci* **961**: 143-153.
- Boulais PE, Frenette PS (2015) Making sense of hematopoietic stem cell niches. *Blood* **125**: 2621-2629.
- Breitbach M, Kimura K, Luis TC, Fuegemann CJ, Woll PS, Hesse M, Facchini R, Rieck S, Jobin K, Reinhardt J (2018) *In vivo* labeling by CD73 marks multipotent stromal cells and highlights endothelial heterogeneity in the bone marrow niche. *Cell Stem Cell* **22**: 262-276. e267.
- Bronckaers A, Hilkens P, Martens W, Gervois P, Ratajczak J, Struys T, Lambrechts I (2014) Mesenchymal stem/stromal cells as a pharmacological and therapeutic approach to accelerate angiogenesis. *Pharmacol Ther* **143**: 181-196.
- Caplan AI (1991) Mesenchymal stem cells. *J Orth Res* **9**: 641-650.
- Caplan AI (2017) Mesenchymal stem cells: time to change the name! *Stem Cells Transl Med* **6**: 1445-1451.
- Cappellen D, Luong-Nguyen N-H, Bongiovanni S, Grenet O, Wanke C, Susa M (2002) Transcriptional program of mouse osteoclast differentiation governed by the macrophage colony-stimulating factor and the ligand for the receptor activator of NF- κ B. *J Biol Chem* **277**: 21971-21982.
- Carlotti F, Zaldumbide A, Loomans CJ, van Rossenberg E, Engelse M, de Koning EJ, Hoeben RC (2010) Isolated human islets contain a distinct population of mesenchymal stem cells. *Islets* **2**: 164-173.
- Caron MM, Emans PJ, Coolsen MM, Voss L, Surtel DA, Cremers A, van Rhijn LW, Welting TJ (2012) Redifferentiation of dedifferentiated human articular chondrocytes: comparison of 2D and 3D cultures. *Osteoarthritis Cartilage* **20**: 1170-1178.
- Carter DR (1984) Mechanical loading histories and cortical bone remodeling. *Calcif Tissue Int* **36**: S19-S24.

- Celil AB, Campbell PG (2005) BMP-2 and insulin-like growth factor-I mediate Osterix (Osx) expression in human mesenchymal stem cells *via* the MAPK and protein kinase D signaling pathways. *J Biol Chem* **280**: 31353-31359.
- Chang J-C, Hsu S-h, Chen DC (2009) The promotion of chondrogenesis in adipose-derived adult stem cells by an RGD-chimeric protein in 3D alginate culture. *Biomaterials* **30**: 6265-6275.
- Chan JK, Glass GE, Ersek A, Freidin A, Williams GA, Gowers K, Espirito Santo AI, Jeffery R, Otto WR, Poulos R, Feldmann M, Rankin SM, Horwood NJ, Nanchahal J (2015) Low-dose TNF augments fracture healing in normal and osteoporotic bone by up-regulating the innate immune response. *EMBO Mol Med* **7**: 547-561.
- Chen CS (2008) Mechanotransduction – a field pulling together? *J Cell Sci* **121**: 3285-3292.
- Chen P-Y, Qin L, Baeyens N, Li G, Afolabi T, Budatha M, Tellides G, Schwartz MA, Simons M (2015) Endothelial-to-mesenchymal transition drives atherosclerosis progression. *J Clin Invest* **125**: 4514-4528.
- Chen X, Katakowski M, Li Y, Lu D, Wang L, Zhang L, Chen J, Xu Y, Gautam S, Mahmood A (2002) Human bone marrow stromal cell cultures conditioned by traumatic brain tissue extracts: growth factor production. *J Neurosci Res* **69**: 687-691.
- Cheng Q, Li X, Liu J, Ye Q, Chen Y, Tan S, Liu J (2017) Multiple myeloma-derived exosomes regulate the functions of mesenchymal stem cells partially *via* modulating miR-21 and miR-146a. *Stem Cells Int* **2017**: 9012152. DOI: 10.1155/2017/9012152.
- Cho D-I, Kim MR, Jeong H-y, Jeong HC, Jeong MH, Yoon SH, Kim YS, Ahn Y (2014) Mesenchymal stem cells reciprocally regulate the M1/M2 balance in mouse bone marrow-derived macrophages. *Exp Mol Med* **46**: e70. DOI: 10.1038/emmm.2013.135.
- Chowdhury R, Webber JP, Gurney M, Mason MD, Tabi Z, Clayton A (2015) Cancer exosomes trigger mesenchymal stem cell differentiation into pro-angiogenic and pro-invasive myofibroblasts. *Oncotarget* **6**: 715-731.
- Ciovacco WA, Cheng YH, Horowitz MC, Kacena MA (2010) Immature and mature megakaryocytes enhance osteoblast proliferation and inhibit osteoclast formation. *J Cell Biochem* **109**: 774-781.
- Cipriani P, Guiducci S, Miniati I, Cinelli M, Urbani S, Marrelli A, Dolo V, Pavan A, Saccardi R, Tyndall A (2007) Impairment of endothelial cell differentiation from bone marrow-derived mesenchymal stem cells: new insight into the pathogenesis of systemic sclerosis. *Arthritis Rheumatol* **56**: 1994-2004.
- Civini S, Jin P, Ren J, Sabatino M, Castiello L, Jin J, Wang H, Zhao Y, Marincola F, Stroncek D (2013) Leukemia cells induce changes in human bone marrow stromal cells. *J Transl Med* **11**: 298. DOI: 10.1186/1479-5876-11-298.
- Cottrill CP, Archer CW, Wolpert L (1987) Cell sorting and chondrogenic aggregate formation in micromass culture. *Dev Biol* **122**: 503-515.
- Cox TR, Erler JT (2011) Remodeling and homeostasis of the extracellular matrix: implications for fibrotic diseases and cancer. *Dis Model Mech* **4**: 165-178.
- Crapo PM, Gilbert TW, Badylak SF (2011) An overview of tissue and whole organ decellularization processes. *Biomaterials* **32**: 3233-3243.
- Crisan M, Dzierzak E (2016) The many faces of hematopoietic stem cell heterogeneity. *Development* **143**: 4571-4581.
- Crisan M, Yap S, Casteilla L, Chen C-W, Corselli M, Park TS, Andriolo G, Sun B, Zheng B, Zhang L, Norotte C, Teng P-N, Traas J, Schugar R, Deasy BM, Badylak S, Bühring H-J, Giacobino J-P, Lazzari L, Huard J, Péault B (2008) A perivascular origin for mesenchymal stem cells in multiple human organs. *Cell Stem Cell* **3**: 301-313.
- Csaki C, Matis U, Mobasheri A, Shakibaei M (2009) Co-culture of canine mesenchymal stem cells with primary bone-derived osteoblasts promotes osteogenic differentiation. *Histochem Cell Biol* **131**: 251-266.
- Curran JM, Chen R, Hunt JA (2006) The guidance of human mesenchymal stem cell differentiation *in vitro* by controlled modifications to the cell substrate. *Biomaterials* **27**: 4783-4793.
- D'Ippolito G, Diabira S, Howard GA, Roos BA, Schiller PC (2006) Low oxygen tension inhibits osteogenic differentiation and enhances stemness of human MIAMI cells. *Bone* **39**: 513-522.
- Dahlin RL, Meretoja VV, Ni M, Kasper FK, Mikos AG (2012) Design of a high-throughput flow perfusion bioreactor system for tissue engineering. *Tissue Eng Part C Methods* **18**: 817-820.
- Dalby MJ, Gadegaard N, Tare R, Andar A, Riehle MO, Herzyk P, Wilkinson CD, Oreffo RO (2007) The control of human mesenchymal cell differentiation using nanoscale symmetry and disorder. *Nat Mater* **6**: 997-1003.
- Datta N, Holtorf HL, Sikavitsas VI, Jansen JA, Mikos AG (2005) Effect of bone extracellular matrix synthesized *in vitro* on the osteoblastic differentiation of marrow stromal cells. *Biomaterials* **26**: 971-977.
- David V, Martin A, Lafage-Proust M-Hln, Malaval L, Peyroche S, Jones DB, Vico L, Guignandon A (2007) Mechanical loading down-regulates peroxisome proliferator-activated receptor γ in bone marrow stromal cells and favors osteoblastogenesis at the expense of adipogenesis. *Endocrinology* **148**: 2553-2562.
- de la Guardia RD, Lopez-Millan B, Lavoie JR, Bueno C, Castaño J, Gómez-Casares M, Vives S, Palomo L, Juan M, Delgado J (2017) Detailed characterization of mesenchymal stem/stromal cells from a large cohort of AML patients demonstrates a definitive link to treatment outcomes. *Stem Cell Rep* **8**: 1573-1586.
- De Luca L, Trino S, Laurenzana I, Simeon V, Calice G, Raimondo S, Podestà M, Santodirocco M, Di Mauro L, La Rocca F (2016) MiRNAs and piRNAs from bone marrow mesenchymal stem cell

extracellular vesicles induce cell survival and inhibit cell differentiation of cord blood hematopoietic stem cells: a new insight in transplantation. *Oncotarget* **7**: 6676-6692.

Deng X, Chen YX, Zhang X, Zhang JP, Yin C, Yue HY, Lin Y, Han ZG, Xie WF (2008) Hepatic stellate cells modulate the differentiation of bone marrow mesenchymal stem cells into hepatocyte-like cells. *J Cell Physiol* **217**: 138-144.

Dessi M, Borzacchiello A, Mohamed TH, Abdel-Fattah WI, Ambrosio L (2013) Novel biomimetic thermosensitive β -tricalcium phosphate/chitosan-based hydrogels for bone tissue engineering. *J Biomed Mater Res A* **101**: 2984-2993.

Devignes C-S, Aslan Y, Brenot A, Devillers A, Schepers K, Fabre S, Chou J, Casbon A-J, Werb Z, Provot S (2018) HIF signaling in osteoblast-lineage cells promotes systemic breast cancer growth and metastasis in mice. *Proc Natl Acad Sci U S A* **115**: E992-E1001.

Dhawan A, von Bonin M, Bray LJ, Freudenberg U, Pishali Bejestani E, Werner C, Hofbauer LC, Wobus M, Bornhäuser M (2016) Functional interference in the bone marrow microenvironment by disseminated breast cancer cells. *Stem Cells* **34**: 2224-2235.

Ding L, Morrison SJ (2013) Haematopoietic stem cells and early lymphoid progenitors occupy distinct bone marrow niches. *Nature* **495**: 231-235.

Dominici M, Le Blanc K, Mueller I, Slaper-Cortenbach I, Marini F, Krause D, Deans R, Keating A, Prockop D, Horwitz E (2006) Minimal criteria for defining multipotent mesenchymal stromal cells. The International Society for Cellular Therapy position statement. *Cytotherapy* **8**: 315-317.

Doron B, Handu M, Kurre P (2018) Concise review: adaptation of the bone marrow stroma in hematopoietic malignancies: current concepts and models. *Stem Cells* **36**: 304-312.

Du P, Suhaeri M, Subbiah R, Van SY, Park J, Kim SH, Park K, Lee K (2016) Elasticity modulation of fibroblast-derived matrix for endothelial cell vascular morphogenesis and mesenchymal stem cell differentiation. *Tissue Eng Part A* **22**: 415-426.

Duncan R, Turner C (1995) Mechanotransduction and the functional response of bone to mechanical strain. *Calcif Tissue Int* **57**: 344-358.

Duttenhoefer F, Lara de Freitas R, Loibl M, Bittermann G, Geoff Richards R, Alini M, Verrier S (2015) Endothelial progenitor cell fraction contained in bone marrow-derived mesenchymal stem cell populations impairs osteogenic differentiation. *BioMed Res Int* **2015**: 659542. DOI: 10.1155/2015/659542.

Duttenhoefer F, Lara de Freitas R, Meury T, Loibl M, Benneker LM, Hermann M, Richards R, Alini M, Verrier S (2013) 3D scaffolds co-seeded with human endothelial progenitor and mesenchymal stem cells: evidence of prevascularisation within 7 days. *Eur Cell Mater* **26**: 64-65.

Eibes G, dos Santos F, Andrade PZ, Boura JS, Abecasis MM, da Silva CL, Cabral JM (2010) Maximizing the *ex vivo* expansion of human

mesenchymal stem cells using a microcarrier-based stirred culture system. *J Biotechnol* **146**: 194-197.

Engler AJ, Sen S, Sweeney HL, Discher DE (2006) Matrix elasticity directs stem cell lineage specification. *Cell* **126**: 677-689.

Erba BG, Gruppi C, Corada M, Pisati F, Rosti V, Villeval J-L, Vannucchi AM, Barosi G, Balduini A, Dejana E (2017) Endothelial-to-mesenchymal transition in bone marrow and spleen of primary myelofibrosis. *Am J Pathol* **187**: 1879-1892.

Fehrer C, Brunauer R, Laschober G, Unterluggauer H, Reitingner S, Kloss F, Güllü C, Gassner R, Lepperdinger G (2007) Reduced oxygen tension attenuates differentiation capacity of human mesenchymal stem cells and prolongs their lifespan. *Aging Cell* **6**: 745-757.

Ferrari G, Angelis D, Coletta M, Paolucci E, Stornaiuolo A, Cossu G, Mavilio F (1998) Muscle regeneration by bone marrow-derived myogenic progenitors. *Science* **279**: 1528-1530.

Fink T, Abildtrup L, Fogd K, Abdallah BM, Kassem M, Ebbesen P, Zachar V (2004) Induction of adipocyte-like phenotype in human mesenchymal stem cells by hypoxia. *Stem Cells* **22**: 1346-1355.

Friedenstein A, Deriglasova U, Kulagina N, Panasuk A, Rudakowa S, Luria E, Ruadkow I (1974) Precursors for fibroblasts in different populations of hematopoietic cells as detected by the *in vitro* colony assay method. *Exp Hematol* **2**: 83-92.

Fukuchi Y, Nakajima H, Sugiyama D, Hirose I, Kitamura T, Tsuji K (2004) Human placenta-derived cells have mesenchymal stem/progenitor cell potential. *Stem Cells* **22**: 649-658.

Galleu A, Riffo-Vasquez Y, Trento C, Lomas C, Dolcetti L, Cheung TS, von Bonin M, Barbieri L, Halai K, Ward S (2017) Apoptosis in mesenchymal stromal cells induces *in vivo* recipient-mediated immunomodulation. *Sci Transl Med* **9**. DOI: 10.1126/scitranslmed.aam7828.

Gamblin A-L, Brennan MA, Renaud A, Yagita H, Lézet F, Heymann D, Trichet V, Layrolle P (2014) Bone tissue formation with human mesenchymal stem cells and biphasic calcium phosphate ceramics: the local implication of osteoclasts and macrophages. *Biomaterials* **35**: 9660-9667.

Garimella R, Kacena MA, Tague SE, Wang J, Horowitz MC, Anderson HC (2007) Expression of bone morphogenetic proteins and their receptors in the bone marrow megakaryocytes of GATA-1low mice: a possible role in osteosclerosis. *J Histochem Cytochem* **55**: 745-752.

Gilpin A, Yang Y (2017) Decellularization strategies for regenerative medicine: from processing techniques to applications. *BioMed research international* **2017**: 9831534. DOI: 10.1155/2017/9831534

Gladman AS, Matsumoto EA, Nuzzo RG, Mahadevan L, Lewis JA (2016) Biomimetic 4D printing. *Nat Mater* **15**: 413-418.

Glueck M, Gardner O, Czekanska E, Alini M, Stoddart MJ, Salzman GM, Schmal H (2015) Induction of osteogenic differentiation in human

mesenchymal stem cells by crosstalk with osteoblasts. *Biores Open Access* 4: 121-130.

Gomariz A, Helbling PM, Isringhausen S, Suessbier U, Becker A, Boss A, Nagasawa T, Paul G, Goksel O, Székely G, Stoma S, Nørrelykke SF, Manz MG, Nombela-Arrieta C (2018) Quantitative spatial analysis of haematopoiesis-regulating stromal cells in the bone marrow microenvironment by 3D microscopy. *Nat Commun* 9: 2532. DOI: 10.1038/s41467-018-04770-z.

Gomez Perdiguero E, Klapproth K, Schulz C, Busch K, Azzoni E, Crozet L, Garner H, Trouillet C, de Bruijn MF, Geissmann F, Rodewald HR (2015) Tissue-resident macrophages originate from yolk-sac-derived erythro-myeloid progenitors. *Nature* 518: 547-551.

Gong M, Yu B, Wang J, Wang Y, Liu M, Paul C, Millard RW, Xiao D-S, Ashraf M, Xu M (2017) Mesenchymal stem cells release exosomes that transfer miRNAs to endothelial cells and promote angiogenesis. *Oncotarget* 8: 4 45200-45212.

Gordon JA, Lisle JW, Alman BA, Lian JB (2014) Disruption of crosstalk between mesenchymal stromal and tumor cells in bone marrow as a therapeutic target to prevent metastatic bone disease. *J Cell Physiol* 229: 1884-1886.

Gronthos S, Mankani M, Brahimi J, Robey PG, Shi S (2000) Postnatal human dental pulp stem cells (DPSCs) *in vitro* and *in vivo*. *Proc Natl Acad Sci U S A* 97: 13625-13630.

Guibentif C, Rönn RE, Böiers C, Lang S, Saxena S, Soneji S, Enver T, Karlsson G, Woods N-B (2017) Single-cell analysis identifies distinct stages of human endothelial-to-hematopoietic transition. *Cell Rep* 19: 10-19.

Guimarães-Camboa N, Cattaneo P, Sun Y, Moore-Morris T, Gu Y, Dalton ND, Rockenstein E, Masliah E, Peterson KL, Stallcup WB (2017) Pericytes of multiple organs do not behave as mesenchymal stem cells *in vivo*. *Cell Stem Cell* 20: 345-359.

Gurkan UA, El Assal R, Yildiz SE, Sung Y, Trachtenberg AJ, Kuo WP, Demirci U (2014) Engineering anisotropic biomimetic fibrocartilage microenvironment by bioprinting mesenchymal stem cells in nanoliter gel droplets. *Mol Pharm* 11: 2151-2159.

Hammoud M, Vlaski M, Duchez P, Chevalerey J, Lafarge X, Boiron JM, Praloran V, Brunet de la Grange P, Ivanovic Z (2012) Combination of low O₂ concentration and mesenchymal stromal cells during culture of cord blood CD34+ cells improves the maintenance and proliferative capacity of hematopoietic stem cells. *J Cell Physiol* 227: 2750-2758.

Hashimoto K, Ochi H, Sunamura S, Kosaka N, Mabuchi Y, Fukuda T, Yao K, Kanda H, Ae K, Okawa A (2018) Cancer-secreted hsa-miR-940 induces an osteoblastic phenotype in the bone metastatic microenvironment *via* targeting ARHGAP1 and FAM134A. *Proc Natl Acad Sci U S A* 115: 2204-2209.

Hass R, Kasper C, Böhm S, Jacobs R (2011) Different populations and sources of human mesenchymal stem cells (MSC): a comparison of adult and neonatal tissue-derived MSC. *Cell Commun Signal* 9: 12. DOI: 10.1186/1478-811X-9-12.

Henriksen K, Sørensen MG, Nielsen RH, Gram J, Schaller S, Dziegiel MH, Everts V, Bollerslev J, Karsdal MA (2006) Degradation of the organic phase of bone by osteoclasts: a secondary role for lysosomal acidification. *J Bone Miner Res* 21: 58-66.

Hermida-Gómez T, Fuentes-Boquete I, Gimeno-Longas MJ, Muiños-López E, Díaz-Prado S, BLANCO FJ (2011) Quantification of cells expressing mesenchymal stem cell markers in healthy and osteoarthritic synovial membranes. *J Rheumatol* 38: 339-349.

Herrmann M, Binder A, Menzel U, Zeiter S, Alini M, Verrier S (2014) CD34/CD133 enriched bone marrow progenitor cells promote neovascularization of tissue engineered constructs *in vivo*. *Stem Cell Res* 13: 465-477.

Herrmann M, Jakob F (2019) Bone marrow niches for skeletal progenitor cells and their inhabitants in health and disease. *Curr Stem Cell Res Ther*. DOI: 10.2174/1574888X14666190123161447.

Hing K, Annaz B, Saeed S, Revell P, Buckland T (2005) Microporosity enhances bioactivity of synthetic bone graft substitutes. *J Mater Sci Mater Med* 16: 467-475.

Hoch AJ, Mittal V, Mitra D, Vollmer N, Zikry CA, Leach JK (2016) Cell-secreted matrices perpetuate the bone-forming phenotype of differentiated mesenchymal stem cells. *Biomaterials* 74: 178-187.

Horwitz E, Le Blanc K, Dominici M, Mueller I, Slaper-Cortenbach I, Marini FC, Deans R, Krause D, Keating A (2005) Clarification of the nomenclature for MSC: The International Society for Cellular Therapy position statement. *Cytherapy* 7: 393-395.

Hoshida T, Lu H, Kawazoe N, Chen G (2010) Decellularized matrices for tissue engineering. *Expert Opin Biol Ther* 10: 1717-1728.

Hosseinkhani H, Hosseinkhani M, Tian F, Kobayashi H, Tabata Y (2006) Ectopic bone formation in collagen sponge self-assembled peptide-amphiphile nanofibers hybrid scaffold in a perfusion culture bioreactor. *Biomaterials* 27: 5089-5098.

Hu J, Zhang G, Liu S (2012) Enzyme-responsive polymeric assemblies, nanoparticles and hydrogels. *Chem Soc Rev* 41: 5933-5949.

Hu X, Yu SP, Fraser JL, Lu Z, Ogle ME, Wang J-A, Wei L (2008) Transplantation of hypoxia-preconditioned mesenchymal stem cells improves infarcted heart function *via* enhanced survival of implanted cells and angiogenesis. *J Thorac Cardiovasc Surg* 135: 799-808.

Huebsch N, Lippens E, Lee K, Mehta M, Koshy ST, Darnell MC, Desai R, Madl CM, Xu M, Zhao X (2015) Matrix elasticity of void-forming hydrogels controls transplanted stem cell-mediated bone formation. *Nat Mater* 14: 1269-1277.

- Indrawattana N, Chen G, Tadokoro M, Shann LH, Ohgushi H, Tateishi T, Tanaka J, Bunyaratvej A (2004) Growth factor combination for chondrogenic induction from human mesenchymal stem cell. *Biochem Biophys Res Commun* **320**: 914-919.
- Itkin T, Gur-Cohen S, Spencer JA, Schajnovitz A, Ramasamy SK, Kusumbe AP, Ledergor G, Jung Y, Milo I, Poulos MG (2016) Distinct bone marrow blood vessels differentially regulate haematopoiesis. *Nature* **532**: 323-328.
- Jalali S, del Pozo MA, Chen K-D, Miao H, Li Y-S, Schwartz MA, Shyy JY-J, Chien S (2001) Integrin-mediated mechanotransduction requires its dynamic interaction with specific extracellular matrix (ECM) ligands. *Proc Natl Acad Sci U S A* **98**: 1042-1046.
- Johnstone B, Hering TM, Caplan AI, Goldberg VM, Yoo JU (1998) *In vitro* chondrogenesis of bone marrow-derived mesenchymal progenitor cells. *Exp Cell Res* **238**: 265-272.
- Jung Y, Song J, Shiozawa Y, Wang J, Wang Z, Williams B, Havens A, Schneider A, Ge C, Franceschi RT (2008) Hematopoietic stem cells regulate mesenchymal stromal cell induction into osteoblasts thereby participating in the formation of the stem cell niche. *Stem Cells* **26**: 2042-2051.
- Kacena MA, Gundberg CM, Horowitz MC (2006) A reciprocal regulatory interaction between megakaryocytes, bone cells, and hematopoietic stem cells. *Bone* **39**: 978-984.
- Kaliva M, Chatziniokolaidou M, Vamvakaki M (2017) Applications of smart multifunctional tissue engineering scaffolds. In: *Smart materials for tissue engineering*. Editor Wang Q, Royal Society of Chemistry, pp: 1-38.
- Kanichai M, Ferguson D, Prendergast PJ, Campbell VA (2008) Hypoxia promotes chondrogenesis in rat mesenchymal stem cells: a role for AKT and hypoxia-inducible factor (HIF)-1 α . *J Cell Physiol* **216**: 708-715.
- Keane T, Saldin L, Badylak S (2016) Decellularization of mammalian tissues: preparing extracellular matrix bioscaffolds. In: *Characterisation and design of tissue scaffolds*. Elsevier, pp: 75-103.
- Khoo ZX, Teoh JEM, Liu Y, Chua CK, Yang S, An J, Leong KF, Yeong WY (2015) 3D printing of smart materials: A review on recent progresses in 4D printing. *Virtual Phys Prototyp* **10**: 103-122.
- Kim JH, Kim K, Kim I, Seong S, Kim N (2018) c-Src-dependent and -independent functions of Matk in osteoclasts and osteoblasts. *J Immunol* **200**: 2455-2463.
- Kim JH, Kim K, Youn BU, Lee J, Kim I, Shin H-I, Akiyama H, Choi Y, Kim N (2014) Kruppel-like factor 4 attenuates osteoblast formation, function, and cross talk with osteoclasts. *J Cell Biol* **204**: 1063-1074.
- King JA, Miller WM (2007) Bioreactor development for stem cell expansion and controlled differentiation. *Curr Opin Chem Biol* **11**: 394-398.
- Klein-Nulend J, Bakker AD, Bacabac RG, Vatsa A, Weinbaum S (2013) Mechanosensation and transduction in osteocytes. *Bone* **54**: 182-190.
- Kleinhans C, Mohan RR, Vacun G, Schwarz T, Haller B, Sun Y, Kahlig A, Kluger P, Finne-Wistrand A, Walles H (2015) A perfusion bioreactor system efficiently generates cell-loaded bone substitute materials for addressing critical size bone defects. *Biotechnol J* **10**: 1727-1738.
- Kratchmarova I, Blagoev B, Haack-Sorensen M, Kassem M, Mann M (2005) Mechanism of divergent growth factor effects in mesenchymal stem cell differentiation. *Science* **308**: 1472-1477.
- Kuboki T, Kidoaki S (2016) Fabrication of elasticity-tunable gelatinous gel for mesenchymal stem cell culture. In: *Mesenchymal stem cells: methods and protocols*. Humana Press, New York, NY, pp 425-441.
- Kusumbe AP, Ramasamy SK, Itkin T, Mäe MA, Langen UH, Betsholtz C, Lapidot T, Adams RH (2016) Age-dependent modulation of vascular niches for haematopoietic stem cells. *Nature* **532**: 380-384.
- Langen UH, Pitulescu ME, Kim JM, Enriquez-Gasca R, Sivaraj KK, Kusumbe AP, Singh A, Di Russo J, Bixel MG, Zhou B, Sorokin L, Vaquerizas JM, Adams RH (2017) Cell-matrix signals specify bone endothelial cells during developmental osteogenesis. *Nat Cell Biol* **19**: 189-201.
- Lee J, Li M, Milwid J, Dunham J, Vinegoni C, Gorbatov R, Iwamoto Y, Wang F, Shen K, Hatfield K (2012) Implantable microenvironments to attract hematopoietic stem/cancer cells. *Proc Natl Acad Sci U S A* **109**: 19638-19643.
- Lee KD, Kuo TKC, Whang-Peng J, Chung YF, Lin CT, Chou SH, Chen JR, Chen YP, Lee OKS (2004) *In vitro* hepatic differentiation of human mesenchymal stem cells. *Hepatology* **40**: 1275-1284.
- Levato R, Visser J, Planell JA, Engel E, Malda J, Mateos-Timoneda MA (2014) Biofabrication of tissue constructs by 3D bioprinting of cell-laden microcarriers. *Biofabrication* **6**: 035020. DOI: 10.1088/1758-5082/6/3/035020.
- Li J-w, Guo X-l, He C-l, Tuo Y-h, Wang Z, Wen J, Jin D (2011) *In vitro* chondrogenesis of the goat bone marrow mesenchymal stem cells directed by chondrocytes in monolayer and 3-dimensional indirect co-culture system. *Chin Med J* **124**: 3080-3086.
- Li L, Xie T (2005) Stem cell niche: structure and function. *Annu Rev Cell Dev Biol* **21**: 605-631.
- Lin L, Du L, Cao K, Huang Y, Yu P, Zhang L, Li F, Wang Y, Shi Y (2016) Tumour cell-derived exosomes endow mesenchymal stromal cells with tumour-promotion capabilities. *Oncogene* **35**: 6038-6042.
- Lin R-Z, Moreno-Luna R, Li D, Jaminet S-C, Greene AK, Melero-Martin JM (2014) Human endothelial colony-forming cells serve as trophic mediators for mesenchymal stem cell engraftment *via* paracrine signaling. *Proc Natl Acad Sci U S A* **111**: 10137-10142.
- Liu H, Liu S, Li Y, Wang X, Xue W, Ge G, Luo X (2012) The role of SDF-1-CXCR4/CXCR7 axis in the therapeutic effects of hypoxia-preconditioned mesenchymal stem cells for renal ischemia/reperfusion injury. *PLoS One* **7**: e34608. DOI: 10.1371/journal.pone.0034608.

- Loh QL, Choong C (2013) Three-dimensional scaffolds for tissue engineering applications: role of porosity and pore size. *Tissue Eng Part B Rev* **19**: 485-502.
- Loibl M, Binder A, Herrmann M, Dutenhoefer F, Richards RG, Nerlich M, Alini M, Verrier S (2014) Direct cell-cell contact between mesenchymal stem cells and endothelial progenitor cells induces a pericyte-like phenotype *in vitro*. *BioMed Res Int* **2014**: 395781. DOI: 10.1155/2014/395781.
- Lu P, Weaver VM, Werb Z (2012) The extracellular matrix: a dynamic niche in cancer progression. *J Cell Biol* **196**: 395-406.
- Lund T, Kramer A, Taisto M, Blake A, Lehrke M (2017) Decellularized bone marrow reveals a novel niche protein that modulate adhesion. *Exp Hematol* **53**: S81. DOI: 10.1016/j.exphem.2017.06.177.
- Luo J, Tang M, Huang J, He B-C, Gao J-L, Chen L, Zuo G-W, Zhang W, Luo Q, Shi Q (2010) TGF β /BMP type I receptors ALK1 and ALK2 are essential for BMP9-induced osteogenic signaling in mesenchymal stem cells. *J Biol Chem* **285**: 29588-29598.
- Luo Q, Song G, Song Y, Xu B, Qin J, Shi Y (2009) Indirect co-culture with tenocytes promotes proliferation and mRNA expression of tendon/ligament related genes in rat bone marrow mesenchymal stem cells. *Cytotechnology* **61**: 1-10.
- Lutolf M, Hubbell J (2005) Synthetic biomaterials as instructive extracellular microenvironments for morphogenesis in tissue engineering. *Nat Biotechnol* **23**: 47-55.
- Lutolf M, Lauer-Fields J, Schmoekel H, Metters AT, Weber F, Fields G, Hubbell JA (2003) Synthetic matrix metalloproteinase-sensitive hydrogels for the conduction of tissue regeneration: engineering cell-invasion characteristics. *Proc Natl Acad Sci U S A* **100**: 5413-5418.
- Lymperi S, Ersek A, Ferraro F, Dazzi F, Horwood NJ (2011) Inhibition of osteoclast function reduces hematopoietic stem cell numbers *in vivo*. *Blood* **117**: 1540-1549.
- Madl CM, Mehta M, Duda GN, Heilshorn SC, Mooney DJ (2014) Presentation of BMP-2 mimicking peptides in 3D hydrogels directs cell fate commitment in osteoblasts and mesenchymal stem cells. *Biomacromolecules* **15**: 445-455.
- Mahrouf-Yorgov M, Augeul L, Da Silva CC, Jourdan M, Rigolet M, Manin S, Ferrera R, Ovize M, Henry A, Guguin A (2017) Mesenchymal stem cells sense mitochondria released from damaged cells as danger signals to activate their rescue properties. *Cell Death Differ* **24**: 1224-1238.
- Maia FR, Lourenco AH, Granja PL, Goncalves RM, Barrias CC (2014) Effect of cell density on mesenchymal stem cells aggregation in RGD-alginate 3D matrices under osteoinductive conditions. *Macromol Biosci* **14**: 759-771.
- Malda J, Visser J, Melchels FP, Jüngst T, Hennink WE, Dhert WJ, Groll J, Hutmacher DW (2013) 25th anniversary article: engineering hydrogels for biofabrication. *Adv Mater* **25**: 5011-5028.
- Maldonado M, Nam J (2013) The role of changes in extracellular matrix of cartilage in the presence of inflammation on the pathology of osteoarthritis. *BioMed Res Int* **2013**: 284873. DOI: 10.1155/2013/284873.
- Manduca P, Castagnino A, Lombardini D, Marchisio S, Soldano S, Ulivi V, Zanotti S, Garbi C, Ferrari N, Palmieri D (2009) Role of MT1-MMP in the osteogenic differentiation. *Bone* **44**: 251-265.
- Mansour A, Abou-Ezzi G, Sitnicka E, Jacobsen SEW, Wakkach A, Blin-Wakkach C (2012) Osteoclasts promote the formation of hematopoietic stem cell niches in the bone marrow. *J Exp Med* **209**: 537-549.
- Marfy-Smith SJ, Clarkin CE (2017) Are mesenchymal stem cells so bloody great after all? *Stem Cells Transl Med* **6**: 3-6.
- Marturano-Kruik A, Nava MM, Yeager K, Chramiec A, Hao L, Robinson S, Guo E, Raimondi MT, Vunjak-Novakovic G (2018) Human bone perivascular niche-on-a-chip for studying metastatic colonization. *Proc Natl Acad Sci U S A* **115**: 1256-1261.
- Matsumoto T, Takami T, Sakaida I (2016) Cell transplantation as a non-invasive strategy for treating liver fibrosis. *Expert Rev Gastroenterol Hepatol* **10**: 639-648.
- McCoy RJ, O'Brien FJ (2010) Influence of shear stress in perfusion bioreactor cultures for the development of three-dimensional bone tissue constructs: a review. *Tissue Eng Part B Rev* **16**: 587-601.
- McMurray RJ (2011) Nanoscale surfaces for the long-term maintenance of mesenchymal stem cell phenotype and multipotency. *Nat Mater* **10**: 637-644.
- McNamara LE, McMurray RJ, Biggs MJ, Kantawong F, Oreffo RO, Dalby MJ (2010) Nanotopographical control of stem cell differentiation. *J Tissue Eng* **2010**: 120623. DOI: 10.4061/2010/120623.
- Medici D, Olsen BR (2012) The role of endothelial-mesenchymal transition in heterotopic ossification. *J Bone Miner Res* **27**: 1619-1622.
- Méndez-Ferrer S, Michurina TV, Ferraro F, Mazloom AR, MacArthur BD, Lira SA, Scadden DT, Ma'ayan A, Enikolopov GN, Frenette PS (2010) Mesenchymal and haematopoietic stem cells form a unique bone marrow niche. *Nature* **466**: 829-834.
- Menon LG, Picinich S, Koneru R, Gao H, Lin SY, Koneru M, Mayer-Kuckuk P, Glod J, Banerjee D (2007) Differential gene expression associated with migration of mesenchymal stem cells to conditioned medium from tumor cells or bone marrow cells. *Stem Cells* **25**: 520-528.
- Muraoka T, Koh CY, Cui H, Stupp SI (2009) Light-triggered bioactivity in three dimensions. *Angew Chem* **121**: 6060-6063.
- Nakamura Y, Arai F, Iwasaki H, Hosokawa K, Kobayashi I, Gomei Y, Matsumoto Y, Yoshihara H, Suda T (2010) Isolation and characterization of endosteal niche cell populations that regulate hematopoietic stem cells. *Blood* **116**: 1422-1432.
- Nicolaidou V, Wong MM, Redpath AN, Ersek A, Baban DF, Williams LM, Cope AP, Horwood NJ

- (2012) Monocytes induce STAT3 activation in human mesenchymal stem cells to promote osteoblast formation. *PLoS One* 7: e39871. DOI: 10.1371/journal.pone.0039871.
- Nishi M, Matsumoto R, Dong J, Uemura T (2013) Engineered bone tissue associated with vascularization utilizing a rotating wall vessel bioreactor. *J Biomed Mater Res A* 101: 421-427.
- Nyberg E, Rindone A, Dorafshar A, Grayson WL (2017) Comparison of 3D-printed poly-ε-caprolactone scaffolds functionalized with tricalcium phosphate, hydroxyapatite, bio-oss, or decellularized bone matrix. *Tissue Eng Part A* 23: 503-514.
- O'Brien FJ (2011) Biomaterials & scaffolds for tissue engineering. *Mater Today* 14: 88-95.
- Oh S, Brammer KS, Li YJ, Teng D, Engler AJ, Chien S, Jin S (2009) Stem cell fate dictated solely by altered nanotube dimension. *Proc Natl Acad Sci U S A* 106: 2130-2135.
- Ono M, Kosaka N, Tominaga N, Yoshioka Y, Takeshita F, Takahashi R-u, Yoshida M, Tsuda H, Tamura K, Ochiya T (2014) Exosomes from bone marrow mesenchymal stem cells contain a microRNA that promotes dormancy in metastatic breast cancer cells. *Sci Signal* 7: ra63. DOI: 10.1126/scisignal.2005231.
- Oshita K, Yamaoka K, Udagawa N, Fukuyo S, Sonomoto K, Maeshima K, Kurihara R, Nakano K, Saito K, Okada Y (2011) Human mesenchymal stem cells inhibit osteoclastogenesis through osteoprotegerin production. *Arthritis Rheumatol* 63: 1658-1667.
- Otsu K, Das S, Houser SD, Quadri SK, Bhattacharya S, Bhattacharya J (2009) Concentration-dependent inhibition of angiogenesis by mesenchymal stem cells. *Blood* 113: 4197-4205.
- Owen M (1988) Marrow stromal stem cells. *J Cell Sci* 1988: 63-76.
- Park JC, Kim JM, Jung IH, Kim JC, Choi SH, Cho KS, Kim CS (2011) Isolation and characterization of human periodontal ligament (PDL) stem cells (PDLSCs) from the inflamed PDL tissue: *in vitro* and *in vivo* evaluations. *J Clin Periodontol* 38: 721-731.
- Park K-H, Kim H, Moon S, Na K (2009) Bone morphogenic protein-2 (BMP-2) loaded nanoparticles mixed with human mesenchymal stem cell in fibrin hydrogel for bone tissue engineering. *J Biosci Bioeng* 108: 530-537.
- Park SJ, Lee E-J, Kim Y-H, Shin J-E, Kang Y-H (2014) Inhibitory effects of gossypin on RANKL-induced osteoclast differentiation and bone resorption in murine macrophages (LB364). *FASEB J* 28: LB364.
- Peired AJ, Sisti A, Romagnani P (2016) Mesenchymal stem cell-based therapy for kidney disease: a review of clinical evidence. *Stem Cells Int* 2016: 4798639.
- Pek YS, Wan AC, Ying JY (2010) The effect of matrix stiffness on mesenchymal stem cell differentiation in a 3D thixotropic gel. *Biomaterials* 31: 385-391.
- Pelaez D, Arita N, Cheung HS (2012) Extracellular signal-regulated kinase (ERK) dictates osteogenic and/or chondrogenic lineage commitment of mesenchymal stem cells under dynamic compression. *Biochem Biophys Res Commun* 417: 1286-1291.
- Pereira RF, O'Hara MD, Laptev AV, Halford KW, Pollard MD, Class R, Simon D, Livezey K, Prockop DJ (1998) Marrow stromal cells as a source of progenitor cells for nonhematopoietic tissues in transgenic mice with a phenotype of osteogenesis imperfecta. *Proc Natl Acad Sci U S A* 95: 1142-1147.
- Phillippi JA, Miller E, Weiss L, Huard J, Waggoner A, Campbell P (2008) Microenvironments engineered by inkjet bioprinting spatially direct adult stem cells toward muscle- and bone-like subpopulations. *Stem Cells* 26: 127-134.
- Phillips JE, Petrie TA, Creighton FP, García AJ (2010) Human mesenchymal stem cell differentiation on self-assembled monolayers presenting different surface chemistries. *Acta Biomater* 6: 12-20.
- Phinney DG, Prockop DJ (2007) Concise review: mesenchymal stem/multipotent stromal cells: the state of transdifferentiation and modes of tissue repair – current views. *Stem Cells* 25: 2896-2902.
- Pina S, Oliveira JM, Reis RL (2016) Biomimetic strategies to engineer mineralized human tissues. In: *Handbook of bioceramics and biocomposites* (Antoniac IV, ed), Springer International Publishing, Cham, pp 503-519.
- Pittenger MF, Mackay AM, Beck SC, Jaiswal RK, Douglas R, Mosca JD, Moorman MA, Simonetti DW, Craig S, Marshak DR (1999) Multilineage potential of adult human mesenchymal stem cells. *Science* 284: 143-147.
- Plotnikov E, Khryapenkova T, Vasileva A, Marey M, Galkina S, Isaev N, Sheval E, Polyakov V, Sukhikh G, Zorov D (2008) Cell-to-cell cross-talk between mesenchymal stem cells and cardiomyocytes in coculture. *J Cell Mol Med* 12: 1622-1631.
- Porter B, Zauel R, Stockman H, Guldborg R, Fyhrie D (2005) 3-D computational modeling of media flow through scaffolds in a perfusion bioreactor. *J Biomech* 38: 543-549.
- Potapova IA, Brink PR, Cohen IS, Doronin SV (2008) Culturing of human mesenchymal stem cells as three-dimensional aggregates induces functional expression of CXCR4 that regulates adhesion to endothelial cells. *J Biol Chem* 283: 13100-13107.
- Prager P, Kunz M, Ebert R, Klein-Hitpass L, Sieker J, Barthel T, Jakob F, Konrads C, Steinert A (2018) Mesenchymal stem cells isolated from the anterior cruciate ligament: characterization and comparison of cells from young and old donors. *Knee Surg Relat Res* 30: 193-205.
- Prockop DJ, Oh JY (2012) Mesenchymal stem/stromal cells (MSCs): role as guardians of inflammation. *Mol Ther* 20: 14-20.
- Qian L, Saltzman WM (2004) Improving the expansion and neuronal differentiation of mesenchymal stem cells through culture surface modification. *Biomaterials* 25: 1331-1337.
- Qin Y, Zhang C (2017) Endothelial progenitor cell-derived extracellular vesicle-mediated cell-to-cell

communication regulates the proliferation and osteoblastic differentiation of bone mesenchymal stromal cells. *Mol Med Rep* **16**: 7018-7024.

Raic A, Rödling L, Kalbacher H, Lee-Thedieck C (2014) Biomimetic macroporous PEG hydrogels as 3D scaffolds for the multiplication of human hematopoietic stem and progenitor cells. *Biomaterials* **35**: 929-940.

Raggatt LJ, Wullschlegel ME, Alexander KA, Wu AC, Millard SM, Kaur S, Maugham ML, Gregory LS, Steck R, Pettit AR (2014) Fracture healing via periosteal callus formation requires macrophages for both initiation and progression of early endochondral ossification. *Am J Pathol* **184**: 3192-3204.

Raicevic G, Najar M, Stamatopoulos B, De Bruyn C, Meuleman N, Bron D, Toungouz M, Lagneaux L (2011) The source of human mesenchymal stromal cells influences their TLR profile as well as their functional properties. *Cell Immunol* **270**: 207-216.

Ramasamy SK, Kusumbe AP, Itkin T, Gur-Cohen S, Lapidot T, Adams RH (2016) Regulation of hematopoiesis and osteogenesis by blood vessel-derived signals. *Annu Rev Cell Dev Biol* **32**: 649-675.

Ranade SS, Syeda R, Patapoutian A (2015) Mechanically activated ion channels. *Neuron* **87**: 1162-1179.

Rao PS, Martinez JS, Keller III TC (2014) Decellularized ECM effects on human mesenchymal stem cell stemness and differentiation. *Differentiation* **88**: 131-143.

Ribeiro C, Correia V, Martins P, Gama F, Lanceros-Mendez S (2016) Proving the suitability of magnetoelectric stimuli for tissue engineering applications. *Colloids Surf B Biointerfaces* **140**: 430-436.

Robey P (2017) "Mesenchymal stem cells": fact or fiction, and implications in their therapeutic use. *F1000 Res* **6**. pii: F1000 Faculty Rev-524. DOI: 10.12688/f1000research.10955.1.

Robins JC, Akeno N, Mukherjee A, Dalal RR, Aronow BJ, Koopman P, Clemens TL (2005) Hypoxia induces chondrocyte-specific gene expression in mesenchymal cells in association with transcriptional activation of Sox9. *Bone* **37**: 313-322.

Roccaro AM, Sacco A, Purschke WG, Moschetta M, Buchner K, Maasch C, Zboralski D, Zöllner S, Vonnhoff S, Mishima Y (2014) SDF-1 inhibition targets the bone marrow niche for cancer therapy. *Cell Rep* **9**: 118-128.

Rojo L, Gharibi B, McLister R, Meenan BJ, Deb S (2016) Self-assembled monolayers of alendronate on Ti6Al4V alloy surfaces enhance osteogenesis in mesenchymal stem cells. *Sci Rep* **6**: 30548. DOI: 10.1038/srep30548.

Rosenkranz K, Kumbruch S, Lebermann K, Marschner K, Jensen A, Dermietzel R, Meier C (2010) The chemokine SDF-1/CXCL12 contributes to the 'homing' of umbilical cord blood cells to a hypoxic-ischemic lesion in the rat brain. *J Neurosci Res* **88**: 1223-1233.

Rosnagl S, Ghura H, Groth C, Altröck E, Jakob F, Schott S, Wimberger P, Link T, Kuhlmann JD, Stenzl A (2018) A subpopulation of stromal cells controls cancer cell homing to the bone marrow. *Cancer Res* **78**: 129-142.

Roy D, Brooks WL, Sumerlin BS (2013) New directions in thermoresponsive polymers. *Chem Soc Rev* **42**: 7214-7243.

Rozario T, DeSimone DW (2010) The extracellular matrix in development and morphogenesis: a dynamic view. *Dev Biol* **341**: 126-140.

Russell WMS, Burch RL, Hume CW (1959) The principles of humane experimental technique. Johns Hopkins University, Baltimore, MD, USA.

Sacchetti B, Funari A, Michienzi S, Di Cesare S, Piersanti S, Saggio I, Tagliafico E, Ferrari S, Robey PG, Riminucci M (2007) Self-renewing osteoprogenitors in bone marrow sinusoids can organize a hematopoietic microenvironment. *Cell* **131**: 324-336.

Sacchetti B, Funari A, Remoli C, Giannicola G, Kogler G, Liedtke S, Cossu G, Serafini M, Sampaolesi M, Tagliafico E (2016) No identical "mesenchymal stem cells" at different times and sites: human committed progenitors of distinct origin and differentiation potential are incorporated as adventitial cells in microvessels. *Stem Cell Rep* **6**: 897-913.

Saleh F, Whyte M, Genever P (2011) Effects of endothelial cells on human mesenchymal stem cell activity in a three-dimensional *in vitro* model. *Eur Cell Mater* **22**: 242-257.

Sart S, Agathos SN, Li Y, Ma T (2016) Regulation of mesenchymal stem cell 3D microenvironment: from macro to microfluidic bioreactors. *Biotechnol J* **11**: 43-57.

Sarugaser R, Lickorish D, Baksh D, Hosseini MM, Davies JE (2005) Human umbilical cord perivascular (HUCPV) cells: a source of mesenchymal progenitors. *Stem Cells* **23**: 220-229.

Saxena P, Heng BC, Bai P, Folcher M, Zulewski H, Fussenegger M (2016) A programmable synthetic lineage-control network that differentiates human iPSCs into glucose-sensitive insulin-secreting beta-like cells. *Nat Commun* **7**: 11247. DOI: 10.1038/ncomms11247.

Scadden DT (2006) The stem-cell niche as an entity of action. *Nature* **441**: 1075-1079.

Schneider PR, Buhrmann C, Mobasher A, Matis U, Shakibaei M (2011) Three-dimensional high-density co-culture with primary tenocytes induces tenogenic differentiation in mesenchymal stem cells. *J Orth Res* **29**: 1351-1360.

Schofield R (1978) The relationship between the spleen colony-forming cell and the haemopoietic stem cell. *Blood Cells* **4**: 7-25.

Schroeder T, Geyh S, Germing U, Haas R (2016) Mesenchymal stromal cells in myeloid malignancies. *Blood Res* **51**: 225-232.

Schultz GS, Wysocki A (2009) Interactions between extracellular matrix and growth factors in wound healing. *Wound Repair Regen* **17**: 153-162.

- Schwab K, Hutchinson P, Gargett C (2008) Identification of surface markers for prospective isolation of human endometrial stromal colony-forming cells. *Hum Reprod* **23**: 934-943.
- Schwartz MA (2010) Integrins and extracellular matrix in mechanotransduction. *Cold Spring Harb Perspect Biol* **2**: a005066. DOI: 10.1101/cshperspect.a005066.
- Seib FP, Prewitz M, Werner C, Bornhäuser M (2009) Matrix elasticity regulates the secretory profile of human bone marrow-derived multipotent mesenchymal stromal cells (MSCs). *Biochem Biophys Res Commun* **389**: 663-667.
- Seo B-M, Miura M, Gronthos S, Bartold PM, Batouli S, Brahimi J, Young M, Robey PG, Wang CY, Shi S (2004) Investigation of multipotent postnatal stem cells from human periodontal ligament. *Lancet* **364**: 149-155.
- Shao B, Liao L, Yu Y, Shuai Y, Su X, Jing H, Yang D, Jin Y (2015) Estrogen preserves Fas ligand levels by inhibiting microRNA-181a in bone marrow-derived mesenchymal stem cells to maintain bone remodeling balance. *FASEB J* **29**: 3935-3944.
- Sharaf-Eldin WE, Abu-Shahba N, Mahmoud M, El-Badri N (2016) The modulatory effects of mesenchymal stem cells on osteoclastogenesis. *Stem Cells Int* **2016**: 1908365. DOI: 10.1155/2016/1908365.
- Shiozawa Y, Eber MR, Berry JE, Taichman RS (2015) Bone marrow as a metastatic niche for disseminated tumor cells from solid tumors. *Bonekey Rep* **4**: 689. DOI: 10.1038/bonekey.2015.57.
- Siciliano C, Chimenti I, Ibrahim M, Napoletano C, Mangino G, Scaletta G, Zoccai GB, Rendina EA, Calogero A, Frati G (2015) Cardiosphere conditioned media influence the plasticity of human mediastinal adipose tissue-derived mesenchymal stem cells. *Cell Transplant* **24**: 2307-2322.
- Simonson OE, Mouggiakakos D, Heldring N, Bassi G, Johansson HJ, Dalén M, Jitschin R, Rodin S, Corbascio M, El Andaloussi S (2015) *In vivo* effects of mesenchymal stromal cells in two patients with severe acute respiratory distress syndrome. *Stem Cells Transl Med* **4**: 1199-1213.
- Sipp D, Robey PG, Turner L (2018) Clear up this stem-cell mess. *Nature* **561**: 455-457.
- Sittichockechaiwut A, Scutt AM, Ryan AJ, Bonewald LF, Reilly GC (2009) Use of rapidly mineralising osteoblasts and short periods of mechanical loading to accelerate matrix maturation in 3D scaffolds. *Bone* **44**: 822-829.
- Song K, Liu T, Cui Z, Li X, Ma X (2008) Three-dimensional fabrication of engineered bone with human bio-derived bone scaffolds in a rotating wall vessel bioreactor. *J Biomed Mater Res A* **86**: 323-332.
- Squillaro T, Peluso G, Galderisi U (2016) Clinical trials with mesenchymal stem cells: an update. *Cell Transplant* **25**: 829-848.
- Stanciu A-M, Flamant Q, Biotteau-Deheuvels K, Stoddart MJ, Anglada M, Porporati AA, Kuntz M, Gremillard L, Alini M, Peroglio M (2018) Human primary osteoblast behaviour on microrough zirconia-toughened alumina and on selectively etched microrough zirconia-toughened alumina. *J Eur Ceram Soc* **38**: 927-937.
- Steinert AF, Kunz M, Prager P, Göbel S, Klein-Hitpass L, Ebert R, Nöth U, Jakob F, Gohlke F (2015) Characterization of bursa subacromialis-derived mesenchymal stem cells. *Stem Cell Res Ther* **6**: 114. DOI: 10.1186/s13287-015-0104-3.
- Stiehler M, Bünger C, Baatrup A, Lind M, Kasse M, Mygind T (2009) Effect of dynamic 3-D culture on proliferation, distribution, and osteogenic differentiation of human mesenchymal stem cells. *J Biomed Mater Res A* **89**: 96-107.
- Strassburg S, Richardson SM, Freemont AJ, Hoyland JA (2010) Co-culture induces mesenchymal stem cell differentiation and modulation of the degenerate human nucleus pulposus cell phenotype. *Regen Med* **5**: 701-711.
- Sun Y, Cai J, Yu S, Chen S, Li F, Fan C (2016) MiR-630 inhibits endothelial-mesenchymal transition by targeting slug in traumatic heterotopic ossification. *Sci Rep* **6**: 22729. DOI: 10.1038/srep22729.
- Sun Y, Chen CS, Fu J (2012a) Forcing stem cells to behave: a biophysical perspective of the cellular microenvironment. *Annu Rev Biophys* **41**: 519-542.
- Sun Y, Weng S, Fu J (2012b) Microengineered synthetic cellular microenvironment for stem cells. *Wiley Interdiscip Rev Nanomed Nanobiotechnol* **4**: 414-427.
- Suzuki S, Narita Y, Yamawaki A, Murase Y, Satake M, Mutsuga M, Okamoto H, Kagami H, Ueda M, Ueda Y (2010) Effects of extracellular matrix on differentiation of human bone marrow-derived mesenchymal stem cells into smooth muscle cell lineage: utility for cardiovascular tissue engineering. *Cells Tissues Organs* **191**: 269-280.
- Swetha M, Sahithi K, Moorthi A, Srinivasan N, Ramasamy K, Selvamurugan N (2010) Biocomposites containing natural polymers and hydroxyapatite for bone tissue engineering. *Int J Biol Macromol* **47**: 1-4.
- Takigawa H, Kitadai Y, Kuwai T, Yuge R, Tanaka S, Chayama K (2017) Mesenchymal stem cells promote epithelial-mesenchymal transition of colon cancer cells *via* direct cell-to-cell contact. *Neoplasia* **19**: 429-438.
- Takizawa N, Okubo N, Kamo M, Chosa N, Mikami T, Suzuki K, Yokota S, Ibi M, Ohtsuka M, Taira M (2017) Bone marrow-derived mesenchymal stem cells propagate immunosuppressive/anti-inflammatory macrophages in cell-to-cell contact-independent and dependent manners under hypoxic culture. *Exp Cell Res* **358**: 411-420.
- Tatárová Z, Abbuehl J, Maerkl S, Huelsken J (2016) Microfluidic co-culture platform to quantify chemotaxis of primary stem cells. *Lab Chip* **16**: 1934-1945.
- Thevenot PT, Nair AM, Shen J, Lotfi P, Ko C-Y, Tang L (2010) The effect of incorporation of SDF-1 α into PLGA scaffolds on stem cell recruitment and the inflammatory response. *Biomaterials* **31**: 3997-4008.

- Thompson CL, Plant JC, Wann AK, Bishop CL, Novak P, Mitchison HM, Beales PL, Chapple JP, Knight MM (2017) Chondrocyte expansion is associated with loss of primary cilia and disrupted hedgehog signalling. *Eur Cell Mater* **34**: 128-141.
- Todd SJ, Farrar D, Gough JE, Ulijn RV (2007) Enzyme-triggered cell attachment to hydrogel surfaces. *Soft Matter* **3**: 547-550.
- Toma C, Pittenger MF, Cahill KS, Byrne BJ, Kessler PD (2002) Human mesenchymal stem cells differentiate to a cardiomyocyte phenotype in the adult murine heart. *Circulation* **105**: 93-98.
- Tondreau T, Meuleman N, Delforge A, Dejeneffe M, Leroy R, Massy M, Mortier C, Bron D, Lagneaux L (2005) Mesenchymal stem cells derived from CD133-positive cells in mobilized peripheral blood and cord blood: proliferation, Oct4 expression, and plasticity. *Stem Cells* **23**: 1105-1112.
- Trento C, Bernardo ME, Nagler A, Kuçi S, Bornhäuser M, Köhl U, Strunk D, Galleu A, Sanchez-Guijo F, Gaipa G (2018) Manufacturing mesenchymal stromal cells for the treatment of graft-versus-host disease: a survey among centers affiliated with the European Society for Blood and Marrow Transplantation. *Biol Blood Marrow Transplant* **24**: 2365-2370.
- Tsimbouri PM, Childs PG, Pemberton GD, Yang J, Jayawarna V, Orapiriyakul W, Burgess K, González-García C, Blackburn G, Thomas D (2017) Stimulation of 3D osteogenesis by mesenchymal stem cells using a nanovibrational bioreactor. *Nat Biomed Eng* **1**: 758-770.
- Usunier B, Benderitter M, Tamarat R, Chapel A (2014) Management of fibrosis: the mesenchymal stromal cells breakthrough. *Stem Cells Int* **2014**: 340257. DOI: 10.1155/2014/340257.
- Varin A, Pontikoglou C, Labat E, Deschaseaux F, Sensebé L (2013) CD200R/CD200 inhibits osteoclastogenesis: new mechanism of osteoclast control by mesenchymal stem cells in human. *PLoS One* **8**: e72831. DOI: 10.1371/journal.pone.0072831.
- Vasandan AB, Jahnavi S, Shashank C, Prasad P, Kumar A, Prasanna SJ (2016) Human mesenchymal stem cells program macrophage plasticity by altering their metabolic status *via* a PGE2-dependent mechanism. *Sci Rep* **6**: 38308. DOI: 10.1038/srep38308.
- Venkatesan J, Kim S-K (2014) Nano-hydroxyapatite composite biomaterials for bone tissue engineering – a review. *J Biomed Nanotechnol* **10**: 3124-3140.
- Veronesi F, Borsari V, Sartori M, Orciani M, Mattioli-Belmonte M, Fini M (2018) The use of cell conditioned medium for musculoskeletal tissue regeneration. *J Cell Physiol* **233**: 4423-4442.
- Visnjic D, Kalajzic Z, Rowe DW, Katavic V, Lorenzo J, Aguila HL (2004) Hematopoiesis is severely altered in mice with an induced osteoblast deficiency. *Blood* **103**: 3258-3264.
- Wang T, Turhan M, Gunasekaran S (2004) Selected properties of pH-sensitive, biodegradable chitosanopoly (vinyl alcohol) hydrogel. *Polym Int* **53**: 911-918.
- Wang W, Itaka K, Ohba S, Nishiyama N, Chung U-i, Yamasaki Y, Kataoka K (2009) 3D spheroid culture system on micropatterned substrates for improved differentiation efficiency of multipotent mesenchymal stem cells. *Biomaterials* **30**: 2705-2715.
- Wang Y, Volloch V, Pindrus MA, Blasioli DJ, Chen J, Kaplan DL (2007) Murine osteoblasts regulate mesenchymal stem cells *via* WNT and cadherin pathways: mechanism depends on cell-cell contact mode. *J Tissue Eng Regen Med* **1**: 39-50.
- Watson EC, Adams RH (2017) Biology of bone: the vasculature of the skeletal system. *Cold Spring Harb Perspect Med* **8**. pii: a031559. DOI: 10.1101/cshperspect.a031559.
- Weber W, Fussenegger M (2012) Emerging biomedical applications of synthetic biology. *Nature Rev Genet* **13**: 21-23.
- Wei Y, Gong K, Zheng Z, Liu L, Wang A, Zhang L, Ao Q, Gong Y, Zhang X (2010) Schwann-like cell differentiation of rat adipose-derived stem cells by indirect co-culture with Schwann cells *in vitro*. *Cell Prolif* **43**: 606-616.
- Wenisch S, Stahl JP, Horas U, Heiss C, Kilian O, Trinkaus K, Hild A, Schnettler R (2003) *In vivo* mechanisms of hydroxyapatite ceramic degradation by osteoclasts: fine structural microscopy. *J Biomed Mater Res A* **67**: 713-718.
- Wingate K, Bonani W, Tan Y, Bryant SJ, Tan W (2012) Compressive elasticity of three-dimensional nanofiber matrix directs mesenchymal stem cell differentiation to vascular cells with endothelial or smooth muscle cell markers. *Acta Biomater* **8**: 1440-1449.
- Winkler IG, Barbier V, Wadley R, Zannettino A, Williams S, Lévesque J-P (2010) Positioning of bone marrow hematopoietic and stromal cells relative to blood flow *in vivo*: serially reconstituting hematopoietic stem cells reside in distinct non-perfused niches. *Blood* **116**: 375-385.
- Wislet-Gendebien S, Hans G, Leprince P, Rigo JM, Moonen G, Rogister B (2005) Plasticity of cultured mesenchymal stem cells: switch from nestin-positive to excitable neuron-like phenotype. *Stem Cells* **23**: 392-402.
- Wohrer S, Knapp DJ, Copley MR, Benz C, Kent DG, Rowe K, Babovic S, Mader H, Oostendorp RA, Eaves CJ (2014) Distinct stromal cell factor combinations can separately control hematopoietic stem cell survival, proliferation, and self-renewal. *Cell Rep* **7**: 1956-1967.
- Woodard JR, Hilldore AJ, Lan SK, Park C, Morgan AW, Eurell JAC, Clark SG, Wheeler MB, Jamison RD, Johnson AJW (2007) The mechanical properties and osteoconductivity of hydroxyapatite bone scaffolds with multi-scale porosity. *Biomaterials* **28**: 45-54.
- Wu C, Rankin EB, Castellini L, Fernandez-Alcudia J, LaGory EL, Andersen R, Rhodes SD, Wilson TL, Mohammad KS, Castillo AB (2015) Oxygen-sensing PHDs regulate bone homeostasis through the modulation of osteoprotegerin. *Genes Dev* **29**: 817-831.

- Xu C, Gao X, Wei Q, Nakahara F, Zimmerman SE, Mar J, Frenette P (2018) Stem cell factor is selectively secreted by arterial endothelial cells in bone marrow. *Nat Commun* 9:2449. DOI: 10.1038/s41467-018-04726-3.
- Xu S, Menu E, Becker AD, Van Camp B, Vanderkerken K, Van Riet I (2012) Bone marrow-derived mesenchymal stromal cells are attracted by multiple myeloma cell-produced chemokine CCL25 and favor myeloma cell growth *in vitro* and *in vivo*. *Stem Cells* 30: 266-279.
- Xu S, Veirman K, Becker A, Vanderkerken K, Riet I (2018) Mesenchymal stem cells in multiple myeloma: a therapeutic tool or target? *Leukemia* 32: 1500-1514.
- Yang C, Tibbitt MW, Basta L, Anseth KS (2014) Mechanical memory and dosing influence stem cell fate. *Nat Mater* 13: 645-652.
- Yang S, Wei D, Wang D, Phimpilai M, Krebsbach PH, Franceschi RT (2003) *In vitro* and *in vivo* synergistic interactions between the Runx2/Cbfa1 transcription factor and bone morphogenetic protein-2 in stimulating osteoblast differentiation. *J Bone Miner Res* 18: 705-715.
- Yeatts AB, Choquette DT, Fisher JP (2013) Bioreactors to influence stem cell fate: augmentation of mesenchymal stem cell signaling pathways via dynamic culture systems. *Biochim Biophys Acta Gen Subj* 1830: 2470-2480.
- Yeatts AB, Fisher JP (2010) Tubular perfusion system for the long-term dynamic culture of human mesenchymal stem cells. *Tissue Eng Part C Methods* 17: 337-348.
- Yim EK, Pang SW, Leong KW (2007) Synthetic nanostructures inducing differentiation of human mesenchymal stem cells into neuronal lineage. *Exp Cell Res* 313: 1820-1829.
- Yim EK, Sheetz MP (2012) Force-dependent cell signaling in stem cell differentiation. *Stem Cell Res Ther* 3: 41 DOI: 10.1186/scrt132.
- Ylöstalo JH, Bartosh TJ, Coble K, Prockop DJ (2012) Human mesenchymal stem/stromal cells cultured as spheroids are self-activated to produce prostaglandin E2 that directs stimulated macrophages into an anti-inflammatory phenotype. *Stem Cells* 30: 2283-2296.
- Yona S, Kim KW, Wolf Y, Mildner A, Varol D, Breker M, Strauss-Ayali D, Viukov S, Williams M, Misharin A, Hume DA, Perlman H, Malissen B, Zelzer E, Jung S (2013) Fate mapping reveals origins and dynamics of monocytes and tissue macrophages under homeostasis. *Immunity* 38: 79-91.
- Yousefi A-M, James PF, Akbarzadeh R, Subramanian A, Flavin C, Oudadesse H (2016) Prospect of stem cells in bone tissue engineering: a review. *Stem Cells Int* 2016: 6180487. DOI: 10.1155/2016/6180487.
- Zanotti L, Angioni R, Cali B, Soldani C, Ploia C, Moalli F, Garghesa M, D'amico G, Elliman S, Tedeschi G (2016) Mouse mesenchymal stem cells inhibit high endothelial cell activation and lymphocyte homing to lymph nodes by releasing TIMP-1. *Leukemia* 30: 1143-1154.
- Zhao F, Grayson WL, Ma T, Bunnell B, Lu WW (2006) Effects of hydroxyapatite in 3-D chitosan-gelatin polymer network on human mesenchymal stem cell construct development. *Biomaterials* 27: 1859-1867.
- Zhao L, Liu L, Wu Z, Zhang Y, Chu PK (2012) Effects of micropitted/nanotubular titania topographies on bone mesenchymal stem cell osteogenic differentiation. *Biomaterials* 33: 2629-2641.
- Zhao Y (2012) Light-responsive block copolymer micelles. *Macromolecules* 45: 3647-3657.
- Zhou BO, Yue R, Murphy MM, Peyer JG, Morrison SJ (2014) Leptin-receptor-expressing mesenchymal stromal cells represent the main source of bone formed by adult bone marrow. *Cell Stem Cell* 15: 154-168.
- Zimmermann EA, Schaible E, Bale H, Barth HD, Tang SY, Reichert P, Busse B, Alliston T, Ager JW, Ritchie RO (2011) Age-related changes in the plasticity and toughness of human cortical bone at multiple length scales. *Proc Natl Acad Sci U S A* 108: 14416-14421.
- Zuk PA, Zhu M, Ashjian P, De Ugarte DA, Huang JJ, Mizuno H, Alfonso ZC, Fraser JK, Benhaim P, Hedrick MH (2002) Human adipose tissue is a source of multipotent stem cells. *Mol Biol Cell* 13: 4279-4295.

Discussion with Reviewer

Reviewer: Given the wide distribution of MSCs and their diversity, there are likely to be a multitude of niches. Will each need to be analyzed separately or will there be common features?

Authors: Stem cells, including MSCs, require particular microenvironments to maintain themselves *in vivo*, otherwise known as niches (Schofield, 1978), where their stemness is protected and the stimulus for differentiation is triggered by cellular signaling with either tissue-adjacent cells, paracrine and endocrine signals from local or systemic sources, or external mechanical forces. Given the theoretically wide distribution of MSCs through several connective tissues in the organism (Crisan *et al.*, 2008), it is reasonable to assume that the inherent chemistry, mechanical structure, and function of different tissues may influence the single MSC entity. Since native stem cell niches at distinct anatomical locations and developmental stages have remained a theoretical construct and criteria for the *in vitro* characterization of MSCs weakly delineate MSCs from other cell types, it remains challenging to compare naïve cells from different niches. However, increasing evidences indicate different transcriptome and differentiation capacity of MSCs-like cells obtained from diverse tissues (Sacchetti *et al.*, 2016), while tissue-specific elements involved in MSC lineage decision still have to be revealed. Based on current knowledge, it

can be assumed that both tissue-specific as well as common mechanisms control MSC fate in distinct niches. However, future research will be required to unravel these mechanisms, which will be also critical to resemble specific niche features in *in vitro* models. Recent technical advances in niche *in vitro* modelling will certainly play a pivotal role in understanding and elucidation of MSC physiology and regulation within different locations.

Reviewer: Are MSCs an *in vitro* artefact?

Authors: Most of the knowledge on MSC biology derives from *in vitro* studies, due to the current lack of sophisticated methods allowing to specifically track MSCs *in vivo*. As discussed in the article, *in vitro* cultures, despite being great mechanistic tools, can often manipulate the cell phenotype in favor of specific differentiation events, by exposing them to highly artificial situations, such as the unnatural 2D environment in monolayer cultures or chemical stimulation. These potentially stressful *in vitro* conditions provoke subcultured MSCs to adjust their physiology (Bara *et al.*, 2014), while their stem cell features, inherent to rare cell population only, may disappear. Thus, regenerative properties of *in vitro* described MSCs are required to be validated *in vivo* with appropriate controls and reproducible protocols, which indeed only some studies have demonstrated

until now. Nevertheless, *in vitro* amplified MSCs show therapeutic potential for certain clinical application, *e.g.* the treatment of graft-*versus*-host disease (Le Blanc *et al.*, 2008; Ringdén *et al.*, 2006; additional references), indicating therapeutic value of these cells independent of the fact that they might be an *in vitro* artefact.

Additional References

Le Blanc K, Frassoni F, Ball L, Locatelli F, Roelofs H, Lewis I, Lanino E, Sundberg B, Bernardo ME, Remberger M, Giorgio D, Maarten E, Andrea B, Willem F, Olle R (2008) Mesenchymal stem cells for treatment of steroid-resistant, severe, acute graft-*versus*-host disease: a phase II study. *The Lancet* **371**: 1579-1586.

Ringdén O, Uzunel M, Rasmusson I, Remberger M, Sundberg B, Lönnies H, Marschall H-U, Dlugosz A, Szakos A, Hassan Z, Omazic B, Aschan J, Barkholt L, Le Blanc K (2006) Mesenchymal stem cells for treatment of therapy-resistant graft-*versus*-host disease. *Transplantation* **81**: 1390-1397.

Editor's note: The Scientific Editor responsible for this paper was Chris Evans.

Chapter 2.

Methods: Development of a decellularized bone scaffold

In this chapter information regarding the manufacturing and handling process of decellularized human-bone scaffolds is methodically described. Further scaffold characterization techniques and corresponding results are shown.

The work presented in this chapter was published as a protocol-article in *Methods in Cell Biology* (Volume 157: Cell-Derived Matrices Part B, Chapter 7). Reprint permission was obtained from all co-authors and from the Elsevier Copyrights department.

*Reference: Pereira AR, Rudert M and Herrmann M. Decellularized human bone as a 3D model to study skeletal progenitor cells in a natural environment. *Methods in cell biology*. Elsevier, 2020, 157, pp.123-141.*

CHAPTER

7

Decellularized human bone as a 3D model to study skeletal progenitor cells in a natural environment

Ana Rita Pereira^a, Maximilian Rudert^b, Marietta Herrmann^{a,c,*}^aIZKF Group Tissue Regeneration in Musculoskeletal Diseases, University Clinics, Wuerzburg, Germany^bDepartment of Orthopaedic Surgery, König-Ludwig-Haus, University of Wuerzburg, Wuerzburg, Germany^cBernhard-Heine Center for Locomotion Research, University of Wuerzburg, Wuerzburg, Germany

*Corresponding author: e-mail address: m-herrmann.klh@uni-wuerzburg.de

Chapter outline

1	Definition	124
2	Rational	125
3	Bone decellularization protocols in literature	125
	3.1 Physical treatments.....	126
	3.2 Chemical treatments.....	127
	3.3 Enzymatic treatments.....	127
4	Material and equipment	128
	4.1 Preparation of decellularized bone scaffolds.....	128
	4.2 Cell culture.....	128
5	Protocol	129
	5.1 Preparation of decellularized bone scaffolds.....	129
	5.2 Cell seeding.....	131
6	Related techniques: Characterization of decellularized bone scaffolds	132
	6.1 Calcium release assay.....	132
	6.2 Cryosectioning and structural characterization.....	133
	6.3 Micro-computed tomography (micro-CT).....	135
	6.4 Cell seeding efficiency.....	136
	6.5 Cell tracking.....	136
	6.6 Metabolic activity of cells: MTT-assay.....	137
7	Safety considerations	138

124 CHAPTER 7 Decellularized human bone as a 3D model

8 Troubleshooting.....	139
9 Conclusion.....	139
References.....	140

Abstract

There has been an increasing interest in exploring naturally derived extracellular matrices as an material mimicking the complexity of the cell microenvironment in vivo. Bone tissue-derived decellularized constructs are able to preserve native structural, biochemical, and bio-mechanical cues of the tissue, therefore providing a suitable environment to study skeletal progenitor cells.

Particularly for bone decellularization, different methods have been reported in the literature. However, the used methods critically affect the final ultrastructure and surface chemistry as well as the decellularization efficiency, consequently causing complications to draw conclusions and compare results in between studies.

In this chapter, an optimized protocol for the preparation of human bone derived scaffolds is described, including processing techniques and further characterization methods, which allow the final construct to be recognized as a major platform for bone therapeutic and/or diagnostic applications.

1 Definition

Tissue decellularization of small and simple tissues was first reported in the 1970s for the treatment of burn victims (Elliott & Hoehn, 1973). Still, the advent of the most forefront techniques arose several years later, with a major impulse from Badylak and coworkers (Badylak, 2004a, 2004b; Badylak, Lantz, Coffey, & Geddes, 1989). Soon after, promising results of tissue-derived biological scaffolds with the purpose of tissue engineering and regenerative medicine applications were reported, such as heart valve substitutes (Bader et al., 1998; Korossis et al., 2002), bladder mucosa grafts (Merguerian et al., 2000; Probst, Piechota, Dahiya, & Tanagho, 2000), skin grafts (Buinewicz & Rosen, 2004; Clark, Saffold, & Israel, 2003; Herson, Mathor, Altran, Capelozzi, & Ferreira, 2001) and liver grafts (Badylak, 2004a, 2004b; Lin, Chan, Badylak, & Bhatia, 2004).

The success of decellularized constructs relies mainly in the fact that these are able to conserve a highly complex tissue-specific combination of structural and functional extracellular matrix features, and therefore direct cell behavior and tissue regeneration in a dynamic way.

Until now, decellularized constructs have been produced from a number of tissues and organs, whereby the methods by which they might be derived are highly dependent on the structure of the organ of interest and may include both physical, chemical and enzymatic treatments. Decellularized bone matrix, in particular, is

gaining a lot of attention as implantable biomaterial for bone tissue repair and regeneration (Freyman, 2008; Lee et al., 2016). However, there is a great variability of protocols in the literature, which may lead to very different biological outcomes. This chapter describes an optimized protocol for the preparation of human bone derived scaffolds, including processing techniques and further characterization methods, which empower the final construct to be recognized as a major platform for therapeutic and/or diagnostic applications.

2 Rational

There has been an increasing interest in exploring naturally derived extracellular matrices, in order to resemble the complexity of the cell microenvironment *in vivo*, which is hardly reached by synthetic scaffolds. The final decellularized constructs are able to preserve their native structural, biochemical, and biomechanical cues. Therefore, tissue-specific and functional molecules, which modulate not only cell behavior but also the synthesis of new extracellular matrix components, are presented in their native three-dimensional distribution and defined concentrations to the cells, thus mimicking the full microenvironmental dynamics.

The goal of decellularization protocols is to preserve the above mentioned biochemical complexity and mechanical integrity of the tissue, while efficiently removing all cellular and nuclear components. Complete removal of antigens and genetic material is critical in order to prevent any rejection or cross-reaction during the repopulation of the scaffold.

Each particular tissue has its own characteristic requirements, e.g., matrix density, chemical composition and geometric factors including tissue thickness and shape, to which the decellularization protocol has to be adapted. Bone has a complex highly organized structure—the organic phase of bone is mainly composed of a strong network of elastic collagen type-I fibers and provides the tissue with flexibility. The inorganic mineral phase is mainly composed of highly organized calcium phosphate known as hydroxyapatite, providing the bone with rigidity and creating the right mechanical balance to provide resistance to fractures. Particularly applied to the decellularization of bone tissue, not only the decellularization efficiency is important, but also the removal of the mineral phase, known as decalcification, is fundamental. Decalcification of bone has been documented already in 1965 to be beneficial to expose biologically active bone morphogenetic proteins in the surface of the produced scaffolds, and consequently increase significantly their osteoinductive properties (Urist, 1965).

3 Bone decellularization protocols in literature

Several alternative techniques have been reported to achieve decellularization of tissues. Decellularization can be accomplished using physical, chemical or enzymatic methods, albeit each strategy has both benefits and drawbacks. For example,

physical treatments often are able to preserve the tissue structure, but fail to meet the requirements for reducing/preventing immunogenicity. In contrast, chemical and enzymatic treatments alone are often not sufficient to remove the total cellular remainings from the tissue. For these reasons, combinatory protocols may be used in the field of decellularization. While requiring longer sample processing times, these protocols offer an improved final material, both in terms of efficient decellularization and overall structure preservation.

Considering bone-specific characteristics such as a high matrix density and challenging geometric features (e.g., high thickness and complex shape), rather harsh decellularization methods must be considered. However, a vast number of protocols for bone decellularization have been described in literature, which are often adapted to the scientific question being pursued by each research group. Therefore, the comparison of biological results among the literature should be performed carefully, taking in consideration the details of the methodology.

3.1 Physical treatments

Commonly used physical methods for decellularization include (1) mechanical agitation, (2) freeze/thaw cycles, (3) sonication and (4) use of high pressures and forces.

Mechanical agitation is highly present in the majority of the protocols as an adjuvant technique applied in most of washing and incubation steps in order to improve the penetration of the solution into the thickness of the tissue.

Thermal shock techniques are also frequently present in bone decellularization protocols. By shock freezing a tissue in liquid nitrogen, ice crystals are created around the cell membrane causing cell lysis. Although the tissue is considered devitalized, it is not decellularized. Therefore, freeze/thawing usually requires complementary washing steps to remove remaining genetic material, either using detergents such as Triton X-100 (Tran et al., 2018), or solvent extraction procedures, e.g., with isopropanol (Bianco et al., 2019). Both techniques have been confirmed to preserve the native 3D bone architecture, including bundles of collagen fibers and glycoproteins, blood vessel structures as well as decellularized cellular niches.

Similarly, sonication methods are also often used to avoid the exposure of prolonged chemical treatments and therefore reduce extracellular matrix damage and ultrastructure disruption. Smith and co-workers reported to have achieved an efficient removal of marrow components (~99.6%) by performing a sequence of three sonication and centrifugation cycles in pre-warmed distilled water followed by a sonication step in peracetic acid to ensure the total removal of cell debris (Smith et al., 2015). Resultant constructs were confirmed to be biomechanically stable compared with fresh frozen samples during compression tests.

High-hydrostatic pressurization has also been applied to bone decellularization protocols. Hashimoto et al. have successfully produced decellularized bone scaffolds after hydrostatically applying a pressure of 980 mPa at 30 °C for 10 min, followed by an enzymatic washing step with nucleases to remove remaining genetic material. The resultant decellularized scaffolds have been shown to improve

in vitro osteogenic differentiation of rat mesenchymal stem cells and no immune reaction was observed when implanted subcutaneously in a rat model (Hashimoto et al., 2011).

3.2 Chemical treatments

Chemical methods commonly used for bone decellularization include (1) acidic and (2) alkaline treatments, (3) nonionic and (4) ionic detergent washing steps, and (5) alcohol sterilization. Usually chemical treatments are recognized to be more abrasive for the ultrastructure and surface chemistry of the tissue; nevertheless, they are essential to ensure the total removal of the cellular material.

Use of alkaline bases, e.g., ammonium hydroxide (Lee et al., 2016), and weak acids, e.g., peracetic acid (Smith et al., 2015), are used to achieve a fast effect on decellularization. The efficacy strongly varies according to the type, concentration and time of exposure; yet, the degree of matrix degradation is proportionally larger. Therefore, the use of those is often used along with an adjuvant physical treatment, such as sonication or mechanical agitation mentioned above, for a short period of time.

Nonionic detergents such as Triton X-100 are widely used (Sun et al., 2011; Tran et al., 2018) since they induce cell lysis through interaction with the lipid bilayer of the cellular membrane—i.e., due to its chemistry, these detergents do not disturb protein-protein interactions, which is a major advantage to preserve the matrix chemistry. Although Triton X-100 has been shown to be an effective decellularization method for several soft tissues (Gilbert, Sellaro, & Badylak, 2006), it is not significantly used in bone decellularization applications.

Ionic detergents, such as SDS, are often used because of their high efficacy in lysing cells (Lee et al., 2016; Sladkova et al., 2019). However, they are considered more detrimental to the matrix structure than nonionic detergents. SDS disrupts cell membranes and denatures proteins, exposing the contents to further degradation. To prevent protein degradation, protocols often contain several sequential washes with low concentrated SDS solutions and incubation at lower temperatures. The complete removal of SDS from samples through several further washing steps is also extremely important, since the presence of SDS is highly toxic for the cells.

Alcohols such as ethanol or methanol are used widely among most of the protocols as a final wash to remove residual nucleic acids. It is also a common strategy applied for sterilization of the final decellularized scaffolds, since it is not unusual that the implementation of the decellularization protocol is not feasible to perform under sterile conditions.

3.3 Enzymatic treatments

Enzymatic agents are often used after physical and/or chemical decellularization to further achieve complete removal of residual nuclear material from the tissue. Nucleases and proteases are the most widely used enzymes for enzymatic decellularization.

128 CHAPTER 7 Decellularized human bone as a 3D model

Nucleases act directly on hydrolyzation of phosphodiester bonds from nucleic acids. The use of deoxyribonuclease (Hashimoto et al., 2011; Sun et al., 2011) or the combined treatment with ribonuclease (Sladkova et al., 2019) have been shown to be very effective in completely removing the genetic material left behind after cell lysis by other pretreatments.

Proteases, such as trypsin, are proteolytic enzymes, which cleave peptide bonds to dissociate adherent cells from the matrix. Proteases are often used with an adjuvant chelation agent, e.g., EDTA that binds calcium ions, and therefore destabilizes calcium-dependent proteins in the cell surface responsible for cell adhesion. Although the combination of trypsin-EDTA has been proven to be efficient for decellularization (Sawkins et al., 2013), due to its specific activity on peptides, long incubation times can severely disrupt matrix proteins, such as collagen, laminin, fibronectin and elastin (Crapo, Gilbert, & Badylak, 2011).

4 Material and equipment

4.1 Preparation of decellularized bone scaffolds

Plexiglas microscope slides (404152, Walter Messner GmbH)
Superglue (1733-0100, Renfert)
Silicon carbide abrasive paper (WSflex 18C, Hermes Schleifmittel GmbH)
Electric saw (300, Exakt)
Diamond cutting band (D64, Walter Messner GmbH)
Hotplate stirrer (WiseStir MSH-A)
Standard testing sieve—250 µm pore size (60BS8F, Advantech Manufacturing Inc.)
Antibiotic-Antimycotic (15240062, Gibco)
Sodium azide (S2002, Sigma-Aldrich)
Chloroform (288306, Sigma-Aldrich)
Methanol (1481, Labsolute)
Tris(hydroxymethyl)aminomethan (161-0716, BioRad)
Ethylenediaminetetraacetic acid (EDTA) (E5134, Sigma-Aldrich)
Sodium dodecyl sulfate (SDS) (A1112, AppliChem)
Deoxyribonuclease I (DNase) (DN25, Sigma-Aldrich)
Ethanol (K928.4, Roth)
Biopsy punch (P0510|PZN 00199131 and P1010|PZN 00258514, Xiomedics Medizintechnik GmbH)
Liophilizator (Alpha 1-4 LSCbasic, Martin Christ Gefriertrocknungsanlagen GmbH)

4.2 Cell culture

Class II Biological Safety Cabinet (Safe 2020, Thermo Scientific)
CO₂ Incubator (BBD 6220, Thermo Scientific)

Dulbecco's Phosphate Buffered Saline (PBS) (D8537, Sigma-Aldrich)
 DMEM/F-12, GlutaMAX™ supplement medium
 Fetal calf serum (Lot#BS211507.5A, FBS.EUA.0500, Bio&Sell)
 Penicillin-Streptomycin (P4333, Sigma-Aldrich)
 HEPES solution (H0887, Sigma-Aldrich)
 Recombinant human FGF basic protein (100-18C, PeproTech)
 Costar® 12-well Not Treated Multiple Well Plate (3737, Corning)
 Trypsin-EDTA 0.5% (15400054, Gibco)

5 Protocol

5.1 Preparation of decellularized bone scaffolds

1. Collect discarded human femoral heads during patient's total hip arthroplasty (see Fig. 1A) with informed consent and agreement of ethical authorities (permission number: 187/18, University Wuerzburg ethics committee). View safety 1.

Note: This protocol has been established with bone samples derived from patients aged ~55–75 years, yet the results of the decellularization process is expected to be transferable for other sets of donors as well.

Pause step: Samples can be stored at -20 or -80 °C before use.

2. In order to avoid bias of results by complications that may affect bone structure, discard samples of donors with indications of osteoporosis and diabetes (based

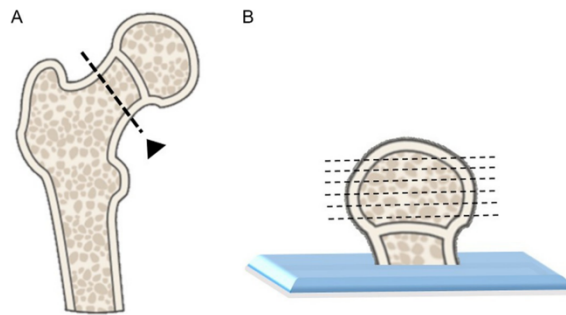


FIG. 1

Schematic view of femoral head slicing steps. (A) During surgery, the cut is performed by the surgeon in the femoral neck region, where the upper section (the femoral head) is stored in a sterile vessel for transportation. (B) After fixation to a slide (step 3), horizontal sections of precisely 3 mm thickness are sawed from the full volume of the femoral head, excluding the femoral neck.

130 CHAPTER 7 Decellularized human bone as a 3D model

on analysis of clinical prescription records or diagnosed osteoporosis based on BMD measurement), and/or with Body Mass Index above 30.

3. Thaw bones in demineralized water at RT for 1 h. Clean remaining blood and remove surrounding tissues.
4. Glue the femoral head to a Plexiglas microscope slide.
Critical step: To ensure a stable fixation, particular irregular contact surfaces can be manually sanded with a silicon carbide abrasive paper.
5. Use an electric diamond band saw to cut slices of 3 mm from each femoral head (see Fig. 1B).
Critical step: Keep demineralized water running on the contact surface between the bone and the saw, in order to avoid overheating and biological degradation of samples.
Pause step: Samples (bone slices) can be stored at -20°C until further use.
6. Wash slices briefly with demineralized water.
Note: From this step on, process each donor individually through the washing steps.
7. Incubate slices in 3 mM sodium azide for 24 h under agitation. View safety 2.
Critical step: For all incubation steps with agitation, use enough volume to completely cover all the slices (approximately $3-4 \times$ volume of bone). Make sure that the stirring speed is able to keep all slices moving and they do not form aggregates, which will critically impair the perfusion of solution in the volume of bone.
8. Remove lipid content from bones by incubation in a mixture of 1:1 chloroform/methanol for 72 h under agitation. View safety 3.
9. Wash $3 \times$ with demineralized water at 37°C for 10–15 min each time.
10. Incubate with 2,5% EDTA in 10 mM Tris at RT under agitation.
Critical step: Keep changing the solution (approximately every 3 days) until the slices can be mechanically bended. This step is highly dependent on the donor. Total time of incubation usually varies between 5 and 12 days.
11. Punch out cylinders with desirable diameter from bone slices using a biopsy punch in the respective size.
Note: The present protocol is optimized for 5 mm diameter scaffolds. Although different sizes can be obtained.
12. Incubate the scaffolds for another additional 3 days with 2,5% EDTA in 10 mM Tris at RT under agitation.
13. Incubate scaffolds with 0,5% SDS in 10 mM Tris for 24 h at RT under agitation.
Critical step: SDS is a detergent, necessary to improve the removal of cytoplasmic and nuclear material; however, it can impair the mechanical properties of the scaffold when to long incubated. Do not prolong this step or increase the concentration of SDS.
14. Wash with excess amount (approximately $6-10 \times$ volume of bone) demineralized water at RT.
15. Incubate with DNase (100 U/mL, approximately $1 \times$ volume of bone) for 6 h at 37°C under agitation.

16. Wash scaffolds in demineralized water at RT under agitation overnight.
17. Incubate scaffolds in dehydrated alcohol for 4h to remove any cellular remnants.
18. Wash with a large amount of deionized water for 2h.
19. Snap-freeze scaffolds in liquid nitrogen for at least 1 min and store them at -80°C for at least 30 min for solidification. Lyophilize scaffolds for 30h under a vacuum pressure of 3,75 mbar.

Pause step: Final samples (Fig. 2) can be stored at -20°C until further use.

5.2 Cell seeding

1. The day prior to cell seeding, incubate scaffolds two times with 70% ethanol for 40 min each at RT under agitation to ensure their sterilization.
Critical step: From this step on, the scaffolds are considered sterile and should be always handled inside the laminar flow hood.
2. Wash scaffolds with abundant amounts of PBS for 10 min at RT under agitation. Repeat two times.
3. Air dry scaffolds under the laminar flow hood overnight.
4. Incubate scaffolds with DMEM/F-12, GlutaMAX™ cell culture medium without any extra additives at 37°C for at least 30 min.

Critical step: This protocol has been established with the absence of FCS during incubation of scaffolds prior to cell seeding in order to promote cell adherence to matrix proteins from the decellularized bone construct. Note that presence of FCS is reported to increase cell attachment (Schönmeyr et al., 2008)

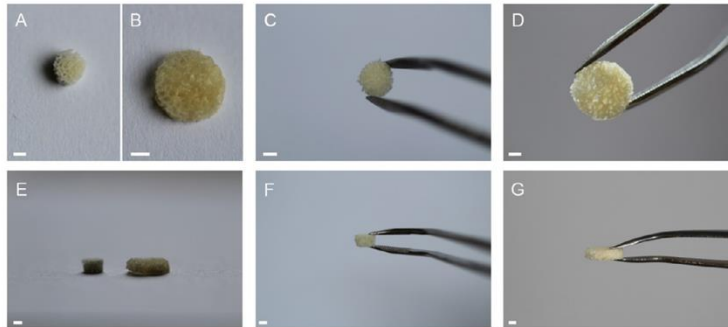


FIG. 2

Macroscopic view of produced scaffolds after the complete protocol. Scaffolds can be obtained with several diameters, images are shown for 5 mm (A, C, F) and 10 mm (B, D, G), while the thickness was maintained for both type of scaffolds at 3 mm (E). Scale bar: 2 mm.

but would mask the effect of the surface proteins in the decellularized constructs and consequently may interfere with the study hypothesis.

5. Expand MSCs isolated from human bone marrow of femoral heads and expand them in cell culture medium supplemented with 10% FCS, 1% P/S, 1% Hepes and 5 ng/mL FGF (see Herrmann et al., 2016 for further information on the isolation procedure).

Critical step: Use cells in passage 2–6 for seeding into scaffolds.

Note: The present protocol has been optimized with human bone marrow derived MSCs but other cells might be theoretically applied.

6. Use trypsin-EDTA solution to detach and count cells.
7. Resuspend 800,000 cells in 20 μ L of cell culture medium.

Note: These values are optimized for one cylindrical scaffold of 3 mm thickness and 5 mm diameter. Other scaffold designs can be used. Adjust the cell number and seeding volume with the respective scaffold volume. Depending on the experimental conditions, cell densities might be adapted as well.

8. Place the scaffolds in the middle of a non-treated well of a 12-well plate.

Critical step: Aspirate the remaining cell culture medium that may be present in the scaffold carefully with a vacuum pump, otherwise cell suspension would be diluted upon seeding.

9. Seed cell suspension drop-wise exactly on top of the scaffold.

Critical step: It is essential that the cell suspension volume does not leak out of the scaffold to the well plate.

10. Transport the plates carefully to an incubator and allow cells to adhere to the scaffold for 3 h at 37°C.

11. Add 3 mL per well of cell culture medium supplemented with 10% FCS, 1% P/S and 1% Hepes to each well and incubate cells again.

12. 24 h after seeding, transfer scaffolds to a new non-treated 12-well plate and add new medium.

Critical step: This step is crucial to discard cells that did not adhere to the scaffold.

6 Related techniques: Characterization of decellularized bone scaffolds

6.1 Calcium release assay

In order to confirm the complete decalcification of the scaffold, a calcium release assay can be performed on scaffolds processed according to the decellularization protocol and compared with native tissue.

1. Incubate scaffolds (approx. 25 mg dry weight each) in 1 mL of 1 M HCl (UN1789, Merck) with mild agitation at room temperature for 24 h.

6 Related techniques: Characterization of decellularized bone scaffolds 133

2. Collect 10 μ L of acid solution overtime (1–24 h) and analyze the calcium present in the solution using a colorimetric kit (CA590, Randox Laboratories Ltd.) according to the manufacturer's recommendations/protocol.

It is expected to measure no calcium ions in the solution from samples previously exposed to the decalcification protocol, while for native tissue a strong release of calcium is expected in the first 4 h of incubation followed by a plateau phase.

6.2 Cryosectioning and structural characterization

With the purpose to gain insight in the final scaffold structure in detail, as well as its protein composition, cryostat embedding techniques and further histology and immunochimistry staining protocols can be applied to the sections of processed scaffolds.

1. Fix processed scaffolds in 4% PFA (11762, Morphisto Laborchemikalien & Histologieservice) at 4 °C for 30 min. View safety 4.
2. Rinse twice with PBS.
3. Embed each scaffold in Tissue-Tek[®] O.C.T.[™] Compound (4583, Sakura Finetek) using a vinyl specimen Tissue-Tek[®] Cryomolds 15 × 15 × 5 mm (4566, Sakura Finetek).
4. Snap-freeze samples in liquid nitrogen. Samples can be stored at –80 °C until further use.
5. Cut sections of 10 μ m thickness in cryostat (CM1850 UV, Leica) with a chamber temperature of –22 °C and mount sections on Superfrost[®] plus microscope slides (J1800AMNZ, Thermo Scientific). Samples can be stored at this point at –20 °C (short term) or –80 °C (long term) until further staining.

To confirm the conservation of tissue morphology, a common Hematoxylin and Eosin (H&E) staining can be performed on the sections (see Fig. 3A). A highly open porous structure and the presence of canaliculi and empty lamellae in the trabecula can be observed (see Fig. 3B). The efficiency of decellularization can be confirmed with a simple nuclei staining, e.g., DAPI, where the absence of signal is indicative of a complete decellularization of the native tissue (see Fig. 3C and D). For analysis of the protein composition, immunofluorescence staining of the sections is required. Several antibodies specific for bone extracellular matrix components can be applied (e.g., collagen type-I, see Fig. 3E).

Note that decellularized bone scaffolds have an intrinsic auto-fluorescence for most of the common fluorescence parameters; therefore, special care should be taken during immunofluorescence analysis. For instance, background signal in DAPI staining is easily distinguished from nuclear positive staining by its low intensity and homogeneous non-specific distribution throughout the entire scaffold, in contrast with the strong and localized nuclear signal to be expected

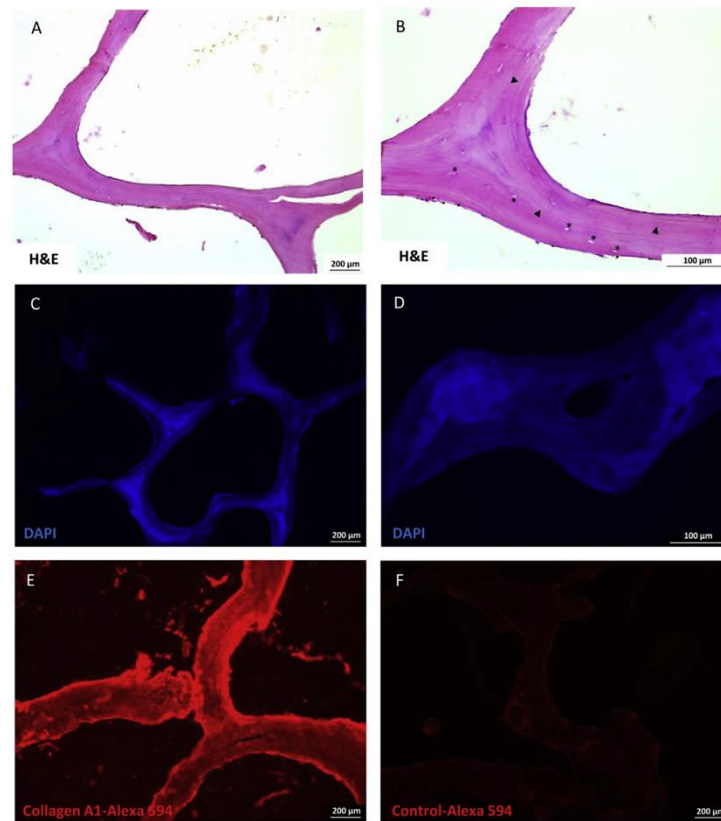


FIG. 3

Decellularized bone structure characterization using cryosectioning and different staining techniques. (A, B) H&E staining. Black asterisks in (B) mark empty lacunae and black arrows point to structural canaliculi in the former bone trabecula. (C, D) DAPI imaging for nucleic acid staining. (E) Collagen type-A1 immunofluorescence using a secondary antibody conjugated with Alexa Fluor 594 dye. (F) Negative control for unspecific binding of the secondary antibody Alexa Fluor 594.

if remaining cells were present (not shown). For immunocytochemistry of proteins, an isotype and/or secondary antibody only control should be used to define unspecific binding noise as well as the background signal due to auto-fluorescence.

6.3 Micro-computed tomography (micro-CT)

The characterization of the porosity of the scaffold, its interconnectivity and anisotropy is a central step in order to have a concrete measure to confirm the preservation of the native human bone structure. Processing of micro-CT scans allows to (i) obtain the bone volume fraction per total volume of the scaffold, which gives the inverted porosity value; (ii) the distribution of actual pore size through 3D thickness maps (see Fig. 4A); and (iii) the distribution of wall thickness (see Fig. 4B) which can be obtained by image digital inversion.

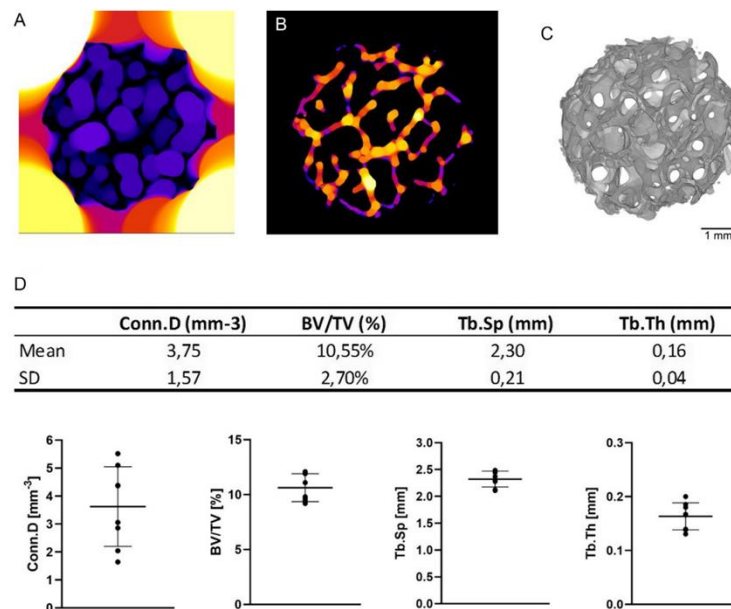


FIG. 4

Micro-CT analysis of decellularized human bone scaffolds. (A) Example of a resultant thickness heat map where it is possible to observe the pore distribution through the z-axis of the ROI. (B) Inverted image of the thickness map results in an illustration of the wall thickness, where brighter signal corresponds to thicker structures. (C) The ImageJ 3D viewer plugin returns a 2D volume projection in z-axis of a full scaffold. (D) Quantitative analysis of structural parameters given by the software, their respective mean and standard deviation ($n=6$). Abbreviations: Conn.D, connectivity density; BV/TV, Bone volume per total volume ratio; Tb.Sp, trabecular separation; Tb.Th, trabecular thickness.

136 CHAPTER 7 Decellularized human bone as a 3D model

1. Place up to three samples of the same donor horizontally in a customized holder for scanning.
2. Scan samples with an X-ray energy of 70kV tension and 0,114mA current for 200ms integration time.
3. Reconstruct the projections with an isotropic voxel size of 0,0105mm using appropriated software, e.g., Amira (Zuse Institute Berlin) or ImageJ (Schindelin et al., 2012) (see Fig. 4C).
4. Define the region of interest in the middle of each scaffold with a z-stack of 100 slices.
5. Apply a median filter of 2,0 points in order to mask the presence of porosity at a smaller scale.
6. Make a binary mask of the auto-threshold result image.
7. Apply a median filter of 4,0 points to reduce noise and smooth the resultant trabeculae mask stack.
8. Use BoneJ plugin (Doube et al., 2010) from ImageJ to obtain values and graphs of connectivity, volume fraction, and trabeculae thickness (see Fig. 4D).

6.4 Cell seeding efficiency

Because of the complexity and heterogeneity in the architecture of the scaffolds, seeding a high density of cells in a homogeneous way throughout the entire scaffold volume is a challenging task. In order to guarantee reproducibility of experiments, seeding efficiency needs to be checked. Efficiency of seeding can be extrapolated by counting the number of unattached cells (i.e., cells attached to the bottom of the well after 3 and 24h of adhesion plus the cells floating in media after 24h of culture), using the following equation:

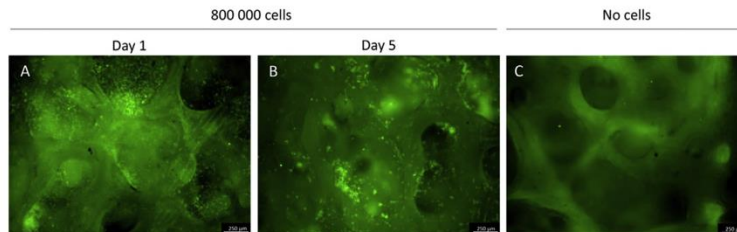
$$Eff = \frac{\text{Number of seeded cells} - \text{Number of unattached cells}}{\text{Number of seeded cells}} \times 100$$

For scaffolds of 5 mm diameter and an initial cell seeding of 800,000 cells, efficiencies between 75% and 90% are observed (n=5).

6.5 Cell tracking

In order to follow up the cell distribution over time as well, as their movement pattern throughout the scaffold volume, it is possible to pre-label cells with a fluorescent dye before seeding.

1. Harvest cells in expansion as described above in Section 5.2. Centrifuge and resuspend cells gently in pre-warmed cell tracking working solution (1 μM) (C2925, Invitrogen) in serum-free medium. Homogenize well in order to achieve a complete and efficient staining of all cells in the suspension.
2. Incubate suspension for 15 min at 37°C.
3. Add same volume of serum to the suspension to stop the labeling reaction.

**FIG. 5**

CellTracker green labeled cells seeded in the decellularized human bone scaffolds. Cells were imaged after 24 h of culture (A) and 5 days (B), where it is possible to observe a homogenous distribution of cells through the scaffold volume that also suggests a sustained cell viability over time. Scaffolds without cells present a strong auto-fluorescence for green laser (C), therefore it is important to compare the positive samples with an empty scaffold for background normalization. Scale bar: 250 μ m.

4. Centrifuge cells and resuspend in complete medium in the desired concentration for seeding.
5. Proceed with the usual cell seeding protocol.
6. Image cells under an inverted fluorescence microscope (Leica, DMI8) at different time-points of the experiment (see Fig. 5).

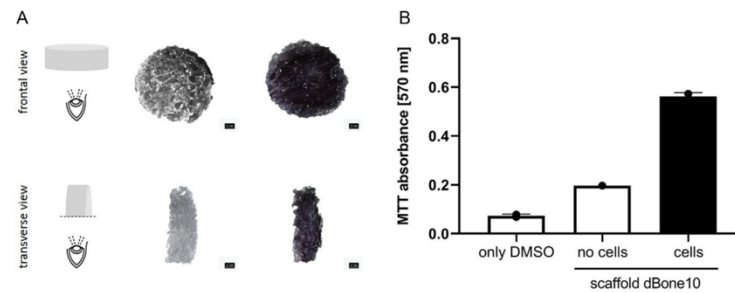
Note 1: It is possible to follow the cells continuously using time-lapse systems, when the microscope is equipped with a sterile chamber with controlled temperature, CO₂ supply and humidity.

Note 2: Inverted microscope imaging only allows for a short penetration depth for opaque samples. Other techniques, e.g., confocal and 2-photon microscopy, might be useful to gain insights of cell distribution in deeper layers of the scaffold.

6.6 Metabolic activity of cells: MTT-assay

Cell viability and distribution over the scaffold volume can be directly related to the conversion rate of thiazolyl blue tetrazolium blue (MTT) (M2128, Sigma-Aldrich) into a purple insoluble formazan by mitochondrial active reductase enzymes. The strong purple precipitates formed in the scaffold allow to take conclusions about homogeneous distribution of cells (see Fig. 6A). While measurements of the supernatant absorbance after dissolving of crystals in dimethyl sulfoxide (DMSO) (D8418, Sigma-Aldrich), returns a quantifiable method to compare cell viability (see Fig. 6B).

1. After culturing cells, add 10% MTT solution (5 mg/mL in PBS) to the total medium volume.
2. Incubate the plate for 3 h at 37 °C.

**FIG. 6**

Cell viability assay: MTT staining and quantification. (A) Decellularized bone scaffolds (dBone) of 10mm diameter seeded with 800,000 cells were stained with MTT after 7 days in basal culture medium. Front and transverse images were acquired. Scaffolds without cells were used as negative control, resulting in only weak background staining (left). A strong and homogenous stain was observed in scaffolds seeded with cells (right), indicating a sustained cell viability and a proper cell distribution over the scaffold volume. Scale bar: 1 mm. (B) Quantification of MTT dye dissolved in DMSO. Scaffolds without cells show absorbance values higher than the DMSO blank measurement due to background noise of the scaffold (n=3).

3. Remove MTT solution carefully.
4. Wash with PBS and take pictures of stained scaffolds under a stereomicroscope (Zeiss, Discovery.V20).
5. Add 1 mL of DMSO into each well. Wrap plate in foil and incubate 40 min at 37°C under gentle agitation.
6. Transfer 100 µL of the supernatant to a new 96-well plate and read absorbance at OD = 570 nm within 1 h.

7 Safety considerations

1. Only after confirmation of negative disease report from the clinic, e.g., HIV, Hepatitis B (HBs antigen and anti-HBc) and Hepatitis C (anti-HCV), samples can be handled in biosafety level 1 facilities, according to German law.
2. Sodium azide is a strong preservative to prevent decomposition by microbial growth. It is fatal if swallowed, inhaled or contact with skin. It may cause damage to organs through prolonged or repeated exposure.
3. The chloroform/methanol mixture is a highly flammable liquid. It is harmful if inhaled and may cause respiratory and digestive tract irritation. For this step and the next two washing steps work under a fume hood.

4. Formaldehyde is a hazardous agent that can trigger an allergic reaction in respiratory and skin tissue after single or repeated exposures. It is classified as a known human carcinogen by the International Agency for Research on Cancer.

8 Troubleshooting

Problem	Possible solutions
1. There is too much remaining fat tissue in the final scaffolds	Chloroform wash (step 8 of protocol for preparation of decellularized bone scaffolds) should be optimized with longer times of incubation and/or higher volumes of wash solution
2. Final scaffolds are still too hard (not completely decalcified)	Decalcification time during EDTA incubation (step 12 of protocol for preparation of decellularized bone scaffolds) can be optimized with a non-invasive X-ray scan. Using as control a sample of the same native not-treated bone, complete decalcification is achieved when no bright spots are detected in X-rays of treated samples
3. Enzymatic treatments are not performing efficiently	In order to avoid to dilute new solutions with the remains of the previous wash, is recommended to use a sieve (60BS8F, Advantech Manufacturing Inc.) to transfer scaffolds between solutions. The use of an absorbent paper to soak the liquid from inside of the scaffolds is also suggested

9 Conclusion

Regardless the potential and recognized aforementioned advantages, there are however limitations to the use of tissue-derived materials in tissue engineering applications. There are significantly different reported methods of tissue decellularization processing, making it challenging to draw conclusions about the efficacy and safety of the final constructs. Due to the lack of guidelines with regards to ECM composition, individual studies are applying different methods, which may cause disruption of the architecture and/or surface composition, resulting in very variable outcomes. It is therefore desirable to decide for a standardized protocol with proven efficiency, as proposed in this manuscript, in order to pave the way for a more consistent and robust research in the field of bone decellularization.

In conclusion, the above described protocol provides a method for the production of standardized scaffolds fulfilling bone tissue engineering requirements. These scaffolds do not only provide physical support for cells but also present a bone-like microenvironment which allows a more complete understanding of the underlying mechanisms of *in vivo* biology and tissue remodeling that may help to bridge the gap between fundamental research and clinical application.

References

- Bader, A., Schilling, T., Teebken, O. E., Brandes, G., Herden, T., Steinhoff, G., et al. (1998). Tissue engineering of heart valves—human endothelial cell seeding of detergent acellularized porcine valves. *European Journal of Cardio-Thoracic Surgery*, 14(3), 279–284.
- Badylak, S. (2004a). *Decellularized liver for repair of tissue and treatment of organ deficiency*. Google Patents.
- Badylak, S. F. (2004b). Xenogeneic extracellular matrix as a scaffold for tissue reconstruction. *Transplant Immunology*, 12(3–4), 367–377.
- Badylak, S. F., Lantz, G. C., Coffey, A., & Geddes, L. A. (1989). Small intestinal submucosa as a large diameter vascular graft in the dog. *Journal of Surgical Research*, 47(1), 74–80.
- Bianco, J. E. R., Rosa, R. G., Congrains-Castillo, A., Joazeiro, P. P., Waldman, S. D., Weber, J. F., et al. (2019). Characterization of a novel decellularized bone marrow scaffold as an inductive environment for hematopoietic stem cells. *Biomaterials Science*, 7(4), 1516–1528.
- Buñewicz, B., & Rosen, B. (2004). Acellular cadaveric dermis (AlloDerm): A new alternative for abdominal hernia repair. *Annals of Plastic Surgery*, 52(2), 188–194.
- Clark, J. M., Saffold, S. H., & Israel, J. M. (2003). Decellularized dermal grafting in cleft palate repair. *Archives of Facial Plastic Surgery*, 5(1), 40–44.
- Crapo, P. M., Gilbert, T. W., & Badylak, S. F. (2011). An overview of tissue and whole organ decellularization processes. *Biomaterials*, 32(12), 3233–3243.
- Doube, M., Klosowski, M. M., Arganda-Carreras, I., Cordelières, F. P., Dougherty, R. P., Jackson, J. S., et al. (2010). BoneJ: Free and extensible bone image analysis in ImageJ. *Bone*, 47(6), 1076–1079.
- Elliott, R. A., Jr., & Hoehn, J. G. (1973). Use of commercial porcine skin for wound dressings. *Plastic Reconstructive Surgery*, 52(4), 401–405.
- Freyman, T. (2008). *Decellularized bone marrow extracellular matrix*. Google Patents.
- Gilbert, T. W., Sellaro, T. L., & Badylak, S. F. (2006). Decellularization of tissues and organs. *Biomaterials*, 27(19), 3675–3683.
- Hashimoto, Y., Funamoto, S., Kimura, T., Nam, K., Fujisato, T., & Kishida, A. (2011). The effect of decellularized bone/bone marrow produced by high-hydrostatic pressurization on the osteogenic differentiation of mesenchymal stem cells. *Biomaterials*, 32(29), 7060–7067.
- Herrmann, M., Bara, J., Sprecher, C., Menzel, U., Jalowiec, J., Osinga, R., et al. (2016). Pericyte plasticity—Comparative investigation of the angiogenic and multilineage potential of pericytes from different human tissues. *Cells & Materials*, 31, 236–241.
- Herson, M. R., Mathor, M. B., Altran, S., Capelozzi, V. L., & Ferreira, M. C. (2001). In vitro construction of a potential skin substitute through direct human keratinocyte plating onto decellularized glycerol-preserved allodermis. *Artificial Organs*, 25(11), 901–906.
- Korossis, S. A., Booth, C., Wilcox, H., Watterson, K., Kearney, J., Fisher, J., et al. (2002). Tissue engineering of cardiac valve prostheses II: Biomechanical characterization of decellularized porcine aortic heart valves. *The Journal of Heart Valve Disease*, 11(4), 463–471.
- Lee, D. J., Diachina, S., Lee, Y. T., Zhao, L., Zou, R., Tang, N., et al. (2016). Decellularized bone matrix grafts for calvaria regeneration. *Journal of Tissue Engineering*, 7, 2041731416680306.
- Lin, P., Chan, W. C., Badylak, S. F., & Bhatia, S. N. (2004). Assessing porcine liver-derived biomatrix for hepatic tissue engineering. *Tissue Engineering*, 10(7–8), 1046–1053.

- Merguerian, P., Reddy, P., Barrieras, D., Wilson, G., Woodhouse, K., Bagli, D., et al. (2000). Acellular bladder matrix allografts in the regeneration of functional bladders: Evaluation of large-segment (>24 cm²) substitution in a porcine model. *BJU International*, 85(7), 894–898.
- Probst, M., Piechota, H., Dahiya, R., & Tanagho, E. (2000). Homologous bladder augmentation in dog with the bladder acellular matrix graft. *BJU International*, 85(3), 362–371.
- Sawkins, M., Bowen, W., Dhadda, P., Markides, H., Sidney, L., Taylor, A., et al. (2013). Hydrogels derived from demineralized and decellularized bone extracellular matrix. *Acta Biomaterialia*, 9(8), 7865–7873.
- Schindelin, J., Arganda-Carreras, I., Frise, E., Kaynig, V., Longair, M., Pietzsch, T., et al. (2012). Fiji: An open-source platform for biological-image analysis. *Nature Methods*, 9(7), 676.
- Schönmeyr, B. H., Wong, A. K., Li, S., Gewalli, F., Cordero, P. G., & Mehrara, B. J. (2008). Treatment of hydroxyapatite scaffolds with fibronectin and fetal calf serum increases osteoblast adhesion and proliferation in vitro. *Plastic and Reconstructive Surgery*, 121(3), 751–762.
- Sladkova, M., Cheng, J., Palmer, M., Chen, S., Lin, C., Xia, W., et al. (2019). Comparison of decellularized cow and human bone for engineering bone grafts with human induced pluripotent stem cells. *Tissue Engineering Part A*, 25(3–4), 288–301.
- Smith, C., Richardson, S., Eagle, M., Rooney, P., Board, T., & Hoyland, J. (2015). The use of a novel bone allograft wash process to generate a biocompatible, mechanically stable and osteoinductive biological scaffold for use in bone tissue engineering. *Journal of Tissue Engineering Regenerative Medicine*, 9(5), 595–604.
- Sun, X.-J., Peng, W., Yang, Z.-L., Ren, M.-L., Zhang, S.-C., Zhang, W.-G., et al. (2011). Heparin-chitosan-coated acellular bone matrix enhances perfusion of blood and vascularization in bone tissue engineering scaffolds. *Tissue Engineering Part A*, 17(19–20), 2369–2378.
- Tran, N. M.-P., Nguyen, D. T., Dai Luong, T., Bui, N. H., Van Toi, V., & Nguyen, T.-H. (2018). Decellularization of bovine cancellous bone for bone tissue engineering application. In *Paper presented at the international conference on the development of biomedical engineering in Vietnam*.
- Urist, M. R. (1965). Bone: Formation by autoinduction. *Science*, 150(3698), 893–899.

Chapter 3.

Results: Decellularized bone ECM for MSC culture

In this chapter, different *in vitro* bone models (2D cell-derived matrices and 3D tissue-derived scaffold) based on decellularization techniques were developed, aiming to provide an alternative method to bypass the limitations imposed by the current approaches to study the stem cell niche. Particularly, for the first time, comparative exploratory proteomics analysis of both models provided significant insights towards the identification of novel targets of native bone tissue-specific ECM.

The work on this chapter was submitted as an original research-article to the Journal of Tissue Engineering. At the time of submission of this thesis, peer-review process is still in progress. Reprint permission was obtained from all co-authors and from the publisher under Creative Commons license (CC BY).

Reference: Pereira AR, Trivanović D, Stahlhut P, Weissenberger M, Groll J and Herrmann M. Preservation of the naïve mesenchymal stromal cell phenotype in vitro: comparison of cell- and bone-derived decellularized extracellular matrix. J. Tissue Eng., 2021 (in revision).

Original Article

Preservation of the naïve features of mesenchymal stromal cells *in vitro*: comparison of cell- and bone-derived decellularized extracellular matrix

Ana Rita Pereira^{1,2}, Drenka Trivanović^{1,2}, Philipp Stahlhut³, Maximilian Rudert⁴, Jürgen Groll³ and Marietta Herrmann^{1,2,*}

¹ IZKF Group Tissue Regeneration in Musculoskeletal Diseases, University Hospital Wuerzburg, Wuerzburg, Germany.

² Bernhard-Heine-Centrum for Locomotion Research, University of Wuerzburg, Wuerzburg, Germany.

³ Chair for Functional Materials in Medicine and Dentistry and Bavarian Polymer Institute, University of Wuerzburg, Wuerzburg, Germany.

⁴ Department of Orthopedic Surgery, Koenig-Ludwig-Haus, University of Wuerzburg, Wuerzburg, Germany.

* Corresponding author: m-herrmann.klh@uni-wuerzburg.de

Abstract

The fate and behavior of bone marrow mesenchymal stem/stromal cells (BM-MSC) is bidirectionally influenced by their microenvironment, the stem cell niche, where a magnitude of biochemical and physical cues communicate in an extremely orchestrated way. It is known that simplified 2D *in vitro* systems for BM-MSC culture do not represent their naïve physiological environment. Here, we developed four different 2D cell-based decellularized matrices (dECM) and a 3D decellularized human trabecular-bone scaffold (dBone) to evaluate BM-MSC behavior. The obtained cell-derived matrices provided a reliable tool for cell shape-based analyses of typical features associated with osteogenic differentiation at high-throughput level. On the other hand, exploratory proteomics analysis identified native bone-specific proteins selectively expressed in dBone but not in dECM models. Together with its architectural complexity, the physico-chemical properties of dBone triggered the upregulation of stemness associated genes and niche-related protein expression, proofing *in vitro* conservation of the naïve features of BM-MSC.

Keywords: Decellularization, bone model, stem cell niche, stemness, osteogenesis, 3D models.

Introduction

Mesenchymal stem/stromal cells (MSC) are rare, self-renewing, multipotent cells, responsible for maintaining skeletal tissues' homeostasis. Since the discovery of MSC in bone marrow (BM)¹, similar cell populations with proliferative competence, an undifferentiated phenotype and the ability to differentiate into osteoblastic, adipogenic and chondrogenic lineages *in vitro*, have been identified and reported in many adult²⁻⁴ and perinatal tissues⁵⁻⁷. Due to MSC's ability to colonize and differentiate into a multitude of tissue and cell types, these cells are suitable candidates to treat many degenerative congenital abnormalities and diseases⁸. Although widely distributed, it seems that MSC are not uniform populations. Moreover, literature exists demonstrating that stem cell fate of MSC is highly dependent and controlled by the tissue-specific surrounding environment⁹, and perturbations in the matrix as a result of inflammation or disease progression^{10,11}. In fact, adult tissues retain unique *milieus*, known as stem cell niches, defined by their anatomic location and protective surrounding, where multipotent cells are self-maintained in quiescence and/or mobilized in response to stimuli. These niches protect stem cells from depletion during adult life, preventing their uncontrolled proliferation and differentiation. The concept of a stem cell niche has become more complex since its first definition was proposed by Schofield in 1978 in the context of the hematopoietic microenvironment¹²; stem cell niches constitute a basic unit of tissue physiology, with not only well-defined anatomical but also with functional dimensions. A primary function of the niche is to provide physical anchorage to stem cells, mainly via RGD-mediated adhesion molecules¹³. In BM, the location and identification of MSC is controversially

discussed due to the lack of distinct surface markers to identify these cells *in vivo*. Recent studies suggested that at least three different osteoblastic niches for skeletal progenitor cells exist, in particular at endosteal, perivascular and stromal regions (reviewed in ¹¹), implying distinct functions in tissue maintenance and regeneration ¹⁴. It is clear that standard *in vitro* monolayer culture approaches do not recapitulate this environmental complexity, thus causing a widely observed translational gap from *in vitro* results to the *in vivo* situation and clinics. Moreover, from a biochemical perspective, the niche-specific extracellular matrix (ECM) regulates stem cell fate in an extremely well-orchestrated manner ¹⁵, triggering intracellular signaling pathways either by (1) directly binding to cellular receptors, or indirectly (2) presenting non-canonical growth factors and (3) generating stress gradients of e.g. oxygen content or mechanical forces due to its physical properties and spatial orientation. In fact, the ECM network is not an arbitrary arrangement of structural proteins. Common ECM proteins such as collagens, fibronectin, vitronectin, and proteoglycans exhibit conserved motifs assigned to keenly bind several growth factors and bone morphogenic proteins (BMPs), hence acting as an insoluble localized reservoir of morphogens ^{16, 17}. Meanwhile, proteolytic enzymes, such as matrix metalloproteinases (MMPs), locally break ECM proteins, resulting in a confined release of soluble growth factors from their insoluble anchorage ^{18, 19}. Likewise, physical properties of the microenvironment such as stiffness, porosity and topography are also constantly being remodeled and may as well influence various anchorage-related biological functions, such as cell division, tissue polarization and cell migration ^{20, 21}. Importantly, all these characteristics and properties are intrinsically related and can mutually influence each other. This becomes even more evident when one considers cell-ECM communication (or relations) as bidirectional interactions, wherein cells constantly rebuild their surroundings, thus untimely influencing their own fate ²²⁻²⁴. It follows from this that great efforts have been made in the field of tissue engineering using advanced biomaterials to recapitulate these unique niche conditions in *ex vivo* culture. The key universal goal is to avoid the persistently observed ‘ageing’ process of cells during long-lasting *in vitro* cultivation – i.e., cell shape change, and significantly decreased colony-forming and differentiation potential ^{25, 26}. Indeed, it is now widely recognized that 2D cultures, despite their numerous advantages in regard to simplicity, impose artificial spatial limits to cell-matrix interactions and mechanical transduction processes. Consequently, those limitations ultimately strongly influence cell biological functions and response to stimuli ²⁷, resulting in potentially misleading results towards clinic applications. A wide variety of material alternatives have been developed to recreate the tissue-specific ECM composition and intricate structure of stem cell niches ²⁸⁻³¹, albeit a single *in vitro* model that reproduces the *in vivo* microenvironment homeostasis remains a bioengineering challenge. Aiming to address this issue, decellularization of cell-derived ECM, tissues and organs came as an ideal reverse-engineering concept able to faithfully mimic the native tissue complexity. Through physical, chemical and/or enzymatic treatments, the central goal of decellularization protocols is to preserve the above-mentioned biochemical complexity and mechanical integrity of the tissue, while efficiently removing all cellular elements to prevent any immunological reaction ³². Decellularized tissue constructs have been successfully applied for several years in tissue engineering and regenerative medicine, mainly designed for rather simple tissues, e.g., heart valve substitutes ^{33, 34}, skin grafts ^{35, 36}, bladder mucosa grafts ^{37, 38}, etc. Particularly, decellularized bone ECM-derived constructs – e.g., (1) *in vitro* MSC-produced decellularized ECM constructs ³⁹ and (2) bioactive 3D scaffolds originated from trabecular ^{40, 41} or cortical decellularized bone ⁴² – have gained a lot of interest as implantable biomaterials for bone tissue repair and regeneration, due to their biochemical properties and their unique mechanical properties and architecture.

In this study, we developed and characterized unique human bone ECM models (2D and 3D) based on decellularization techniques, aiming to identify intrinsic ECM regulatory factors in either basal or osteogenic settings, which may be responsible for maintenance of MSC stem-cell competence *in vitro* and their response to homeostatic and extrinsic signals.

Materials and methods

BM-MSc isolation and expansion

MSC were isolated from human BM acetabular reaming of patients undergoing hip arthroplasty surgery after obtaining informed consent of the patient (Ethical approval (187/18)). Briefly, mononuclear cells were collected from BM material by Ficoll (Histopaque®-1077, Sigma-Aldrich, Germany) density gradient centrifugation and repeatedly washed. To obtain adherent BM-MSc fraction, cells were cultured and further expanded in culture medium (DMEM/F-12 GlutaMAX, 31331-028, Gibco, Germany) supplemented with 10% fetal calf serum (FCS, Bio&Sell, Germany), 1% Pen/Strep (P4333, Gibco), 1% HEPES (H0887, Sigma-Aldrich), and 5 ng/mL fibroblast growth factor (FGF, 100-18C, PeproTech, Germany) at 37°C in a humidified atmosphere and 5% CO₂. Culture medium was replaced 3 times a week. Cells were detached from culture flasks by trypsinization (T4174, Sigma-Aldrich), centrifuged and washed. Cell number and viability were assessed with the trypan-blue dye (93595, Sigma-Aldrich) exclusion test. BM-MSc in passage 4-6 were used for the experiments.

2D decellularized matrices (dECM) production

We often observed delamination of newly formed ECM of decellularization cultures on conventional tissue culture plastic well plates (data not shown). In order to achieve robustly anchored native dECM, BM-MSc were seeded on 13 mm treated-coverslips (174950, Thermo Scientific Nunc, USA) at a density of 2×10^4 cells/cm². Cells were cultivated for an accommodation period of 48 h in DMEM/F-12 GlutaMAX medium supplemented with 10% FCS, 1% Pen/Strep and 1% HEPES, before starting the matrix production phase. Four different models were created combining two variables: the time of culture (10 or 21 days) and media supplementation (basal: DMEM/F-12 GlutaMAX medium supplemented with 10% FCS, 1% Pen/Strep, 1% HEPES, and 50 µg/mL L-Ascorbic acid 2-phosphate (ASC, A8960, Sigma-Aldrich); osteo: DMEM low glucose medium (D6046, Sigma-Aldrich) supplemented with 10% FCS, 1% Pen/Strep, 1% HEPES, 50 µg/mL ASC, 5 mM β-Glycerophosphate disodium salt (β-GP, G9422, Sigma-Aldrich) and 10 nM dexamethasone (D4902, Sigma-Aldrich)). After the matrix production phase, all different types of cultures were exposed to a mild decellularization protocol. First, monolayers were washed 2 times with phosphate-buffered saline without calcium and magnesium (PBS, D8537, Sigma-Aldrich), and incubated in lysis buffer (20 mM ammonia (1.05432.1011, Merck, Germany) in 0.5% (v/v) PBS-Triton X100 (3051.3, Carl Roth, Germany) solution) for 10 min at 37°C under gentle agitation. Next, monolayers were washed repeatedly with excess of PBS before complete decellularization of matrices with DNase 100 Units/mL (DN25, Sigma-Aldrich) dissolved in 0.15 M sodium chloride (NaCl, P029.3, Carl Roth) incubation for 1 h at 37°C under gentle agitation. dECM were finally washed twice with PBS and stored for no longer than 1 month at 4°C in PBS supplemented with 1% Pen/Strep until allogenic BM-MSc seeding.

Decellularization efficiency

In order to access the efficiency of the decellularization protocol, matrices for each condition were fixed in 4% paraformaldehyde (PFA, 11762, Morphisto, Germany) just after the matrix production phase and respectively after the complete decellularization protocol. Monolayers were washed twice with excess of PBS, followed by staining of cell nuclei with 4',6-diamidino-2-phenylindole (DAPI, H-1200, Vectashield, USA). Coverslips were mounted on slides for fluorescence microscopy and DAPI channel images were acquired (DMI8, Leica, Germany) for each condition. Cell counting was performed with a Fiji analysis plugin (version 2.1.0/1.53f) and calculated for a total area of 1 cm² per sample (4 region of interested selected per condition for 7 individual experiment).

Preparation of Decellularized Bone Scaffolds

Decellularized bone scaffolds were obtained from human trabecular femoral head specimens (permission number: 187/18, University of Wuerzburg ethics committee), as previously described in ^{24, 43}. Briefly, freshly thawed samples (kept at -20°C for no more than 4 months after surgery) were precisely cut in 3 mm thick slices using an electric diamond band saw (300 Exakt D64, Walter Messner, Germany) to ensure homogeneous penetration of washing solutions through the complete sample volume. Blood and residual fat material were removed by several washing cycles in water and a chloroform (288306, Sigma-Aldrich) and methanol (8388.6, Carl-Roth) mix solution. Further decalcification of bone slices was achieved by incubation for several days in 2.5% ethylenediaminetetraacetic acid (EDTA, E5134, Sigma-Aldrich) in 10 mM Tris-base (T6066, Sigma-Aldrich), from where cylindrical constructs with a diameter of 5 mm were shaped using a biopsy punch (05.SF004, Stiefel, Germany). Complete decellularization of bone samples was achieved by enzymatic treatment with 100 Units/mL DNase and finalized with lyophilization (Martin Christ, Alpha 1–2 LDplus, Germany) for 4 days under a vacuum pressure of 1 mbar. Processed bone scaffolds were stored at -20 °C. For sterilization, scaffolds were incubated with 70% ethanol one day before cell seeding.

Protein extraction: electrophoresis and western-blot

For analysis of protein content in the decellularized models, matrices were collected in 1mL of RIPA buffer (89901, Thermo Fisher Scientific) supplemented with proteinase inhibitor cocktail (78440, Thermo Fisher Scientific). Homogenization of samples was performed by cycles of sonification (20x: 2 s 80% peak followed by 28 s break, Sonopus HD 4100, Bandelin, Germany) and the total amount of protein quantified using a Pierce BCA kit (23227, Thermo Fisher Scientific). Samples were reduced in the presence of 2-mercaptoethanol at 95°C for 10 min and 10 µg of total protein per condition were loaded on 10% polyacrylamide gels followed by sodium dodecyl sulfate (SDS) separation through electrophoresis (PAGE). Coomassie staining was performed for dECM characterization – enriched rat-tail Collagen-type I (C3867, Sigma-Aldrich) and FCS were run in parallel as controls. For western-blot analysis, 3 individual donors were used for each condition. Proteins were transferred to the nitrocellulose membrane (10600001, GE Healthcare, Germany) for 1 h and then blocked overnight at 4°C with 5% BSA in Tris (A4577, Applichem, Germany)-buffered saline with 0.1% Tween-20 (P1379, Sigma-Aldrich). Next, membranes were incubated with primary antibodies (dilution 1:2000, Col1 (ab35710, abcam, Germany), type-VI collagen (Col6, MA5-32412, Thermo Fisher Scientific) and Fetuin-A (Fet-A, homemade serum no. 5359 kindly provided by Prof. W. Jahnen-Dechent, RWTH Aachen University)) overnight at 4°C following incubation with secondary anti-rabbit immunoglobulin G (IgG) antibody conjugated with horseradish peroxidase (dilution 1:5000, ab205718, abcam). Finally, blots were developed by the enhanced chemiluminescence method with Chemiluminescent HRP substrate (541015, Biozym, Germany) and images acquired with the FluorChem Q imaging System (Cell Biosciences, Germany). Semi-quantification of the bands was carried out by optical densitometry and analyzed using the Fiji Gel plugin menu (version 2.1.0/1.53f). The expression of each protein is presented in relation to Col1 expression.

Proteomics analysis: mass spectrometry (MS)

For proteomics studies one sample for each condition was analyzed by MS. Briefly, protein precipitation was performed overnight at -20°C with 4x volume of acetone. Pellets were washed with acetone at -20°C. Precipitated proteins were dissolved in NuPAGE® LDS sample buffer (NP0007, Thermo Fisher Scientific), reduced with 50 mM DTT at 70 °C for 10 minutes and alkylated with 120 mM Iodoacetamide at room temperature for 20 minutes. Separation was performed on NuPAGE® Novex® 4-12 % Bis-Tris gels (NP0321PK2, Thermo Fisher Scientific) with MOPS buffer according to manufacturer's instructions. Gels were washed three times for 5 min with water and stained for 1 h

with Simply Blue™ Safe Stain (LC6065, Thermo Fisher Scientific). After washing with water for 1 h, each gel lane was cut into 15 slices. The excised gel bands were destained with 30 % acetonitrile in 0.1 M NH₄HCO₃ (pH 8), shrunk with 100 % acetonitrile, and dried in a vacuum concentrator (5301, Eppendorf, Germany). Digests were performed with 0.1 µg trypsin per gel band overnight at 37 °C in 0.1 M NH₄HCO₃ (pH 8). After removing the supernatant, peptides were extracted from the gel slices with 5 % formic acid, and extracted peptides were pooled with the supernatant.

NanoLC-MS/MS analyses were performed on a LTQ-Orbitrap Velos Pro (Thermo Fisher Scientific) equipped with a PicoView Ion Source (New Objective) and coupled to an EASY-nLC 1000 (Thermo Fisher Scientific). Peptides were loaded on a trapping column (2 cm x 150 µm ID, PepSep) and separated on capillary columns (30 cm x 150 µm ID, PepSep, Denmark) both packed with 1.9 µm C18 ReproSil and separated with a 30 min linear gradient from 3% to 30% acetonitrile and 0.1% formic acid and a flow rate of 500 nL/min. MS scans were acquired in the Orbitrap analyzer with a resolution of 30000 at m/z 400, MS/MS scans were acquired in the Orbitrap analyzer with a resolution of 7500 at m/z 400 using HCD fragmentation with 30% normalized collision energy. A TOP5 data-dependent MS/MS method was used; dynamic exclusion was applied with a repeat count of 1 and an exclusion duration of 30 seconds; singly charged precursors were excluded from selection. Minimum signal threshold for precursor selection was set to 50000. Predictive AGC was used with AGC target a value of 1e6 for MS scans and 5e4 for MS/MS scans. Lock mass option was applied for internal calibration in all runs using background ions from protonated decamethylcyclopentasiloxane (m/z 371.10124). Raw MS data files were analyzed with MaxQuant version 1.6.2.2⁴⁴. Database search was performed with Andromeda, which is integrated in the utilized version of MaxQuant. The search was performed against the UniProt Human database. Additionally, a database containing common contaminants was used. The search was performed with tryptic cleavage specificity with 3 allowed miscleavages. Protein identification was under control of the false-discovery rate (1% FDR on protein and peptide level). In addition to MaxQuant default settings, the search was performed against following variable modifications: Protein N-terminal acetylation, Gln to pyro-Glu formation (N-term. Gln) and oxidation (Met). Carbamidomethyl (Cys) was set as fixed modification.

Proteins of particular interest were selected based on their involvement in the following groups: bone extracellular matrix components, intracellular and membrane proteins, and hematopoietic compartment related proteins. The intensity based absolute quantification (iBAQ) log₁₀ transformed values calculated by the software algorithm were plotted in heatmap graphs corresponding to the molar quantities found for each protein using official gene symbols.

Scanning electron microscopy (SEM) and energy dispersive x-ray spectroscopy (EDS)

The ultrastructure of decellularized-matrices and BM-MSc morphology (initial seeding: 10⁴ cells per cm²) were evaluated for each cell-seeded model after 48 h of basal culture, i.e., cultivation in standard BM-MSc expansion medium without FGF, by SEM (Crossbeam 340 with secondary electron detector, Carl Zeiss, Germany). The samples were fixed on ice for 15 min with 6% glutaraldehyde (G5882, Sigma-Aldrich), dehydrated in a serial dilution of ethanol, dried in hexamethyldisilazane (440191, Sigma-Aldrich) and stored at 4°C. Prior to imaging, all samples were sputter-coated (EM ACE600, Leica, Germany) with a 4 nm film of platinum to ensure conductivity of the sample's surface. Images were taken at an acceleration voltage equal to 2-3 kV. Cellular details were artificially colored on magnified images using Photoshop® CS6 (Adobe, v13.0.1) for visualization purposes.

Additionally, dECM models without cells were also prepared and the surface atomic composition was evaluated using energy dispersive X-ray spectroscopy with a silicon drift detector (X-MaxN 50, Oxford Instruments, United Kingdom) setting the acceleration voltage of the SEM's electron beam to 10 kV. Two random areas of interest were evaluated for each sample. Mineral distribution and composition were analyzed using AZTech (Oxford Instruments).

Immunofluorescence staining and microscopy

Immunofluorescence analysis of matrix-associated bone proteins was performed to visualize their presence and distribution in the generated dECM models. Briefly, decellularized-monolayers were fixed in 4% PFA for 15 min at 4°C followed by blocking with 1% BSA-PBS (10735086001, Roch, Germany) for 1 h at room temperature and incubation with primary antibody (anti-Col1 (sc-293182, Santacruz, Germany), anti-laminin (sc-74418, Santacruz), anti-osteopontin (sc-21742, Santacruz), 1:500 dilution in 1% BSA-PBS) overnight at 4°C. After washing, samples were incubated with secondary antibody (goat anti-mouse IgG-FITC, sc-516140, Santacruz) for 2 h at room temperature. Finally, samples were slide-mounted for microscopy (H-1000, Vectashield, Germany) and representative pictures were acquired using a fluorescence microscope (DMI8, Leica).

To confirm expression of CXCL12 by BM-MSCs seeded on decellularized models after 5 days in basal culture (initial seeding: 10^4 cells per cm^2 for dECM models and 4×10^5 cells per dBone scaffold, seeding protocol previously described in ⁴³), immunofluorescence analysis was performed on both dECM monolayers and 12 μm cryosections of dBone scaffolds (sectioning protocol previously described in ⁴³). Samples were fixed in 4% PFA for 15 min at 4°C and permeabilized with 0.1% (v/v) Triton-X /PBS for 30 min at room temperature. BSA-blocking was performed for 1h before the overnight incubation with CXCL12-primary antibody (dilution 1:100, MAB350, R&D System, Germany) at 4°C. In addition, Phalloidin-iFluor 488 (dilution 1:500, ab176753, abcam) was added during primary antibody incubation for cell cytoskeleton visualization. After washing, samples were incubated with secondary antibody (dilution 1:100, goat anti-mouse IgG conjugated with Alexa Fluor® 594, ab150116, abcam) for 2 h at room temperature and embedded in mounting medium containing DAPI for nuclei staining. For all stainings, secondary antibody specificity controls were performed by executing the full protocol for each sample in the absence of primary antibody.

Cell shape analysis

For BM-MSCs morphology analysis, cells were seeded on dECM matrices at a density of 10^4 cells per cm^2 for 48 h in basal culture and then fixed with 4% PFA for 15 min. Cell and nuclear morphology were assessed using phalloidin and DAPI staining respectively, as previously described. Automated quantification of cellular shape features was performed using CellProfiler ⁴⁵ (version 4.0.6, pipeline description in Supplementary Fig. S1). Selection of poorly thresholded cells or overlapping parts was performed by unique numbering of individual segmented cells exported to the spreadsheet. At least 350 cells were assessed for each experimental group, with approximately equal numbers of cells analyzed from each of seven independent experiments. Overall morphological signatures were constructed for each group using nine cellular descriptive features (form factor, eccentricity, area, solidity, perimeter, aspect ratio, extent, orientation, compactness, area, aspect ratio and compactness).

Separate principal component analysis (PCA) was performed using single-cell morphological data (200 cells presented in density plots of PC space) using all available CellProfiler data given for four experiments ($n = 4$). Representative cells were chosen randomly from the centroids for each condition. Statistical significance of each significant parameter was evaluated with the mean value corresponding to each independent experiment ($n = 7$).

Alizarin-red staining

Matrix-mineral deposition was measured by Alizarin-red staining and subsequent quantification, according to standard protocols. To test the effect of the decellularization protocol, analysis was performed before and after decellularization for each dECM model. In addition, we assessed the osteogenic differentiation potential of seeded BM-MSCs (initial seeding: 2×10^4 cells per cm^2) after 21 days in osteogenic medium (DMEM low glucose medium supplemented with 10% FCS, 1% Pen/Strep, 1% HEPES, 50 $\mu\text{g}/\text{mL}$ ASC, 5 mM β -GP and 10 nM dexamethasone) or control conditions (osteogenic

medium without differentiation factors). Briefly, at the analysis timepoint cells were washed twice with cold PBS and fixed in 70% ethanol (T913.3, Carl Roth) for 1 h at -20°C. Monolayers were allowed to air-dry and mineral deposition was stained with 2% Alizarin-red solution (0223, ScienCell, USA) for 15 min at room temperature under gentle agitation. After repeated washing steps, representative images were taken, followed by absorbance quantification of the resulting staining. Staining was eluted in 10% cetylpyridinium chloride (C0732, Sigma-Aldrich) solution for 20 min under gentle agitation. Absorbance of samples and standard were measured (infinite M200, Tecan, Switzerland) in a 96-well plate at 570 nm in duplicates. Results were calculated as mM (or µg/mL) of Alizarin-red.

Resazurin viability assay

Cell metabolic activity of BM-MSC seeded on different decellularized models was accessed over a total period of 10 days in basal culture (initial seeding: 10⁴ cells per cm² for dECM models and 4x10⁵ cells per dBone scaffold) with a resazurin reduction assay. Briefly, at day 0 (4 hours after seeding), 2, 5 and 10 BM-MSC seeded on each model were incubated with 10% sterile solution of resazurin (R7017, Sigma-Aldrich) in cell culture medium. The reduction assay was performed for 4 h, followed by fluorescence reading of metabolized resazurin-product at 560 nm emission/590 nm absorption wavelengths. Measurements were normalized with blank (no cells) and for each model controls without cells were tested in parallel to confirm their respective biologic inertness.

Flow cytometry

For quantification of cell viability and analysis of cell cycle stage, BM-MSC (initial seeding: 10⁴ cells per cm² for dECM models and 4x10⁵ cells per dBone scaffold) cultured on decellularized models were collected by trypsinization for 20 min at 37°C under strong agitation, and pooled (six wells for each dECM model and two dBone scaffolds) for flow cytometry staining. Cells were washed twice in PBS and incubated with Fixable Viability Dye eFluor™ 780 (65-0865-14, Thermo Fisher Scientific) for 30 min at 4°C in the dark according to manufactures recommendations, followed by repeated washing in 1% FCS-PBS. To detect cells entering different apoptotic stages, cells were then prepared and stained with fluorochrome-conjugated Annexin V (A35111, Thermo Fisher Scientific) for 15 min at room temperature. Finally, cells were fixed with 2% PFA for 15 min at 4°C and stained with 10 µg/mL DAPI solution in 1%FCS-PBS for DNA amount detection. Samples were analyzed at the Attune NxT Flow Cytometer (Thermo Fisher Scientific) and data evaluated using the software FlowJo (version 10.5.3).

Real-time quantitative polymerase chain reaction (PCR)

To analyze early gene expression response of BM-MSC to the decellularized models, cells from six 13 mm wells or two scaffolds were pooled together for RNA harvesting in Tri-Reagent (T9424, Sigma-Aldrich) after 5 days in basal culture (initial seeding: 10⁴ cells per cm² for dECM models and 4x10⁵ cells per dBone scaffold). BM-MSC cultured on coverslips were used as controls. Homogenization and cell lysis were performed by mechanical disruption for 5 min at 50 Hz (TissueLyser LT, Qiagen, Germany). Samples were stored at -80°C until further processing. RNA was isolated by 1-bromo-3-chloropropane (B9673, Sigma- Aldrich) phase separation followed by column separation according to the manufacturer's instructions (NucleoSpin RNA, Macherey-Nagel, Germany). cDNA was synthesized by reverse transcription (Oligo (dT) C110A, dNTP Mix U151A, M-MLV RT 5x Buffer M531A, and M-MLV Reverse Transcriptase M1708, Promega, Germany) from 1 µg of RNA. Real-time PCR was performed by CFX96 Real-Time System (1845096, Bio-Rad, Germany) using SYBR Green dye (GoTaq® qPCR Master Mix, A600A, Promega) following a standardized program: 2 min at 95°C, 45x [30 sec at 95°C and 1 min at 60°C], melting curve at 65–95°C. Primers for stem marker genes (Nestin and Octamer-binding transcription factor 4 (Oct4)) and genes related with niche-microenvironment (Survivin and C-X-C Motif Chemokine Ligand 12 (CXCL12)), and osteogenesis

(RUNX Family Transcription Factor 2 (Runx2), Alkaline phosphatase (ALP), Col1 and Secreted Phosphoprotein 1/Osteopontin (SPP1)) were designed in the Primer Blast tool from NCBI and purchased from Biomers.net (Germany). Primer sequences and NCBI reference numbers appear in Supplementary Table S1. Expression of target genes was normalized with beta-2-microglobulin (B2M) as the reference gene, and results displayed as relative values ($10^4 \times 2^{-\Delta Ct}$).

Statistical analysis

Quantitative data was analyzed using Graphpad Prism software (version 9.1) and presented as the mean \pm standard error of the mean. Statistical significance was generally determined using the Kruskal–Wallis method followed by Dunn’s multiple comparisons test. Statistical significance was set to $p \leq 0.05$. n refers to number of BM-MSD donors independently tested.

Results and Discussion

Preparation and characterization of 2D dECM models

Here, we generated 2D dECM *in vitro* models by inducing human BM-MSD to synthesize and secrete *de novo* ECM proteins during a total time of 10 or 21 days, in presence of osteogenic differentiation medium (O-matrix) or in basal medium supplemented with ASC (B-matrix), followed by a mild decellularization protocol (Fig.1a). Based on previously published work on cell culture-derived ECM as cell niche models⁴⁶⁻⁴⁸, we hypothesized that by controlling the cell culture environment, we would be able to trigger synthesis of ECM key components necessary to either influence differentiation⁴⁹ or preserve BM-MSD’s stemness properties⁵⁰. Numerous decellularization protocols for virtual all types of tissues and *in vitro* systems have been described, although no standard criteria have yet been defined. Generally, the protocols involve a combination of physical, chemical, and enzymatic techniques tailored to balance the preservation of unique physical and biochemical properties, and the complete removal of cellular and antigen epitopes material^{32, 39}. In this study, we first optimized the decellularization protocol considering each matrix (data not shown). The selected protocol involved treatment of cell-monolayers with a sequential series of short incubations in Triton X-100 and ammonia to disrupt the cell membranes and lyse the cells, followed by slow DNase enzymatic removal of remaining nuclear material alongside with continuous gentle agitation. DAPI staining of the matrices (Fig.1b) showed efficient removal of cells and nuclei for all conditions after the decellularization protocol, resulting in a residual average of 2.8 nuclei counted per cm^2 compared to 127.6 before. Considering that the whole process of decellularization naturally disrupts the ECM to some extent⁵¹, we then examined the structure and biochemical composition of the resulting dECM matrices. We observed presence of homogeneously distributed fibrillar type-I collagen (Col1) in all decellularized matrices (Fig.1d). Col1 is the most abundant extracellular protein in bone and plays a fundamental role in the structure and mechanical strength of the tissue^{52, 53}. Therefore, we decided to supplement the basal control cultures with ASC to generate a collagen-rich ECM as well⁵⁴. Bone-specific ECM proteins⁵⁵ such as laminin and osteopontin, on the contrary, have been only detected punctually distributed in the 21-day decellularized osteogenic matrix (O21). Similarly, Coomassie stained SDS-PAGE (Fig.1c) revealed a strong band at 138kDa and 129kDa for all matrices, most likely accounting for presence of Col1 $\alpha 1$ and $\alpha 2$ -chains, respectively, as indicated by the purified Col1a control. Not surprisingly, these matrices also exhibited presence of bands (67 kDa) that can be speculated to be associated with albumin derived from cell culture FCS. Nonetheless, each matrix shows an overall complex and unique protein pattern, similar to what has been reported in literature^{46, 56}. Lastly, we explored the effect of the decellularization protocol on the mineralization residues of the produced matrices.

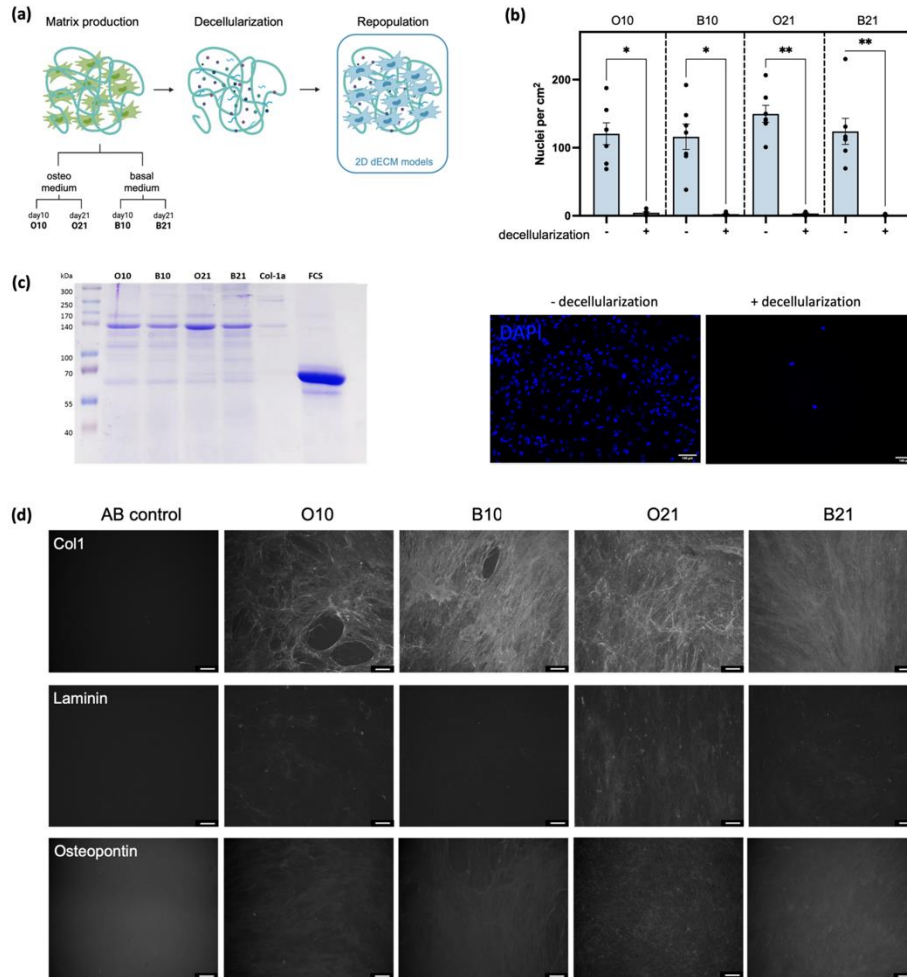


Figure 1. Production and characterization of BM-MSC-derived 2D dECM: **(a)** Schematic protocol of the development of dECM models. The first phase involves the key period of synthesis and secretion of ECM proteins by BM-MSC, where unique stimuli target the production of specific environments. Next, monolayers are treated by a multi-step decellularization protocol, therefore eliminating any nuclear material yet retaining the biochemical and structural complexity of the previously produced matrices. Finally, the last step is the repopulation of the dECM models and the study of the differential behavior of BM-MSC seeded on each matrix. Images created with BioRender.com. **(b)** Decellularization efficiency analysis. ECM-cell monolayers were fixed before and after the decellularization protocol and cell nuclei stained with DAPI. Quantitative and qualitative (representative images) analysis was performed, confirming the efficient decellularization protocol for all types of matrices. (Statistic: Kruskal–Wallis one-way test, * $p < 0.05$, $n = 7$). **(c)** Coomassie stained SDS-PAGE of collected matrices in reduction conditions. Rat-tail derived Col1 concentrated solution and FCS were used as control in order to identify specific bands in the samples. Total protein loaded per well 10 μg. **(d)** Immunofluorescence staining of bone-ECM proteins (Col1, Laminin and osteopontin). Absence of detectable signal in secondary antibody (AB) controls (left column) confirms that they do not bind unspecifically to matrix-associated proteins, therefore validating the positive signaling detected in presence of each individual antibody. Acquired raw images are shown. Scale bar: 100 μm.

Quantification of Alizarin-red dye (Supplementary Fig. S2) for all conditions showed a general decrease of mineral content after decellularization. Particularly, O21 matrices showed a high concentration of mineral residues before decellularization, however EDS analysis (Supplementary Fig. S3) revealed no detectable presence of minerals, such as calcium and magnesium, after decellularization.

Effect of dECM models on BM-MSC's osteogenic potential

Cellular morphology has traditionally been considered as an important qualitative indicator of cell behavior and state. Interestingly, while changes in cell shape are associated with descriptive traits of specific biology processes, studies have shown that cell shape in turn plays an important role in regulating cell fate, emerging as a fine bond between the interplay of physics and cell biology^{57, 58}.

In order to access the effect of dECM substrates on cell behavior, we first analyzed cell morphology of seeded BM-MSC after 2 days of culture by SEM (Fig.2a). Cells seeded on coverslips (CS) were used as controls. CS-cultured cells displayed a widespread morphology. In contrast, cells on dECM seem to have acquired an explicit orientation and rather favor cell-ECM interactions. High-magnification images reveal the complexity of BM-MSC (colored in blue) interactions with the fibrous-collagen rich dECM substrates through numerous cytoplasmic extensions, which corroborates the functionality and relevance of the dECM models. In fact, the morphology of a cell is known to be primarily determined by a combination of physical and biochemical interactions with its surrounding ECM, reflecting an integrative effect across a wide range of multiple processes and signaling pathways, such as migration^{59, 60}, lineage commitment⁶¹⁻⁶³, function or dysfunction⁶⁴ and cancer progression⁶⁵. Therefore, monitoring cellular morphology has also been used as a practical and non-invasive approach to predict lineage commitment of stem cells. While these assessments have historically been applied qualitatively and require experienced interpretation, recently high-throughput single-cell bioimaging has enabled quantification of numerous shape descriptors from a heterogeneous cell population. Particularly, Marklein *et al.*⁶⁶ demonstrated the prediction of BM-MSC mineralization at day 35 from several human donors, based on automated morphometric descriptor analysis at day 3 of osteogenic induction with over 90% accuracy.

Here, we developed a robust protocol (pipeline in supplement Fig.1S) for automated high-throughput quantification of cell shape descriptors, based on fluorescent-labelled cytoskeletal images of seeded BM-MSC on dECM matrices after 2 days of culture. Supporting the cell morphology observations in SEM, the integration of the multi-parametric acquired features into a principal-component analysis (Fig.2b) revealed a clear segmentation of matrix-seeded BM-MSC when compared to the tissue culture plastic control, both by qualitative observation of segmented single-cell images and by quantitative analysis of cell shape descriptors. With the purpose of obtaining reliable and biological significant results⁶⁷, from nine shape descriptors acquired (form factor, eccentricity, area, solidity, perimeter, aspect ratio, extent, orientation and compactness, Fig.2c), three significant parameters (area, aspect ratio and compactness) were selected, considering both their definition and interpretation, for further analysis (Fig.2d). In fact, due to the combined results of these three parameters, individual clusters could be identified in a 3D graph of multiple variables (Fig.2e). Control CS-seeded BM-MSC are categorically bigger in size (area > 4 000 μm^2) and display a rather simple (i.e., low compact values, stucked to its spatial boundaries) and spherical shape (aspect ratio values closer to 1). In opposite, cells seeded on dECM models, particular day 21-matrices (O21 and B21), reveal an evident shift from the CS cluster in all 3 dimensions – cell size/area is significantly reduced, while cells exhibit a rather elliptical and complex shape, creating a state of cytoskeletal tension, characteristic of a pre-osteogenic differentiation phenotype⁶⁸.

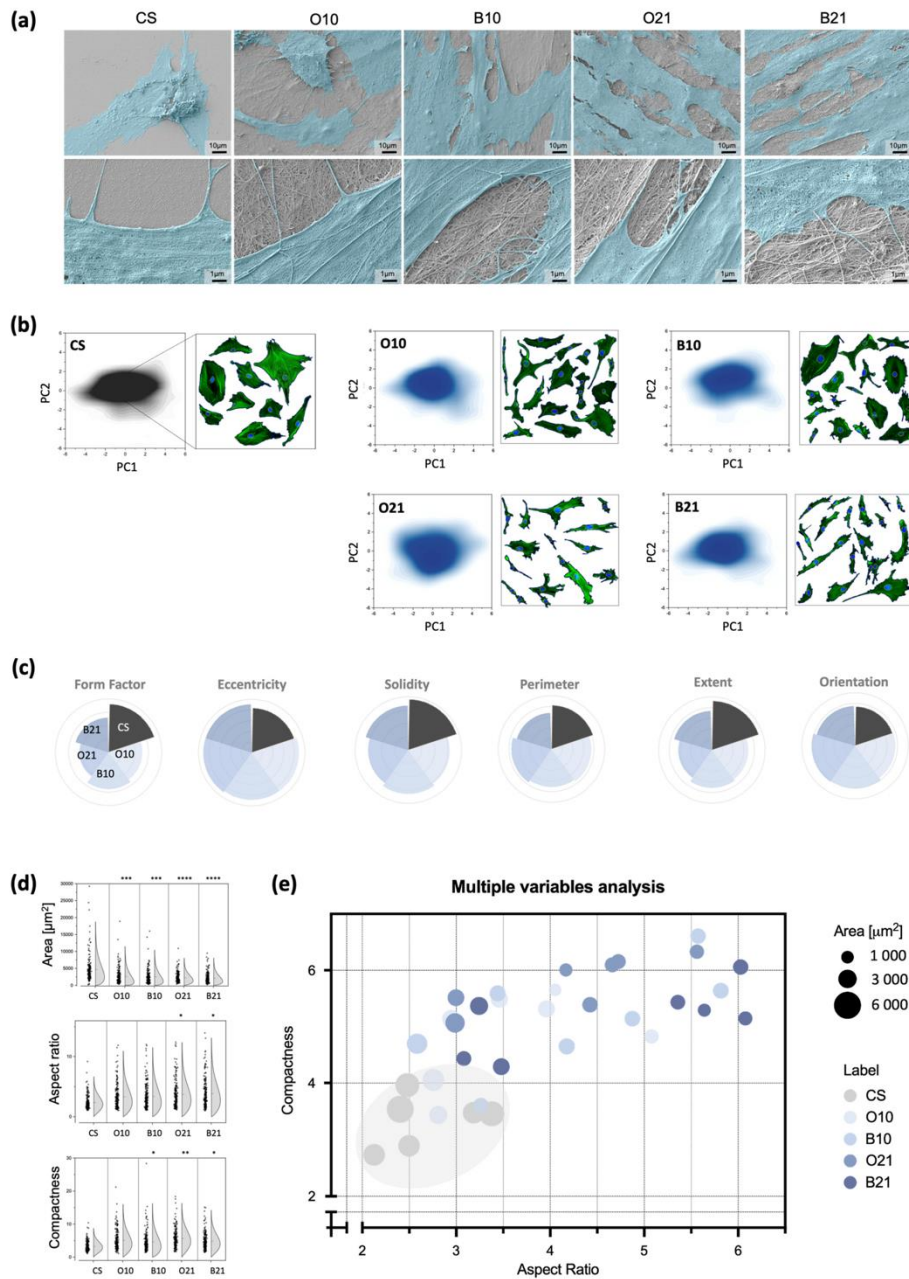


Figure 2. Cell shape analysis of human BM-MSC cultured on dECM for 2 days: **(a)** Representative SEM images of BM-MSC's early morphological response to the culture substrate. For visualization purposes the cell surface was artificially colored in blue with Photoshop. Low magnification images (first row) uncover the overall cell shape morphology of BM-MSC on each culture substrate, where a clear elongation and orientation is enforced on dECM cultured BM-MSC, particularly on O21 and B21 matrices. Scale bar: 10 μm. High magnification images

(bottom row) illustrate single cell interactions with the ECM through cytoplasmic extensions. A highly complex fibrous collagen-like matrix is detected for all dECM models. Scale bar: 1 μm . **(b)** Principal-component (PC) analysis from single-cell morphological data of fluorescently labeled cells (β -actin and DAPI staining) ($n = 200$ total points per condition, collected from 4 individual experiments). PC1 accounted for 44-47% of the data variance. Representative segmented boundaries, exported from CellProfiler pipeline, are illustrated (right column) for each condition as qualitative evidence. **(c)** Substrate-specific cell shape descriptor variance. Pie-charts corresponding to the variance of six non-significantly different shape-parameters exported from the CellProfiler pipeline (form factor, eccentricity, solidity, perimeter, extent, and orientation, $n = 200$ from 4 individual experiments). **(d)** Normal distribution and statistical analysis of the three significant shape-parameters selected (area, aspect ratio and compactness, repeated measures (RM) one-way ANOVA, * $p < 0.05$, ** $p < 0.01$, *** $p < 0.001$, **** $p < 0.0001$, $n = 350$ from 7 individual experiments). **(e)** Three-dimensional multiple variable analysis showing connection between the top three morphological features: area (symbol size), aspect ratio (x-axis) and compactness (y-axis) with the BM-MS culture substrate (color map shown on the right of the graph, $n = 350$ from 7 individual experiments).

Previous literature has shown that osteogenic lineage determination occurs within the cell cytoskeleton itself, i.e., adhesion protein complexes communicate the cell tension state to the cell nucleus via mechanotransductive cascade involving yes-associated protein 1 (YAP)/transcriptional coactivator with PDZ-binding motif (TAZ), leading to the activation of RhoA-associated signaling pathways, therefore specifically promoting the osteogenic differentiation process^{61,69}.

Thus, we further compared the osteogenic potential of BM-MS seeded on dECM in presence and absence of osteogenic factors, i.e., ASC, dexamethasone and β -GP, by means of mineral deposition at day 21 (Fig.3). Interestingly, there was no apparent effect on differentiation of BM-MS (red bars) when cultured on different substrates, with observed mineral deposition for all conditions. Yet, BM-MS cultured on dECM models in absence of external differentiation factors (white bars) show a trend towards an increased mineral deposition in comparison to CS control cultures, particularly significant for the O21 condition. Furthermore, an increased number of competent colony-forming cells in the dECM models was observed in comparison with CS control cultures, advocating for the superior supportive-effect of decellularized ECM models as a culture substrate for BM-MS expansion (Fig. S4). It seems that BM-MS interaction with dECM topography- and chemical-associated features governs the initial cell adhesion, resulting in a stronger intercellular connectivity in the early phase of cell culture. It follows from this that enhanced cell-cell contacts accelerate the osteogenic differentiation cascade⁷⁰. Hence, these findings validate the cell-shape prediction results, which shows to be in line with a common organogenesis theory hypothesizing that cellular function may indeed follow form⁷¹. Notwithstanding, BM-MS lineage fate decision is a complex process influenced by several microenvironmental factors; whilst topography imposes a physical constrain to cells and ultimately to tissue structure (in a process known as mechanotransduction)⁷², integrin-matrix interactions likewise play a pivotal role in gene expression, phenotype and eventually cell fate by direct signal transducing to the nucleus. In contrast to the artificial over-imposing chemically-induced osteogenic differentiation methods, commonly applied in research, dECM models seems to provide a rather natural substrate for BM-MS expansion, while specific features on ECM osteogenic-produced matrices are able to trigger spontaneous osteogenic differentiation of BM-MS.

dECM and dBone comparative chemical-composition analysis

As the native niche develops, most of the local microenvironmental cues are highly heterogeneous and continuously dynamic over time. The complexity of this process imposes difficulties in uncovering the role of individual features of well-defined ECM properties and signals in cellular responses. Several biomaterials have been designed to capture key molecular cues that mimic particular aspects of the natural extracellular milieu, such as mechanical properties, structural characteristics, chemical composition, and bioactive compounds^{73,74}; however, they still represent a rather simplistic approach to the full complexity of the tissue. Therefore, full tissue decellularization techniques appear as a

straightforward method to retain the physical and chemical complexity of the naïve environment. We have previously established a human decellularized trabecular bone 3D scaffold (dBone, dB), proved to be a suitable *in vitro* model to study the complexity of the bone skeletal environment⁴³. We speculate that beyond the dimensionality, specific protein expression patterns in cell-based and bone-derived decellularized models might play a significant role in BM-MSCs *in vitro* cell fate.

Thus, here we conducted a comparative investigation considering the chemical composition and subsequent behavioral differences of cells interacting with both dECM and dBone models.

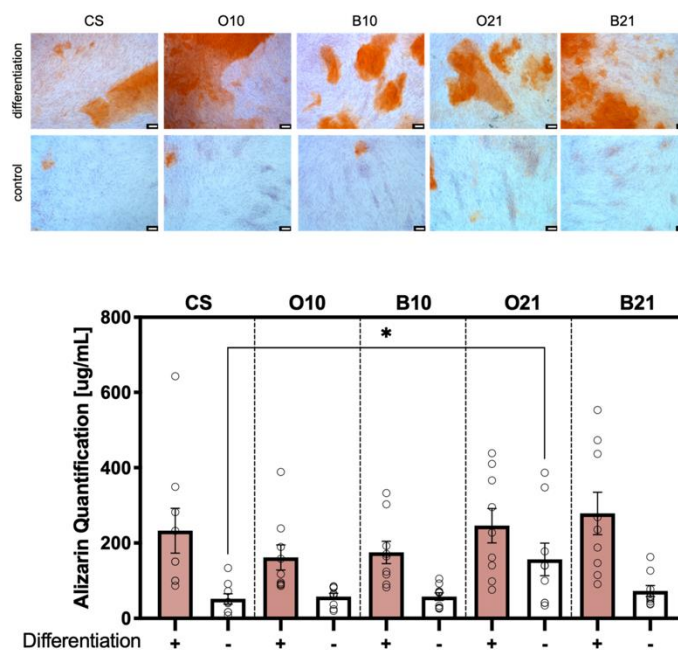


Figure 3. Human BM-MSCs' osteogenic potential accessed by mineral deposition analysis at day 21. Representative images of Alizarin Red S staining at day 21 of osteogenic culture (top panel). Osteogenic differentiation was stimulated by supplementation of low-glucose cell culture medium with osteogenic factors (i.e., ASC, dexamethasone and β -GP). Control cultures for each substrate were performed in parallel in absence of osteogenic-inducing factors. Scale bar: 100 μ m. Quantification of Alizarin Red S staining (bottom panel) shows no effect of dECM on BM-MSCs mineralization in presence of differentiation-inducing medium (red bars). Although in absence of external differentiation factors (white bars), a significant increase of mineral deposition of BM-MSCs seeded on O21 matrix was detected when compared with cells cultured in the same conditions on CS substrate (2way ANOVA multiple comparisons, * $p < 0.05$, $n = 9$).

To this end, mass spectrometry-based high-throughput proteomics techniques provide a feasible exploratory approach towards the identification of important bone factors that might be absent in certain models and therefore not fully reflecting the naïve environment. LC-MS detected a total of 735 proteins identified in at least one of the samples (excluding contaminants). Of these, 128 proteins were found in both dECM and 3D dBone proteome, indicating high homology of obtained dECM models to the *in vivo* bone niche⁷⁵. This homology is found to particularly be evident for intracellular and membrane proteins. Interestingly, we found by gene ontology (GO) analysis (Fig.4a) that there were proteins specifically enriched in the dBone scaffold. These differentially expressed proteins were associated with bone matrix structure and metabolism, e.g., secreted phosphoprotein 24 (SPP2), α 2-HS-glycoprotein (AHSG) also referred to as fetuin-A; while intracellular proteins were rather enriched in dECM matrices, e.g., tubulin (TUB), actin (ACT) and laminin (LMNA), recapping the cell lysis during

the decellularization protocol, which have been documented likewise in other studies ⁷⁶. Moreover, further GO analysis of biological processes revealed singular expression of proteins associated with the hematopoietic compartment function, such as immune effector process and antimicrobial humoral response, e.g., proteoglycans (PRG), hemoglobin (HBB) and F2 (prothrombin), specifically in dBone but not dECM, resembling the native-complexity of dBone scaffolds. Col1 accounts for nearly 95% of the entire collagen amount in the organic bone matrix and about 80% of the total proteins present in bone, playing a substantial role in the mechanical properties of the tissue, particularly for its toughness (i.e., ability to absorb energy before rupturing) ⁷⁷. Therefore, the consistent expression of Col1 throughout all models was confirmed by Western Blot analysis for 3 independent donors (Fig.4b).

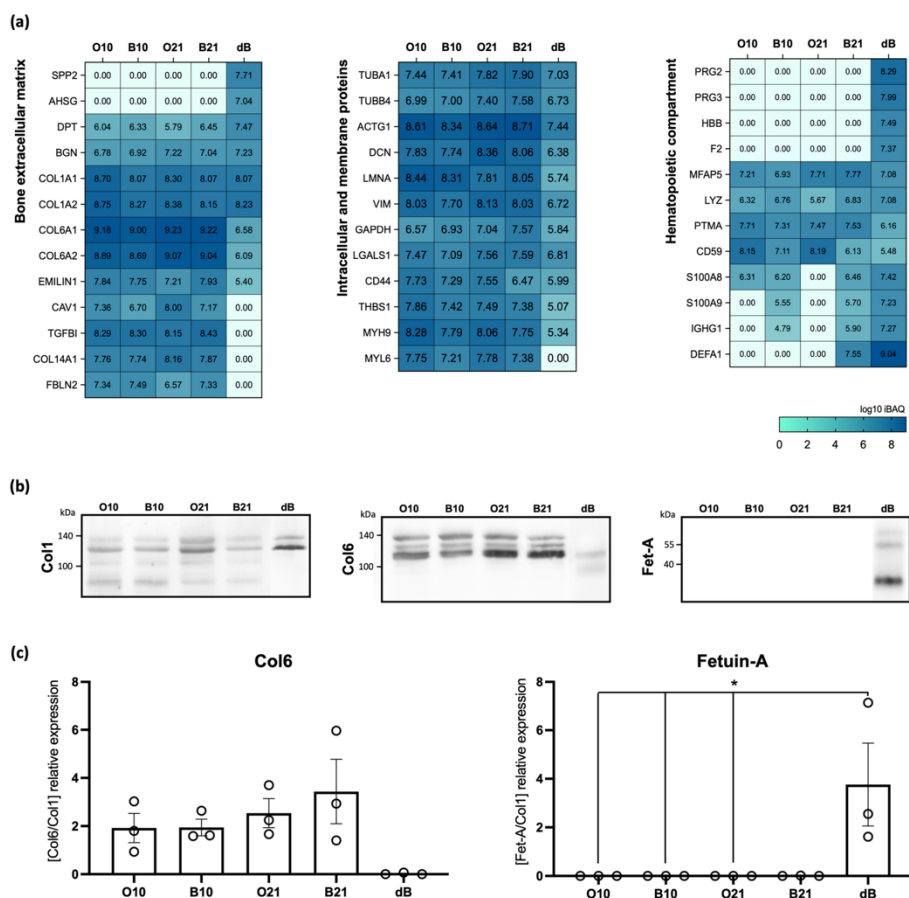


Figure 4. Proteomic analysis of collected dECM and dBone samples: **(a)** SDS-PAGE was performed under reduction conditions and followed by mass spectrometry analysis (n = 1). Heatmaps show the log10 value of the relative abundance of proteins in the decellularized models (iBAQ calculated by MaxQuant). Detected proteins of interest were grouped under three main groups (bone extracellular matrix, intracellular and membrane proteins and hematopoietic compartment), showing different patterns of expression across each model (gradient blue color code). **(b)** Western blot analyses from electrophoresis gel separation (9 μ g of total protein), of three proteins (Col1, Col6 and Fet-A), validating proteomics results (representative image of 3 replicates). **(c)** Relative quantifications of Col6 and Fet-A Western blot band expression normalized to the respective expression of Col1. Quantification of band area was performed in ImageJ using the Analyze Gel plugin (2way ANOVA multiple comparisons, * p < 0.05, n = 3).

The observation of an obvious band at the 138 kDa mark for all conditions confirmed the anticipated presence of a collagen-rich matrix, therefore validating the proteomic results. We were further interested in exploring expression patterns of differentially enriched proteins in different models. Col1 basal expression was used to normalize the quantification of Col6 and Fet-A, in the samples (Fig.4c). Interestingly, we observed a very strong expression of Col6 (108 kDa and 134.7 kDa) in dECM, particularly for day-21 matrices, whereas the detection in dBone samples was significantly reduced, evident for both proteomics and western blot analysis. Col6 is a nonfibrillar collagen commonly associated with ECM remodeling, specifically important in processes such as wound healing⁷⁸ and cancer progression⁷⁹. Altogether, we postulate that stronger expression of Col6 specifically in dECM models may be a result of artificial *in vitro* culture, which may affect BM-MSc behavior, particularly cell motility and spreading⁸⁰. Likewise, the detection of analogous patterns of Col14 expression may be postulated as an *in vitro* artefact as well. Col14 has been known as regulator of fibrillogenesis⁸¹, and is often present in areas of high tissue mechanical stress⁸², advocating towards the aforementioned artificial excessive ECM remodeling in *in vitro* culture.

Although there is limited literature describing the isolation of *in vitro* cell-produced ECM and its proteomic analysis^{83,84}, ECM-associated proteins selectively expressed in dBone but not in dECM models may be extremely significant to identify novel targets involved in bone-niche processes. In particular, fetuin-A (55 kDa), is one of the most abundant non-collagenous proteins found in mineralized bone. Primarily produced in the liver, fetuin-A binds to hydroxyapatite minerals in bone matrix and acts as a potent inhibitor of ectopic mineralization^{85,86}. Despite its' affinity to bind to TGF- β /BMP receptors blocking osteogenic signaling, fetuin-A may also sequester cytokines in the matrix, thereby generating a reservoir of osteoinductive activity when released⁸⁷. Similarly to fetuin-A, secreted phosphoprotein-24 (SPP2) is a liver-derived precursor of pro-osteogenic proteins, playing an important role in the rate and magnitude of BMP2-dependent bone formation⁸⁸. Collectively, the acquired data highlight that, although structurally important proteins for cell adhesion and proliferation such as Col1 are present on both dECM and dBone models, extracellular proteins importantly involved in the bioactivity of the bone mineral phase are not detected in manufactured dECM models, due to their peripheral synthesis followed by bloodstream-transportation to the bone, which may well have an implication on the functionality of those models.

BM-MSc behavior and transcriptional activity on decellularized models

In order to study the effect of the here developed decellularized models on BM-MSc behavior, we first looked at cell metabolism over a period of 10 days in basal culture conditions (Fig.5a). In order to revalidate the metabolic inertness of the models *per se*, the signal of constructs without cells for all conditions and timepoints was assessed. The observed near-zero values with insignificant small variance confirm the abovementioned success of the decellularization protocol. Human BM-MSc seeded on the decellularized models were compared with control cultures on coverslip (CS). Generally, a positive and sustained increase of cell metabolic activity over time was observed in all conditions, verifying once more the cytocompatibility of the models. Moreover, the superior initial (day 0) metabolic values observed for cells seeded in the decellularized models in comparison with CS controls, confirm the previously claimed extraordinary cell adhesion facilitated by the ECM-associated features. For 3D matrices, the initial cell number was adapted to the total scaffold volume in order to achieve an equivalent confluent cell density (previously described in⁴³), which explains the elevated baseline signal in the dBone model. Subsequently, we took particular interest in assessing further biological changes in BM-MSc after 5 days in basal culture. Cell viability was quantified by flow cytometry of labelled cells with Annexin-V and viability dye, and live, early apoptotic, late apoptotic or dead populations identified (Fig.5b).

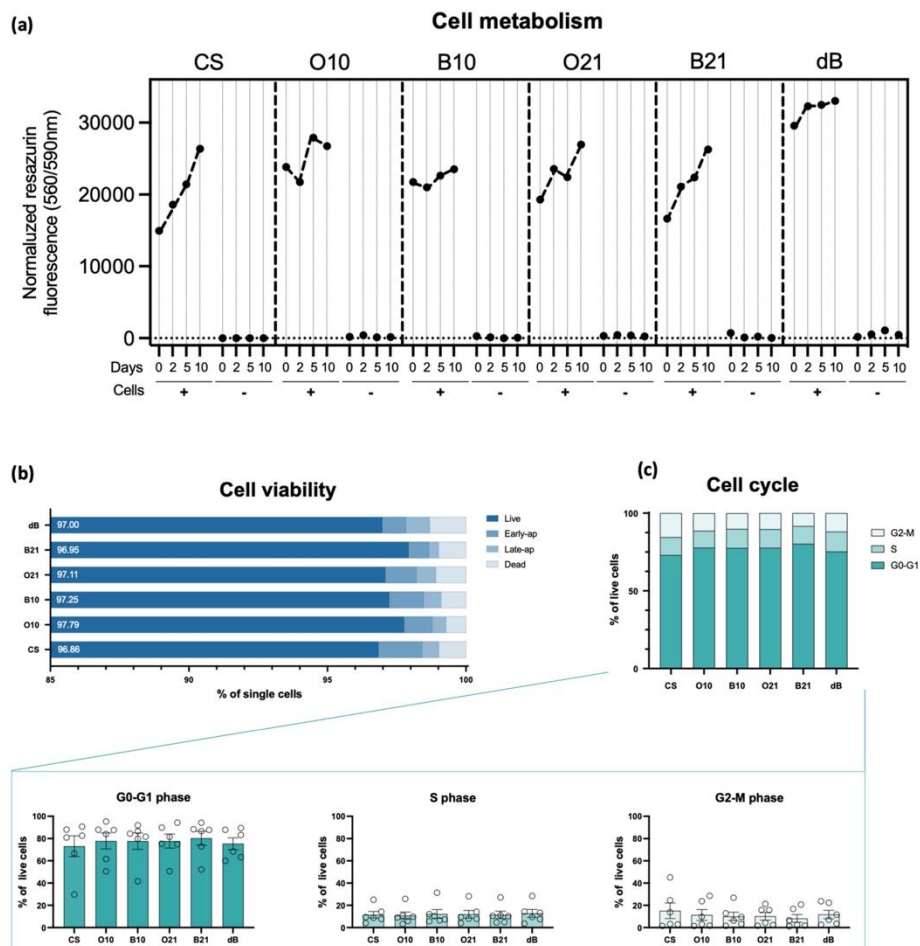


Figure 5. Analysis of metabolic activity of BM-MSC seeded on dECM and dBone models during early timepoints: **(a)** Metabolic analysis of BM-MSC in basal culture over time (0-10 days) measured by resazurin reduction assay shows a stable and sustained growth of BM-MSC in all models. Values were normalized with blank measurements (10% resazurin solution in cell culture medium). For each condition controls without cells were tested to prove the inert activity of decellularized models ($n = 3$). **(b)** Flow cytometry analysis of BM-MSC viability at day 5 of culture in decellularized models. BM-MSC in all conditions show similar results to CS control samples with live cells percentage values consistently higher than 98% ($n = 6$). **(c)** BM-MSC cell cycle stage analysis performed by flow cytometry based of DAPI-DNA labelled histograms. Upper panel displays the cumulative cell percentage quantification for each condition, whereas in the bottom panel individual values are displayed for enhanced visualization and interpretation ($n = 6$).

As anticipated from the resazurin assay results, a high percentage of viable cells was observed for all conditions, with the percentage of the live population being consistent higher than 98%. Analysis of the cell cycle stage was performed on the population of live cells, based on measurement of cellular DNA content, albeit no significant changes were observed.

In order to further investigate the hypothesized niche-phenotype of BM-MSC in the different decellularized models, we performed an extensive analysis of gene markers associated with different BM-MSC stages (Fig.6a). Firstly, we observe an explicitly dBone-associated upregulation of stem cell-related markers when compared with BM-MSC in control conditions and dECM models.

CXCL12 is a soluble ligand secreted by niche-resident BM-MSC reported to be highly involved in hematopoietic stem cells (HSC) communication and associated with cell-homing, especially during fracture healing⁸⁹. To confirm the significance of CXCL12 gene expression upregulation in the dBone condition, we further performed an immunostaining targeting protein expression of CXCL12 in BM-MSC seeded on the different substrates (Fig.6b). Interestingly, no expression of CXCL12 was detected in control or any dECM model. Contrarily, a high percentage of cells, but not all, cultured in the dBone model exhibited intracellular CXCL12 expression, corroborating the previous results towards a dBone-conferred niche-like environment for BM-MSC. Nestin is a recognized stem marker found *in vivo* particularly on BM-MSC at perivascular sites adjacent to the bone and marrow parenchyma, known to be closely associated with HSC communication in bone marrow⁹⁰. Despite the high donor variance, the emerging transcription of Nestin, together with an increased gene expression of transcription factor Oct4 (p-value = 0.0651 to CS control), a factor well-known to be associated with pluripotency of stem cells⁹¹, as well as the enhanced CXCL12 expression at gene and protein level⁹², suggests that the 3D dBone model is capable to preserve the property of a primary BM stem cell niche, i.e., to provide a sheltered environment for BM-MSC to maintain their stem phenotype. The supported stem-cell potential of recovered BM-MSC from decellularized bone models was functionally validated by a colony-forming unit (CFU) efficiency assay (Fig. S5a), where a slightly increased number of competent colony-forming cells was observed in dBone-recovered cells compared with controls. Moreover, a decreased level of Survivin mRNA in 3D dBone when compared to 2D cultures might be indicative of the structure-induced sheltered effect by protecting BM-MSC from external proliferation and mobilization stimuli, therefore allowing for the preservation of a rather quiescent phenotype⁹³. In fact, cellular quiescence is a native key property of adult stem cells observed *in vivo* allowing BM-MSC to temporarily suppress proliferation but re-enter cell cycle upon stimuli⁹⁴. However, literature regarding biology of quiescent BM-MSC in culture is poor due to the difficulty of maintaining the BM-MSC naïve phenotype during cell expansion in traditional culture-plastic surfaces²⁵.

Next, we were interested to explore early microenvironment-related BM-MSC lineage commitment decisions. Thus, osteogenesis (Runx2, ALP, Col1 and SPP1) specific gene markers were investigated for BM-MSC at 5 day-basal culture on the different decellularized-models. Expression of Runx2 did not show to be predictive of the material-osteoconductive properties previously observed. In principle, the time-point of analysis and the no-differentiation culture condition, were not sufficient to induce spontaneous detectable differences of the osteogenesis transcription factor by BM-MSC. Furthermore, while no obvious trend was identified for gene expression of ALP in BM-MSC seeded either on control coverslips or in decellularized models, the predicted osteo-supportive potential of the dBone models, was further validated functionally by ALP activity detection at day 7 of osteogenic culture (Fig. S5b). Col1 expression appears to present some donor-to-donor variability, yet while the collagen-rich dECM models seem to generally inhibit new formation of Col1 fibers on seeded BM-MSC, the native properties of dBone might induce synthesis of newly formed bone-matrix by BM-MSC (our previous results²⁴), contributing to the augmentation of a cell-fitting niche. Additionally, there is evidence of BM-MSC osteoblastic differentiation induced by Col1-mediated $\alpha2\beta1$ integrin interaction through Runx2 transcriptional cascade activation^{95,96}. Finally, a significant upregulation of SPP1 was detected in BM-MSC seeded in dBone. SPP1 expression is known to be particularly sensible to physical environment and mechanical stimuli, possibly due to its dual role in cell adhesion⁹⁷ and ECM-calcium sequestering competence⁹⁸.

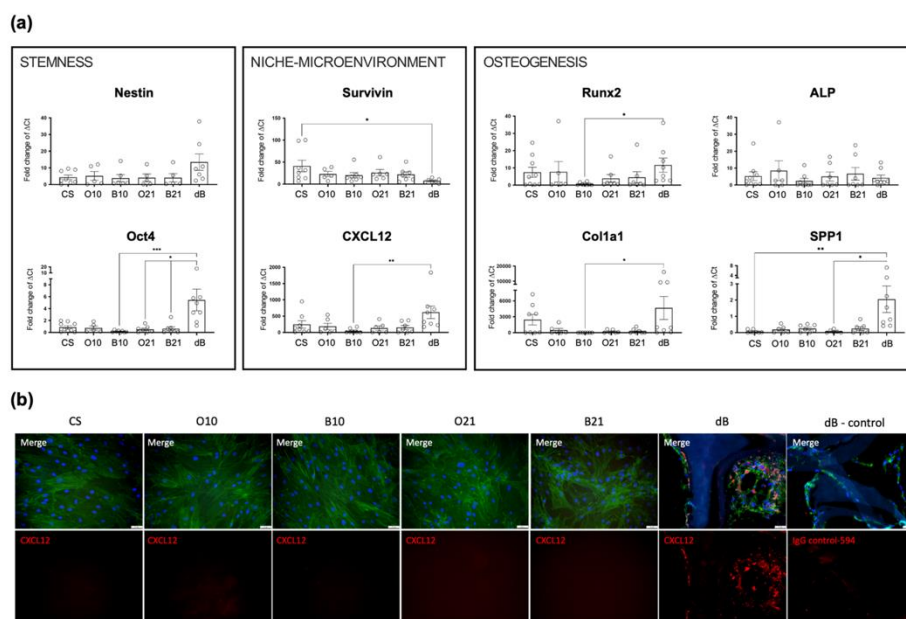


Figure 6. Analysis of the BM-niche signature of cells seeded in dECM and dBone models after 5 days in basal culture: **(a)** Relative gene expression ($10^4 \times 2^{-\Delta C_t}$) normalized to B2M housekeeping gene. A combination of genes associated with stemness: Nestin and Oct4; niche microenvironment cues: Survivin and CXCL12; and osteogenesis: Runx2, ALP, Col1 and SPP1 were analysed. Statistics: Kruskal–Wallis one-way test, * $p < 0.05$, ** $p < 0.01$, *** $p < 0.001$, $n = 4-10$. **(b)** Representative images of CXCL12-stained samples ($n = 2$). Top panel: merge composite images of nuclei (DAPI, blue), F-actin (phalloidin, green) and CXCL12 (red) channels. Bottom panel: individual CXCL12-staining for better visualization. No observable signal in dECM models was detected, yet a strong intracellular staining in BM-MSC seeded in dBone was found. Absence of signal in secondary antibody control (on right) confirms the specificity of the secondary to the primary antibody and absence of sample auto-fluorescence. Scale bar: 50 μm .

In fact, early SPP1 mRNA and protein expression in response to mechanical cues has been strongly associated with bone remodeling process via osteoclast and osteoblast interaction⁹⁹, also observed in our previous study on BM-MSC seeded in dBone²⁴. Taken together, the results suggest that 2D dECM matrices are extremely accessible models which might be used as a BM-MSC culture substrate supporting their proliferation and differentiation potential. On the other hand, the 3D dBone model has shown to support the preservation of a naïve-like cell phenotype, hence providing a suitable *in vitro* model to study the overall functions of BM-MSC in a physiological relevant microenvironment.

Conclusion

The complexity of adult stem cell niches and the relevance of its' different elements for MSC physiology remains elusive with the current *in vitro* manufactured alternatives, which cannot fully mimic the biochemistry and architecture of the native tissue-specific ECM. Decellularization of cell culture sheets and/or whole tissues may provide an alternative method to bypass these limitations. In this study, we showed that cell-derived ECM models can be tailored by manipulating the cell culture conditions, particularly through biochemical additives during culture, in line with previous literature results. The established 2D dECM models proved to be a suitable culture substrate for BM-MSC, allowing cell-matrix interactions that more closely mimic the bone environment *in vivo*. The observed

BM-MSc morphological shape changes suggested a superior cell adhesion to the substrates facilitated by the chemical properties of dECM models. Moreover, mature osteogenic day 21-matrices triggered spontaneous early osteogenic commitment of BM-MSc, where mineralization was detected in absence of external osteogenic differentiation factors. Furthermore, here we report on a 3D human-derived decellularized trabecular bone model developed in our laboratory as a promising scaffolding material to study the complexity of the bone skeletal environment. As far as we know, here we provided for the first time a comparative proteomic analysis between cell-derived dECM and human 3D dBone ECM, hence revealing key proteins involved in regulation of BM-MSc behavior and functions, such as adhesion, metabolic activity and osteogenic differentiation. Interestingly, BM-MSc seeded in dBone scaffolds exhibited, when compared with control and dECM cultures, upregulation of BM stem cell-niche related genes, suggesting the recapitulation of the naïve BM-MSc phenotype. Taken together, the here developed decellularization-based bone models, prominently the 3D dBone scaffold, seem to hold potential to provide a novel platform for advanced BM-MSc *in vitro* culture where mechanisms of activation, proliferation and lineage determination can be studied in a physiological relevant context.

Acknowledgements: We thank Dr. Andreas Schlosser (Rudolf-Virchow-Zentrum, Center for Integrative and Translational Bioimaging) for the help in the MS-proteomics data acquisition and analysis.

Author contributions: Conceptualization, M.H. and A.R.P.; investigation, A.R.P., P.S. and D.T.; resources, M.H., M.W., J.G.; original draft preparation, A.R.P.; review and editing, M.H., D.T. and P.S.; project administration, M.H.; funding acquisition, M.H. and J.G. All authors have read and agreed to the published version of the manuscript.

Declaration of conflicting interests: The authors declare no conflict of interest.

Ethical approval: The study was conducted according to the guidelines of the Declaration of Helsinki and approved by the Ethics Committee of the University of Wuerzburg (187/18). Informed consent was obtained from all subjects involved in the study.

Funding: This research was supported by the Interdisciplinary Center for Clinical Research (IZKF) at the University of Wuerzburg (Project D-361). We thank the Deutsche Forschungsgemeinschaft for funding the crossbeam scanning electron microscope Zeiss CB 340 (INST 105022/58-1 FUGG) within the DFG State Major Instrumentation Programme.

References

1. Friedenstein A, Deriglasova U, Kulagina N, et al. Precursors for fibroblasts in different populations of hematopoietic cells as detected by the in vitro colony assay method. *Experimental hematology* 1974; 2: 83-92.
2. Tuli R, Tuli S, Nandi S, et al. Characterization of multipotential mesenchymal progenitor cells derived from human trabecular bone. *Stem cells* 2003; 21: 681-693.
3. Zuk PA, Zhu M, Ashjian P, et al. Human adipose tissue is a source of multipotent stem cells. *Molecular biology of the cell* 2002; 13: 4279-4295.
4. Tondreau T, Meuleman N, Delforge A, et al. Mesenchymal stem cells derived from CD133-positive cells in mobilized peripheral blood and cord blood: proliferation, Oct4 expression, and plasticity. *Stem cells* 2005; 23: 1105-1112.
5. Sarugaser R, Lickorish D, Baksh D, et al. Human umbilical cord perivascular (HUCPV) cells: a source of mesenchymal progenitors. *Stem cells* 2005; 23: 220-229.
6. Lee OK, Kuo TK, Chen W-M, et al. Isolation of multipotent mesenchymal stem cells from umbilical cord blood. *Blood* 2004; 103: 1669-1675.
7. In't Anker PS, Scherjon SA, Kleijburg-van der Keur C, et al. Isolation of mesenchymal stem cells of fetal or maternal origin from human placenta. *Stem cells* 2004; 22: 1338-1345.
8. Murphy MB, Moncivais K and Caplan AI. Mesenchymal stem cells: environmentally responsive therapeutics for regenerative medicine. *Experimental & molecular medicine* 2013; 45: e54-e54.
9. Gattazzo F, Urciuolo A and Bonaldo P. Extracellular matrix: a dynamic microenvironment for stem cell niche. *Biochimica et Biophysica Acta (BBA)-General Subjects* 2014; 1840: 2506-2519.

10. Bergfeld SA and DeClerck YA. Bone marrow-derived mesenchymal stem cells and the tumor microenvironment. *Cancer and Metastasis Reviews* 2010; 29: 249-261.
11. Herrmann M and Jakob F. Bone marrow niches for skeletal progenitor cells and their inhabitants in health and disease. *Current stem cell research & therapy* 2019; 14: 305-319.
12. Schofield R. The relationship between the spleen colony-forming cell and the haemopoietic stem cell. *Blood cells* 1978; 4: 7-25.
13. Brizzi MF, Tarone G and Defilippi P. Extracellular matrix, integrins, and growth factors as tailors of the stem cell niche. *Current opinion in cell biology* 2012; 24: 645-651.
14. Sacchetti B, Funari A, Remoli C, et al. No identical “mesenchymal stem cells” at different times and sites: human committed progenitors of distinct origin and differentiation potential are incorporated as adventitial cells in microvessels. *Stem cell reports* 2016; 6: 897-913.
15. Reilly GC and Engler AJ. Intrinsic extracellular matrix properties regulate stem cell differentiation. *Journal of biomechanics* 2010; 43: 55-62.
16. Hynes RO. The extracellular matrix: not just pretty fibrils. *Science* 2009; 326: 1216-1219.
17. Schultz GS and Wysocki A. Interactions between extracellular matrix and growth factors in wound healing. *Wound repair and regeneration* 2009; 17: 153-162.
18. Midwood KS, Williams LV and Schwarzbauer JE. Tissue repair and the dynamics of the extracellular matrix. *The international journal of biochemistry & cell biology* 2004; 36: 1031-1037.
19. Lu P, Takai K, Weaver VM, et al. Extracellular matrix degradation and remodeling in development and disease. *Cold Spring Harbor perspectives in biology* 2011; 3: a005058.
20. Guimarães CF, Gasperini L, Marques AP, et al. The stiffness of living tissues and its implications for tissue engineering. *Nature Reviews Materials* 2020; 5: 351-370.
21. Dalby MJ. Topographically induced direct cell mechanotransduction. *Medical engineering & physics* 2005; 27: 730-742.
22. Gjorevski N and Nelson CM. Bidirectional extracellular matrix signaling during tissue morphogenesis. *Cytokine & growth factor reviews* 2009; 20: 459-465.
23. Loebel C, Mauck RL and Burdick JA. Local nascent protein deposition and remodelling guide mesenchymal stromal cell mechanosensing and fate in three-dimensional hydrogels. *Nature materials* 2019; 18: 883-891.
24. Pereira AR, Lipphaus A, Ergin M, et al. Modeling of the Human Bone Environment: Mechanical Stimuli Guide Mesenchymal Stem Cell–Extracellular Matrix Interactions. *Materials* 2021; 14: 4431.
25. Bara JJ, Richards RG, Alini M, et al. Concise review: Bone marrow-derived mesenchymal stem cells change phenotype following in vitro culture: implications for basic research and the clinic. *Stem cells* 2014; 32: 1713-1723.
26. Herrmann M and Bara JJ. Biological changes in human mesenchymal stromal cells during monolayer culture. *The Biology and Therapeutic Application of Mesenchymal Cells* 2016: 58-74.
27. Baker BM and Chen CS. Deconstructing the third dimension—how 3D culture microenvironments alter cellular cues. *Journal of cell science* 2012; 125: 3015-3024.
28. Lutolf M and Hubbell J. Synthetic biomaterials as instructive extracellular microenvironments for morphogenesis in tissue engineering. *Nature biotechnology* 2005; 23: 47.
29. Pereira A, Trivanović D and Herrmann M. Approaches to mimic the complexity of the skeletal mesenchymal stem/stromal cell niche in vitro. *European cells & materials* 2019; 37: 88-112.
30. Blache U, Stevens MM and Gentleman E. Harnessing the secreted extracellular matrix to engineer tissues. *Nature biomedical engineering* 2020; 4: 357-363.
31. Ramírez-Rodríguez GB, Pereira AR, Herrmann M, et al. Biomimetic Mineralization Promotes Viability and Differentiation of Human Mesenchymal Stem Cells in a Perfusion Bioreactor. *International journal of molecular sciences* 2021; 22: 1447.
32. Hussey GS, Dziki JL and Badyrak SF. Extracellular matrix-based materials for regenerative medicine. *Nature Reviews Materials* 2018; 3: 159-173.
33. Stock UA and Schenke-Layland K. Performance of decellularized xenogeneic tissue in heart valve replacement. *Biomaterials* 2006; 27: 1-2.
34. Neumann A, Cebotari S, Tudorache I, et al. Heart valve engineering: decellularized allograft matrices in clinical practice. *Biomedizinische Technik/Biomedical Engineering* 2013; 58: 453-456.
35. Chen R-N, Ho H-O, Tsai Y-T, et al. Process development of an acellular dermal matrix (ADM) for biomedical applications. *Biomaterials* 2004; 25: 2679-2686.
36. Milan PB, Pazouki A, Joghataei MT, et al. Decellularization and preservation of human skin: A platform for tissue engineering and reconstructive surgery. *Methods* 2020; 171: 62-67.
37. Merguerian P, Reddy P, Barrieras D, et al. Acellular bladder matrix allografts in the regeneration of functional bladders: evaluation of large-segment (> 24 cm²) substitution in a porcine model. *BJU international* 2000; 85: 894-898.

38. Rosario DJ, Reilly GC, Ali Salah E, et al. Decellularization and sterilization of porcine urinary bladder matrix for tissue engineering in the lower urinary tract. 2008.
39. Hoshiba T, Lu H, Kawazoe N, et al. Decellularized matrices for tissue engineering. *Expert opinion on biological therapy* 2010; 10: 1717-1728.
40. Smith CA, Board TN, Rooney P, et al. Human decellularized bone scaffolds from aged donors show improved osteoinductive capacity compared to young donor bone. *PloS one* 2017; 12: e0177416.
41. Duarte MM, Ribeiro N, Silva IV, et al. Fast decellularization process using supercritical carbon dioxide for trabecular bone. *The Journal of Supercritical Fluids* 2021; 172: 105194.
42. Taylor B, Indano S, Yankannah Y, et al. Decellularized cortical bone scaffold promotes organized neovascularization in vivo. *Tissue Engineering Part A* 2019; 25: 964-977.
43. Pereira AR, Rudert M and Herrmann M. Decellularized human bone as a 3D model to study skeletal progenitor cells in a natural environment. *Methods in cell biology*. Elsevier, 2020, pp.123-141.
44. Cox J and Mann M. MaxQuant enables high peptide identification rates, individualized ppb-range mass accuracies and proteome-wide protein quantification. *Nature biotechnology* 2008; 26: 1367-1372.
45. Carpenter AE, Jones TR, Lamprecht MR, et al. CellProfiler: image analysis software for identifying and quantifying cell phenotypes. *Genome biology* 2006; 7: 1-11.
46. Prewitz MC, Seib FP, Von Bonin M, et al. Tightly anchored tissue-mimetic matrices as instructive stem cell microenvironments. *Nature methods* 2013; 10: 788-794.
47. Marinkovic M, Block TJ, Rakian R, et al. One size does not fit all: developing a cell-specific niche for in vitro study of cell behavior. *Matrix Biology* 2016; 52: 426-441.
48. Cai R, Nakamoto T, Hoshiba T, et al. Matrices secreted during simultaneous osteogenesis and adipogenesis of mesenchymal stem cells affect stem cells differentiation. *Acta biomaterialia* 2016; 35: 185-193.
49. Zeitouni S, Krause U, Clough BH, et al. Human mesenchymal stem cell-derived matrices for enhanced osteoregeneration. *Science translational medicine* 2012; 4: 132ra155-132ra155.
50. Chen XD, Dusevich V, Feng JQ, et al. Extracellular matrix made by bone marrow cells facilitates expansion of marrow-derived mesenchymal progenitor cells and prevents their differentiation into osteoblasts. *Journal of bone and mineral research* 2007; 22: 1943-1956.
51. Fernández-Pérez J and Ahearn M. The impact of decellularization methods on extracellular matrix derived hydrogels. *Scientific reports* 2019; 9: 1-12.
52. Rossert J and de Crombrughe B. Type I collagen: structure, synthesis, and regulation. *Principles of bone biology*. Elsevier, 2002, pp.189-XVIII.
53. Rico-Llanos GA, Borrego-González S, Moncayo-Donoso M, et al. Collagen type I Biomaterials as scaffolds for bone tissue engineering. *Polymers* 2021; 13: 599.
54. Choi K-M, Seo Y-K, Yoon H-H, et al. Effect of ascorbic acid on bone marrow-derived mesenchymal stem cell proliferation and differentiation. *Journal of bioscience and bioengineering* 2008; 105: 586-594.
55. Robey PG and Boskey AL. The composition of bone. *Primer on the metabolic bone diseases and disorders of mineral metabolism* 2008; 7: 32-38.
56. Lin H, Yang G, Tan J, et al. Influence of decellularized matrix derived from human mesenchymal stem cells on their proliferation, migration and multi-lineage differentiation potential. *Biomaterials* 2012; 33: 4480-4489.
57. Guilak F, Cohen DM, Estes BT, et al. Control of stem cell fate by physical interactions with the extracellular matrix. *Cell stem cell* 2009; 5: 17-26.
58. Rozario T and DeSimone DW. The extracellular matrix in development and morphogenesis: a dynamic view. *Developmental biology* 2010; 341: 126-140.
59. Jiang X, Bruzewicz DA, Wong AP, et al. Directing cell migration with asymmetric micropatterns. *Proceedings of the National Academy of Sciences* 2005; 102: 975-978.
60. Doyle AD, Wang FW, Matsumoto K, et al. One-dimensional topography underlies three-dimensional fibrillar cell migration. *Journal of cell biology* 2009; 184: 481-490.
61. McBeath R, Pirone DM, Nelson CM, et al. Cell shape, cytoskeletal tension, and RhoA regulate stem cell lineage commitment. *Developmental cell* 2004; 6: 483-495.
62. Treiser MD, Yang EH, Gordonov S, et al. Cytoskeleton-based forecasting of stem cell lineage fates. *Proceedings of the National Academy of Sciences* 2010; 107: 610-615.
63. Chen D, Sarkar S, Candia J, et al. Machine learning based methodology to identify cell shape phenotypes associated with microenvironmental cues. *Biomaterials* 2016; 104: 104-118.
64. Anlaş AA and Nelson CM. Tissue mechanics regulates form, function, and dysfunction. *Current opinion in cell biology* 2018; 54: 98-105.
65. Clark AG and Vignjevic DM. Modes of cancer cell invasion and the role of the microenvironment. *Current opinion in cell biology* 2015; 36: 13-22.
66. Marklein RA, Lo Surdo JL, Bellayr IH, et al. High content imaging of early morphological signatures predicts long term mineralization capacity of human mesenchymal stem cells upon osteogenic induction. *Stem Cells* 2016; 34: 935-947.

67. Prasad A and Alizadeh E. Cell form and function: interpreting and controlling the shape of adherent cells. *Trends in biotechnology* 2019; 37: 347-357.
68. Jaiswal N, Haynesworth SE, Caplan AI, et al. Osteogenic differentiation of purified, culture-expanded human mesenchymal stem cells in vitro. *Journal of cellular biochemistry* 1997; 64: 295-312.
69. Dupont S, Morsut L, Aragona M, et al. Role of YAP/TAZ in mechanotransduction. *Nature* 2011; 474: 179-183.
70. Stein GS and Lian JB. Molecular mechanisms mediating proliferation/differentiation interrelationships during progressive development of the osteoblast phenotype. *Endocrine reviews* 1993; 14: 424-442.
71. Ingber DE. Mechanical control of tissue growth: function follows form. *Proceedings of the National Academy of Sciences* 2005; 102: 11571-11572.
72. Dalby MJ, Gadegaard N and Oreffo RO. Harnessing nanotopography and integrin-matrix interactions to influence stem cell fate. *Nature materials* 2014; 13: 558-569.
73. Murphy WL, McDevitt TC and Engler AJ. Materials as stem cell regulators. *Nature materials* 2014; 13: 547-557.
74. Huang G, Li F, Zhao X, et al. Functional and biomimetic materials for engineering of the three-dimensional cell microenvironment. *Chemical reviews* 2017; 117: 12764-12850.
75. Baroncelli M, Van Der Eerden BC, Chatterji S, et al. Human osteoblast-derived extracellular matrix with high homology to bone proteome is osteopromotive. *Tissue Engineering Part A* 2018; 24: 1377-1389.
76. Alves RD, Demmers JA, Bezstarosti K, et al. Unraveling the human bone microenvironment beyond the classical extracellular matrix proteins: a human bone protein library. *Journal of proteome research* 2011; 10: 4725-4733.
77. Viguet-Carrin S, Garnero P and Delmas P. The role of collagen in bone strength. *Osteoporosis international* 2006; 17: 319-336.
78. Oono T, Specks U, Eckes B, et al. Expression of type VI collagen mRNA during wound healing. *Journal of investigative dermatology* 1993; 100: 329-334.
79. Sherman-Baust CA, Weeraratna AT, Rangel LB, et al. Remodeling of the extracellular matrix through overexpression of collagen VI contributes to cisplatin resistance in ovarian cancer cells. *Cancer cell* 2003; 3: 377-386.
80. Theocharidis G, Drymoussi Z, Kao AP, et al. Type VI collagen regulates dermal matrix assembly and fibroblast motility. *Journal of investigative dermatology* 2016; 136: 74-83.
81. Anson HL, Meng X, Zhang G, et al. Type XIV collagen regulates fibrillogenesis. *Journal of Biological Chemistry* 2009; 284: 8427-8438.
82. Niyibizi C, Visconti CS, Kavalkovich K, et al. Collagens in an adult bovine medial collateral ligament: immunofluorescence localization by confocal microscopy reveals that type XIV collagen predominates at the ligament-bone junction. *Matrix biology* 1995; 14: 743-751.
83. Byron A, Humphries JD and Humphries MJ. Defining the extracellular matrix using proteomics. *International journal of experimental pathology* 2013; 94: 75-92.
84. Harvey A, Yen T-Y, Aizman I, et al. Proteomic analysis of the extracellular matrix produced by mesenchymal stromal cells: implications for cell therapy mechanism. *PloS one* 2013; 8: e79283.
85. Brylka L and Jahnke-Dechent W. The role of fetuin-A in physiological and pathological mineralization. *Calcified tissue international* 2013; 93: 355-364.
86. Herrmann M, Kinkeldey A and Jahnke-Dechent W. Fetuin-A function in systemic mineral metabolism. *Trends in cardiovascular medicine* 2012; 22: 197-201.
87. Jahnke-Dechent W, Heiss A, Schäfer C, et al. Fetuin-A regulation of calcified matrix metabolism. *Circulation research* 2011; 108: 1494-1509.
88. Behnam K, Phillips ML, Silva JDP, et al. BMP binding peptide: a BMP-2 enhancing factor deduced from the sequence of native bovine bone morphogenetic protein/non-collagenous protein. *Journal of orthopaedic research* 2005; 23: 175-180.
89. Sugiyama T, Kohara H, Noda M, et al. Maintenance of the hematopoietic stem cell pool by CXCL12-CXCR4 chemokine signaling in bone marrow stromal cell niches. *Immunity* 2006; 25: 977-988.
90. Xie L, Zeng X, Hu J, et al. Characterization of nestin, a selective marker for bone marrow derived mesenchymal stem cells. *Stem cells international* 2015; 2015.
91. Pan GJ, Chang ZY, Schöler HR, et al. Stem cell pluripotency and transcription factor Oct4. *Cell research* 2002; 12: 321-329.
92. Asada N, Kunisaki Y, Pierce H, et al. Differential cytokine contributions of perivascular haematopoietic stem cell niches. *Nature cell biology* 2017; 19: 214-223.
93. Singh P, Fukuda S, Liu L, et al. Survivin is required for mouse and human bone marrow mesenchymal stromal cell function. *Stem Cells* 2018; 36: 123-129.
94. Rumman M, Dhawan J and Kassem M. Concise review: quiescence in adult stem cells: biological significance and relevance to tissue regeneration. *Stem cells* 2015; 33: 2903-2912.

95. Mizuno M, Fujisawa R and Kuboki Y. Type I collagen-induced osteoblastic differentiation of bone-marrow cells mediated by collagen- $\alpha 2\beta 1$ integrin interaction. *Journal of cellular physiology* 2000; 184: 207-213.
96. Elango J, Robinson J, Zhang J, et al. Collagen peptide upregulates osteoblastogenesis from bone marrow mesenchymal stem cells through MAPK-Runx2. *Cells* 2019; 8: 446.
97. Chen Q, Shou P, Zhang L, et al. An osteopontin-integrin interaction plays a critical role in directing adipogenesis and osteogenesis by mesenchymal stem cells. *Stem cells* 2014; 32: 327-337.
98. Zappone B, Thurner PJ, Adams J, et al. Effect of Ca^{2+} ions on the adhesion and mechanical properties of adsorbed layers of human osteopontin. *Biophysical journal* 2008; 95: 2939-2950.
99. Morinobu M, Ishijima M, Rittling SR, et al. Osteopontin expression in osteoblasts and osteocytes during bone formation under mechanical stress in the calvarial suture in vivo. *Journal of Bone and Mineral Research* 2003; 18: 1706-1715.

Supplementary data

Table S1. RT-qPCR primer sequences were generated with Primer-BLAST tool from NCBI for this study. Gene name, forward and reverse primer sequence, NCBI reference number, and product length (pair of bases) is shown.

Gene	Forward sequence 5'-3'	Reverse sequence 5'-3'	NCBI Nr.	Product length
BMP-2	GGAACGGACATTCGGTCCTT	CACCATGGTCGACCTTTAGGA	NM_001200.4	127
Nestin	CTCAGCTTTCAGGACCCCAAG	AGCAAAGATCCAAGACGCCG	NM_006617.2	74
Oct4	TCGAGAACCGAGTGAGAGG	GAACCACACTCGGACCACA	NM_002701.6	125
Survivin	GACGACCCCATAGAGGAAC	CCTTTGCAATTTTGTCTTG	NM_001168.3	136
CXCL12	GTGCCCTTCAGATTGTAGCC	ACTGTAAGGGTTCCTCAGGC	NM_000609.6	150
Runx2	GAGTGGACGAGGCAAGAGTT	CTGTCTGTGCCTTCTGGGTT	NM_001024630.3	127
ALP	AGAACCCCAAGGCTTCTTC	CTTGGCTTTTCCTTCATGGT	BC021289.2	74
Col1	GGTCAGATGGGCCCCCG	GCACCATCATTTCCACGAGC	NM_000088.3	86
SPP1	TCTGGGAGGGCTTGGTTGTC	GGTAGTGAGTTTTCCTTGGTCG	NM_000582.2	124

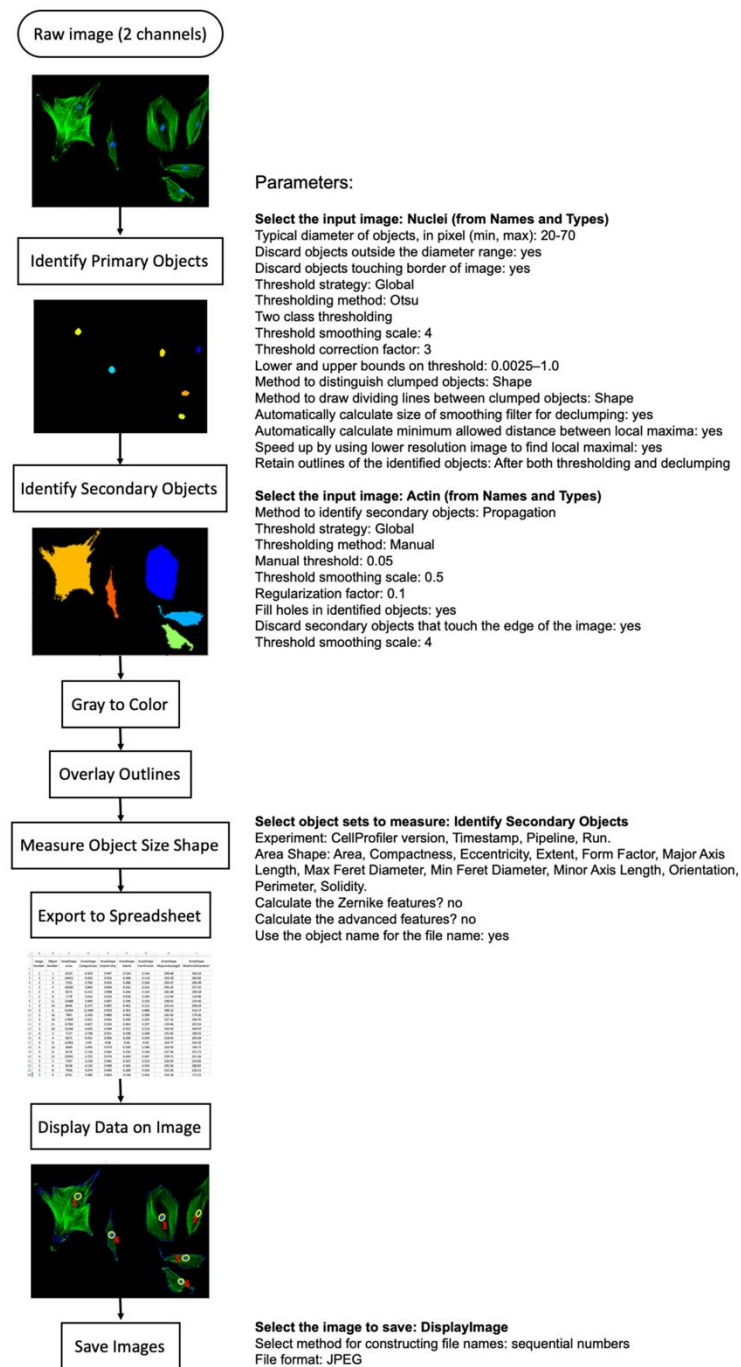


Figure S1. CellProfiler pipeline used in this study to automatically quantify single-cell morphological features.

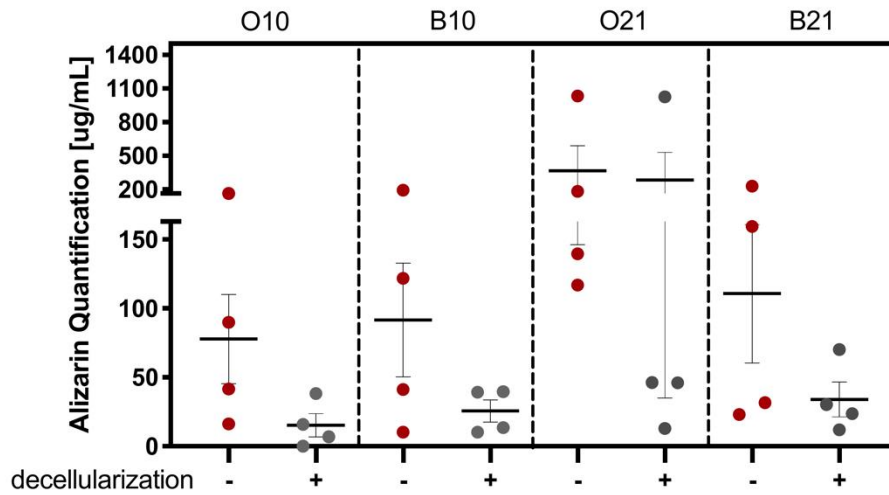


Figure S2. Quantification of Alizarin-red staining corresponding to mineralization content of dECM matrices before (red) and after (gray) the decellularization protocol (n = 4). To note that O21 model after decellularization exhibits a high mean value, comparable with the respective mean value for O21 matrix before decellularization. However, that results majorly from the contribution of an outlier point. Therefore, it is concluded that no significant mineral content is present in the decellularized models for all conditions.

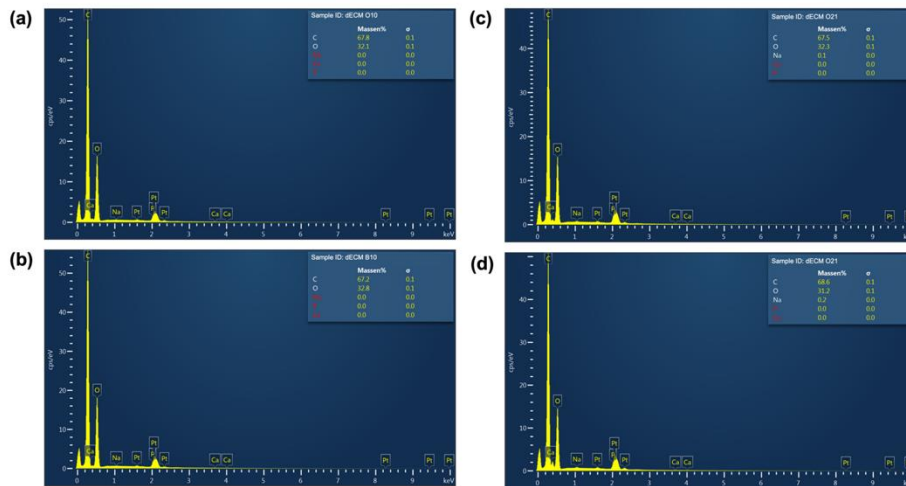


Figure S3. Representative EDS spectra of dECM (a) O10, (b) B10, (c) O21 and (d) B21 surface and respective quantification atomic element weight percentage (%). C: carbon, O: oxygen, Na: sodium, P: phosphorus, and Ca: calcium.

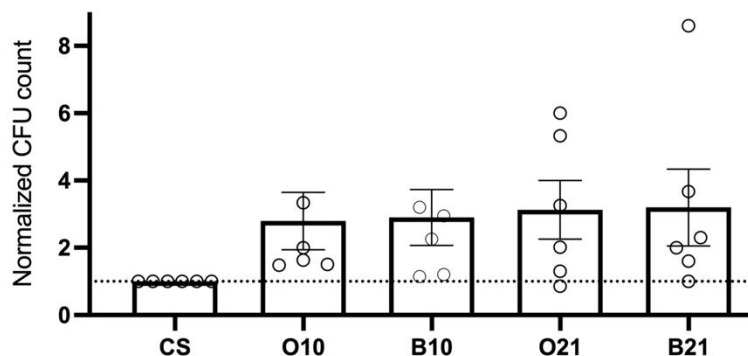


Figure S4. Colony-forming unit (CFU) assay of BM-MS C recovered from 5 day-basal culture in dECM. Count of colonies were performed after 15 days basal culture (without FGF) of 250 cells seeded cells per well in a 6-well plate stained with 1% crystal-violet in methanol. Values were normalized to BM-MS C expanded on coverslip (CS) control. Results exhibit a general trend of increased colony-forming unit capacity of BM-MS C previously cultivated in dECM models, particularly in O21 and B21 conditions, with adjusted p values of 0.0785 and 0.0662, respectively (n = 5 to 6).

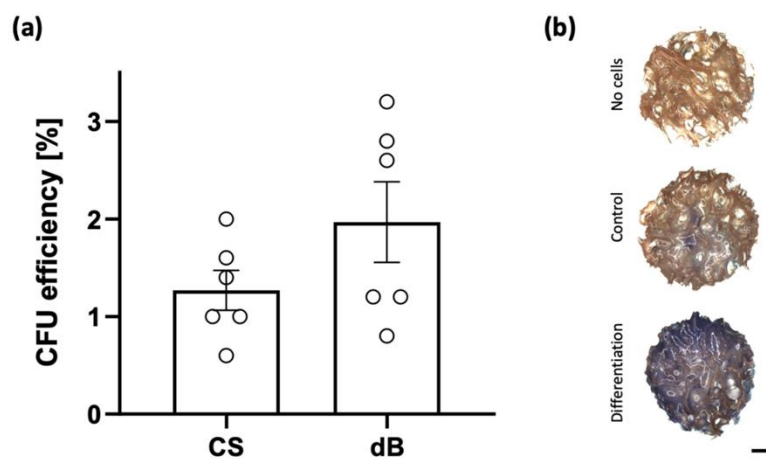


Figure S5. Validation of functional assays of BM-MS C in dBone scaffolds. (a) CFU efficiency assay of BM-MS C recovered from 5 day-basal culture in dBone. Count of colonies were performed after 15 days basal culture (without FGF) of 250 cells seeded cells per well in a 6-well plate stained with 1% crystal-violet in methanol. Control samples were used from BM-MS C expanded on standard coverslips (n = 6). (b) Representative images of ALP staining (86C-1KT, Sigma-Aldrich) of BM-MS C seeded (initial cell density: 800 000 cells per scaffold) in dBone scaffolds after 7 days in osteogenic differentiation medium (n = 4, scale bar: 1mm). Control scaffolds without cells and seeded-scaffolds in medium without osteogenic factors were used as controls.

Chapter 4.

Results: Role of mineral nucleation on osteogenesis

Here, the osteoconductive function of mineralization was addressed through biomimetic functionalization of recombinant organic collagen with hydroxyapatite nanocrystals in presence of magnesium. Additionally, the implementation of a perfusion system was used to facilitate cell seeding and 3D culture. This work provides biological insights to material science applications towards the development of *in vitro* models which can better recapitulate the *in vivo* cell niche.

The work in this chapter was previously published as an original research-article in the International Journal of Molecular Sciences. Reprint permission was obtained from all co-authors and from the publisher under Creative Commons license (CC BY). The author of this thesis, AR Pereira, shares the first authorship of the mentioned article with GB R-Rodríguez, material-scientist from University of Granada, as a result of a collaborative partnership, whereas both assumed a major contribution in all aspects of the study design, data acquisition/analysis and manuscript writing (detailed information in APPENDIX B).

Reference: Ramírez-Rodríguez GB, Pereira AR, Herrmann M, Hansmann J, Delgado-López JM, Sprio S, Tampieri A and Sandri M. Biomimetic mineralization promotes viability and differentiation of human mesenchymal stem cells in a perfusion bioreactor. Int. J. Mol. Sci. 2021, 22, p. 1447.



Article

Biomimetic Mineralization Promotes Viability and Differentiation of Human Mesenchymal Stem Cells in a Perfusion Bioreactor

Gloria Belén Ramírez-Rodríguez ^{1,*}, Ana Rita Pereira ^{2,3,†}, Marietta Herrmann ^{2,3}, Jan Hansmann ², José Manuel Delgado-López ¹, Simone Sprio ⁴, Anna Tampieri ⁴ and Monica Sandri ⁴

¹ BioNanoMet Group, Department of Inorganic Chemistry, University of Granada, 18071 Granada, Spain; jmdl@ugr.es

² IZKF Group Tissue Regeneration in Musculoskeletal Diseases, University Hospital Wuerzburg, 97070 Wuerzburg, Germany; r-pereira.klh@uni-wuerzburg.de (A.R.P.); m-herrmann.klh@uni-wuerzburg.de (M.H.); jan.hansmann@uni-wuerzburg.de (J.H.)

³ Bernhard-Heine-Centrum for Locomotion Research, University of Wuerzburg, 97070 Wuerzburg, Germany

⁴ Institute of Science and Technology for Ceramics (ISTEC-CNR), 48018 Faenza, Italy; simone.sprio@istec.cnr.it (S.S.); anna.tampieri@istec.cnr.it (A.T.); monica.sandri@istec.cnr.it (M.S.)

* Correspondence: gloria@ugr.es

† These authors contributed equally to this work.



Citation: Ramírez-Rodríguez, G.B.; Pereira, A.R.; Herrmann, M.; Hansmann, J.; Delgado-López, J.M.; Sprio, S.; Tampieri, A.; Sandri, M. Biomimetic Mineralization Promotes Viability and Differentiation of Human Mesenchymal Stem Cells in a Perfusion Bioreactor. *Int. J. Mol. Sci.* **2021**, *22*, 1447. <https://doi.org/10.3390/ijms22031447>

Academic Editor: Amir A. Zadpoor
Received: 3 December 2020
Accepted: 26 January 2021
Published: 1 February 2021

Publisher's Note: MDPI stays neutral with regard to jurisdictional claims in published maps and institutional affiliations.



Copyright: © 2021 by the authors. Licensee MDPI, Basel, Switzerland. This article is an open access article distributed under the terms and conditions of the Creative Commons Attribution (CC BY) license (<https://creativecommons.org/licenses/by/4.0/>).

Abstract: In bone tissue engineering, the design of 3D systems capable of recreating composition, architecture and micromechanical environment of the native extracellular matrix (ECM) is still a challenge. While perfusion bioreactors have been proposed as potential tool to apply biomechanical stimuli, its use has been limited to a low number of biomaterials. In this work, we propose the culture of human mesenchymal stem cells (hMSC) in biomimetic mineralized recombinant collagen scaffolds with a perfusion bioreactor to simultaneously provide biochemical and biophysical cues guiding stem cell fate. The scaffolds were fabricated by mineralization of recombinant collagen in the presence of magnesium (RCP.MgAp). The organic matrix was homogeneously mineralized with apatite nanocrystals, similar in composition to those found in bone. X-Ray microtomography images revealed isotropic porous structure with optimum porosity for cell ingrowth. In fact, an optimal cell repopulation through the entire scaffolds was obtained after 1 day of dynamic seeding in the bioreactor. Remarkably, RCP.MgAp scaffolds exhibited higher cell viability and a clear trend of up-regulation of osteogenic genes than control (non-mineralized) scaffolds. Results demonstrate the potential of the combination of biomimetic mineralization of recombinant collagen in presence of magnesium and dynamic culture of hMSC as a promising strategy to closely mimic bone ECM.

Keywords: scaffold; perfusion bioreactor; collagen; apatite nanoparticles; magnesium; human mesenchymal stem cell; osteogenesis

1. Introduction

Severe trauma, congenital malformations or disease can compromise the integrity and functionality of the skeletal system to the extent of requiring bone implants [1]. Over 2 million bone surgeries are conducted each year in the United States and around 10 million of Chinese patients suffered from limited limb functions [2]. Bone is the second most transplanted tissue after blood and an ever-increasing worldwide demand of bone graft substitutes can be expected in the coming years [1]. The forefront of tissue engineering involves the isolation of stem cells from bone marrow or adipose tissue aspirated from the patient, their expansion and differentiation on synthetic porous scaffolds and the further implantation of the composite with the aim of fostering osteoinduction and osteoconduction for rapid repair of the defect site [3,4]. The design of ideal bone biomaterial plays a vital role in bone repair. Biomaterial design aims to recapitulate the organization and

composition of natural bone extracellular matrix (ECM) where stem cells grow in vivo. To guide stem cell interaction and fate, multiple stimulus including physical (porosity, surface nanotopography, stiffness, shear stress and electrical forces) and biochemical (surface chemistry, growth factors or proteins) have been proposed [2,5–7].

In vivo bone mineralization has inspired the design of advanced biomaterials, so-called biomimetic, mimicking the hierarchical organization and composition of native tissue at nanoscale level [8–11]. Bone is a nanocomposite made up of self-assembled collagen fibers (accounting for 35 wt.%) strengthened by inter and intrafibrillar mineralization of apatite (Ap) nanocrystals (65 wt.%) [12]. Ap nanoparticles consist on non-stoichiometric hydroxyapatite $[\text{HA}, \text{Ca}_{10}(\text{PO}_4)_6(\text{OH})_2]$ containing foreign ions in its structure, e.g., CO_3^{2-} , Mg^{2+} , Sr^{2+} [13]. Bone grafts have been designed through a biologically inspired mineralization protocol by which magnesium-substituted hydroxyapatite nanoparticles crystallized into naturally derived type I collagen fibers mimicking the process occurring during biological neo-ossification [9,14–17]. In vitro studies demonstrated the potential of this hybrid scaffolds to induce, orchestrate, and harmonize the osteogenic differentiation of human bone marrow stem cells (hMSCs) and in vivo studies revealed its osteoinductive nature [17]. However, the difficulties in processing and purification with batch-to-batch variability and the risk of disease transmission of natural collagen have stimulated keen interest in devising biomaterial based on recombinant collagen [18,19]. Recombinant collagen is engineered with precise chemical composition and molecular weight, enabling the introduction of specific amino acid sequences and the large-scale production for industrial exploitation [18]. Recently, we have investigated the biomimetic mineralization of recombinant collagen peptide (RCP) based on human collagen type I enriched in arginine-glycine-aspartic acid sequences, which are specific sites favoring the attachment of a large number of adhesive ECM, blood and cell surface proteins [20]. We carried out RCP mineralization in the presence of magnesium to closer mimic bone Ap composition (0.5–1%) [21] and we observed that Mg stabilized the precursor amorphous calcium phosphate and inhibited apatite crystal growth along *c*-axis, resulting in more isometric Ap nanocrystals than mineralization protocol without magnesium [20]. Atomic force microscopy observations revealed that mineralization in the presence of Mg provided homogeneous mineral distribution in the organic matrix and surface roughness similar to that found in bone [20]. Further in vitro studies demonstrated that RCP mineralization in the presence of magnesium potentially promoted cell migration through the inner areas of the scaffold and higher gene and protein expressions of osteogenic markers comparing with the results of mouse mesenchymal stem cells grown on mineralized scaffolds without magnesium [22]. In spite of these good results, even after 14 days of cell culture, few cells arrived to the bottom inner part of the scaffolds [22]. This is likely due to the fact that in vitro static cell culture on tridimensional scaffolds presents scarce mass transport prompting to limited cell colonization through few hundred microns and apoptosis or necrosis of cells at the central core of the scaffold [23].

Over the last decade, bioreactor systems have been engineered to improve the transport of gases and nutrients and enhance cell distribution, overcoming the main limitations of static cell culture [7,23–25]. Perfusion bioreactors also generate dynamic biophysical stimuli such as shear stress and mechanical loading [7,23–25]. Cells in bone tissues (i.e., osteoclast, osteoblast, osteocytes and MSCs) are mechanosensitive and respond to biophysical factors in the environment [23]. It has been widely demonstrated that dynamic cell culture in different type of scaffolds such as ceramic scaffolds, metallic scaffolds, decellularized bone matrix from animal sources, synthetic polymer scaffolds, e.g., poly (l-lactic acid), or hybrid scaffolds made of HA and chitosan, enhanced cell proliferation and osteogenic differentiation [26,27]. Several in vivo studies also demonstrated that MSC preconditioning in bioreactor prior to implantation enhanced in vivo results as quantity and quality of new bone [23,28,29]. A more recent work demonstrated that bioreactor-based preconditioning augments the bone-forming potential of human bone marrow aspirates [30].

Despite the numerous works on dynamic culture of MSC in perfusion bioreactor, there is still a lack of simulation of the real environment due to the low biomimicry of

used scaffold. In this work, we propose the combination of perfusion bioreactor and recombinant collagen scaffolds mineralized in the presence of magnesium (RCP.MgAp) to simultaneously provide biochemical and biophysical cues and closely simulate the growth environment of stem cells *in vivo*. The structure and chemical composition of biomimetic scaffold (RCP.MgAp) was deeply characterized. Then, hMSC seeding on the resulting 3D biomaterial was assessed under static and dynamic conditions in a perfusion bioreactor. We also evaluated the osteogenic potential of biomimetic mineralized recombinant collagen scaffolds versus control recombinant collagen scaffolds by gene expression.

2. Results

2.1. Scaffold Characterization

The microstructure of RCP.MgAp scaffold was evaluated via micro-computed tomography (μ CT). Tridimensional porous scaffolds with interconnected and randomly distributed pores (i.e., isotropic structure) were obtained via freeze-drying of mineralized solutions (Figure 1). Analysis of surface pore size of 200 μ CT scans revealed a wide pore size distribution ranging from 50 to 600 μ m and giving rise to $90 \pm 0.4\%$ of porosity. Non-mineralized recombinant collagen scaffolds used as a control on *in vitro* assay showed similar pore size distribution (Figure S1) and porosity ($88 \pm 0.6\%$).

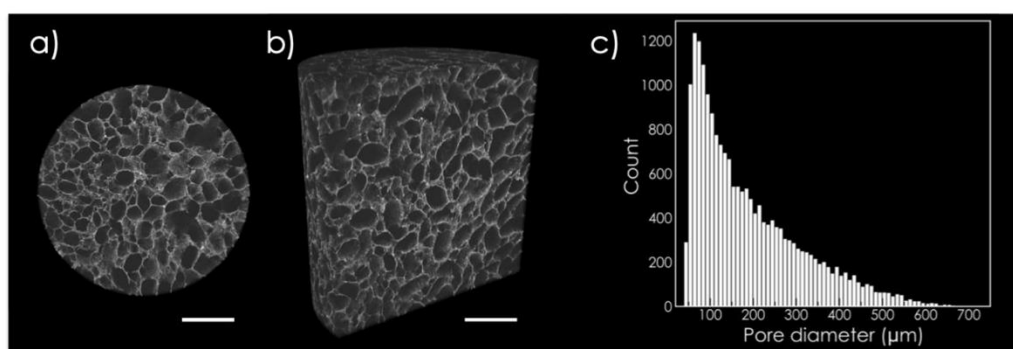


Figure 1. Structural characterization of recombinant collagen in the presence of magnesium (RCP.MgAp) scaffold (diameter = 4 mm; height = 4 mm) by micro-computed tomography. (a) Transversal and (b) longitudinal section of the scaffold. Scale bar=1 mm. (c) Graph bar displays pore size distribution estimated with ImageJ software.

Scanning electron microscope (SEM) image of RCP.MgAp scaffold shows pores diameter between 100–300 μ m (Figure 2). The energy dispersive X-ray spectroscopy (EDS) mapping of the cross-section (Figure 2) reveals a uniform distribution of calcium, phosphorus and magnesium belonging to the mineral phase along with the nitrogen of the organic matrix. From these results we can infer that a homogeneous hybrid material was obtained through the biomimetic mineralization of RCP. In fact, the Ap nanoparticles are completely embedded in the organic matrix as indicated by the SEM images at high magnification of the wall of the pore (Figure 3a). The nanoparticles have a length of approximately 150–250 nm and a width of around 30–50 nm (Figure 3a), as previously observed by transmission electron images of MgAp nanoparticles synthesized through the same biomimetic mineralization approach [20].

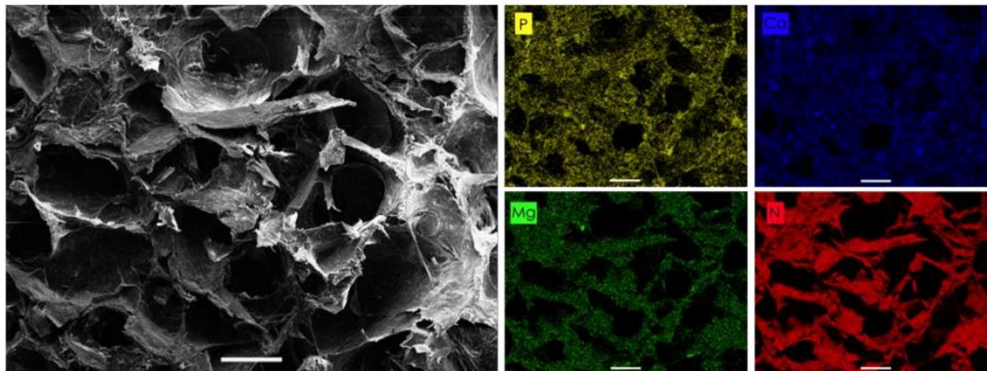


Figure 2. Energy dispersive X-ray spectroscopy (EDS) elemental maps of an area of RCP.MgAp scaffold showing the presence of P (yellow), Ca (blue) and Mg (green) of the mineral phase closely related to the N signal of the collagen (red). SEM image of the scaffold on the left displays the area of the mapping. Scale bar = 100 µm.

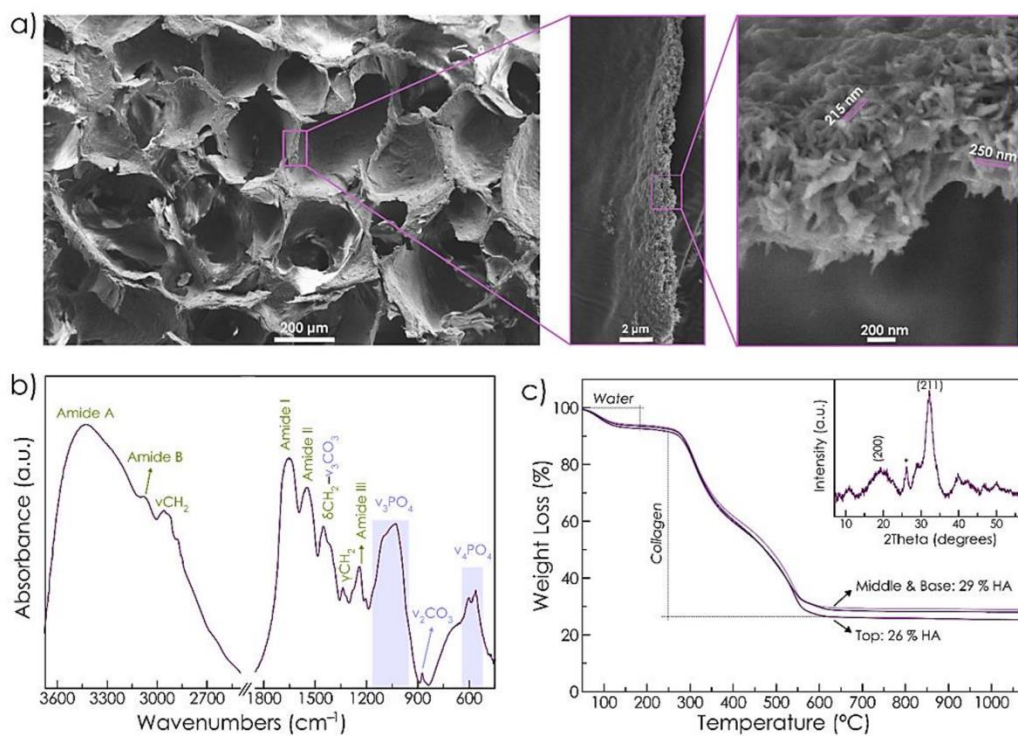


Figure 3. (a) SEM images of cross-section of RCP.MgAp scaffold. High magnification image of the wall of the pores shows the incorporation of Ap into the organic matrix. (b) Fourier-transform infrared spectroscopy (FTIR) spectrum of RCP.MgAp scaffold. (c) TGA curve of the top, middle and base of the scaffold. Inset displays X-ray diffraction (XRD) pattern of the sample exhibiting characteristic reflections of hydroxyapatite (HA, ASTM card file No 09-432).

The chemical composition and structure of RCP.MgAp scaffolds were also analyzed by Fourier-transform infrared spectroscopy (FTIR), thermogravimetric analysis (TGA) and X-ray diffraction (XRD). FTIR spectrum (Figure 3b) shows the amide bands of recombinant collagen at 1245 cm^{-1} (amide III), 1540 cm^{-1} (amide II), 1650 cm^{-1} (amide I), 3074 cm^{-1} (amide B) and 3421 cm^{-1} (amide A) [31,32]. The wagging (γ), bending (δ) and asymmetrical stretching (ν) modes of CH_2 of collagen are also visible [31]. It also displays characteristic bands of Ap: the triply degenerated asymmetric stretching mode of phosphate group ($\nu_3\text{PO}_4$) at 1032 cm^{-1} with shoulders at 1046 cm^{-1} and 1087 cm^{-1} and triply degenerated bending mode of phosphate ($\nu_4\text{PO}_4$) at 561 cm^{-1} and 602 cm^{-1} [33]. FTIR spectrum shows bending ($\nu_2\text{CO}_3$) and stretching ($\nu_3\text{CO}_3$) vibration mode of carbonate that corresponds with B-type carbonated apatite (partial substitution of PO_4^{3-} groups mainly by CO_3^{2-} ions) [33]. The formation of nanocrystalline apatite was confirmed by XRD. Figure 3c (inset) exhibits broad reflections ascribed to hydroxyapatite (HA, ASTM card file No 09-432). The broadness of the peaks indicates low crystallinity and nanosized dimensions of the diffracting crystal domains. The ratio of mineral content of RCP.MgAp scaffold was quantitatively assessed by TGA of the top, middle and base of the scaffold to evaluate the mineral distribution (Figure 3c). TGA curves mainly exhibit three decomposition steps: the first loss from $25\text{ }^\circ\text{C}$ to $170\text{ }^\circ\text{C}$ due to the decomposition of adsorbed and bound water (accounting for 6–7 wt.%); the second loss from $170\text{ }^\circ\text{C}$ to $420\text{ }^\circ\text{C}$ due to degradation of recombinant collagen; and the third loss from $420\text{ }^\circ\text{C}$ to $650\text{ }^\circ\text{C}$ attributed to the combustion of organic residues. The resultant residue after $650\text{ }^\circ\text{C}$ corresponds directly to the inorganic phase amount, which was 26 wt.% at the top and around 29 wt.% at the middle and base of the scaffold. This finding confirms a homogeneous distribution of Ap along the scaffold. Chemical composition of hybrid scaffolds was quantitatively evaluated by inductively coupled plasma optical emission spectroscopy (ICP-OES) indicating the following composition: Ca ($9.4 \pm 0.8\text{ wt.}\%$), PO_4 ($12.0 \pm 1.4\text{ wt.}\%$) and Mg ($0.8 \pm 0.1\text{ wt.}\%$).

2.2. In Vitro Studies

2.2.1. Optimization of hMSC Seeding on Scaffolds

Cell seeding was initially optimized in order to achieve a homogeneous distribution of cells over the scaffold volume. First, 2×10^6 cells were seeded on top of the scaffolds and maintained in static culture for 24 h (Figure 4a). This strategy led to the formation of cell clusters at the top and the edges of both mineralized (RCP.MgAp) and non-mineralized (RCP) scaffolds (Figure 4b). To overcome this undesired cell distribution, perfusion bioreactor was used for dynamic cell seeding using the same cell density (Section 4.4.3). The homogeneity of cell distribution within the scaffold improved significantly after 24 h of dynamic cell culture. Nonetheless, the MTT staining showed low cell density (pale violet) likely due to the large volume of the scaffolds (Figure 4b)), giving rise to low MTT absorbance value (Supplementary Figure S2). The increase of cell suspension density to 5×10^6 cells per scaffold allowed to obtain a homogeneous cell distribution with higher cell density through the whole volume, as shown MTT staining images of the lateral surface and the cross-section of the scaffolds (Figure 4b) and MTT absorbance graph (Supplementary Figure S2). These conditions were then used to further evaluate the capability of RCP.MgAp scaffold in inducing osteogenic differentiation of hMSC using a perfusion bioreactor.

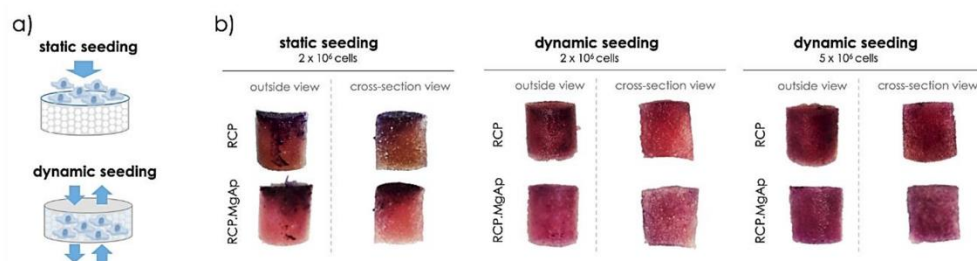


Figure 4. Cell seeding optimization. (a) Schematic design of the cell seeding approaches: static seeding in a well-plate and dynamic seeding in a perfusion bioreactor. (b) Representative images of MTT staining obtained after 24 h of hMSC culture on mineralized (RCP.MgAp) and non-mineralized (RCP) scaffolds. Full scaffolds were cross-sectioned in half in order to assess the cell distribution also in the center of the scaffold.

2.2.2. Dynamic Osteogenic Differentiation in a Perfusion Bioreactor

The impact of the mineral phase on osteogenic differentiation of hMSC was studied after 15 days of dynamic cell culture in the perfusion bioreactor. At the end of the experiment, scaffolds were stained with MTT to assess cell viability and distribution over the scaffolds (Figure 5) and cells were collected for gene expression analysis (Figure 6). Interestingly, the presence of mineral provides a significant increase on cell viability for hMSC on RCP.MgAp scaffolds in comparison to the non-mineralized RCP scaffolds (Figure 5a). However, it was observed a homogeneously distributed staining for both materials (Figure 5b). As expected, the not-seeded scaffolds (control) showed no staining. Therefore, the increase of MTT absorbance is assumed to be associated with an increase of hMSC proliferation on mineralized scaffolds, rather than a hitch from the RCP scaffolds.

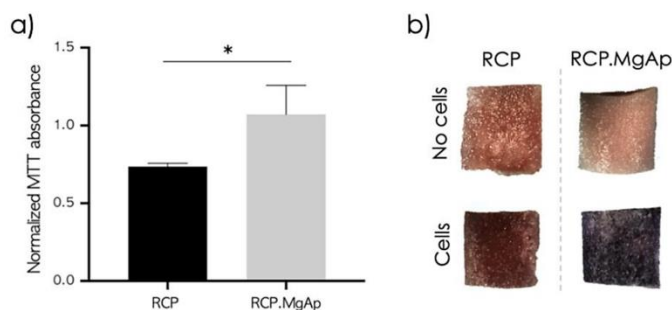


Figure 5. Cell viability of hMSC after 15 days of dynamic osteogenic culture. (a) MTT absorbance from full scaffolds was measured and normalized with dimethyl sulfoxide blank values. Statistical analysis using student *t*-test, * $p < 0.05$, n (RCP) = 3, n (RCP.MgAp) = 5. (b) Representative cross-sections images from MTT staining of non-seeded scaffolds (on top) and hMSC seeded scaffolds (on bottom) after 15 days of dynamic culture with osteogenic differentiation factors.

Regarding the gene expression analysis, hMSC cultivated on RCP.MgAp scaffolds showed the trend of superior osteogenic gene expression than hMSC cultivated on scaffolds without mineral (RCP) (Figure 6). Remarkably, the expression of Col1a1 on RCP.MgAp scaffolds showed a considerable increase in comparison to the control. Despite this clear trend, statistical analysis indicated no significance ($p > 0.05$). These results are indicative of an augmented differentiation into osteogenic lineage of hMSC cultivated in the mineralized scaffolds.

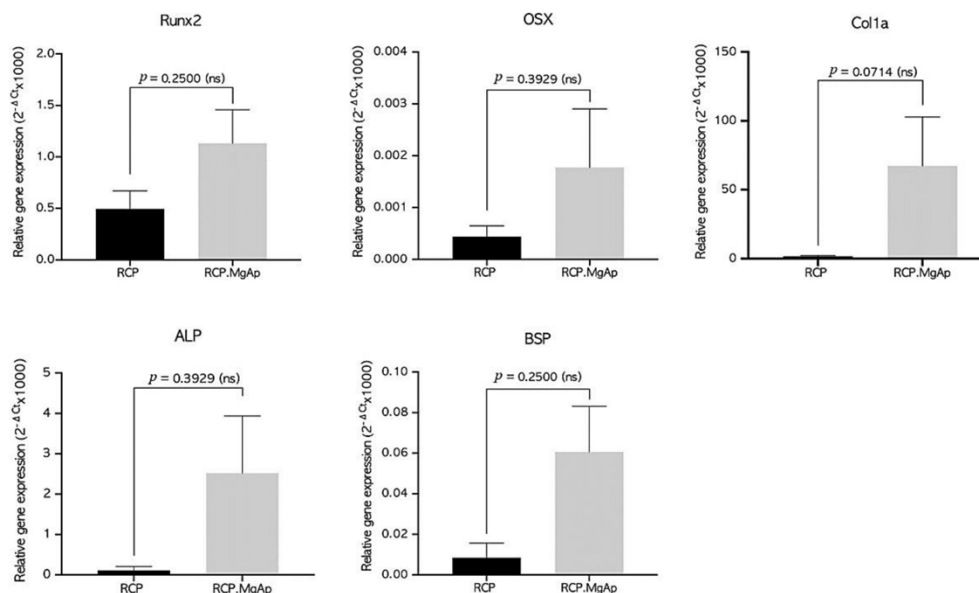


Figure 6. Relative gene expression ($2^{-\Delta Ct}$) after 15 days. GAPDH housekeeping gene was used to normalize data. RUNX2 = runt-related transcription factor 2, ALP = alkaline phosphatase, Col1a = collagen type I alpha 1, OSX = osterix, BSP = bone sialoprotein. Statistical analysis using student *t*-test, *n* (RCP) = 3, *n* (RCP.MgAp) = 5.

3. Discussion

The synergy of 3D scaffolds and perfusion bioreactors represents a promising strategy to more accurately simulate growth environment of stem cells in the human body [34]. In bone tissue engineering, 3D scaffolds must be designed to provide a more conducive structure for hMSC attachment, growth and osteogenic differentiation [34]. Herein, bioinspired scaffolds mimicking the osteogenic niche of cancellous bone have been designed through biomimetic mineralization of recombinant collagen and freeze-drying. This technique is one of the most common methodologies used to fabricate tridimensional porous scaffolds with tailored pore size, porosity and pore distribution (aligned or isotropic structures) [10,35]. These are critical parameters that directly affect the fluid shear stress sensed by the cells when cell medium is perfused through the scaffold in the bioreactor [36]. This mechanical stimulus has been pointed out as a potent promoter of hMSC osteodifferentiation [27,37]. A recent review suggests that the cultivation of hMSC under oscillatory or pulsative flow in 3D scaffolds (100–800 μm) and in the presence of osteoinductive supplements provides optimal effect on hMSC osteogenesis [23]. In this line, we obtained 3D scaffolds with pore size distribution (50–700 μm) inside the range previously commented. Moreover, the most frequent value of pore diameter (100–300 μm) has been designated as the optimum cell migration and new bone formation [38–40]. The porosity, closed to that found in cancellous bone, also provides a suitable structure for cell colonization and fluid exchanges [38–40]. Conversely, porosity has a detrimental effect on the scaffold mechanical properties, as reviewed by Deville et al. [35]. Future work, also involving *in vivo* studies, will require a thorough study to achieve a compromise between the requirements of porosity for cell ingrowth and fluid exchange and the need of suitable mechanical properties.

Biomimetic mineralization of RCP in the presence of magnesium promoted the nucleation of Ap nanoparticles into the organic matrix providing a homogeneous integration of the mineral phase along the entire scaffolds, as indicated by EDS map and TGA analysis.

SEM image of the wall of the pores confirmed the formation of acicular nanoparticles in the organic matrix. These results fit with previous atomic force microscopy observations revealing a homogeneous distribution of Ap nanoparticles into the RCP matrix at nanoscale level when mineralization was carried out in the presence of Mg [20]. Conversely, RCP mineralization in the absence of Mg prompted to Ap nanoparticle aggregation, heterogeneous mineral distribution at nanoscopic scale and therefore, higher surface roughness value [20]. Regarding the chemical composition, these nanoparticles contain magnesium (close to the values found in bone, 0.5–1%) [21] and carbonate ions substituting phosphate group in apatite crystal structure, named as B-type carbonate substitution. This type of carbonate substitution is the preferred in bone apatite [41]. Whereas carbonate ions are by far the most abundant exogenous ion of bone apatite [41], magnesium is one of the more important minor cations in bone tissue [42]. Both ions, magnesium and carbonate, are typically found in younger bone triggering to poor crystalline apatite [14,43]. In fact, XRD pattern of RCP.MgAp scaffolds confirmed the precipitation of poor crystalline apatite as biological ones [12].

In addition to biomaterial features, cell distribution, mass transport and biomechanical stimulation are also highly relevant factors on bone regeneration [44]. In this scenario, perfusion bioreactors have been demonstrated to provide a homogeneous distribution of cells inside 3D scaffolds, an adequate transport of nutrients and oxygen and mechanical stimuli by way of fluid shear stress [26,44,45]. In this work, hMSC have been cultured on mineralized recombinant collagen scaffolds in the presence of Mg in a perfusion bioreactor in order to simultaneously provide them with the adequate physico-chemical and mechanical stimuli for osteogenic differentiation. The first step was to optimize hMSC seeding on 3D hybrid scaffolds. Whereas some authors carried out cell seeding in static conditions and then moved cell/scaffold construction inside the bioreactor for dynamic culture [46–49], others studies implemented dynamic conditions for cell seeding and culture [30,50,51]. Static cell seeding is by far the most commonly used seeding method but it provides low seeding efficiencies and non-uniform cell distribution [52]. Herein, the static cell seeding promoted the formation of capsule cell layer at the surface of the scaffold (closer to 2D system) due to the physical limitation of fluid penetration extensively reported in the literature, especially for bone substitutes constructs where a large scaffold volume is often required [53–55]. The dynamic seeding provided a more uniform cell distribution in both scaffolds, mineralized (RCP.MgAp) and non-mineralized ones (RCP, control), revealing their feasibility to support cell attachment. After 15 days of dynamic cell culture, mineralized scaffolds showed a significant increase on cell growth and scaffold repopulation comparing with non-mineralized scaffolds. This effect may be associated to the scaffold surface chemistry and topography [6]. Respect to the former, apatite nanoparticles are widely considered as ideal biomaterial for bone regeneration due to its excellent biocompatibility, biodegradability and osteoconductive and osteoinductive potential [5]. Moreover, the presence of magnesium may favor cell proliferation on mineralized scaffolds since magnesium is involved in bone homeostasis by enhancing attachment and differentiation of osteoblastic cells and accelerating the mineralization process [56]. Another factor to consider is the unique surface properties of nanocomposite materials that are capable of mediating specific protein adsorption and promoting cell adhesion, proliferation and differentiation [6]. In fact, a clear trend for upregulation of genes related to osteogenic commitment of primary hMSC cultured in mineralized scaffolds (RCP.MgAp) when compared with non-modified scaffolds (RCP) was observed. Despite this trend, no statistically significant differences in the expression of the tested genes were observed due to variations between donors, a fact widely reported and accepted in the literature for primary cells derived from different patients [57]. Moreover, the presence of osteogenic factors (L-ascorbic acid, dexamethasone and β -glycerophosphate) also induced dramatic differences in levels of bone-specific gene induction in hMSC exposed to osteo-inductive media, as previously reported by Donald G. Phinney et al. [58]. Yet, a prominent upregulation of Col1a1, an early precursor protein

responsible for the formation of very strong mature type I collagen fibers, was observed for RCP.MgAp scaffolds.

In a nutshell, the biomimetic mineralization of RCP in the presence of magnesium might provide chemical signaling favoring hMSC viability and osteogenesis while perfusion bioreactor enhances cell distribution inside the scaffolds, closely recreating 3D bone ECM environment. Further studies are required in order to verify the osteogenic potential of mineralized recombinant collagen scaffolds. In addition, this work paves the way on the development of in vitro models that better recapitulate the in vivo cell niche, which are essential for the progress of fundamental biology and clinical translation (review in [59]).

4. Materials and Methods

4.1. Materials

Recombinant collagen peptide (RCP), commercially available as Cellnest™ (Fujifilm, Tilburg, The Netherlands), is produced by a fermentation process using genetically modified yeast as described previously [60]. RCP sequence is based on human collagen type I and comprises 571 amino acids. Unless noted, all reagents were purchased from Sigma-Aldrich (Taufkirchen, Germany).

4.2. Fabrication of Hybrid Scaffolds

Mineralization of RCP was carried out by a neutralization reaction in order to obtain a hybrid scaffold with a 30 wt.% of mineral content (i.e., magnesium-doped hydroxyapatite). Briefly, 0.75g of RCP was dissolved in 5 mL of phosphoric acid aqueous solution (270 mM) through magnetically stirring at 40 °C. Once that RCP was completely dissolved, it was added dropwise into 5 mL of a calcium hydroxide aqueous suspension (450 mM) containing magnesium ions in a molar ratio Mg/Ca of 0.15. After 2 h of mineral maturation at room temperature, the mineralized solution was poured into a 48-well plate, frozen at −20 °C overnight and freeze-dried (0.1 mbar; 5Pascal; Cinquepascal srl, Trezzano sul Naviglio, Italy). RCP aqueous solution (7.5 wt.%) was also freeze-dried in 48-well plate to fabricate control scaffolds for in vitro experiments. We obtained cylindrical scaffolds with a diameter of 10 mm and a height of 10 mm. The scaffolds were crosslinked by dehydrothermal treatment (DHT) at 160 °C under vacuum for 48 h. Finally, the scaffolds were sterilized by autoclaving.

4.3. Characterization of the Material

4.3.1. Structural Characterization

The porosity of the scaffold and its three-dimensional structure was determined by X-ray computerized axial microtomograph (Zeiss Xradia 510 Versa, Oberkochen, Germany) of the Centre for Scientific Instrumentation (University of Granada, CIC-UGR). For each scaffold (d = 4 mm, h = 4 mm), 2000 radiographic images (image resolution: 5 µm, X-ray energy: 80 keV, exposure time = 3 s) were obtained. ImageJ software (version 1.48v; NIH, Bethesda, MD, USA) was used to analyze pore size distribution and porosity in 200 images. The 3D image reconstruction of the scaffold was performed with Dragonfly Pro (Object Research System, Montreal, QC, Canada).

Scaffold structure and composition was analyzed with a Field Emission Scanning Electron Microscope (FESEM, Zeiss SUPRA40V from CIC-UGR) equipped with an Oxford energy-dispersive X-ray spectrophotometer (EDS) and operating at 3–15 KeV. Scaffolds were cut with a razor blade, mounted on aluminum stubs using a carbon tape and sputtered with a thin carbon film. Mineral distribution and composition were analyzed with Aztec 3.0 SP1 EDS software.

4.3.2. Characterization of Chemical Composition

Fourier-transform infrared (FTIR) spectrum of RCP.MgAp scaffolds was recorded on a Nicolet 380 FTIR spectrometer (Thermo Fisher Scientific, Waltham, MA, United States of America). Scaffold was cut with a razor blade in a small piece of 5 mg that was mixed

with 250 mg of potassium bromide (KBr). Then, the mixture was pressed at 10 tons into 7 mm diameter disk. A pure KBr disk was used as blank. The spectrum was registered from 4000 cm^{-1} to 400 cm^{-1} with a resolution of 2 cm^{-1} by accumulating 100 scans.

Thermogravimetry analysis was performed using a simultaneous thermal analyzer (STA 449 Jupiter Netzsch Gerätebau, Selb, Germany) with a heating rate of 10 $^{\circ}\text{C}/\text{min}$ up to 1000 $^{\circ}\text{C}$ in nitrogen flow.

X-Ray diffraction (XRD) pattern of RCP.MgAp scaffolds was recorded in a D8 Advance diffractometer (Bruker, Germany) using a Cu $K\alpha$ radiation ($\lambda = 1.5418 \text{ \AA}$) generated at 40 kV and 40 mA. The pattern was recorded from 10 $^{\circ}$ to 60 $^{\circ}$ (2θ) with a step size of 0.002 $^{\circ}$ and a scan rate of 5 s step^{-1} .

The chemical composition (Ca, P and Mg) was analyzed by inductively coupled plasma optical emission spectrometry (ICP-OES; Agilent Technologies 5100 ICP-OES, Santa Clara, CA, USA). A 20 mg portion of scaffold was dissolved in 2 mL of ultrapure nitric acid and then diluted up to 100 mL with Milli-Q water. Three replicates were prepared and the Ca, P and Mg content were measured three times each replicate at analytical emission wavelengths of 422 nm (Ca), 279 nm (Mg) and 214 nm (P).

4.4. In Vitro Studies in Dynamic Conditions

4.4.1. Cell Isolation and Expansion

hMSC were isolated from human bone marrow of femoral heads after informed consent of the patient and ethical approval (186/18), as previously described [61]. Then, hMSC were expanded in DMEM GlutaMAX medium (Gibco, Dreieich, Germany) supplemented with 10% FCS (Bio&Sell, Feucht, Germany), 1% Pen/Strep (Sigma-Aldrich), 1% HEPES (Sigma-Aldrich) and 5 ng/mL of recombinant human fibroblast growth factor (FGF, PeproTech, Hamburg, Germany) at 37 $^{\circ}\text{C}$ in a humidified atmosphere of 5% CO_2 . Culture medium was replaced 3 times a week. Cells were detached from culture flasks by trypsinization, centrifuged and resuspended. Cell number and viability were assessed with the trypan-blue dye exclusion test. hMSC in passage 4–6 were used for the experiments.

hMSC characterization of these cell population, such as surface markers analysis and in vitro osteogenic and adipogenic potential, have been proven in ref. [62].

4.4.2. Perfusion Bioreactor

This perfusion bioreactor consists of a computer-controlled pump connected by silicon tubes to a scaffold chamber and a flask reservoir in a closed cyclic system (Figure 7). The scaffold chamber is sealed with silicone tube with an inner diameter of 10 mm, the same diameter as the RCP.MgAp scaffolds (Figure 7h). The scaffold chamber was mounted on a bioreactor cartridge that ensures the homogeneous conditions, avoiding the extravasation of overflow out of the system, while allowing gas exchange with the bioreactor environment. The bioreactor was maintained in aseptic conditions in a controlled chamber (Figure 7f) at 37 $^{\circ}\text{C}$ and with 5% CO_2 . This bioreactor has been satisfactorily used for dynamic culture of hMSC on synthetic polymeric scaffolds (non-mineralized) to evaluate its osteogenic differentiation with or without external mechanical stimulation as deformation strain [50,63].

4.4.3. Optimization of hMSC Seeding in 3D Scaffolds

Non-mineralized RCP scaffolds were used as a control for in vitro test. All scaffolds (10 mm in diameter and 10 mm of height) were pre-incubated with complete culture medium at 37 $^{\circ}\text{C}$ overnight before cell seeding.

Two different strategies (static and dynamic) of cell seeding were evaluated. For static seeding, scaffolds were placed in a 24-well plate and each seeded by carefully dropping 100 μL of cell suspension containing 2.0×10^6 cells onto the upper surface, allowing cell attachment for 90 min at 37 $^{\circ}\text{C}$ with 5% CO_2 . Then, 1.5 mL of expansion medium supplemented with 10 mM β -glycerophosphate (Sigma-Aldrich), 50 $\mu\text{g}/\text{mL}$ L-ascorbic acid (Sigma-Aldrich) and 100 nM dexamethasone (Sigma-Aldrich) were added to each well and hMSC were cultured for 1 day.

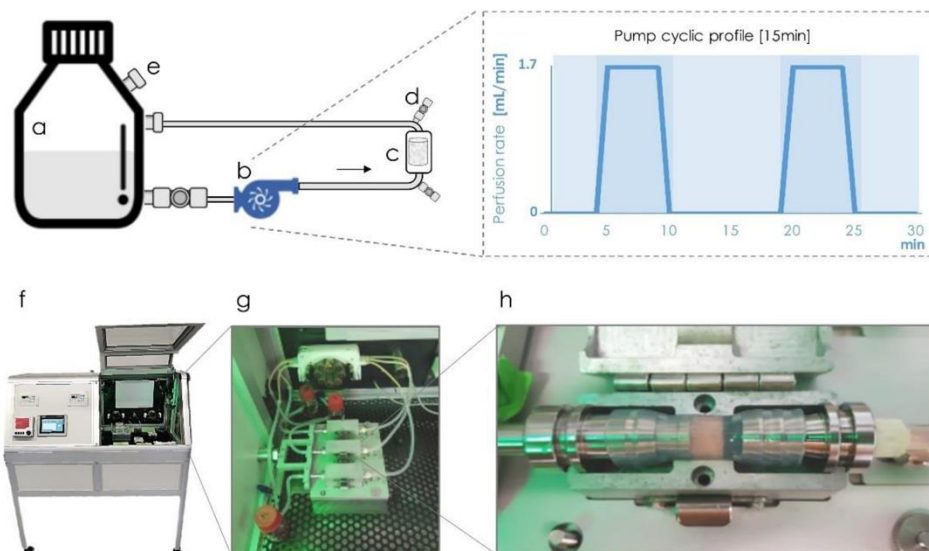


Figure 7. Schematic representation of the bioreactor design. The cell culture media is kept in a controlled environment at 37 °C in a flask reservoir (a) and driven through silicon tubes with a controllable pump (b) towards the scaffold chamber (c/h) and back to the reservoir. The system includes additional connections (d) strategically in the inlet and outlet of the chamber for cell seeding. A valve equipped with a sterile filter (e) on the reservoir guarantees the gas exchange with the external environment. The pump is programmed to actively perfuse cell culture medium for 5 min at a rate of 1.7 mL/min and stop for 10 min in cycles of 15 min, as illustrated on the right graph. The incubation chamber (f) includes temperature and CO₂ control where multi bioreactor systems can be mounted in parallel (g).

For dynamic seeding, the scaffolds were placed in the bioreactor chamber and then, 750 μ L of cell suspension containing 2.0×10^6 or 5.0×10^6 cells were manually inserted in the bioreactor chamber through connection named as d (Figure 7). After five backward-forward cycles, cells were allowed to adhere for 90 min at 37 °C with 5% CO₂. Then, the complete supplemented culture medium (35 mL) was added to the reservoir flask and driven through silicon tubes (towards the scaffold chamber and back to the reservoir) at a rate of 1.7 mL/min for 5 min every 15 min for 1 day.

Cell viability and distribution in the scaffolds were assessed with MTT [3-(4,5-dimethylthiazol-2-yl)-2,5-diphenyltetrazolium bromide] assay. Briefly, cell-laden scaffolds were incubated for 2 h in a solution of 10% MTT (5 mg/mL) in cell culture medium. The metabolically active cells react with the tetrazolium salt in the MTT reagent producing a formazan dye. Pictures of scaffold cross-section were taken under a stereomicroscope (Zeiss, Discovery.V20).

4.4.4. Osteogenic Differentiation of hMSC under Flow Perfusion

5.0×10^6 cells were seeded and cultured under dynamic conditions (as previously described in Section 4.4.2) for 15 days to evaluate the osteogenic differentiation. Media change was carried out 3 times per week. A total of 3 donors were used as biological replicas for RCP control samples, while 5 hMSC donors were tested for RCP.MgAp scaffolds.

Cell viability was evaluated by MTT assay (see above). After taking some pictures, scaffolds were transferred to a tube containing dimethyl sulfoxide (DMSO) that dissolves formazan crystal and absorbance was read at 570 nm using a Tecan's NanoQuant plate reader.

The osteoblastic differentiation was evaluated by analyzing the expression of osteogenic genes by real-time polymerase chain reaction (RT-qPCR). Scaffolds were homogenized in 1 mL of TRI Reagent (Sigma-Aldrich) for 5 min at 50 Hz using a QIAGEN TissueLyser LT (Hilden, Germany). Supernatant was collected and RNA extracted according to the manufacturer's protocol (NucleoSpin RNA, Macherey-Nagel, Dueren, Germany). cDNA was synthesized using Promega reverse transcriptase reagents. Real-time Polymerase chain reaction (PCR) was performed on the CFX96 Real-Time System (Bio-Rad, Postfach, Germany). Selected osteogenic marker genes were detected using Runx2 (NM 001015051.3), ALP (NM 001631.3), Col1a1 (NM 000088.3), OSX (NM 001173467.2), and BSP (NM 004967.3) primers, all purchased from Applied Biosystems (Dreieich, Germany). GAPDH (NM 002046.3) was used as a housekeeping gene. Non-mineralized scaffolds (RCP) were used as control. Relative quantification of mRNA targets was performed according to the comparative $2^{-\Delta Ct} \times 1000$ method [64].

4.5. Statistical Analysis

Results are expressed as the mean \pm standard error of the mean (SEM). Data analysis was made by *t*-test, followed by non-parametric analysis using Mann–Whitney test. Statistical analyses were performed with the GraphPad Prism software (version 6.0) and statistical significance set at $p < 0.05$

5. Conclusions

In this study, the combination of mineralized recombinant collagen scaffolds in the presence of magnesium with dynamic culture of hMSC was investigated for the first time. 3D porous structure with suitable pore size and porosity of cell ingrowth was obtained via freeze-drying. Biomimetic mineralization in the presence of Mg provided a homogeneous mineral incorporation into the organic matrix. This mineral phase consisted of poor crystalline apatite nanoparticles containing carbonate and magnesium, two relevant ions found in bone apatite. Dynamic seeding of hMSC provided a more uniform cell distribution along the inner areas of the scaffolds compared to static cell seeding approach, thus resulting in a genuine 3D culture system. After 15 days of dynamic culture, mineralized scaffolds enhanced hMSC viability and showed a clear trend of enhancement of osteogenic differentiation compared to non-mineralized scaffolds, revealing the pivotal role of biomimetic mineral phase on cell behavior. Further studies are required in order to verify this hypothesis and optimize the system towards specialized tissue-engineered constructs for bone replacement.

Supplementary Materials: The following are available online at <https://www.mdpi.com/1422-0067/22/3/1447/s1>, Figure S1: Structural characterization of non-mineralized collagen scaffolds (Control, RCP) by micro-computed tomography. Figure S2: MTT absorbance of cell seeding optimization experiment.

Author Contributions: Conceptualization, A.T., M.S., S.S., M.H. and G.B.R.-R.; investigation, G.B.R.-R., A.R.P.; writing—original draft preparation, G.B.R.-R., A.R.P., M.H. and J.M.D.-L.; writing—review and editing, all the authors. All authors have read and agreed to the published version of the manuscript.

Funding: This research was funded by the EU Marie Curie Project “Bio-Inspired Bone Regeneration” (BIOINSPIRE: Grant No. 607051, FP7-PEOPLE-2013-ITN) and Spanish Ministry of Science, Innovation and Universities (MCIU) with projects NanoSmart (RYC-2016-21042) and NanoVIT (RTI-2018-095794-A-C22). G.B.R.R. acknowledges to MCIU for her postdoctoral contract within Juan de la Cierva Program (JdC-2017). R.P. and M.H. are funded by the Interdisciplinary Center for Clinical Research (IZKF) at the University of Wuerzburg (Project D-361).

Institutional Review Board Statement: The study was conducted according to the guidelines of the Declaration of Helsinki, and approved by the Ethics Committee of University of Wuerzburg (186/18).

Informed Consent Statement: Informed consent was obtained from all subjects involved in the study.

Data Availability Statement: MDPI Research Data Policies.

Acknowledgments: We acknowledge Fujifilm Manufacturing Europe BV for supplying Cellnest, Davide Confalonieri for supplying hMSC and Ramkumar Ramani Mohan for his advises on perfusion bioreactor. We also acknowledge Isabel Guerra and Fátima Linares from CIC-UGR.

Conflicts of Interest: The authors declare no conflict of interest.

Abbreviations

3D	Three-dimensional
ECM	Extracellular matrix
hMSC	Human mesenchymal stem cells
Ap	Apatite
RCP	Recombinant collagen peptide
RCP.MgAp	Mineralized recombinant collagen scaffold in presence of magnesium
μCT	Micro-computed tomography
SEM	Scanning electron microscopy
EDS	Energy dispersive X-ray spectroscopy
FTIR	Fourier-transform infrared spectroscopy (FTIR)
TGA	Thermogravimetric analysis
XRD	X-ray diffraction
MTT	3-(4,5-dimethylthiazol-2-yl)-2,5-diphenyltetrazolium bromide
DMSO	Dimethyl sulfoxide
RUNX-2	Runt-related transcription factor
ALP	Alkaline phosphatase
Col1a	Collagen type I alpha
OSX	Osterix
BSP	Bone sialoprotein

References

- Haugen, H.J.; Lyngstadaas, S.P.; Rossi, F.; Perale, G. Bone grafts: Which is the ideal biomaterial? *J. Clin. Periodontol.* **2019**, *46*, 92–102. [[CrossRef](#)] [[PubMed](#)]
- Gao, C.; Peng, S.; Feng, P.; Shuai, C. Bone biomaterials and interactions with stem cells. *Bone Res.* **2017**, *5*, 1–33. [[CrossRef](#)]
- Vacanti, J.P.; Langer, R. Tissue engineering: The design and fabrication of living replacement devices for surgical reconstruction and transplantation. *Lancet* **1999**, *354*, S32–S34. [[CrossRef](#)]
- Lanza, R.; Langer, R.; Vacanti, J.P.; Atala, A. *Principles of Tissue Engineering*; Academic Press: Cambridge, MA, USA, 2020; ISBN 0128214015.
- Samavedi, S.; Whittington, A.R.; Goldstein, A.S. Calcium phosphate ceramics in bone tissue engineering: A review of properties and their influence on cell behavior. *Acta Biomater.* **2013**, *9*, 8037–8045. [[CrossRef](#)] [[PubMed](#)]
- Zhang, L.; Webster, T.J. Nanotechnology and nanomaterials: Promises for improved tissue regeneration. *Nano Today* **2009**, *4*, 66–80. [[CrossRef](#)]
- Fernandez-Yague, M.A.; Abbah, S.A.; McNamara, L.; Zeugolis, D.I.; Pandit, A.; Biggs, M.J. Biomimetic approaches in bone tissue engineering: Integrating biological and physicochemical strategies. *Adv. Drug Deliv. Rev.* **2015**, *84*, 1–29. [[CrossRef](#)]
- Nudelman, F.; Sommerdijk, N.A.J.M. Biomineralization as an Inspiration for Materials Chemistry. *Angew. Chem. Int. Ed.* **2012**, *51*, 6582–6596. [[CrossRef](#)]
- Sprio, S.; Sandri, M.; Panseri, S.; Iafisco, M. Bone substitutes based on biomineralization. *Bone Substit. Biomater.* **2014**, *1*.
- Ramírez Rodríguez, G.; Patrício, T.; Delgado López, J. *Natural Polymers for Bone Repair*, 2nd ed.; Elsevier Ltd.: Amsterdam, The Netherlands, 2019; ISBN 9780081024515.
- Wegst, U.G.K.; Bai, H.; Saiz, E.; Tomsia, A.P.; Ritchie, R.O. Bioinspired structural materials. *Nat. Mater.* **2014**, *14*, 23. [[CrossRef](#)]
- Olszta, M.J.; Cheng, X.; Jee, S.S.; Kumar, R.; Kim, Y.-Y.; Kaufman, M.J.; Douglas, E.P.; Gower, L.B. Bone structure and formation: A new perspective. *Mater. Sci. Eng. R Rep.* **2007**, *58*, 77–116. [[CrossRef](#)]
- Gómez-Morales, J.; Iafisco, M.; Delgado-López, J.M.; Sarda, S.; Drouet, C. Progress on the preparation of nanocrystalline apatites and surface characterization: Overview of fundamental and applied aspects. In *Progress in Crystal Growth and Characterization of Materials*; Elsevier: Amsterdam, The Netherlands, 2013; Volume 59, pp. 1–46.
- Landi, E.; Logroscino, G.; Proietti, L.; Tampieri, A.; Sandri, M.; Sprio, S. Biomimetic Mg-substituted hydroxyapatite: From synthesis to in vivo behaviour. *J. Mater. Sci. Mater. Med.* **2008**, *19*, 239–247. [[CrossRef](#)] [[PubMed](#)]
- Tampieri, A.; Sandri, M.; Landi, E.; Pressato, D.; Francioli, S.; Quarto, R.; Martin, I. Design of graded biomimetic osteochondral composite scaffolds. *Biomaterials* **2008**, *29*, 3539–3546. [[CrossRef](#)] [[PubMed](#)]

16. Tampieri, A.; Celotti, G.; Landi, E.; Sandri, M.; Roveri, N.; Falini, G. Biologically inspired synthesis of bone-like composite: Self-assembled collagen fibers/hydroxyapatite nanocrystals. *J. Biomed. Mater. Res. Part A* **2003**, *67A*, 618–625. [[CrossRef](#)] [[PubMed](#)]
17. Minardi, S.; Taraballi, F.; Cabrera, F.J.; Van Eps, J.; Wang, X.; Gazze, S.A.; Fernandez-Mourev, J.S.; Tampieri, A.; Francis, L.; Weiner, B.K. Biomimetic hydroxyapatite/collagen composite drives bone niche recapitulation in a rabbit orthotopic model. *Mater. Today Bio* **2019**, *2*, 100005. [[CrossRef](#)] [[PubMed](#)]
18. Olsen, D.; Yang, C.; Bodo, M.; Chang, R.; Leigh, S.; Baez, J.; Carmichael, D.; Perälä, M.; Hämäläinen, E.-R.; Jarvinen, M.; et al. Recombinant collagen and gelatin for drug delivery. *Adv. Drug Deliv. Rev.* **2003**, *55*, 1547–1567. [[CrossRef](#)] [[PubMed](#)]
19. Shrivats, A.R.; McDermott, M.C.; Hollinger, J.O. Bone tissue engineering: State of the union. *Drug Discov. Today* **2014**, *19*, 781–786. [[CrossRef](#)] [[PubMed](#)]
20. Ramirez-Rodríguez, G.B.; Sprio, S.; Montesi, M.; Delgado-López, J.M.; Iafisco, M.; Sandri, M.; Tampieri, A. Biomimetic mineralization of recombinant collagen type I derived protein to obtain hybrid matrices for bone regeneration. *J. Struct. Biol.* **2016**, *196*, 138–146. [[CrossRef](#)]
21. Wallach, S. Effects of magnesium on skeletal metabolism. *Magnes. Trace Elem.* **1989**, *9*, 1–14.
22. Ramirez-Rodríguez, G.B.; Montesi, M.; Panseri, S.; Sprio, S.; Tampieri, A.; Sandri, M. Biomimetic mineralized recombinant collagen-based scaffold mimicking native bone enhances mesenchymal stem cell interaction and differentiation. *Tissue Eng. Part A* **2017**, *23*. [[CrossRef](#)]
23. Yong, K.W.; Choi, J.R.; Choi, J.Y.; Cowie, A.C. Recent Advances in Mechanically Loaded Human Mesenchymal Stem Cells for Bone Tissue Engineering. *Int. J. Mol. Sci.* **2020**, *21*, 5816. [[CrossRef](#)]
24. Meinel, L.; Karageorgiou, V.; Fajardo, R.; Snyder, B.; Shinde-Patil, V.; Zichner, L.; Kaplan, D.; Langer, R.; Vunjak-Novakovic, G. Bone tissue engineering using human mesenchymal stem cells: Effects of scaffold material and medium flow. *Ann. Biomed. Eng.* **2004**, *32*, 112–122. [[CrossRef](#)] [[PubMed](#)]
25. Jaasma, M.J.; Plunkett, N.A.; O'Brien, F.J. Design and validation of a dynamic flow perfusion bioreactor for use with compliant tissue engineering scaffolds. *J. Biotechnol.* **2008**, *133*, 490–496. [[CrossRef](#)] [[PubMed](#)]
26. Sladkova, M.; de Peppo, G.M. Bioreactor systems for human bone tissue engineering. *Processes* **2014**, *2*, 494–525. [[CrossRef](#)]
27. Yeatts, A.B.; Fisher, J.P. Bone tissue engineering bioreactors: Dynamic culture and the influence of shear stress. *Bone* **2011**, *48*, 171–181. [[CrossRef](#)] [[PubMed](#)]
28. Bhumiratana, S.; Bernhard, J.C.; Alfi, D.M.; Yeager, K.; Eton, R.E.; Bova, J.; Gimble, J.M.; Lopez, M.J.; Eisig, S.B.; Vunjak-Novakovic, G. Tissue-engineered autologous grafts for facial bone reconstruction. *Sci. Transl. Med.* **2016**, *8*, 343ra83. [[CrossRef](#)]
29. Mitra, D.; Whitehead, J.; Yasui, O.W.; Leach, J.K. Bioreactor culture duration of engineered constructs influences bone formation by mesenchymal stem cells. *Biomaterials* **2017**, *146*, 29–39. [[CrossRef](#)]
30. Harvestine, J.N.; Gonzalez-Fernandez, T.; Sebastian, A.; Hum, N.R.; Genetos, D.C.; Loots, G.G.; Leach, J.K. Osteogenic preconditioning in perfusion bioreactors improves vascularization and bone formation by human bone marrow aspirates. *Sci. Adv.* **2020**, *6*, eaay2387. [[CrossRef](#)]
31. Muyonga, J.H.; Cole, C.G.B.; Duodu, K.G. Fourier transform infrared (FTIR) spectroscopic study of acid soluble collagen and gelatin from skins and bones of young and adult Nile perch (*Lates niloticus*). *Food Chem.* **2004**, *86*, 325–332. [[CrossRef](#)]
32. Morris, M.D.; Finney, W.F. Recent developments in Raman and infrared spectroscopy and imaging of bone tissue. *Spectrosc. Int. J.* **2004**, *18*, 155–159. [[CrossRef](#)]
33. Koutopoulos, S. Synthesis and characterization of hydroxyapatite crystals: A review study on the analytical methods. *J. Biomed. Mater. Res.* **2002**, *62*, 600–612. [[CrossRef](#)]
34. Yi, T.; Huang, S.; Liu, G.; Li, T.; Kang, Y.; Luo, Y.; Wu, J. Bioreactor Synergy with 3D Scaffolds: New Era for Stem Cells Culture. *ACS Appl. Bio Mater.* **2018**, *1*, 193–209. [[CrossRef](#)]
35. Deville, S. Freeze-Casting of Porous Ceramics: A Review of Current Achievements and Issues. *Adv. Eng. Mater.* **2008**, *10*, 155–169. [[CrossRef](#)]
36. McCoy, R.J.; Jungreuthmayer, C.; O'Brien, F.J. Influence of flow rate and scaffold pore size on cell behavior during mechanical stimulation in a flow perfusion bioreactor. *Biotechnol. Bioeng.* **2012**, *109*, 1583–1594. [[CrossRef](#)] [[PubMed](#)]
37. Zhao, F.; Chella, R.; Ma, T. Effects of shear stress on 3-D human mesenchymal stem cell construct development in a perfusion bioreactor system: Experiments and hydrodynamic modeling. *Biotechnol. Bioeng.* **2007**, *96*, 584–595. [[CrossRef](#)]
38. Salgado, A.J.; Coutinho, O.P.; Reis, R.L. Bone tissue engineering: State of the art and future trends. *Macromol. Biosci.* **2004**, *4*, 743–765. [[CrossRef](#)]
39. Karageorgiou, V.; Kaplan, D. Porosity of 3D biomaterial scaffolds and osteogenesis. *Biomaterials* **2005**, *26*, 5474–5491. [[CrossRef](#)]
40. Hutmacher, D.W. Scaffolds in tissue engineering bone and cartilage. *Biomaterials* **2000**, *21*, 2529–2543. [[CrossRef](#)]
41. Rey, C.; Renugopalakrishnan, V.; Collins, B.; Glimcher, M. Fourier transform infrared spectroscopic study of the carbonate ions in bone mineral during aging. *Calcif. Tissue Int.* **1991**, *49*, 251–258. [[CrossRef](#)]
42. Tsuboi, S.; Nakagaki, H.; Ishiguro, K.; Kondo, K.; Mukai, M.; Robinson, C.; Weatherell, J.A. Magnesium distribution in human bone. *Calcif. Tissue Int.* **1994**, *54*, 34–37. [[CrossRef](#)]
43. Rey, C.; Combes, C.; Drouet, C.; Glimcher, M.J. Bone mineral: Update on chemical composition and structure. *Osteoporos. Int.* **2009**, *20*, 1013–1021. [[CrossRef](#)]

44. Sikavitsas, V.I.; Temenoff, J.S.; Mikos, A.G. Biomaterials and bone mechanotransduction. *Biomaterials* **2001**, *22*, 2581–2593. [[CrossRef](#)]
45. Bancroft, G.N.; Sikavitsas, V.I.; Mikos, A.G. Design of a flow perfusion bioreactor system for bone tissue-engineering applications. *Tissue Eng.* **2003**, *9*, 549–554. [[CrossRef](#)] [[PubMed](#)]
46. Goldstein, A.S.; Juarez, T.M.; Helmke, C.D.; Gustin, M.C.; Mikos, A.G. Effect of convection on osteoblastic cell growth and function in biodegradable polymer foam scaffolds. *Biomaterials* **2001**, *22*, 1279–1288. [[CrossRef](#)]
47. Liu, L.; Guo, Y.; Chen, X.; Li, R.; Li, Z.; Wang, L.; Wan, Z.; Li, J.; Hao, Q.; Li, H. Three-dimensional dynamic culture of pre-osteoblasts seeded in HA-CS/Col/nHAP composite scaffolds and treated with α -ZAL. *Acta Biochim. Biophys.* **2012**, *44*, 669–677. [[CrossRef](#)] [[PubMed](#)]
48. Poh, P.S.P.; Hutmacher, D.W.; Holzappel, B.M.; Solanki, A.K.; Stevens, M.M.; Woodruff, M.A. In vitro and in vivo bone formation potential of surface calcium phosphate-coated polycaprolactone and polycaprolactone/bioactive glass composite scaffolds. *Acta Biomater.* **2016**, *30*, 319–333. [[CrossRef](#)]
49. Salifu, A.A.; Obayemi, J.D.; Uzonwanne, V.O.; Soboyejo, W.O. Mechanical stimulation improves osteogenesis and the mechanical properties of osteoblast-laden RGD-functionalized polycaprolactone/hydroxyapatite scaffolds. *J. Biomed. Mater. Res. Part A* **2020**. [[CrossRef](#)]
50. Kleinhans, C.; Mohan, R.R.; Vacun, G.; Schwarz, T.; Haller, B.; Sun, Y.; Kahlig, A.; Kluger, P.; Finne-Wistrand, A.; Walles, H. A perfusion bioreactor system efficiently generates cell-loaded bone substitute materials for addressing critical size bone defects. *Biotechnol. J.* **2015**, *10*, 1727–1738. [[CrossRef](#)]
51. Janssen, F.W.; Oostra, J.; van Oorschot, A.; van Blitterswijk, C.A. A perfusion bioreactor system capable of producing clinically relevant volumes of tissue-engineered bone: In vivo bone formation showing proof of concept. *Biomaterials* **2006**, *27*, 315–323. [[CrossRef](#)]
52. Grayson, W.L.; Bhumiratana, S.; Cannizzaro, C.; Chao, P.-H.G.; Lennon, D.P.; Caplan, A.I.; Vunjak-Novakovic, G. Effects of initial seeding density and fluid perfusion rate on formation of tissue-engineered bone. *Tissue Eng. Part A* **2008**, *14*, 1809–1820. [[CrossRef](#)]
53. Wendt, D.; Marsano, A.; Jakob, M.; Heberer, M.; Martin, I. Oscillating perfusion of cell suspensions through three-dimensional scaffolds enhances cell seeding efficiency and uniformity. *Biotechnol. Bioeng.* **2003**, *84*, 205–214. [[CrossRef](#)]
54. Petrenko, Y.A.; Ivanov, R.V.; Lozinsky, V.I.; Petrenko, A.Y. Comparison of the methods for seeding human bone marrow mesenchymal stem cells to macroporous alginate cryogel carriers. *Bull. Exp. Biol. Med.* **2011**, *150*, 543–546. [[CrossRef](#)] [[PubMed](#)]
55. Rodina, A.V.; Tenchurin, T.K.; Saprykin, V.P.; Shepelev, A.D.; Mamagulashvili, V.G.; Grigor'ev, T.E.; Lukanina, K.I.; Orekhov, A.S.; Moskaleva, E.Y.; Chvalun, S.N. Migration and proliferative activity of mesenchymal stem cells in 3D polylactide scaffolds depends on cell seeding technique and collagen modification. *Bull. Exp. Biol. Med.* **2016**, *162*, 120–126. [[CrossRef](#)] [[PubMed](#)]
56. Zhang, Y.; Xu, J.; Ruan, Y.C.; Yu, M.K.; O'Laughlin, M.; Wise, H.; Chen, D.; Tian, L.; Shi, D.; Wang, J. Implant-derived magnesium induces local neuronal production of CGRP to improve bone-fracture healing in rats. *Nat. Med.* **2016**, *22*, 1160–1169. [[CrossRef](#)] [[PubMed](#)]
57. Rady, D.; Abbass, M.; El-Rashidy, A.A.; El Moshy, S.; Radwan, I.A.; Dörfer, C.E.; Fawzy El-Sayed, K.M. Mesenchymal Stem/Progenitor Cells: The Prospect of Human Clinical Translation. *Stem Cells Int.* **2020**, *2020*. [[CrossRef](#)]
58. Phinney, D.G.; Kopen, G.; Righter, W.; Webster, S.; Tremain, N.; Prockop, D.J. Donor variation in the growth properties and osteogenic potential of human marrow stromal cells. *J. Cell. Biochem.* **1999**, *75*, 424–436. [[CrossRef](#)]
59. Pereira, A.R.; Trivanović, D.; Herrmann, M. Approaches to mimic the complexity of the skeletal mesenchymal stem/stromal cell niche in vitro. *Eur. Cell. Mater.* **2019**, *37*, 88–112. [[CrossRef](#)]
60. De Boer, A.L.; Van Urk, H.; Bouwstra, J.B.; Van Asten, P.F.T.M. RGD Containing Recombinant Gelatin 2012. U.S. Patent No. 8,198,047, 12 June 2012.
61. Herrmann, M.; Bara, J.J.; Sprecher, C.M.; Menzel, U.; Jalowiec, J.M.; Osinga, R.; Scherberich, A.; Alini, M.; Verrier, S. Pericyte plasticity—comparative investigation of the angiogenic and multilineage potential of pericytes from different human tissues. *Eur. Cells Mater.* **2016**, *31*, 236–249. [[CrossRef](#)]
62. Wagenbrenner, M.; Heinz, T.; Horas, K.; Jakuscheit, A.; Arnholdt, J.; Herrmann, M.; Rudert, M.; Holzappel, B.M.; Steinert, A.F.; Weisenberger, M. The human arthritic hip joint is a source of mesenchymal stromal cells (MSCs) with extensive multipotent differentiation potential. *BMC Musculoskelet. Disord.* **2020**, *21*, 297. [[CrossRef](#)]
63. Ramani-Mohan, R.; Schwedhelm, I.; Finne-Wistrand, A.; Krug, M.; Schwarz, T.; Jakob, F.; Walles, H.; Hansmann, J. Deformation strain is the main physical driver for skeletal precursors to undergo osteogenesis in earlier stages of osteogenic cell maturation. *J. Tissue Eng. Regen. Med.* **2018**, *12*, e1474–e1479. [[CrossRef](#)]
64. Melms, H.; Herrmann, M.; Förstner, K.; Bharti, R.; Schneider, D.; Mentrup, B.; Rudert, M.; Schlagenhaut, U.; Jakob, F.; Graser, S. Novel molecular cues for dental defects in hypophosphatasia. *Exp. Cell Res.* **2020**, *112026*. [[CrossRef](#)]

Supplementary information

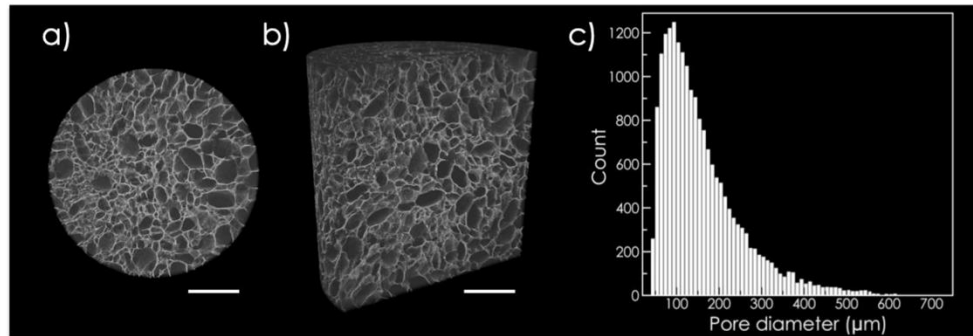


Figure 1. Structural characterization of non-mineralized collagen scaffolds (Control, RCP) by micro-computed tomography (diameter = 4mm; height = 4 mm). (a) Transversal and (b) longitudinal section of scaffold. Scale bar= 1 mm. (c) Graph bar display pore size distribution.

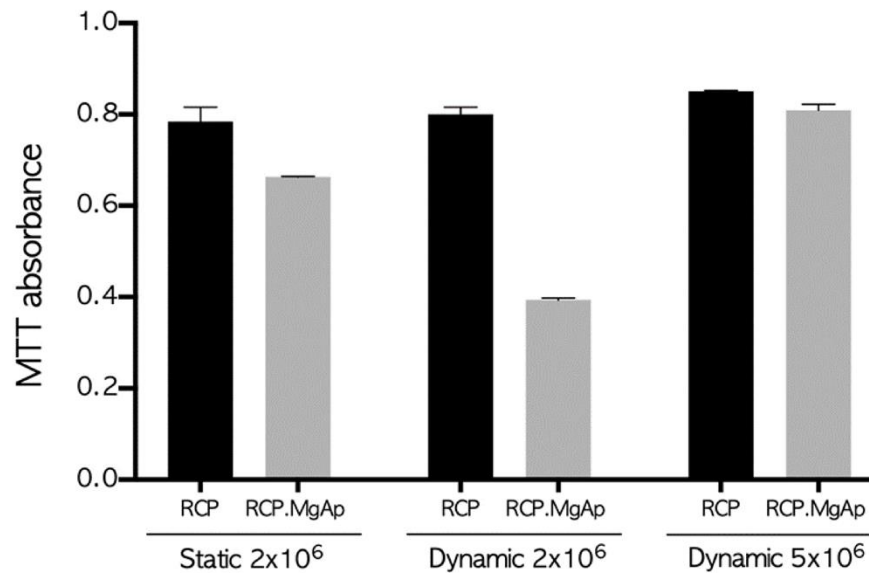


Figure S2. MTT absorbance of cell seeding optimization experiment. n=2 technical replicates. Mean \pm SEM.

Chapter 5.

Results: Effect of mechanical stimuli on osteogenesis







In this chapter, for the first-time the combined effect of the naïve human trabecular bone ECM and a dynamic culture system reflecting physiological mechanical forces was simultaneously addressed. This study provides a foundation for exploring the early effects of external mechanical stimuli on MSCs behavior in a biologically meaningful *in vitro* environment, opening new opportunities to study bone development, remodeling, and pathologies.

The work presented in Chapter 5 was published as an original research-article in Materials journal. Reprint permission was obtained from all co-authors and from the publisher under Creative Commons license (CC BY).

Reference: Pereira AR, Lipphaus A, Ergin M, Salehi S, Gehweiler D, Rudert M, Hansmann J and Herrmann M. Modeling of the Human Bone Environment: Mechanical Stimuli Guide Mesenchymal Stem Cell–Extracellular Matrix Interactions. Materials, 2021, 14(16), 4431.

Article

Modeling of the Human Bone Environment: Mechanical Stimuli Guide Mesenchymal Stem Cell–Extracellular Matrix Interactions

Ana Rita Pereira ^{1,2} , Andreas Lipphaus ³ , Mert Ergin ^{1,4}, Sahar Salehi ⁴ , Dominic Gehweiler ⁵ , Maximilian Rudert ⁶ , Jan Hansmann ⁷ and Marietta Herrmann ^{1,2,*} 

- ¹ IZKF Group Tissue Regeneration in Musculoskeletal Diseases, University Hospital Wuerzburg, 97070 Wuerzburg, Germany; r-pereira.klh@uni-wuerzburg.de (A.R.P.); mertergin.de@gmail.com (M.E.)
² Bernhard-Heine-Centrum for Locomotion Research, University of Wuerzburg, 97074 Wuerzburg, Germany
³ Biomechanics Research Group, Ruhr-University Bochum, 44801 Bochum, Germany; andreas.lipphaus@rub.de
⁴ Department of Biomaterials, Center of Energy Technology und Materials Science (TAO), University of Bayreuth, 95447 Bayreuth, Germany; sahar.salehi@bm.uni-bayreuth.de
⁵ AO Research Institute Davos, 7270 Davos, Switzerland; dominic.gehweiler@aofoundation.org
⁶ Department of Orthopedic Surgery, Koenig-Ludwig-Haus, University of Wuerzburg, 97074 Wuerzburg, Germany; m-rudert.klh@uni-wuerzburg.de
⁷ Fraunhofer Institute for Silicate Research, Translational Center for Regenerative Therapies, 97082 Wuerzburg, Germany; jan.hansmann@isc.fraunhofer.de
* Correspondence: m-herrmann.klh@uni-wuerzburg.de



Citation: Pereira, A.R.; Lipphaus, A.; Ergin, M.; Salehi, S.; Gehweiler, D.; Rudert, M.; Hansmann, J.; Herrmann, M. Modeling of the Human Bone Environment: Mechanical Stimuli Guide Mesenchymal Stem Cell–Extracellular Matrix Interactions. *Materials* **2021**, *14*, 4431. <https://doi.org/10.3390/ma14164431>

Academic Editor: Franz E. Weber

Received: 2 July 2021
 Accepted: 3 August 2021
 Published: 7 August 2021

Publisher's Note: MDPI stays neutral with regard to jurisdictional claims in published maps and institutional affiliations.



Copyright: © 2021 by the authors. Licensee MDPI, Basel, Switzerland. This article is an open access article distributed under the terms and conditions of the Creative Commons Attribution (CC BY) license (<https://creativecommons.org/licenses/by/4.0/>).

Abstract: In bone tissue engineering, the design of in vitro models able to recreate both the chemical composition, the structural architecture, and the overall mechanical environment of the native tissue is still often neglected. In this study, we apply a bioreactor system where human bone-marrow hMSCs are seeded in human femoral head-derived decellularized bone scaffolds and subjected to dynamic culture, i.e., shear stress induced by continuous cell culture medium perfusion at 1.7 mL/min flow rate and compressive stress by 10% uniaxial load at 1 Hz for 1 h per day. In silico modeling revealed that continuous medium flow generates a mean shear stress of 8.5 mPa sensed by hMSCs seeded on 3D bone scaffolds. Experimentally, both dynamic conditions improved cell repopulation within the scaffold and boosted ECM production compared with static controls. Early response of hMSCs to mechanical stimuli comprises evident cell shape changes and stronger integrin-mediated adhesion to the matrix. Stress-induced Col6 and SPP1 gene expression suggests an early hMSC commitment towards osteogenic lineage independent of Runx2 signaling. This study provides a foundation for exploring the early effects of external mechanical stimuli on hMSC behavior in a biologically meaningful in vitro environment, opening new opportunities to study bone development, remodeling, and pathologies.

Keywords: bone tissue engineering; human trabecular bone decellularization; in vitro modeling; shear stress; compressive load; fluid simulation; cell-matrix interaction; mechanotransduction

1. Introduction

Bone tissue unveils remarkable mechanical properties and regeneration potential, mainly provided by its particular extracellular matrix (ECM) composition and organization. Bone ECM consists of 30–45% of organic matrix, primarily composed of collagen type I (Col1) assembled in twisted microfibrils [1,2]. These fibrils interact with other collagenous (e.g., type III and V collagen) and non-collagenous proteins (e.g., bone sialoproteins, proteoglycans, osteocalcin, osteopontin (SPP1), etc.), establishing an optimal biochemical and physical environment for bone-resident cells [3]. Simultaneously, Col1 fibrils provide a template for hydroxyapatite crystals to nucleate parallel along their axis and therefore grant mechanical competence to the tissue [4,5].

ECM is, in principle, a very dynamic structure that controls and is controlled by its surrounding environment, adapting its structural arrangement and composition to external

stimuli [6–9]. In fact, bone tissue is mainly subjected to two types of mechanical signals: (1) strain caused by tension or compression triggered by physical activity, and (2) shear stress as a result of interstitial fluid movement through bone lacunae. These deformations are sensed by bone resident cells, namely, osteoblasts and osteocytes, through their ion channels and/or cell membrane receptors (e.g., transmembrane integrins and cadherins) and transduced into intracellular biochemical signals in a process known as mechanotransduction [10,11]. Particularly, fluid shear stress has been shown to induce synthesis of non-collagenous proteins by osteoblasts, and therefore influence mineralization [12,13]. The Wnt/ β -Catenin canonical pathway is well established to be activated in response to mechanical stimulation, inducing downstream expression of secretory proteins, such as SPP1, and thereby influencing osteoblastogenesis and bone formation [14,15]. In vitro bioreactor studies have shown that cyclic compression loads prompt osteoblast division, matrix production, and increase levels of alkaline phosphatase (ALP) activity, which result in an improvement of the compressive modulus of the entire structure [16,17]. Furthermore, not only the magnitude and type of stimuli, but also the rate and frequency can influence the quality of new bone formation, and consequently, bone formation efficiency [18].

As such, understanding the detailed biomechanical aspects of bone homeostasis and regeneration is essential for transferring useful knowledge related to the integration of complex stimuli to which cells are subjected, either in physiological or pathological conditions. Generally, there are two possibilities to approach this: (1) experimental methods and (2) computational modeling. Notwithstanding, in silico modeling can provide valuable projections for the design and optimization of experimental strategies [19,20]. However, the complexity of in vivo biochemical and biomechanical features is the primary limitation of these studies, which require extreme processing competencies in order to formulate and solve several finite elements iterations. On the other hand, experimental methods make use of standard models from which representative clinical outcomes are foreseeable; particularly, animal models are currently a keystone of biomedical research. Yet, several limitations are raised when studying human diseases, as experimental animals often fail to recapitulate critical aspects, e.g., the age of patients and the specific human microenvironmental architecture and physiology [21–23]. On those grounds, over the last decade, bone tissue engineering strategies have been the focus of the research field as they allow us to recapitulate developmental processes in tridimensional (3D) in vitro settings [9,24]. Different types of materials have been used to engineer bone. Synthetic materials (e.g., polymers, composites, bioceramics, etc.) gained recognition mostly due to their great flexibility, reproducibility, and control over scaffold functionalization, and therefore the possibility to tune their composition, structural, and mechanical properties [25]. However, these materials still represent a very artificial environment to the cells, often exposing problems of biocompatibility and poor osteoinductive properties [26]. Natural-derived polymers (e.g., collagen, fibrin, chitosan, etc.) are constituted of naive ECM and show high biocompatibility but present poor mechanical properties and do not represent the structural organization of the native bone tissue [27]. As a matter of fact, the internal architecture of the scaffold, e.g., particularly the porosity and pore size, is shown to directly affect cell proliferation, signaling, and osteogenic differentiation [28,29]. In recent years, decellularization of tissues or organs has been widely explored since the resulting construct is able to preserve both the biochemistry and the architecture of the native ECM of the respective tissue [30,31]. Specifically for bone decellularization, partial or full demineralization is shown to further enable the exposition of soluble and insoluble osteogenic molecules that otherwise were embedded in the calcified matrix [32]. Therefore, the direct interaction of these molecules with seeded cells reportedly triggers osteogenic differentiation processes and consequently enhances bone formation [33].

In this study, we aim to investigate the early influence of mechanical stimuli on the behavior of bone marrow mesenchymal stem/stromal cells (hMSC) seeded in a physiologically relevant environment. Besides the native chemistry and mechanical properties of the bone environment offered by the decellularized human bone scaffold, a perfusion

bioreactor with a uniaxial compression load was used to mimic external forces to which bone cells are subjected in vivo. Finite element analysis of the applied forces did support the reliability of the model.

Finally, the design of multimodal bone tissue models, such as the one developed here, opens new opportunities to validate bone development, remodeling, and pathology studies, as it provides biologically meaningful in vitro systems in which specific experimental parameters can be systematically controlled.

2. Materials and Methods

2.1. Preparation of Decellularized Bone Scaffolds

Decellularized bone scaffolds were obtained from human trabecular femoral head specimens (permission number: 187/18, University of Wuerzburg ethics committee), as previously described in [34]. Briefly, freshly thawed samples were precisely cut in 3 mm thick slides using an electric diamond band saw (300, Exakt; D64, Walter Messner GmbH, Oststeinbek, Germany) to ensure homogeneous penetration of washing solutions through the complete sample volume. Blood and residual fat material were firstly removed by several cycles of washing in water and a chloroform (288306, Sigma-Aldrich, Steinheim, Germany) and methanol (8388.6, Carl-Roth, Karlsruhe, Germany) mix solution. Further decalcification of bone slices was achieved by incubation for several days in 2.5% ethylenediaminetetraacetic acid (EDTA, E5134, Sigma-Aldrich) in 10 mM Tris-base (T6066, Sigma-Aldrich), from where cylindrical constructs were shaped using a 10 mm biopsy punch. Complete decellularization of bone samples was achieved by enzymatic treatment with 100 Units/mL DNase (DN25, Sigma-Aldrich) and finalized with lyophilization (Martin Christ, Alpha 1–2 LDplus, Osterode am Harz, Germany) for 4 days under a vacuum pressure of 1 mbar. Processed bone scaffolds were stored at $-20\text{ }^{\circ}\text{C}$, and sterilization with 70% ethanol was always performed freshly the day before cell seeding.

2.2. Elastic Modulus Measurements

A TA ElectroForce[®] 5500/BOSE device (New Castle, PA, USA) equipped with a 200 N load cell in an unconfined compression test setup was used to assess the elastic modulus of scaffolds. Both native and decellularized cylindrical samples (3 mm height and 10 mm diameter; 3 technical replicates from 5 donors) were mounted in the setup and exposed to a compression load resulting in a total displacement of 13% ($=-0.39\text{ mm}$) at a rate of 0.001 mm/s or 0.005 mm/s, respectively. WinTest7[®] (version 7.2) software continuously recorded the resulting force (Newton) applied on scaffolds during testing. Elastic modulus results were obtained by linear regression of strain versus stress values for each sample.

2.3. Pore Size Measurements

Decellularized bone scaffolds from five donors were scanned using micro computed tomography (microCT, vivaCT40, SCANCO Medical AG, Brüttisellen, Switzerland), with an x-ray energy of 70 kV and a 0.114 mA tube current with 200 ms integration time and reconstructed with an isotropic voxel size of 0.0105 mm. Image data were exported to ImageJ (version 1.53c) [35]. Data were collected by measuring the Ferret diameter of 50 pores randomly distributed through the full volume of each sample using ROI manual selection and the Analyze menu.

2.4. Dynamic Bioreactor

A custom-made bioreactor system, previously described in [36], was designed to mimic the mechanical environment to which bone tissue is subjected in vivo, where both shear stress and cyclic compression can be applied to the cell-seeded scaffolds. Briefly, the system can be separated into three compartments—(1) the bioreactor cartridge, where the cell-seeded scaffolds are harbored inside a 10.4 mm diameter silicone housing, which allows gas exchange while avoiding fluid extravasation; (2) a computer-controllable peristaltic pump that ensures the continuous fluid flow of the cell culture medium through a

unidirectional closed-circuit centered between the bioreactor-cartridge and the medium reservoir; and (3) an uniaxial loading unit directly connected with the bioreactor cartridge, where frequency and magnitude of the piston displacement can be tailored. The bioreactor was maintained in aseptic conditions in a controlled chamber at 37 °C and with 5% CO₂.

2.5. Computational Fluid Dynamic

Two computational finite element models were established to calculate wall shear stress, pressure, and velocity in the bioreactor system and the decellularized bone scaffold. First, a model of the full system based on CAD data was set up by importing the geometry to ANSYS Fluent (version 19.2). The volume model was meshed with 195138 nodes. Liquid water with a dynamic viscosity of 0.6913 mPa·s in accordance with a temperature of 37 °C was set as the material model for the fluid. The inlet was modeled as velocity inlet with a velocity of 1.7 mL/min and the outlet as the outflow, as environmental condition atmospheric pressure was used. The scaffold geometry was simplified as a porous medium with a porosity of 90%. To access permeability, the differential pressure of three bone scaffolds of different donors was experimentally measured, and the permeability was calculated according to Darcy's law. Contact areas between the solid and fluid phases were modeled as interfaces. After initialization using the hybrid initialization method, the model was solved with five iterations. A second detailed model of the bone scaffold was established based on microCT data of decellularized bone scaffolds. Briefly, images of microCT data and chamber geometry were imported into ScanIP (Simpleware, version 14) for segmentation and meshing. After adjusting for size and application of the median filter, segmentations with two different thresholds were combined using a Booleans operation and dilate and close-Filter, as well as Gaussian smoothing. Flood fill was used on segmented masks to remove floating islands. After inlet, outlet, and walls were defined as boundary conditions, the model was meshed using the +FEGrid meshing algorithm as a msh-file containing 36212059 nodes and imported to Fluent (Version 19.2). Boundaries and material properties were set accordingly to the first model.

2.6. Mesenchymal Stem/Stromal Cells Isolation and Loading Protocol

hMSCs were isolated from human bone marrow from acetabular reaming in patients undergoing hip arthroplasty surgery after obtaining informed consent of the patient and ethical approval (187/18).

Briefly, mononuclear cells were collected from bone marrow aspirates by a Ficoll (Histopaque-1077, Sigma-Aldrich) density gradient centrifugation and repeatedly washed. The cell count was determined, and cells were cultured for adhesion selection of hMSCs. Cells were further expanded with basal medium (DMEM/F-12 GlutaMAX, Gibco, Bleiswijk, Netherlands) supplemented with 10% fetal bovine serum (FCS, Bio&Sell, Feucht, Germany), 1% Pen/Strep (100 U/mL, Gibco), 1% HEPES (Sigma-Aldrich), and 5 ng/mL fibroblast growth factor (FGF, 100-18C, PeproTech, Hamburg, Germany) until passage 4–6 and seeded in decellularized bone scaffolds as previously described in [34]. Briefly, 50 µL containing 1.5×10^6 cells was distributed on top of each scaffold and incubated for 3 h at 37 °C with 5% CO₂ to allow cell attachment, followed by 21 h static incubation with the supplemented basal medium.

For each dynamic condition, i.e., (1) only perfusion or (2) perfusion plus compression, three scaffolds were stacked in a bioreactor cartridge, and osteogenic differentiation cell culture medium (DMEM low glucose (Gibco) supplemented with 10% FCS, 1% Pen/Strep, 1% HEPES, 50 µg/mL L-Ascorbic acid 2-phosphate (Sigma-Aldrich), 5 mM β-Glycerophosphate disodium salt (Sigma-Aldrich), and 10 nM dexamethasone (Sigma-Aldrich)) was continuously perfused at 1.7 mL/min. Uniaxial compression loading was applied for 1 h per day at a frequency of 1 Hz and amplitude of 10%, whilst perfusion was temporarily halted.

The total differentiation culture duration was either one or seven days. On day four, half of the cell culture medium was renewed. Cells were harvested for further analysis

always 6 h after the last loading cycle. For all experiments, constructs in static conditions were implemented as controls.

2.7. Viability Assays

To confirm cell viability and scaffold integration, cell metabolic activity and distribution within the scaffold were assessed both by (1) MTT (3-(4,5-dimethylthiazol-2-yl)-2,5-diphenyltetrazolium bromide, 20395.04, Serva Electrophoresis, Heidelberg, Germany) assay and by histological staining of cryostat sections with Hematoxylin and Eosin (H&E).

Briefly, after 7 days of differentiation culture, each scaffold was cut in the middle and incubated at 37 °C for 3 h in 10% MTT (5 mg/mL) solution in a cell culture medium. Pictures from the top and the cross-section view of the entire scaffold were acquired using a stereomicroscope (Zeiss, Discovery V20, Oberkochen, Germany). Blank samples without cells were used as controls.

In parallel, samples were fixed and snap-frozen in Tissue-Tek® O.C.T.™ Compound (4583, Sakura Finetek, Hartenstein, Wuerzburg, Germany), from where 8 µm-thick cryosections were collected and stained with H&E. Scaffold integration and cell proliferation within each sample was examined under a light microscope (Leica, DMi8, Wetzlar, Germany).

Representative images are shown from three individual experiments.

2.8. Immunofluorescence Analysis

Immunofluorescence analysis of 7-day samples was performed to visualize the presence and location of either native or newly formed ECM proteins. Briefly, the cryosections were permeabilized with 0.1% (*v/v*) Triton-X (3051.3, Carl-Roth) for 30 min at RT and blocked with 1% (*w/v*) Bovine Serum Albumin (BSA, A1391, AppliChem, Darmstadt, Germany) for 1 h prior to treatment with primary antibodies (Collagen-type1, anti-Col1, dilution 1:300, ab34710, abcam, Cambridge, UK; Osteopontin, anti-SPP1, dilution 1:500, HPA027541, Sigma-Aldrich) overnight at 4 °C. After washing, samples were incubated with secondary antibody (goat anti-rabbit IgG conjugated with Alexa Fluor® 594, ab150080, abcam) for 2 h at RT. Finally, samples were embedded in Vectashield®-containing DAPI (H-1200, Vector Laboratories, Biozol, Eching, Germany) for nuclei staining. In addition, Phalloidin-iFluor 488 (ab176753, abcam) was added during primary antibody incubation for cell cytoskeleton visualization.

Antibody specificity control was performed by incubating the samples in 1% BSA without the first antibody, i.e., anti-Col1 and anti-SPP1, respectively, followed by standard incubation with secondary antibody and detection reagents.

2.9. Scanning Electron Microscopy and Energy Dispersive X-ray Spectroscopy

Scaffold structure and hMSC morphology were evaluated for each culture protocol after 30 h post differentiation by scanning electron microscopy (SEM) (Thermo Fischer Scientific, FEI Apero VS, Darmstadt, Germany). The samples were fixed in 4% formaldehyde, dehydrated in a serial dilution of ethanol, dried in tert-butanol, and immediately freeze-dried. Prior to imaging, all samples were sputter-coated (Leica, EM ACE600) with a 2 nm film of platinum to ensure conductivity of the sample's surface. Images were taken at an accelerating voltage equal to 1.5–3 kV and a magnification of ×200 and ×5000. Cellular details were artificially colored on magnified images using Photoshop® CS6 (Adobe, v13.0.1) for visualization purposes.

In addition, a dispersive energy X-ray (EDS) detector (Carl Zeiss, Gemini Sigma 300 VP, Oberkochen, Germany) operating at 10 KeV was used to determine the surface atomic composition of the decellularized bone scaffolds. Three random areas of interest were evaluated for each sample.

2.10. Gene Transcription Analysis

To analyze the early gene response of hMSC to mechanical stimuli, two scaffolds for each condition were harvested in Trizol (Sigma), and cells were lysed for 5 min at

50 Hz (TissueLyser LT, Quiagen, Hilden, Germany). RNA was isolated by 1-bromo-3-chloropropane (B9673, Sigma-Aldrich) phase separation followed by column separation according to the manufacturer's instructions (NucleoSpin RNA, Macherey-Nagel, Dueren, Germany). cDNA was synthesized by reverse transcription (Promega, Walldorf, Germany) from 1 µg of RNA.

Real-time Polymerase chain reaction (PCR) was performed by CFX96 Real-Time System (Bio-Rad). Primers for genes targeting either mechanosensory functions—fos proto-oncogen (cFos), prostaglandin-endoperoxide synthase 2 (Cox2), integrin subunit beta 5 (ITGb5), osteopontin (SPP1), bone morphogenetic protein 2 (BMP-2)—or osteochondral early differentiation—collagen type-VI (Col6), runt-related transcription factor 2 (Runx2), SRY-Box Transcription Factor 9 (Sox9)—were designed in the Primer Blast tool from NCBI and purchased from Biomers.net (Ulm, Germany). Primers sequence and NCBI reference numbers appear in Supplementary Table S1.

Expression of target genes was normalized with beta-2-microglobulin (B2M, NM_00448.2) as the reference gene, and results displayed as relative values ($10,000 \times 2^{-\Delta Ct}$).

2.11. Statistical Analysis

Qualitative data were analyzed using Graphpad Prism software (version 9.1) and presented as the mean \pm standard error of the mean. Statistical significance was investigated using the Kruskal–Wallis method followed by Dunn's multiple comparisons test. Statistical significance was set at $p \leq 0.05$.

3. Results

3.1. Scaffold Structure Characterization

The microstructure of decellularized bone scaffolds was evaluated by microCT reconstruction (Figure 1a). Three-dimensional porous scaffolds with highly interconnected anisotropically distributed pores were obtained from a combination of chemical, enzymatic and physical decellularization of human femoral head-derived trabecular bone.

Analysis of trabecular thickness (Figure 1b) and pore size distribution (Figure 1c) confirmed a preserved native bone tissue architecture with an overall trabeculae thickness average of 120.7 ± 17.8 µm and a wide Gaussian pore size distribution ranging from 100 to 2000 µm.

The stiffness of both native and decellularized constructs was determined by mechanical compression of 10% of the total scaffold length, i.e., approximately 0.3 mm (Figure 1d). Despite high both inter- and intra-donor variance, the elastic modulus of decellularized scaffolds (30.5 ± 4.6 kPa) evidently decreased about tenfold in comparison with native trabecular constructs (329 ± 36.6 kPa) due to the EDTA-induced decalcification occasioned by the decellularization protocol. Yet, EDS spectra obtained from decellularized bone scaffolds surface (Figure 1e) shows the remaining presence of bone minerals, such as calcium and phosphorus, 0.47 and 0.6 weight %, respectively.

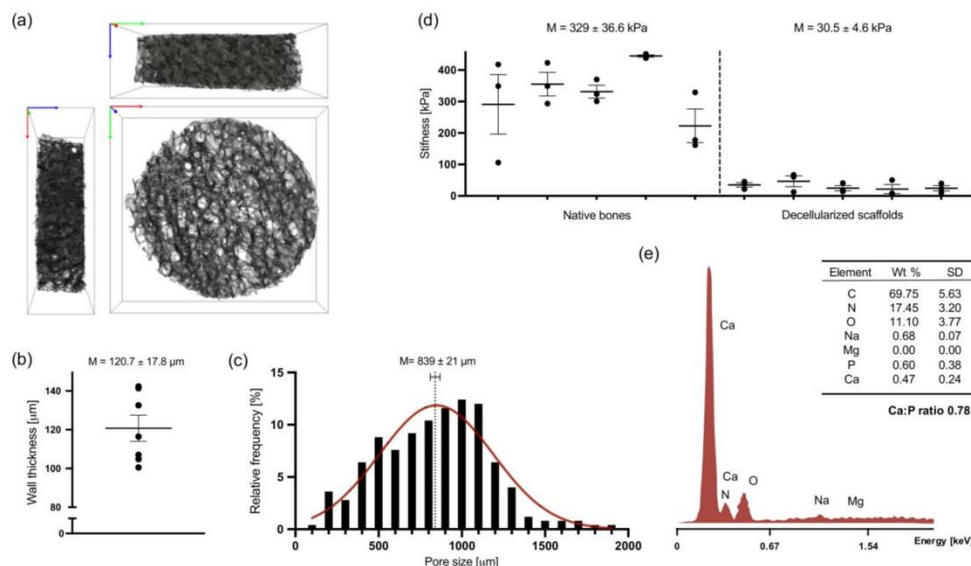


Figure 1. Structural characterization of human femoral head-derived decellularized bone scaffolds. (a) A 3D volume rendering obtained from mesh segmentation (10^6 tetrahedra elements) of microCT scan of a representative scaffold. Box dimension: $10 \times 10 \times 3$ mm. Axis: x—green, y—red, z—blue. (b) Wall thickness, or trabeculae thickness (Tb.Th), calculated from the total volume of interest (VOI) determined on Simpleware™ ScanIP respectively for each segmented mesh sample ($n = 7$). (c) Histogram of the relative frequency of pore size diameter ($n = 5$). Data assume a Gaussian distribution shown in red. (d) Stiffness of native and decellularized constructs, shown as means of elastic modulus obtained by mechanical compression testing ($n = 5$). The same shape and size were used for measurements of both native and decellularized samples. (e) Representative EDS spectra of decellularized scaffolds surface and respective quantification of atomic element weight percentage (wt%, $n = 2$). C—carbon, N—nitrogen, O—oxygen, Na—sodium, Mg—magnesium, P—phosphorus, and Ca—calcium.

3.2. Computational Modeling

In order to estimate mechanical conditions sensed by hMSCs in this specific complex in vitro system, finite element models of both (1) a simplified CAD model of the bioreactor and (2) a complex microCT model of the bone scaffold structure were established. For the porous media, permeability k was calculated taking into consideration the fluid flow $Q = 1.7$ mL/min, dynamic viscosity $\eta = 0.6913$ mPa·s (assumed for water at 37°C), length of the bone scaffolds $L = 9$ mm, the cross-sectional area of the bioreactor cartridge $A = 78.5$ mm² and experimentally measured differential pressure Δp using Darcy's law $k = \frac{Q \mu L}{A \Delta p}$, resulting in a mean permeability of $6.64 \times 10^{-12} \pm 1.22 \times 10^{-12}$ m². Using this value for the simplified CAD model, the velocity in the bioreactor cartridge was calculated as 0.16 mm/s. Please note that the velocity in the pipes is higher than in the bioreactor cartridge because of the different diameters of the tubing (Figure 2a). The fluid-induced wall shear stress on the scaffold in the microCT model was on average 8.5 mPa. Wall shear stress did not markedly differ between the first (Figure 2d) and third scaffold (Figure 2c). However, the highest values of wall shear stress were observed at the edges of the bone scaffold, while larger internal areas further away from the pores showed lower to zero wall shear stress values. The mean velocity in the fluid phase was calculated for the microCT model as 0.166 mm/s (Figure 2e), matching the result of the simplified CAD model, and the mean pressure as 40 mPa (Figure 2f). Notably, velocity peaked near the inlet and outlet

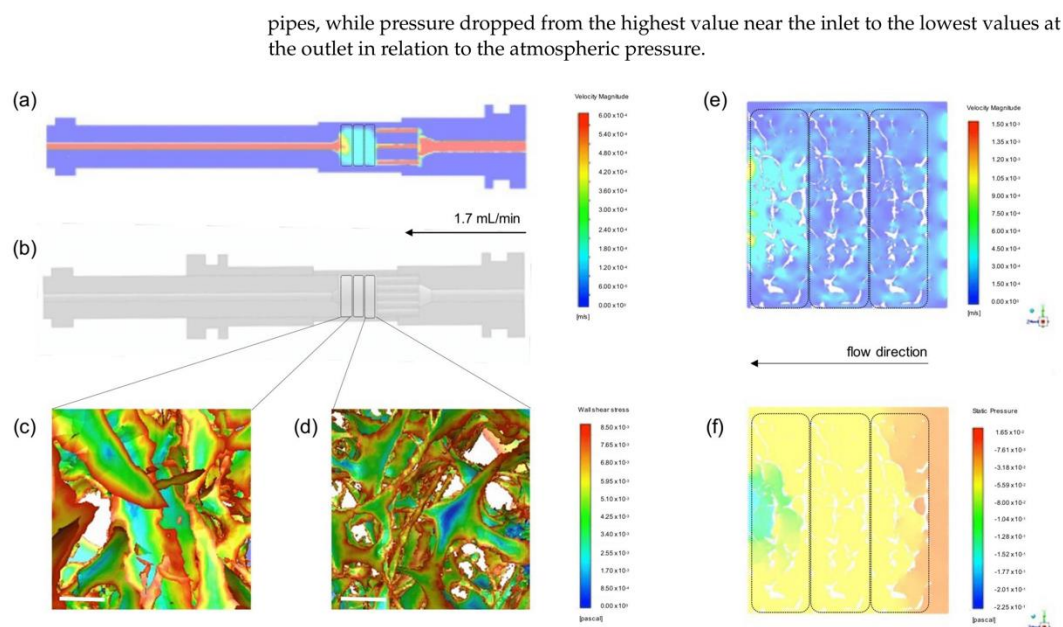


Figure 2. Computational fluid simulation. (a) Velocity profile of the simplified CAD model. Perfusion direction from the right (inlet) to the left (outlet). (b) A 3D rendering model of bioreactor parts visualized on AutoDesk Inventor software. (c,d) Close-up view of wall shear stress calculated in the microCT model for the scaffolds nearest the outlet and inlet, respectively. Scale-bar: 200 μm . (e) Cross-section of the velocity profile in the fluid phase from microCT model surrounding the bone scaffolds. (f) Cross-section of the pressure profile in the fluid phase from microCT model surrounding the bone scaffolds. In overview figures, the region where scaffolds are positioned is highlighted with traced line.

3.3. In Vitro Studies

3.3.1. hMSC—Scaffold Integration in the Static and Dynamic Culture

The impact of different cell culture regimens, i.e., static culture, flow perfusion, and combination with compressive loading, on hMSCs was initially studied after 7 days of culture. hMSC viability and distribution through the scaffold volume were evaluated by MTT staining (Figure 3a–d). Strong and consistent positive staining was observed for all conditions, indicating that the decellularized human bone scaffolds indeed provide a base for cell attachment and proliferation, promoting cell viability over time. Particularly better homogeneous distribution is visible in 3D scaffold cross-sections where perfusion is present, i.e., both perfusion only (Figure 3c) and perfusion + compression (Figure 3d) regimens.

To support this observation, histological staining of scaffolds' cryosections (Figure 3e–l) further shows a superior scaffold integration of hMSC in both dynamic conditions (Figure 3h,l) compared with static culture images (Figure 3f). Likewise, major cell growth is apparent only in dynamic conditions; there, hMSC are tidily densely packed around the high porous scaffold structure, and ECM deposition is observed at higher magnifications (Figure 3k,l).

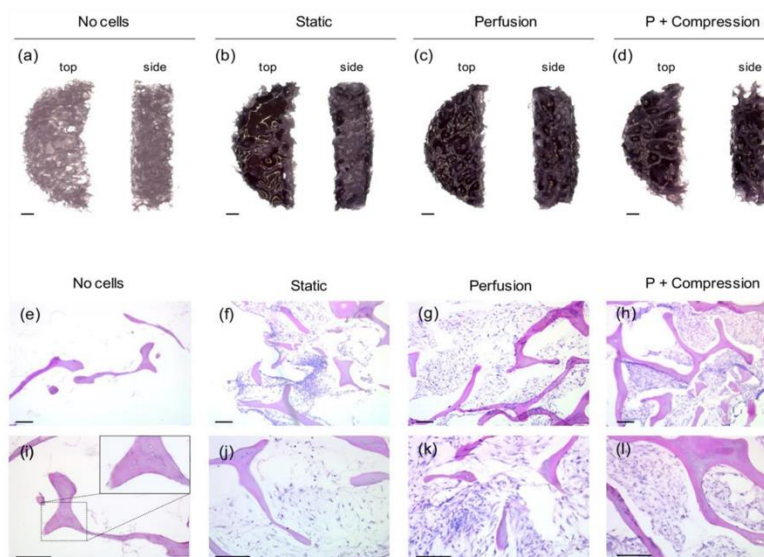


Figure 3. hMSC viability and scaffold integration after 7 days in osteogenic culture in different regiments. (a–d) Representative images of cell viability MTT staining of the top (left) and cross-section (right) view of scaffolds acquired by RGB-stereomicroscopy. (Scale-bar: 100 μm , $n = 3$). (e–l) Representative images of H&E staining from 8 μm -thick scaffold cryosections. Successful hMSC integration within the decellularized bone scaffold (strong pink color) is observed for all cell-laden conditions (purple color), while ECM deposition (light pink color) is rather visible in both perfusion (k) and perfusion + compression (l) conditions. A close-up zoom image (right upper corner) of non-cellular scaffolds (i) shows empty lacunae without the presence of osteocytes. (Scale-bar: 200 μm , $n = 3$).

Sections of non-cellular scaffolds (Figure 3e,i) show the presence of canaliculi and empty lacunae, confirming once more the maintenance of trabeculae native structures and the efficiency of the decellularization protocol.

hMSC integration within the scaffold, particularly cellular interaction with ECM bone proteins, was further investigated by immunofluorescence staining of Coll1 (Figure 4) and SPP1 (Figure 5).

An organized collagen fibrillar network is observed for all samples, including in the non-seeded control scaffold, validating the biochemical and structural preservation of collagen fibers as the most dominant organic ECM component in native bone tissue. Interestingly, a specific co-localization between collagen fibers and the presence of hMSC is observed, indicating the close contact between the cells and collagen fibers as an anchoring structure for cell attachment and proliferation. Confirming the above results, a higher cell density for both dynamic conditions is observed, where the collagen fiber's structure seems to be broadly arranged in space, in contrast with the static environment where the high cell density seems to shrink the soft matrix fibers.

Distinctively, an intrinsic SPP1 expression is mainly detected within the trabecular structures of decellularized bone scaffolds in all samples. Note that the positive signal is only attributed to SPP1-specific binding since that secondary antibody control (Figure S1) shows no detectable autofluorescence signal. Locally nascent SPP1 deposition is further observed in the pericellular matrix space only in mechanically stimulated conditions, i.e., perfusion only and perfusion and compression.

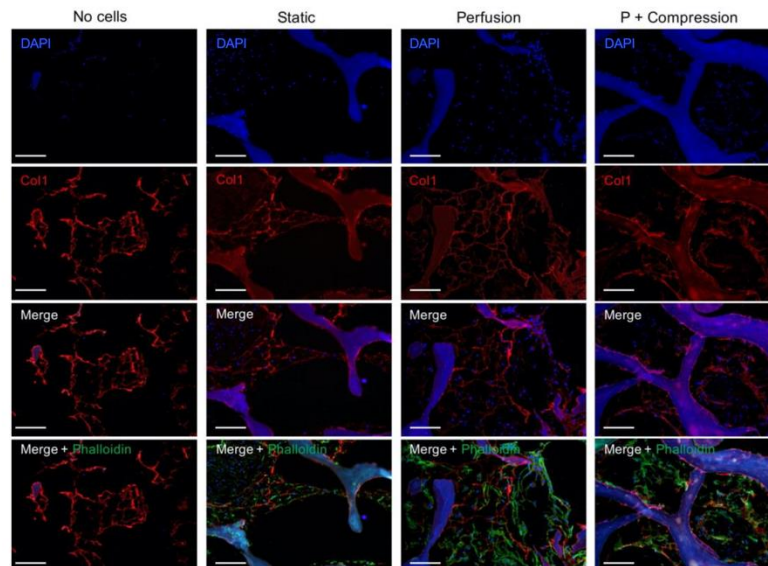


Figure 4. Immunofluorescence analysis of Col1 in acellular and cellular constructs in different culture conditions. Individual channels of nuclei (DAPI, blue) staining and Col1 (red) are shown in the first two rows, followed by the corresponding overlay images, also including cell cytoskeleton staining (Phalloidin, green). Due to an intrinsic auto-fluorescence of decellularized bone scaffolds for most of the common fluorescence channels, e.g., DAPI and FITC, the brightness of green-channel images was occasionally altered with Photoshop for visualization purposes. The biological interpretation of the images was not distorted. (Scale bar 200 μm , $n = 3$).

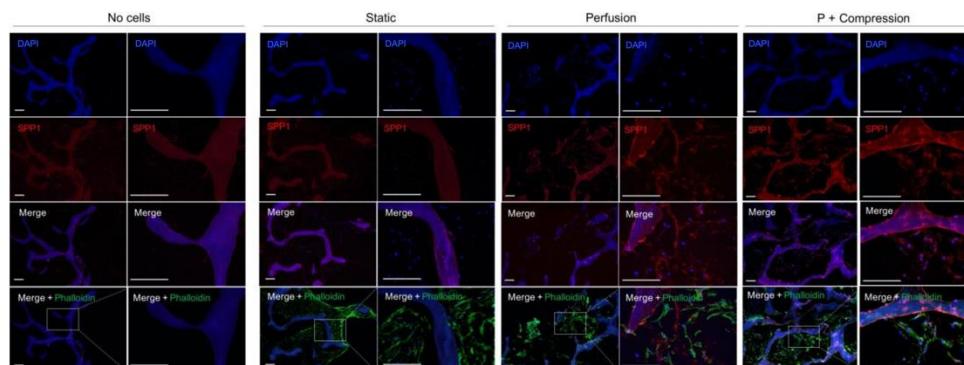


Figure 5. Immunofluorescence analysis of SPP1 in acellular and cellular constructs in different culture conditions. Individual channels of nuclei (DAPI, blue) staining and Col1 (red) are shown in the first two rows, followed by the corresponding overlay images, also including cell cytoskeleton staining (Phalloidin, green). Specificity control without the anti-SPP1 antibody is shown in Supplementary Figure S1. For each condition, a representative higher magnification picture is shown on the left, and a detailed high magnification from the field of interest is shown on the right. (Scale bar 200 μm , $n = 3$). Due to an intrinsic auto-fluorescence of decellularized bone scaffolds for most of the common fluorescence channels, e.g., DAPI and FITC, the brightness of green-channel images was occasionally altered with Photoshop for visualization purposes. The biological interpretation of the images was not distorted. (Scale bar 200 μm , $n = 3$).

ALP expression (data not shown) was also investigated for all conditions showing common positive staining, yet no obvious differences were detected between the different groups for this time point.

3.3.2. hMSC Early Response to Mechanical Stimuli

Considering the successful results of hMSC scaffold integration and bone-ECM protein accumulation, particularly under mechanical stress induced conditions, the early response of hMSC to mechanical stimuli was further investigated. Both hMSC morphology (Figure 6) and gene expression analysis (Figure 7) were assessed after only one cycle of loading, i.e., the total time of incubation was adjusted to 30 h.

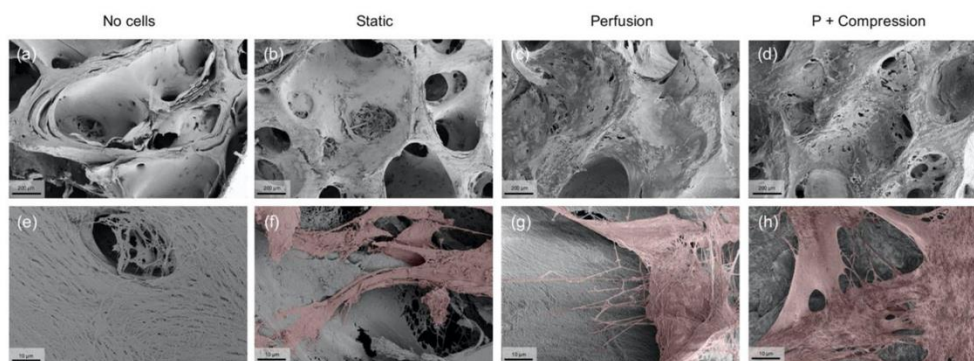


Figure 6. Representative SEM images of hMSC's early morphological response to mechanical stimuli. (a–d) 200× low magnification images confirm once more the presence of a highly porous structure, where hMSCs attach physically to the scaffold walls. (Scale bar 200 μm). (e–h) 5000× high magnification images show single cell interactions with the ECM through cytoplasm extensions, such as filopodia, present in samples subjected to dynamic culture. For visualization purposes only, cell surface areas were artificially colored in red with Photoshop. (Scale bar 10 μm).

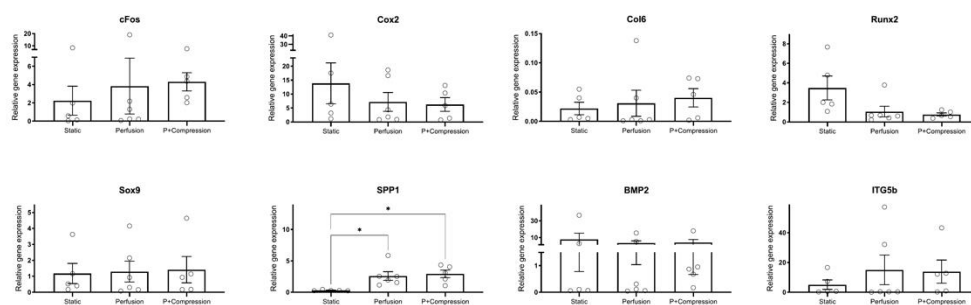


Figure 7. Gene expression analysis of hMSC's early response to mechanical stimuli. Expression of targeted genes involved in mechanosensory functions (cFos, Cox2, ITGB5, SPP1, BMP-2) unveil a general upregulation in dynamic conditions compared with static, whereas osteochondral early differentiation markers (Col6, Runx2, Sox9) expression seems to be inconclusive for this early time point. Expression of target genes was normalized with B2M as reference gene, and results displayed as relative values ($10000 \times 2^{-\Delta Ct}$). Statistical analysis using student Kruskal–Wallis one-way method followed by Dunn's multiple comparisons tests (* $p < 0.05$, $n = 5-6$).

Promptly, low magnification SEM images reveal a less-efficient hMSC integration in static (Figure 6b), compared with highly efficient cell dispersion in both dynamic conditions (Figure 6c,d). These results confirm and support the previous experiments, uncovering

the early determination of superior homogeneous cell distribution inflicted by dynamic conditions.

In high magnification images, it is possible to observe further the complex organic structure of the acellular scaffold (Figure 6e), mainly composed of collagen network fibers naturally present in the trabecular bone, as shown by immunofluorescence assays. Very interestingly, single hMSCs in both dynamic conditions (Figure 6g,h) seem to exhibit several filopodia extensions granting the cells to interact with the ECM environment actively, whereas in static conditions (Figure 6f), hMSC seems to display a steadier morphology, where the observed cell extrusions are smaller and rather orientated towards cell–cell than cell–ECM integrations.

Regarding the gene expression analysis (Figure 7), large donor-specific variations were observed due to the primary origin of hMSCs. Donor-to-donor differences are widely reported in the literature in various contexts, recognized to be a reflection of not only the age or overall health of the donor, but also of the diversity of environments from which hMSCs may be isolated [37,38].

hMSCs cultivated in both dynamic conditions showed, as expected, a trend of up-regulation for mechanosensitive factors (cFos, ITGb5, SPP1). Despite this trend, statistical analysis indicated no significance ($p > 0.05$) for most of the genes, except for SPP1. Cox2, a very early mechanical responsive gene, showed an opposite trend. BMP-2 expression, despite specific donor variation, does not seem to be significantly affected by mechanical stimulation in our experiments.

Considering markers related to osteochondral differentiation (Col6, Runx2, Sox9), no clear lineage commitment could be observed. Col6 appears to be upregulated in dynamic conditions, particularly when compressive loading is imposed, indicating an augmented differentiation into osteogenic lineage of hMSCs; in contrast, Runx2 was downregulated upon dynamic stimulation, while Sox9 expression was not altered.

4. Discussion

In vivo, hMSCs reside in specialized niches that are known for regulating stem cell fate throughout their life span [39,40]. In this work, we established a human decellularized bone scaffold as a model to mimic the native human bone extracellular matrix microenvironment. For the first time, we combined the naïve biochemical and architectural properties retained in these scaffolds with a dynamic culture system, reflecting the physiological mechanical forces to which native bone is subjected in vivo. Our data suggest that hMSCs sense and dynamically adapt to their environment mainly through cell–ECM interactions.

Decellularization techniques have been used in the bone tissue engineering field with the purpose of creating an immunogenic free material while preserving the native tissue structure and its innate osteoinductive qualities [30,31]. Rodriguez et al. [41] identified by mass spectrometry the maintenance of structural ECM proteins (e.g., Col1, Col4, Col6, etc.) present in human bone-derived demineralized fibers, in addition to several growth factors (e.g., BMP-2, BMP-4, BMP-7) and numerous other proteins supporting a variety of intra- and extracellular signaling pathways (e.g., fibronectin, fibrinogen, vitronectin, and laminin). Furthermore, it has been reported that partially or fully demineralized bone can provide not only osteoinductive factors, but also superior mechanical, biochemical, and architectural properties supporting scaffold functionality into physiological conditions [42,43]. We have previously developed a protocol based on physical, chemical, and enzymatic methods to consistently achieve human-femoral head-derived decellularized bone scaffolds [34]. The effective removal of all cellular components was previously confirmed, and the cell seeding protocol was optimized to ensure sustained cell viability. Here, we show the suitability of these scaffolds to investigate the response of hMSCs to mechanical stimuli in a naïve ECM environment.

Scaffolds' ultra-topography, particularly their trabeculae structure and pore size, has been shown to have a major influence on hMSCs proliferation and osteogenic commitment [44,45]. Interestingly, Smith et al. [42] concluded that decellularized scaffolds derived

from elderly bone donors with Tb.Th values comparable with the ones obtained in the present study (average of 120.7 μm) showed improved osteoinductive capacity with higher osteogenic gene expression and ALP activity [46]. Due to the propitious combination of abundant surface area for cell attachment and high distribution of large and interconnected pores (average of 839 μm), cell penetration, growth, and exchange of oxygen and nutrients are wholly provided [47–49].

Not only is the physical arrangement of the environment the main constraint to resembling the *in vivo* niche, but the stiffness of the matrix is likewise widely recognized and accounted for favoring cell–ECM mechanosignaling [50]. However, as a result of the partial decalcification protocol, the stiffness of the native trabecular bones exhibits much higher values (average of 329 kPa) compared with decellularized bone scaffolds (average of 30.5 kPa); the stiffness value obtained compares to previous studies. In fact, matrices with an elastic modulus between 25–40 kPa have been demonstrated to favor osteogenic lineage differentiation, associated with distinctively high expression of the osteogenic transcription factor Runx2 [51,52]. An essential element of human bone structure is hydroxyapatite, a mineral form based on Ca and P, conferring rigidity and mechanical competence to the tissue. However, in bone decellularization protocols, partial decalcification is often applied, mainly for handling purposes, but also for improving osteoinductive properties. Urist et al. [32] showed decades ago that the decalcification of native bone is able to not only retain bone morphogenic proteins and growth factors entrapped in the bone matrix, but even to further expose them and therefore facilitate specific cell–ECM interactions [53,54].

Yet, in the present study, a residual presence of both minerals was visible by EDS (Ca/P ratio = 0.78), which is significant to potentially trigger *de novo* mineral nucleation [55–57]. Future experiments will validate these findings.

Computational fluid simulations allow obtaining non-invasively and in high-resolution knowledge about mechanical conditions inside a 3D structure. Shear stress and hydrostatic pressure are assumed to be the main mechanical stimuli sensed by hMSCs [58–60], and finite element analysis can calculate their values even for extremely complex geometries. Models simplifying the bone scaffold to porous media as well as based on microCT scans have been reported using a broad range of perfusion velocity, porosity, and permeability. Shear stress caused by fluid perfusion is in fact widely recognized in the literature as a trigger of hMSC pro-osteogenic commitment (reviewed in [61]). Particularly, Melke et al. [62] concluded that a wall shear stress of 0.5–10 mPa promotes mineralization. Here, we present experimental data of superior scaffold integration of hMSCs due to dynamic rather than static conditions, while computational simulation revealed a mean wall shear stress of 8.5 mPa. Previously, simulations on a similar bioreactor setup showed that intermittent shear stress ranging from 0 to 13.35 mPa was able to induce osteogenic differentiation of rat-derived bone marrow stem cells seeded on a synthetic copolymer scaffold with a comparable porosity to ours, but with higher permeability, in the absence of any chemical stimuli [63]. Notably, our results show that mechanical conditions vary slightly depending on the position considered, *i.e.*, velocity is highest near the inlet and outlet and more homogenous in the middle, while pressure showed a gradient between the inlet and outlet. The potential of microCT scanning is widely recognized for studying complex structures and fine details [64,65], *e.g.*, inter-pore walls and/or pore size wide distribution, which are not taken in consideration in simplified models and can cause bias in the final analysis. Here, map visualization of wall shear stress in the microCT model reveals no distinct differences between the position in the bioreactor cartridge; rather, the heterogeneous complex geometry of the trabecular bone directs the shear stress sensed locally by the cells.

The here-developed human femoral head-derived decellularized bone scaffolds were consistently shown to provide hMSCs a valuable environment able to boost cell viability and ECM production, particularly in dynamic conditions. The presence of continuous perfusion has been shown to improve cell distribution throughout the scaffold, avoiding a preferential accumulation of cells on the edges as observed in static conditions. This is in line with previous studies where perfusion bioreactors and loading systems have been

shown to not only provide appropriate oxygen and nutrient supply, but also to have a direct accelerating effect on hMSC matrix production quality and quantity [66–68].

Furthermore, dynamic conditions also seem to influence cell-ECM interactions; in particular, mechanical stimulation seems to prevent the Col1 network shrinkage frequently reported in the literature to be provoked by high cell densities in static conditions [69,70]. Therefore, the wide Col1 network observed in dynamic conditions provides hMSCs with a higher surface area throughout the trabecular pores for adhesion and migration with abundant oxygen and nutrients access. Besides the Col1 scaffolding function as a major structural protein in the bone ECM, several studies have shown that ECM proteins, including collagen and non-collagen proteins, have a direct effect on both osteoconduction and osteoinduction [3,71]. Elango et al. [72] showed that Col1 fibrils modulate osteogenesis by binding to integrins of progenitor cells, triggering the differentiation cascade through MAPK-Runx2 activation. Likewise, due to the dual role of SPP1 as a protein-containing pro-adhesive tripeptide motif -RGD [73,74], as well as ECM calcium sequestering competence [75], native expression of SPP1 also plays a fundamental role in the dynamics of bone ECM. In fact, several studies have previously recognized an early SPP1 mRNA and protein expression in response to mechanical stress, elucidating its role in bone remodeling by affecting both osteoclastogenesis and osteoblastogenesis [76–79]. Consistently, we detected intrinsic SPP1 accumulation within the trabecular structure of all samples after 7 days of differentiation, yet locally nascent deposition in the pericellular matrix space was only clearly observed in hMSCs subjected to dynamic culture, validating the SPP1 role in response to mechanical stimuli.

In fact, an early response of hMSCs to mechanical conditions was observed even after only 1 day of stimulation. One relevant factor for hMSCs' mechanotransduction response is the exposure time to mechanical signals [80]. Our results show that dynamic culture has a pivotal role in determining the initial spreading of cells into the highly porous 3D scaffold. Furthermore, the combined effect of physical cues of the decellularized bone scaffold ultrastructure and the applied mechanical stimuli are able to control single-cell morphology. Indeed, specific micro- or nanoscale patterns capable of guiding early hMSCs differentiation commitment simply by confining cell shape are often reported in the literature [81–83]. In this study, a more spread morphology and the presence of cytoplasmic extensions, known as filopodia, able to sense and interact with the environment [84,85] were observed precisely in hMSCs exposed to dynamic conditions, which further corroborates the functionality and relevance of the human bone in vitro model achieved in this study. Supporting this observation, gene expression of hMSCs cultured in dynamic settings revealed signs of a stress-induced early osteogenic commitment, which has to be proofed in long-term experiments in the future. We observed a higher expression of cFos in hMSCs subjected to dynamic conditions, particularly when perfusion was combined with compression, while Cox2 transient expression after stimuli was probably outpaced at this timepoint. The expression of cFos and Cox2, genes associated with osteogenic mechanotransduction, is known to be quick and short lived [86,87]. Müller-Deubert et al. [88] reported a transient Cox2 mRNA expression in hMSCs for 2 h after stress with a peak of expression at 30 min. Nevertheless, both cFos and Cox2 mechanosensitive genes are described to follow a coordinated expression pattern attributed to early osteogenic but not chondrogenic differentiation [89,90].

In addition, we observed a remarkable upregulation of SPP1 for both dynamic conditions compared with static culture, followed by an increased protein accumulation seen in histology. As previously discussed, SPP1 is an abundant non-collagenous bone matrix protein with multifaceted functions involving cell interactions and ECM modulation [91,92]. Corroborating our findings, SPP1 has been frequently described as a mechanoresponsive target [76], and therefore has been shown to be critical for unloading-induced bone remodeling shown in vitro [93] and in vivo [79,94]. Likewise, upregulation of Col6 was detected—Col6 is a bone anabolic ECM protein and a constituent of the basement membrane involved fundamentally in cell adhesion [95,96], yet simultaneously exhibits a stimulatory effect

on osteogenesis in vitro [97,98]. Thereby, it is reasonable to assume that hMSCs establish stronger attachments to their environment in response to mechanical stress by increasing Col6 and SPP1 matrix deposition since both proteins contain RGD peptide sequences as well as connection domains to focal adhesion-related proteins. This assumption is further validated by the increased expression of ITG5b in hMSCs subjected to dynamic conditions in our study, which may, at a cellular level, trigger a cascade of downstream osteogenic differentiation in hMSCs [74,99–101].

In contrast, no clear expression pattern could be seen for BMP2, due to high donor variance. BMP2 is similarly a recognized target of mechanotransduction [102,103], and its role in bone repair is well established [104,105]. In fact, BMP2 autocrine signaling is known to be required for the downstream transcription of load-induced Runx2 by hMSCs [106,107], which may explain the low expression of Runx2 observed in our results as well. On the other hand, constant expression of Sox9 suggests that possible chondrogenesis commitment induced by mechanical stimuli [108,109] was absent in our model.

Taken together, the novelty of this study lies in the shared resembling of both biochemical and mechanical properties of human bone tissue elements in a simple in vitro model. Therefore, by providing a better understanding of mechanobiological interactions of cells with their environment, we aim to further identify key interactions to efficiently direct bone formation in homeostasis or pathologic scenarios.

5. Conclusions

Bone tissue-engineered constructs often fail to recapitulate either the chemistry, the ultrastructural physical cues, or the external mechanical properties that native bone is exposed to in the human body. In this study, the synergic effects of (1) 3D decellularized human trabecular bone-derived scaffold properties, namely, its trabecular morphology, heterogeneous porosity, and retained osteoinductive factors, and (2) the dynamic culture imposed by perfusion flow and compressive load are shown to be a promising strategy to accurately mimic the complex regiments occurring in vivo.

Here, we first elucidated the structure–function relations in our system by modeling the fluid flow through the highly complex structure interstices of the decellularized bone scaffold by integrating microCT data. Experimentally, we validated the improved effect of dynamic conditions in scaffold integration of hMSCs and reported a boost of ECM production. The early response of hMSCs to mechanical stimuli manifested in evident cell shape changes and stronger integrin-mediated adhesion to the matrix, promoting hMSCs commitment towards osteogenic lineage independently of Runx2 expression.

Although this study has demonstrated favorable improvements towards the synergetic effect of mechanical stimuli in a native human bone environment in vitro, there are still limitations that need to be addressed. Particularly, further long-term osteogenic functional assays would be crucial to accelerate its prospects in the translation of routine scientific practices in the bone engineering field.

Supplementary Materials: The following are available online at <https://www.mdpi.com/article/10.3390/ma14164431/s1>, Figure S1: Immunofluorescence secondary antibody control. The absence of detectable signal in the red channel confirms that positive staining is produced from detection of the antigen by the primary antibody (anti-Col1 or anti-SPP1, respectively) and not by the detection system or auto-fluorescence of the sample. Representative images of hMSCs in perfusion + compression condition. (Scale bar 200 μ m). Table S1: RT-qPCR primer sequences were generated with the Primer-BLAST tool from NCBI for this study. Gene name, forward and reverse primer sequence, NCBI reference number, and product length (pb: pair of bases) is shown.

Author Contributions: Conceptualization, M.H. and A.R.P.; investigation, A.R.P., A.L., S.S., D.G. and M.E.; resources, S.S., M.R., D.G. and J.H.; writing—original draft preparation, A.R.P. and A.L.; writing—review and editing, M.H., S.S., D.G., M.E., J.H., M.R.; project administration, M.H.; funding acquisition, M.H. and M.R. All authors have read and agreed to the published version of the manuscript.

Funding: This research was supported by the Interdisciplinary Center for Clinical Research (IZKF) at the University of Wuerzburg (Project D-361). Parts of this project were supported by the Max Buchner Research Foundation (Grant number 3775).

Institutional Review Board Statement: The study was conducted according to the guidelines of the Declaration of Helsinki and approved by the Ethics Committee of the University of Wuerzburg (186/18).

Informed Consent Statement: Informed consent was obtained from all subjects involved in the study.

Data Availability Statement: MDPI Research Data Policies. Data not shown can be obtained from the corresponding author upon reasonable request.

Conflicts of Interest: The authors declare no conflict of interest.

References

- Fuchs, R.; Warden, S.; Turner, C. Bone anatomy, physiology and adaptation to mechanical loading. In *Bone Repair Biomaterials*; Elsevier: Sawston, UK, 2009; pp. 25–68.
- Weiner, S.; Wagner, H.D. The material bone: Structure-mechanical function relations. *Annu. Rev. Mater. Sci.* **1998**, *28*, 271–298. [[CrossRef](#)]
- Lin, X.; Patil, S.; Gao, Y.-G.; Qian, A. The bone extracellular matrix in bone formation and regeneration. *Front. Pharmacol.* **2020**, *11*, 757. [[CrossRef](#)]
- Li, Y.; Aparicio, C. Discerning the subfibrillar structure of mineralized collagen fibrils: A model for the ultrastructure of bone. *PLoS ONE* **2013**, *8*, e76782. [[CrossRef](#)] [[PubMed](#)]
- Gautieri, A.; Vesentini, S.; Redaelli, A.; Buehler, M.J. Hierarchical structure and nanomechanics of collagen microfibrils from the atomistic scale up. *Nano Lett.* **2011**, *11*, 757–766. [[CrossRef](#)]
- Fan, D.; Creemers, E.E.; Kassiri, Z. Matrix as an interstitial transport system. *Circ. Res.* **2014**, *114*, 889–902. [[CrossRef](#)] [[PubMed](#)]
- Humphrey, J.D.; Dufresne, E.R.; Schwartz, M.A. Mechanotransduction and extracellular matrix homeostasis. *Nat. Rev. Mol. Cell Biol.* **2014**, *15*, 802–812. [[CrossRef](#)]
- Alford, A.I.; Kozloff, K.M.; Hankenson, K.D. Extracellular matrix networks in bone remodeling. *Int. J. Biochem. Cell Biol.* **2015**, *65*, 20–31. [[CrossRef](#)]
- Pereira, A.; Trivanović, D.; Herrmann, M. Approaches to mimic the complexity of the skeletal mesenchymal stem/stromal cell niche in vitro. *Eur. Cells Mater.* **2019**, *37*, 88–112. [[CrossRef](#)] [[PubMed](#)]
- Burger, E.H.; Klein-Nulend, J. Mechanotransduction in bone—Role of the lacunocanalicular network. *FASEB J.* **1999**, *13*, S101–S112. [[CrossRef](#)] [[PubMed](#)]
- Huang, C.; Ogawa, R. Mechanotransduction in bone repair and regeneration. *FASEB J.* **2010**, *24*, 3625–3632. [[CrossRef](#)] [[PubMed](#)]
- Grellier, M.; Bareille, R.; Bourget, C.; Amédée, J. Responsiveness of human bone marrow stromal cells to shear stress. *J. Tissue Eng. Regen. Med.* **2009**, *3*, 302–309. [[CrossRef](#)]
- Yourek, G.; McCormick, S.M.; Mao, J.J.; Reilly, G.C. Shear stress induces osteogenic differentiation of human mesenchymal stem cells. *Regen. Med.* **2010**, *5*, 713–724. [[CrossRef](#)] [[PubMed](#)]
- Robinson, J.A.; Chatterjee-Kishore, M.; Yaworsky, P.J.; Cullen, D.M.; Zhao, W.; Li, C.; Kharode, Y.; Sauter, L.; Babji, P.; Brown, E.L. Wnt/ β -catenin signaling is a normal physiological response to mechanical loading in bone. *J. Biol. Chem.* **2006**, *281*, 31720–31728. [[CrossRef](#)]
- Qin, L.; Liu, W.; Cao, H.; Xiao, G. Molecular mechanosensors in osteocytes. *Bone Res.* **2020**, *8*, 1–24. [[CrossRef](#)] [[PubMed](#)]
- Sittichokechaiwut, A.; Scutt, A.M.; Ryan, A.J.; Bonewald, L.F.; Reilly, G.C. Use of rapidly mineralising osteoblasts and short periods of mechanical loading to accelerate matrix maturation in 3D scaffolds. *Bone* **2009**, *44*, 822–829. [[CrossRef](#)] [[PubMed](#)]
- Ravichandran, A.; Lim, J.; Chong, M.S.K.; Wen, F.; Liu, Y.; Pillay, Y.T.; Chan, J.K.; Teoh, S.H. In vitro cyclic compressive loads potentiate early osteogenic events in engineered bone tissue. *J. Biomed. Mater. Res. Appl. Biomater.* **2017**, *105*, 2366–2375. [[CrossRef](#)]
- Hsieh, Y.F.; Turner, C.H. Effects of loading frequency on mechanically induced bone formation. *J. Bone Miner. Res.* **2001**, *16*, 918–924. [[CrossRef](#)] [[PubMed](#)]
- Geris, L.; Guyot, Y.; Schrooten, J.; Papantoniou, I. In silico regenerative medicine: How computational tools allow regulatory and financial challenges to be addressed in a volatile market. *Interface Focus* **2016**, *6*, 20150105. [[CrossRef](#)] [[PubMed](#)]
- Giorgi, M.; Verbruggen, S.W.; Lacroix, D. In silico bone mechanobiology: Modeling a multifaceted biological system. *Wiley Interdiscip. Rev. Syst. Biol. Med.* **2016**, *8*, 485–505. [[CrossRef](#)]
- Muschler, G.F.; Raut, V.P.; Patterson, T.E.; Wenke, J.C.; Hollinger, J.O. The design and use of animal models for translational research in bone tissue engineering and regenerative medicine. *Tissue Eng. Rev.* **2010**, *16*, 123–145. [[CrossRef](#)]
- Turner, A.S. Animal models of osteoporosis—Necessity and limitations. *Eur. Cell Mater* **2001**, *1*, 13.
- Zeiter, S.; Koschitzki, K.; Alini, M.; Jakob, F.; Rudert, M.; Herrmann, M. Evaluation of preclinical models for the testing of bone tissue-engineered constructs. *Tissue Eng. Methods* **2020**, *26*, 107–117. [[CrossRef](#)]
- Roseti, L.; Parisi, V.; Petretta, M.; Cavallo, C.; Desando, G.; Bartolotti, L.; Grigolo, B. Scaffolds for bone tissue engineering: State of the art and new perspectives. *Mater. Sci. Eng.* **2017**, *78*, 1246–1262. [[CrossRef](#)] [[PubMed](#)]

25. Lutolf, M.; Hubbell, J. Synthetic biomaterials as instructive extracellular microenvironments for morphogenesis in tissue engineering. *Nat. Biotechnol.* **2005**, *23*, 47. [[CrossRef](#)] [[PubMed](#)]
26. Nuss, K.M.; von Rechenberg, B. Biocompatibility issues with modern implants in bone—A review for clinical orthopedics. *Open Orthop. J.* **2008**, *2*, 66. [[CrossRef](#)]
27. Prasadh, S.; Wong, R.C.W. Unraveling the mechanical strength of biomaterials used as a bone scaffold in oral and maxillofacial defects. *Oral Sci. Int.* **2018**, *15*, 48–55. [[CrossRef](#)]
28. Loh, Q.L.; Choong, C. Three-dimensional scaffolds for tissue engineering applications: Role of porosity and pore size. *Tissue Eng. Rev.* **2013**, *19*, 485–502. [[CrossRef](#)]
29. Murphy, C.M.; Haugh, M.G.; O'Brien, F.J. The effect of mean pore size on cell attachment, proliferation and migration in collagen—Glycosaminoglycan scaffolds for bone tissue engineering. *Biomaterials* **2010**, *31*, 461–466. [[CrossRef](#)]
30. Gilbert, T.W.; Sellaro, T.L.; Badylak, S.F. Decellularization of tissues and organs. *Biomaterials* **2006**, *27*, 3675–3683. [[CrossRef](#)]
31. Rothrauff, B.B.; Tuan, R.S. Decellularized bone extracellular matrix in skeletal tissue engineering. *Biochem. Soc. Trans.* **2020**, *48*, BT20190079. [[CrossRef](#)]
32. Urist, M.R. Bone: Formation by autoinduction. *Science* **1965**, *150*, 893–899. [[CrossRef](#)]
33. Zhang, M.; Powers, R.M.; Wolfenbarger, L. Effect(s) of the demineralization process on the osteoinductivity of demineralized bone matrix. *J. Periodontol.* **1997**, *68*, 1085–1092. [[CrossRef](#)]
34. Pereira, A.R.; Rudert, M.; Herrmann, M. Decellularized human bone as a 3D model to study skeletal progenitor cells in a natural environment. In *Methods in Cell Biology*; Elsevier: Amsterdam, The Netherlands, 2020; Volume 157, pp. 123–141.
35. Schindelin, J.; Arganda-Carreras, I.; Frise, E.; Kaynig, V.; Longair, M.; Pietzsch, T.; Preibisch, S.; Rueden, C.; Saalfeld, S.; Schmid, B. Fiji: An open-source platform for biological-image analysis. *Nat. Methods* **2012**, *9*, 676–682. [[CrossRef](#)]
36. Ramani-Mohan, R.K.; Schwedhelm, I.; Finne-Wistrand, A.; Krug, M.; Schwarz, T.; Jakob, F.; Walles, H.; Hansmann, J. Deformation strain is the main physical driver for skeletal precursors to undergo osteogenesis in earlier stages of osteogenic cell maturation. *J. Tissue Eng. Regen. Med.* **2018**, *12*, e1474–e1479. [[CrossRef](#)]
37. Phinney, D.G.; Kopen, G.; Righter, W.; Webster, S.; Tremain, N.; Prockop, D.J. Donor variation in the growth properties and osteogenic potential of human marrow stromal cells. *J. Cell. Biochem.* **1999**, *75*, 424–436. [[CrossRef](#)]
38. Rady, D.; Abbass, M.; El-Rashidy, A.A.; El Moshy, S.; Radwan, I.A.; Dörfer, C.E.; Fawzy El-Sayed, K.M. Mesenchymal stem/progenitor cells: The prospect of human clinical translation. *Stem Cells Int.* **2020**, *2020*, 1–45. [[CrossRef](#)] [[PubMed](#)]
39. Herrmann, M.; Jakob, F. Bone marrow niches for skeletal progenitor cells and their inhabitants in health and disease. *Curr. Stem Cell Res. Ther.* **2019**, *14*, 305–319. [[CrossRef](#)] [[PubMed](#)]
40. Andrzejewska, A.; Lukomska, B.; Janowski, M. Concise review: Mesenchymal stem cells: From roots to boost. *Stem Cells* **2019**, *37*, 855–864. [[CrossRef](#)] [[PubMed](#)]
41. Rodriguez, R.U.; Kemper, N.; Breathwaite, E.; Dutta, S.M.; Huber, A.; Murchison, A.; Chen, S.; Hsu, E.L.; Hsu, W.K.; Francis, M.P. Demineralized bone matrix fibers formable as general and custom 3D printed mold-based implants for promoting bone regeneration. *Biofabrication* **2016**, *8*, 035007. [[CrossRef](#)]
42. Smith, C.A.; Board, T.N.; Rooney, P.; Eagle, M.J.; Richardson, S.M.; Hoyland, J.A. Human decellularized bone scaffolds from aged donors show improved osteoinductive capacity compared to young donor bone. *PLoS ONE* **2017**, *12*, e0177416. [[CrossRef](#)]
43. Bianco, J.E.R.; Rosa, R.G.; Congrains-Castillo, A.; Joazeiro, P.P.; Waldman, S.D.; Weber, J.F.; Saad, S.T.O. Characterization of a novel decellularized bone marrow scaffold as an inductive environment for hematopoietic stem cells. *Biomater. Sci.* **2019**, *7*, 1516–1528. [[CrossRef](#)]
44. Rubert, M.; Vetsch, J.R.; Lehtoviita, I.; Sommer, M.; Zhao, F.; Studart, A.R.; Müller, R.; Hofmann, S. Scaffold pore geometry influences bone-like tissue formation in dynamic cell culture conditions. *BioRxiv* **2020**.
45. Van Tol, A.F.; Schemenz, V.; Wagermaier, W.; Roschger, A.; Razi, H.; Vitiennes, I.; Fratzl, P.; Willie, B.M.; Weinkamer, R. The mechanoresponse of bone is closely related to the osteocyte lacunocanalicular network architecture. *Proc. Natl. Acad. Sci. USA* **2020**, *117*, 32251–32259. [[CrossRef](#)] [[PubMed](#)]
46. Chen, H.; Zhou, X.; Shoumura, S.; Emura, S.; Bunai, Y. Age- and gender-dependent changes in three-dimensional microstructure of cortical and trabecular bone at the human femoral neck. *Osteoporos. Int.* **2010**, *21*, 627–636. [[CrossRef](#)]
47. Lee, D.J.; Kwon, J.; Kim, Y.I.; Wang, X.; Wu, T.J.; Lee, Y.T.; Kim, S.; Miguez, P.; Ko, C.C. Effect of pore size in bone regeneration using polydopamine-laced hydroxyapatite collagen calcium silicate scaffolds fabricated by 3D mould printing technology. *Orthod. Craniofacial Res.* **2019**, *22*, 127–133. [[CrossRef](#)] [[PubMed](#)]
48. Kasten, P.; Beyen, I.; Niemeyer, P.; Luginbühl, R.; Bohner, M.; Richter, W. Porosity and pore size of β -tricalcium phosphate scaffold can influence protein production and osteogenic differentiation of human mesenchymal stem cells: An in vitro and in vivo study. *Acta Biomater.* **2008**, *4*, 1904–1915. [[CrossRef](#)] [[PubMed](#)]
49. Marcos-Campos, I.; Marolt, D.; Petridis, P.; Bhumiratana, S.; Schmidt, D.; Vunjak-Novakovic, G. Bone scaffold architecture modulates the development of mineralized bone matrix by human embryonic stem cells. *Biomaterials* **2012**, *33*, 8329–8342. [[CrossRef](#)]
50. Guimarães, C.F.; Gasperini, L.; Marques, A.P.; Reis, R.L. The stiffness of living tissues and its implications for tissue engineering. *Nat. Rev. Mater.* **2020**, *5*, 351–370. [[CrossRef](#)]
51. Xue, R.; Li, J.Y.S.; Yeh, Y.; Yang, L.; Chien, S. Effects of matrix elasticity and cell density on human mesenchymal stem cells differentiation. *J. Orthop. Res.* **2013**, *31*, 1360–1365. [[CrossRef](#)] [[PubMed](#)]

52. Engler, A.J.; Sen, S.; Sweeney, H.L.; Discher, D.E. Matrix elasticity directs stem cell lineage specification. *Cell* **2006**, *126*, 677–689. [[CrossRef](#)] [[PubMed](#)]
53. Yu, S.H.; Chan, H.L.; Chong, L.Y.; Jheng, Y.H.; Chang, P.C. Evaluation of the osteogenic potential of growth factor—Rich demineralized bone matrix in vivo. *J. Periodontol.* **2015**, *86*, 36–43. [[CrossRef](#)] [[PubMed](#)]
54. Liu, S.; Wang, Y.; Wang, J.; Qiu, P.; Wang, S.; Shi, Y.; Li, M.; Chen, P.; Lin, X.; Fang, X. A cancellous bone matrix system with specific mineralisation degrees for mesenchymal stem cell differentiation and bone regeneration. *Biomater. Sci.* **2019**, *7*, 2452–2467. [[CrossRef](#)]
55. Palmer, L.C.; Newcomb, C.J.; Kaltz, S.R.; Spoerke, E.D.; Stupp, S.I. Biomimetic systems for hydroxyapatite mineralization inspired by bone and enamel. *Chem. Rev.* **2008**, *108*, 4754–4783. [[CrossRef](#)] [[PubMed](#)]
56. Ramírez-Rodríguez, G.B.; Montesi, M.; Panseri, S.; Sprio, S.; Tampieri, A.; Sandri, M. Biomimetic recombinant collagen-based scaffold mimicking native bone enhances mesenchymal stem cell interaction and differentiation. *Tissue Eng.* **2017**, *23*, 1423–1435. [[CrossRef](#)] [[PubMed](#)]
57. Ramírez-Rodríguez, G.B.; Pereira, A.R.; Herrmann, M.; Hansmann, J.; Delgado-López, J.M.; Sprio, S.; Tampieri, A.; Sandri, M. Biomimetic mineralization promotes viability and differentiation of human mesenchymal stem cells in a perfusion bioreactor. *Int. J. Mol. Sci.* **2021**, *22*, 1447. [[CrossRef](#)]
58. Bequart, P.; Cruel, M.; Hoc, T.; Sudre, L.; Pernelle, K.; Bizios, R.; Logeart-Avramoglou, D.; Petite, H.; Bensidhoum, M. Human mesenchymal stem cell responses to hydrostatic pressure and shear stress. *Eur. Cell Mater.* **2016**, *31*, 160–173. [[CrossRef](#)]
59. Metzger, T.A.; Schwane, S.A.; LaNeve, A.J.; Kreipke, T.C.; Niebur, G.L. Pressure and shear stress in trabecular bone marrow during whole bone loading. *J. Biomech.* **2015**, *48*, 3035–3043. [[CrossRef](#)]
60. Hao, J.; Zhang, Y.; Jing, D.; Shen, Y.; Tang, G.; Huang, S.; Zhao, Z. Mechanobiology of mesenchymal stem cells: Perspective into mechanical induction of MSC fate. *Acta Biomater.* **2015**, *20*, 1–9. [[CrossRef](#)] [[PubMed](#)]
61. Arora, S.; Srinivasan, A.; Leung, C.M.; Toh, Y.-C. Bio-mimicking shear stress environments for enhancing mesenchymal stem cell differentiation. *Curr. Stem Cell Res. Ther.* **2020**, *15*, 414–427. [[CrossRef](#)]
62. Melke, J.; Zhao, F.; van Rietbergen, B.; Ito, K.; Hofmann, S. Localisation of mineralised tissue in a complex spinner flask environment correlates with predicted wall shear stress level localisation. *Eur. Cells Mater.* **2018**, *36*, 57–68. [[CrossRef](#)]
63. Yamada, M.A.Y.; Schwarz, T.; Hansmann, J.; Mustafa, K. Induction of osteogenic differentiation of bone marrow stromal cells on 3D polyester-based scaffolds solely by subphysiological fluidic stimulation in a laminar flow bioreactor. *J. Tissue Eng.* **2021**, *12*, 1–17. [[CrossRef](#)] [[PubMed](#)]
64. Palmroth, A.; Pitkänen, S.; Hannula, M.; Paakinaho, K.; Hyttinen, J.; Miettinen, S.; Kellomäki, M. Evaluation of scaffold microstructure and comparison of cell seeding methods using micro-computed tomography-based tools. *J. R. Soc. Interface* **2020**, *17*, 20200102. [[CrossRef](#)] [[PubMed](#)]
65. Ho, S.T.; Hutmacher, D.W. A comparison of micro CT with other techniques used in the characterization of scaffolds. *Biomaterials* **2006**, *27*, 1362–1376. [[CrossRef](#)]
66. De Girolamo, L.; Sartori, M.; Arrigoni, E.; Rimondini, L.; Albisetti, W.; Weinstein, R.; Brini, A.T. Human adipose-derived stem cells as future tools in tissue regeneration: Osteogenic differentiation and cell-scaffold interaction. *Int. J. Artif. Organs* **2008**, *31*, 467–479. [[CrossRef](#)] [[PubMed](#)]
67. Sittichokechaiwut, A.; Edwards, J.; Scutt, A.; Reilly, G. Short bouts of mechanical loading are as effective as dexamethasone at inducing matrix production by human bone marrow mesenchymal stem cell. *Eur. Cells Mater.* **2010**, *20*, 45–57. [[CrossRef](#)]
68. Morris, H.; Reed, C.; Haycock, J.; Reilly, G. Mechanisms of fluid-flow-induced matrix production in bone tissue engineering. *Proc. Inst. Mech. Eng. J. Eng. Med.* **2010**, *224*, 1509–1521. [[CrossRef](#)] [[PubMed](#)]
69. Schneider, R.K.; Puellen, A.; Kramann, R.; Raupach, K.; Bornemann, J.; Knuechel, R.; Pérez-Bouza, A.; Neuss, S. The osteogenic differentiation of adult bone marrow and perinatal umbilical mesenchymal stem cells and matrix remodelling in three-dimensional collagen scaffolds. *Biomaterials* **2010**, *31*, 467–480. [[CrossRef](#)]
70. Toosi, S.; Naderi-Meshkin, H.; Kalalinia, F.; Peivandi, M.T.; HosseinKhani, H.; Bahrami, A.R.; Heirani-Tabasi, A.; Mirahmadi, M.; Behravan, J. PGA-incorporated collagen: Toward a biodegradable composite scaffold for bone-tissue engineering. *J. Biomed. Mater. Res.* **2016**, *104*, 2020–2028. [[CrossRef](#)] [[PubMed](#)]
71. Ravindran, S.; Gao, Q.; Kotecha, M.; Magin, R.L.; Karol, S.; Bedran-Russo, A.; George, A. Biomimetic extracellular matrix-incorporated scaffold induces osteogenic gene expression in human marrow stromal cells. *Tissue Eng.* **2012**, *18*, 295–309. [[CrossRef](#)] [[PubMed](#)]
72. Elango, J.; Robinson, J.; Zhang, J.; Bao, B.; Ma, N.; de Val, J.E.M.S.; Wu, W. Collagen peptide upregulates osteoblastogenesis from bone marrow mesenchymal stem cells through MAPK-Runx2. *Cells* **2019**, *8*, 446. [[CrossRef](#)]
73. Bautista, D.S.; Xuan, J.; Hota, C.; Chambers, A.F.; Harris, J.F. Inhibition of Arg-Gly-Asp (RGD)-mediated cell adhesion to osteopontin by a monoclonal antibody against osteopontin. *J. Biol. Chem.* **1994**, *269*, 23280–23285. [[CrossRef](#)]
74. Chen, Q.; Shou, P.; Zhang, L.; Xu, C.; Zheng, C.; Han, Y.; Li, W.; Huang, Y.; Zhang, X.; Shao, C. An osteopontin-integrin interaction plays a critical role in directing adipogenesis and osteogenesis by mesenchymal stem cells. *Stem Cells* **2014**, *32*, 327–337. [[CrossRef](#)]
75. Zappone, B.; Thurner, P.J.; Adams, J.; Fantner, G.E.; Hansma, P.K. Effect of Ca²⁺ ions on the adhesion and mechanical properties of adsorbed layers of human osteopontin. *Biophys. J.* **2008**, *95*, 2939–2950. [[CrossRef](#)]
76. Terai, K.; Takano-Yamamoto, T.; Ohba, Y.; Hiura, K.; Sugimoto, M.; Sato, M.; Kawahata, H.; Inaguma, N.; Kitamura, Y.; Nomura, S. Role of osteopontin in bone remodeling caused by mechanical stress. *J. Bone Miner. Res.* **1999**, *14*, 839–849. [[CrossRef](#)] [[PubMed](#)]

77. Denhardt, D.T.; Noda, M.; O'Regan, A.W.; Pavlin, D.; Berman, J.S. Osteopontin as a means to cope with environmental insults: Regulation of inflammation, tissue remodeling, and cell survival. *J. Clin. Investig.* **2001**, *107*, 1055–1061. [[CrossRef](#)] [[PubMed](#)]
78. Wang, K.X.; Denhardt, D.T. Osteopontin: Role in immune regulation and stress responses. *Cytokine Growth Factor Rev.* **2008**, *19*, 333–345. [[CrossRef](#)]
79. Morinobu, M.; Ishijima, M.; Rittling, S.R.; Tsuji, K.; Yamamoto, H.; Nifuji, A.; Denhardt, D.T.; Noda, M. Osteopontin expression in osteoblasts and osteocytes during bone formation under mechanical stress in the calvarial suture in vivo. *J. Bone Miner. Res.* **2003**, *18*, 1706–1715. [[CrossRef](#)]
80. Darnell, M. Mechanotransduction Across Time and Length Scales. PhD Thesis, Harvard University, Cambridge, MA, USA, 2017.
81. Dalby, M.J. Topographically induced direct cell mechanotransduction. *Med. Eng. Phys.* **2005**, *27*, 730–742. [[CrossRef](#)]
82. McBeath, R.; Pirone, D.M.; Nelson, C.M.; Bhadriraju, K.; Chen, C.S. Cell shape, cytoskeletal tension, and RhoA regulate stem cell lineage commitment. *Dev. Cell* **2004**, *6*, 483–495. [[CrossRef](#)]
83. Mathieu, P.S.; Lobo, E.G. Cytoskeletal and focal adhesion influences on mesenchymal stem cell shape, mechanical properties, and differentiation down osteogenic, adipogenic, and chondrogenic pathways. *Tissue Eng. Rev.* **2012**, *18*, 436–444. [[CrossRef](#)] [[PubMed](#)]
84. Heckman, C.A.; Plummer, H. Filopodia as sensors. *Cell. Signal.* **2013**, *25*, 2298–2311. [[CrossRef](#)]
85. Kelly, D.J.; Jacobs, C.R. The role of mechanical signals in regulating chondrogenesis and osteogenesis of mesenchymal stem cells. *Birth Defects Res. Embryo Today Rev.* **2010**, *90*, 75–85. [[CrossRef](#)]
86. Peake, M.; Cooling, L.; Magnay, J.; Thomas, P.; El Haj, A. Selected contribution: Regulatory pathways involved in mechanical induction of c-fos gene expression in bone cells. *J. Appl. Physiol.* **2000**. [[CrossRef](#)]
87. Joldersma, M.; Burger, E.H.; Semeins, C.M.; Klein-Nulend, J. Mechanical stress induces COX-2 mRNA expression in bone cells from elderly women. *J. Biomech.* **2000**, *33*, 53–61. [[CrossRef](#)]
88. Müller-Deubert, S.; Seefried, L.; Krug, M.; Jakob, F.; Ebert, R. Epidermal growth factor as a mechanosensitizer in human bone marrow stromal cells. *Stem Cell Res.* **2017**, *24*, 69–76. [[CrossRef](#)] [[PubMed](#)]
89. Friedl, G.; Schmidt, H.; Rehak, I.; Kostner, G.; Schauenstein, K.; Windhager, R. Undifferentiated human mesenchymal stem cells (hMSCs) are highly sensitive to mechanical strain: Transcriptionally controlled early osteo-chondrogenic response in vitro. *Osteoarthr. Cartil.* **2007**, *15*, 1293–1300. [[CrossRef](#)] [[PubMed](#)]
90. Lu, L.Y.; Loi, F.; Nathan, K.; Lin, T.H.; Pajarinen, J.; Gibon, E.; Nabeshima, A.; Cordova, L.; Jämsen, E.; Yao, Z. Pro-inflammatory M1 macrophages promote Osteogenesis by mesenchymal stem cells via the COX-2-prostaglandin E2 pathway. *J. Orthop. Res.* **2017**, *35*, 2378–2385. [[CrossRef](#)]
91. Gilbert, M.; Shaw, W.J.; Long, J.R.; Nelson, K.; Drobny, G.P.; Giachelli, C.M.; Stayton, P.S. Chimeric peptides of statherin and osteopontin that bind hydroxyapatite and mediate cell adhesion. *J. Biol. Chem.* **2000**, *275*, 16213–16218. [[CrossRef](#)]
92. Si, J.; Wang, C.; Zhang, D.; Wang, B.; Hou, W.; Zhou, Y. Osteopontin in bone metabolism and bone diseases. *Med. Sci. Monit. Int. Med. J. Exp. Clin. Res.* **2020**, *26*, e919159-1–e919159-9. [[CrossRef](#)]
93. Klein-Nulend, J.; Roelofs, J.; Semeins, C.M.; Bronckers, A.L.; Burger, E.H. Mechanical stimulation of osteopontin mRNA expression and synthesis in bone cell cultures. *J. Cell. Physiol.* **1997**, *170*, 174–181. [[CrossRef](#)]
94. Ishijima, M.; Tsuji, K.; Rittling, S.R.; Yamashita, T.; Kurosawa, H.; Denhardt, D.T.; Nifuji, A.; Ezura, Y.; Noda, M. Osteopontin is required for mechanical stress-dependent signals to bone marrow cells. *J. Endocrinol.* **2007**, *193*, 235–243. [[CrossRef](#)]
95. McNeill, E.P.; Zeitouni, S.; Pan, S.; Haskell, A.; Cesarek, M.; Tahan, D.; Clough, B.H.; Krause, U.; Dobson, L.K.; Garcia, M. Characterization of a pluripotent stem cell-derived matrix with powerful osteoregenerative capabilities. *Nat. Commun.* **2020**, *11*, 1–15. [[CrossRef](#)] [[PubMed](#)]
96. Hanssen, E.; Reinboth, B.; Gibson, M.A. Covalent and non-covalent interactions of β ig-h3 with collagen VI: β ig-h3 is covalently attached to the amino-terminal region of collagen VI in tissue microfibrils. *J. Biol. Chem.* **2003**, *278*, 24334–24341. [[CrossRef](#)] [[PubMed](#)]
97. Clough, B.H.; McCarley, M.R.; Krause, U.; Zeitouni, S.; Froese, J.J.; McNeill, E.P.; Chaput, C.D.; Sampson, H.W.; Gregory, C.A. Bone regeneration with osteogenically enhanced mesenchymal stem cells and their extracellular matrix proteins. *J. Bone Miner. Res.* **2015**, *30*, 83–94. [[CrossRef](#)]
98. Izu, Y.; Ezura, Y.; Koch, M.; Birk, D.E.; Noda, M. Collagens VI and XII form complexes mediating osteoblast interactions during osteogenesis. *Cell Tissue Res.* **2016**, *364*, 623–635. [[CrossRef](#)]
99. Toma, C.; Ashkar, S.; Gray, M.; Schaffer, J.; Gerstenfeld, L. Signal transduction of mechanical stimuli is dependent on microfilament integrity: Identification of osteopontin as a mechanically induced gene in osteoblasts. *J. Bone Miner. Res.* **1997**, *12*, 1626–1636. [[CrossRef](#)]
100. Hu, D.D.; Lin, E.C.; Kovach, N.L.; Hoyer, J.R.; Smith, J.W. A biochemical characterization of the binding of osteopontin to integrins α v β 1 and α v β 5. *J. Biol. Chem.* **1995**, *270*, 26232–26238. [[CrossRef](#)] [[PubMed](#)]
101. Yang, J.; McNamara, L.E.; Gadegaard, N.; Alakpa, E.V.; Burgess, K.V.; Meek, R.D.; Dalby, M.J. Nanotopographical induction of osteogenesis through adhesion, bone morphogenic protein cosignaling, and regulation of microRNAs. *ACS Nano* **2014**, *8*, 9941–9953. [[CrossRef](#)]
102. Rui, Y.F.; Lui, P.P.Y.; Lee, Y.W.; Chan, K.M. Higher BMP receptor expression and BMP-2-induced osteogenic differentiation in tendon-derived stem cells compared with bone-marrow-derived mesenchymal stem cells. *Int. Orthop.* **2012**, *36*, 1099–1107. [[CrossRef](#)]

103. Sumanasinghe, R.D.; Bernacki, S.H.; Lobo, E.G. Osteogenic differentiation of human mesenchymal stem cells in collagen matrices: Effect of uniaxial cyclic tensile strain on bone morphogenetic protein (BMP-2) mRNA expression. *Tissue Eng.* **2006**, *12*, 3459–3465. [[CrossRef](#)]
104. Tsuji, K.; Bandyopadhyay, A.; Harfe, B.D.; Cox, K.; Kakar, S.; Gerstenfeld, L.; Einhorn, T.; Tabin, C.J.; Rosen, V. BMP2 activity, although dispensable for bone formation, is required for the initiation of fracture healing. *Nat. Genet.* **2006**, *38*, 1424–1429. [[CrossRef](#)] [[PubMed](#)]
105. Wulsten, D.; Glatt, V.; Ellinghaus, A.; Schmidt-Bleek, K.; Petersen, A.; Schell, H.; Lienau, J.; Sebald, W.; Plöger, F.; Seemann, P. Time kinetics of bone defect healing in response to BMP-2 and GDF-5 characterised by in vivo biomechanics. *Eur. Cell Mater.* **2011**, *21*, 177–192. [[CrossRef](#)] [[PubMed](#)]
106. Nishimura, I.; Hisanaga, R.; Sato, T.; Arano, T.; Nomoto, S.; Ikada, Y.; Yoshinari, M. Effect of osteogenic differentiation medium on proliferation and differentiation of human mesenchymal stem cells in three-dimensional culture with radial flow bioreactor. *Regen. Ther.* **2015**, *2*, 24–31. [[CrossRef](#)]
107. Schreivogel, S.; Kuchibhotla, V.; Knaus, P.; Duda, G.N.; Petersen, A. Load-induced osteogenic differentiation of mesenchymal stromal cells is caused by mechano-regulated autocrine signaling. *J. Tissue Eng. Regen. Med.* **2019**, *13*, 1992–2008. [[CrossRef](#)] [[PubMed](#)]
108. Hardingham, T.E.; Oldershaw, R.A.; Tew, S.R. Cartilage, SOX9 and Notch signals in chondrogenesis. *J. Anat.* **2006**, *209*, 469–480. [[CrossRef](#)]
109. Kupcsik, L.; Stoddart, M.J.; Li, Z.; Benneker, L.M.; Alini, M. Improving chondrogenesis: Potential and limitations of SOX9 gene transfer and mechanical stimulation for cartilage tissue engineering. *Tissue Eng.* **2010**, *16*, 1845–1855. [[CrossRef](#)]

Supplementary Materials

Modeling of the Human Bone Environment: Mechanical Stimuli Guide Mesenchymal Stem Cell–Extracellular Matrix Interactions

Ana Rita Pereira ^{1,2}, Andreas Lipphaus ³, Mert Ergin ^{1,4}, Sahar Salehi ⁴, Dominic Gehweiler ⁵, Maximilian Rudert ⁶, Jan Hansmann ⁷ and Marietta Herrmann ^{1,2,*}

¹ IZKF Group Tissue Regeneration in Musculoskeletal Diseases, University Hospital Wuerzburg, 97070 Wuerzburg, Germany; r-pereira.klh@uni-wuerzburg.de (A.R.P.); mertergin.de@gmail.com (M.E.)

² Bernhard-Heine-Centrum for Locomotion Research, University of Wuerzburg, 97074 Wuerzburg, Germany

³ Biomechanics Research Group, Ruhr-University Bochum, 44801 Bochum, Germany; andreas.lipphaus@rub.de

⁴ Department of Biomaterials, Center of Energy Technology und Materials Science (TAO), University of Bayreuth, 95447 Bayreuth, Germany; sahar.salehi@bm.uni-bayreuth.de

⁵ AO Research Institute Davos, 7270 Davos, Switzerland; dominic.gehweiler@aofoundation.org

⁶ Department of Orthopedic Surgery, Koenig-Ludwig-Haus, University of Wuerzburg, 97074 Wuerzburg, Germany; m-rudert.klh@uni-wuerzburg.de

⁷ Fraunhofer Institute for Silicate Research, Translational Center for Regenerative Therapies, 97082 Wuerzburg, Germany; jan.hansmann@isc.fraunhofer.de

* Correspondence: m-herrmann.klh@uni-wuerzburg.de

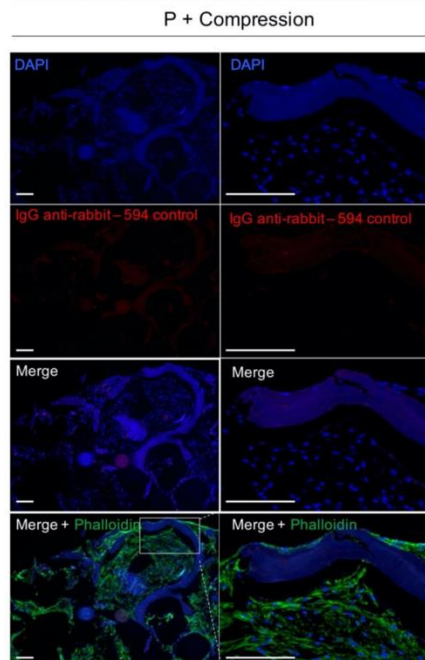


Figure S1. Immunofluorescence secondary antibody control. The absence of detectable signal in the red channel confirms that positive staining is produced from detection of the antigen by the primary antibody (anti-Col1 or anti-SPP1, respectively) and not by the detection system or autofluorescence of the sample. Representing images of hMSC in perfusion + compression condition. (Scale bar 200 μ m).

Table S1. RT-qPCR primer sequences were generated with Primer-BLAST tool from NCBI for this study. Gene name, forward and reverse primer sequence, NCBI reference number, and product length (pb: pair of bases) is shown.

Gene	Forward sequence 5'-3'	Reverse sequence 5'-3'	NCBI number	Product length (pb)
BMP-2	GGAAC- GGACATTCGGTCCTT	CACCATGGTCGAC- CTTTAGGA	NM_001200.4	127
cFos	GGGGCAAGGTGGAACAG- TTA	AGTTGGTCTGTCTCCGCTTG	NM_005252.4	139
Cox2	CAAATTGCTGG- CAGGGITGC	AGGGCTTCAGCATAAAGCGT	NM_000963.4	139
ITGb5	CCGGCTCGCAGGTCTCA	CACCAGGCACATTTTGGGTG	NM_002213.5	87
SPP1	TCTGGGAGGGCTTGGTTGTC	GGTAGTGAGTTTTTCCTT- GGTCG	NM_000582.2	124
BMP-2	GGAAC- GGACATTCGGTCCTT	CACCATGGTCGAC- CTTTAGGA	NM_001200.4	127
Col6 a1	TCTCAGATGGCAACTCG- CAG	ACCACGAAGATCTCGATGCC	NM_001848.3	91
Runx2	GAGTGGACGAGGCAA- GAGTT	CTGTCTGTGCCTTCTGGGTT	NM_001024630.3	127
SOX9	GCAGGCCGACTCGCCACAC	GGATTGCCCGAG- TGCTCGCC	NM_000346.3	73

Chapter 6.

Concluding remarks

Despite the recent developments towards *in vitro* models seeking to mimic the native biochemical and architectural complexity of adult stem cell niches, the significance of local interactions for MSCs physiology still remains elusive. In fact, most of the MSC biology knowledge derives from *in vitro* studies, evidently exposing cells to highly artificial situations that do not recapitulate the complexity of the naïve environment [53]. As a result, an ambiguous distinction between the physiological function of isolated MSCs in culture and their presumed *in vivo* counterpart often leads to a translation gap of results towards the clinics.

In this thesis, human cell and tissue-derived decellularized models were developed in order to address the influence of ECM-chemistry and -biomechanics on MSC behavior.

At first, cell culture-derived 2D matrices were generated by inducing MSCs to synthesize and secrete *de novo* ECM, followed by a mild decellularization protocol. Distinctly, osteo- and basal- cell culture environments resulted in four different models with unique chemical composition, in line with literature work [57, 58]. For instance, while collagen type-I, the most abundant protein of bone ECM [2, 59], was homogeneously detected in all the models, bone-specific ECM proteins [4] such as laminin and osteopontin, on the contrary, have been only detected punctually distributed in the long-term cultured osteogenic-induced matrix. Literature studies have previously shown that MSCs osteogenic lineage determination may result from communication of cell tension signals via mechanotransduction to the cell nucleus [60, 61]. Here was showed that reseeded MSCs establish early-detectable cytoplasmic-extension interactions with the fibrous-collagen rich ECM matrices, consequently inciting a significant elliptical-orientated cell morphological change. Corroborating those assumptions, osteo-induction functionality of the long-term cultured osteogenic-induced matrix and its relevance as a rather natural substrate for *in vitro* MSC culture was validated by alizarin-red staining of

MSCs mineral deposition after 21 days of culture without external supplementation of osteogenic differentiation factors.

In order to implement the aforementioned tissue third dimensionality, in this thesis a human decellularized trabecular bone 3D scaffold was further established as a straightforward tissue decellularization-based approach able to retain the bone naïve physical and chemical complexity.

The ultra-topography of the scaffold, particularly its retained-native trabeculae structure and pore size distribution and interconnectivity, has been shown to have a major influence on MSC proliferation and osteogenic commitment [62, 63]. Not only the physical arrangement of the environment is a main constraint to resemble the *in vivo* niche, but the stiffness of the matrix is likewise widely recognized and accounted in favor of cell-ECM mechanosignaling [64, 65]. In fact, culture of MSCs in softer materials (15-1.5 kPa), in opposition to conventional stiff cell culture materials (GPa range) such as glass or tissue culture polystyrene, has shown to favor stem-like MSCs phenotype [66]. In line with these literature reports, here the stemness potential of MSCs recovered from decellularized bone models was confirmed by upregulation of Oct4 and Nestin gene expression, and further functionally validated by increased efficiency of colony-forming capability of cells.

Beyond the dimensionality, proteins specifically present in cell- and/or bone-derived decellularized models surely play a significant role in MSC *in vitro* cell fate. In this thesis for the first-time a comparative proteomic analysis was performed in order to speculate on novel ECM target molecules involved in regulation of MSC behavior and functions, such as adhesion, metabolic activity and osteogenic differentiation. Interestingly, several proteins involved in hematopoietic compartment function, such as immune effector process and antimicrobial humoral response, e.g., proteoglycans, hemoglobin, prothrombin, *etc.*, were exclusively detected in the bone-decellularized scaffold, resembling the close association of MSCs to the hematopoietic stem cell niche in bone marrow [26]. Further supporting data corroborating the preservation of MSCs naïve phenotype was obtained by the detectable expression of CXCL12, an important niche factor associated with hematopoietic stem cells maintenance, quiescence and mobilization [67], at gene and protein level in MSCs cultured for 5 days in basal conditions in 3D bone-decellularized scaffolds.

Additionally, proteomics results further revealed exclusive-presence of important non-collagenous proteins produced by hepatic cells in decellularized scaffolds, transported to bone by bloodstream, such as fetuin-A [68, 69] and secreted phosphoprotein-24 [70]. Both proteins are involved in the bioactivity of the bone mineral phase exhibiting high affinity to osteoinductive chemokines and growth factors, possibly manifested in an enhanced osteogenic potential of reseeded MSCs observed by alkaline phosphatase activity staining as early as day 7 of differentiation.

Undoubtedly, bone tissue is a particularly complex composite with multiple stages of hierarchical organization. At the molecular level, self-assembly collagen triple helices fibrils intercalate with hydroxyapatite that grow within the fibrils, regulating their nucleation and growth [5]. However, in bone decellularization protocols partial decalcification is usually required, mainly for handling purposes but also to enhance the exposition of bone morphogenic proteins and growth factors entrapped in the matrix [71]. Accurately, energy-dispersive x-ray spectrometry shown no detectable presence of minerals in the 2D cell-derived decellularized matrices. On the other hand, residual below-physiological values of calcium and phosphate were detected in 3D decellularized scaffolds, therefore conjectured to provide a nucleation initial point for augmented mineral deposition during osteogenesis. In order to explore the presence of minerals on osteogenesis, in this thesis recombinant collagen-based scaffolds mimicking the mineralization of native bone have been manufactured in presence of magnesium, a stabilizer for hydroxyapatite crystals nucleation, by freeze-drying. Mineralized scaffolds showed to significantly support an increase cell growth and scaffold repopulation compared to non-mineralized scaffolds. This observed effect was shown to be a combined result from the biocompatibility and osteoinductive properties associated with chemistry of hydroxyapatite [72], with the unique rough-topography created by the homogeneous incorporation of minerals in the collagen-organic matrix, therefore favoring cell adhesion and protein absorption [73].

Furthermore, biomimetic mineralization has shown to not only improve cell viability, but also trigger the osteogenic potential of MSCs with a clear trend of upregulated osteogenesis related genes, particularly type-I collagen. Therefore, revealing the pivotal interplay between the organic and inorganic components in the bone tissue, which ultimately coordinate MSCs fate.

It is widely accepted that *in vitro* models should not be confined to stationary conditions [56, 74]. Literature is vast when recognizing the effect of shear stress on promoting pro-osteogenic commitment of MSCs [75, 76]. In here, experimental data showed superior scaffold repopulation of MSCs due to dynamic rather than static conditions, for both decellularized bone and collagen-functionalized scaffolds. Notably, flow-induced wall shear stress simulated in micro-computed tomography data for the decellularized bone model, revealed a mean value of 8.5 mPa, fitting in the literature range reported to promote mineralization [76]. However, local map-visualization showed heterogeneous distributed trabeculae-shape dependent shear stress locally sensed by the cells, unraveling the naïve heterogeneity of MSCs population where particular cells remain physically sheltered to mechanical stimuli.

Furthermore, dynamic conditions also seem to influence MSC-ECM interactions through integrin-mediated cell cytoplasmic extensions [77, 78]. In particular, mechanical stimulation seems to reinforce collagen network fiber assembly, therefore providing MSCs with a higher surface area for adhesion and migration with abundant oxygen and nutrients access. This is in line with previous studies, where perfusion bioreactors and loading systems have been shown to not only provide appropriate gas exchange but also to have a direct accelerating effect on MSCs-matrix *de novo* production quality and quantity [79-81]. Corroborating these findings, genes expression of proteins associated with bone anabolic ECM, such as osteopontin [82] and type-VI collagen [83, 84] were found to be early upregulated in dynamic conditions, particularly when compressive loading was imposed, indicating an augmented MSC osteogenic lineage determination.

Finally, the novelty of this thesis lays in the step-wise approach towards the complexity of *in vitro* modelling of MSCs interaction within the skeletal niche. Altogether, the results provided suitable *in vitro* models to study the overall functions of MSCs in a physiological relevant microenvironment, sharing both biochemical and mechanical properties of human bone tissue elements. Ultimately, this work surely offers a valuable tool for both fundamental prospective study of MSCs identity counterpart *in vivo*, as well as for clinical biology modelling of diseases and pharmacology approaches.

Future perspectives

It is widely recognized that the interplay with systemic factors and cells of different maturation and activation states from each particular niche region surely plays a pivot role in MSC behavior and function determination. Reproducing these interactions in experimental systems, such as the ones described in this thesis, surely provides a foundation to answer significant open questions in the field of fundamental regenerative processes as well as to explore novel rational cell-based therapeutic strategies. Some potential further model increments of complexity and future applications are mentioned:

Addressing the mineralization on decellularized models

In this thesis the lack of physiological-mineralization due to the limitations of the decellularization techniques was addressed by material-functionalization of a collagen-based scaffold. However, the rich-organic composition offered by the decellularized ECM was not fully addressed in this system either. Although a material science challenge to be addressed, functionalization of the decellularized ECM with hydroxyapatite crystals would certainly provide a remarkable interesting tool to study the bio-synergetic effect of the fully-mimicking bone ECM on MSCs behavior.

Addressing other types of mechanical loading

The relations between mechanical loading and bone metabolism have been recognized for more than one century, particularly since Wolff based on anatomical dissection studies described how bone mass, and consequently function, is determined by the local mechanical stress perceived by the tissue [85]. Different experimental both *in vivo* and *in vitro* models have been used to study how bone remodeling is affected by mechanical forces, for a large spectrum of mechanical deformation. Moreover, the literature is vast and occasionally conflicting in regards of how loading approaches affect the response of cells towards viability and/or osteogenic differentiation. Namely changes on the amplitude of the stimuli [86], the frequency [87], the wave form, i.e., triangular, sinusoidal, or trapezoidal shape [88], the total duration, i.e. number of cycles [89], and the periodicity of resting [90] may directly influence the outcomes. Given that, addressing further combination of loading setting features on the here developed dynamic model,

certainly would provide a key fundamental understanding of bone mechanical adaptation processes, which are up to now not fully understood.

Addressing systemic paracrine signals

It is known that MSCs are recruited to sites of stress or inflammation through biochemical toll-like receptor recognition and further signaling activation [91]. As so, the chemotaxis profile and functional effect of inflammatory factors on MSC behavior should be addressed with perspectives for new therapeutic approaches. Although most work is often performed by stimulation of MSCs to single cytokines [92, 93], platelet-rich plasma has successfully been used to mimic the combinatorial effect of several growth factors and cytokines that are released during inflammation, e.g., transforming growth factor- β , vascular endothelial growth factor, insulin-like growth factor I, basic fibroblast growth factor, endothelial growth factor, *etc.* [94, 95]. Platelet-released factors showed to not only enhance MSCs recruitment, proliferation and osteogenic lineage commitment, but also promote MSCs immunomodulatory and paracrine activity [96]. Thus, the incorporation of such stimuli in experimental designs using the here developed 3D decellularized bone model would be of extreme scientific urge in order to access MSCs immunomodulatory behavior in the course of regeneration in a unique *in vitro* model.

Addressing the hematopoietic stem cell niche

In this thesis, exclusively MSCs behavior in culture was addressed. Yet, a single culture approach is fairly reductant when aiming to model the stem cell niche, particularly in respects with the interactions with other neighboring cells.

The crosstalk between MSCs and hematopoietic cells in bone marrow homeostasis have been widely studied in the context of adult tissue regeneration [97, 98]. Interestingly, it has been shown that MSC secreted factors, such as stem cell factor and CXCL12 are able to control hematopoietic stem cells quiescence, survival, proliferation, self-renewal and mobilization [99, 100]. In turn, hematopoietic cells may trigger osteogenic differentiation of MSCs through BMP2 and BMP6 signaling [101]. Due to the experimentally observed rushed *ex vivo* differentiation of hematopoietic cells in culture, development of improved amplifying strategies where cells retain the stem phenotype are a promising tool to support translation to clinical applications. In fact, MSCs have been shown to support expansion of hematopoietic stem cells in co-culture systems [102],

advocating for the potential of the here developed 3D bone-decellularized model with naïve architecture and chemical composition, towards an optimized *in vitro* tool for recapitulation of the bone marrow stromal niche.

Addressing the bone remodeling multicellular unit

Bone homeostasis depends on the resorption of aged bone by osteoclasts and formation of new bone by osteoblasts [103]. Imbalance of this tightly coupled process can cause diseases such as osteoporosis. Studies suggested that osteoblasts could regulate osteoclast formation [104, 105], while osteoclasts have been shown to also be able to dynamically affect MSCs-osteoblastic differentiation [106] through direct cell-cell contact, cytokines and extracellular matrix interaction [107]. Hence, the study of mechanisms that regulate communication between osteoclasts and osteoblasts in a complex system may be addressed through the 3D bone-decellularized model in order to facilitate the macromolecular spatial interactions within the skeletal niche.

Addressing the perivascular function

Tissue formation and regeneration, as well as the survival of bone grafts, are under the control of vessels, which supply oxygen and nutrients to the cells [108]. At perivascular sites, MSCs assume a pericyte-like function as stabilizers of newly formed blood vessels, thus modulating the angiogenic response through cross-talk with endothelial cells [109-111]. Likewise, MSCs pericyte activity is reported to control hematopoietic cells mobility, i.e., low permeable endosteal vessels with high integrity (H-type) favor hematopoietic cells niche retention, while sinusoidal vessels with low integrity (L-type) offer a facilitated cell transference [112]. Therefore, exploring the co-culture effect of MSCs with endothelial cells may provide significant insights towards stem cells mobility and potential role in the systemic response.

Addressing cancer progression

Bone marrow niches can also be targeted by metastasizing cancer cells, developing a malignant vicious cycle between niche and tumor cells, where the ECM is dynamically adapted to each step of tumor progression [113]. It is proposed that MSCs and their progeny may in fact facilitate neoplastic growth [114]. MSC derived CXCL12-gradient is one of the most described explanations for tumor-to-bone marrow homing, as result of a

chemo-attractant gradient for CXCR4-expressing cancer cells [115]. However, the interactions with bone resident cells and tissue functionality are still to be further explored, particularly in relation with the dynamic of the bone remodeling unit, e.g., prostate cancer cells induce an osteoblastic-type lesion, in contrast to breast cancer and myeloma cells, which create typically osteolytic bone lesions [116]. Furthermore, functional modification of MSCs in hematologic malignancies, including acute lymphoblastic, myeloid leukemia, lymphomas, chronic myeloid leukemia, and myelodysplastic syndromes must be further addressed, while it is still unknown whether malignant hematopoietic progenitors modified MSCs or if leukemia-triggering changes occurred first in MSCs and the healthy marrow niche [117, 118].

In addition, a major feature of solid tumors is hypoxia, which increases patient treatment resistance and favors tumor progression [119, 120]. It is known that hypoxia environment activates transcription factors such as hypoxia-inducible factor [121], thus implicating a broad range of genes targeting several cellular functions such as angiogenesis, cell survival/death, metabolism, pH regulation, adhesion, extracellular matrix remodeling, migration and metastasis. Although now recognized as a major contributor to cancer progression and to treatment failure, the functional consequences of hypoxia signaling in cancer should be further addressed. The here developed 3D model may provide a unique tool for the study of such experimental setups by recapitulating the complex architectural network of bone trabeculae.

Addressing the aging process

Lastly, the dynamics of the bone marrow niche is reported to vary strongly also with age. Quiescence-to-senescence transition of niche-residing MSCs are reported to occur during aging, assumed to be driven either by the age-associated fat tissue expansion [122] and/or the inherent modulation of number and type of vessels in bone and bone marrow [123]. This phenomenon, albeit still not completely elucidated, strongly impairs the interactive signaling network of the overall niche system and ultimately the complete regenerative activity. Thus, the possibility to explore co-culture interactions of MSCs with mature adipocyte cells in a mimetic complex system that resembles the skeletal niche here presented, may provide useful knowledge regarding the root-developing causes of MSC senescence phenotype, hardly addressed in the literature.

References

1. Bilezikian, J.P., L.G. Raisz, and T.J. Martin, *Principles of bone biology*. 2008: Academic press.
2. Rossert, J. and B. de Crombrughe, *Type I collagen: structure, synthesis, and regulation*, in *Principles of bone biology*. 2002, Elsevier. p. 189-XVIII.
3. Viguet-Carrin, S., P. Garnero, and P. Delmas, *The role of collagen in bone strength*. Osteoporosis international, 2006. **17**(3): p. 319-336.
4. Robey, P.G. and A.L. Boskey, *The composition of bone*. Primer on the metabolic bone diseases and disorders of mineral metabolism, 2008. **7**: p. 32-38.
5. Zhang, W., et al., *Nucleation sites of calcium phosphate crystals during collagen mineralization*. Journal of the American Ceramic Society, 2003. **86**(6): p. 1052-1054.
6. Buck, D.W. and G.A. Dumanian, *Bone biology and physiology: Part I. The fundamentals*. Plastic and reconstructive surgery, 2012. **129**(6): p. 1314-1320.
7. Teti, A., *Bone development: overview of bone cells and signaling*. Current osteoporosis reports, 2011. **9**(4): p. 264-273.
8. Henriksen, K., et al., *Local communication on and within bone controls bone remodeling*. Bone, 2009. **44**(6): p. 1026-1033.
9. Burger, E.H. and J. Klein-Nulend, *Mechanotransduction in bone—role of the lacunocanalicular network*. The FASEB journal, 1999. **13**(9001): p. S101-S112.
10. Loh, Q.L. and C. Choong, *Three-dimensional scaffolds for tissue engineering applications: role of porosity and pore size*. Tissue Engineering Part B: Reviews, 2013. **19**(6): p. 485-502.
11. Dalby, M.J., et al., *The control of human mesenchymal cell differentiation using nanoscale symmetry and disorder*. Nature materials, 2007. **6**(12): p. 997.
12. Engler, A.J., et al., *Matrix elasticity directs stem cell lineage specification*. Cell, 2006. **126**(4): p. 677-689.
13. Grellier, M., et al., *Responsiveness of human bone marrow stromal cells to shear stress*. Journal of tissue engineering and regenerative medicine, 2009. **3**(4): p. 302-309.
14. Morse, A., et al., *Mechanical load increases in bone formation via a sclerostin-independent pathway*. Journal of Bone and Mineral Research, 2014. **29**(11): p. 2456-2467.
15. Friedenstein, A., et al., *Precursors for fibroblasts in different populations of hematopoietic cells as detected by the in vitro colony assay method*. Experimental hematology, 1974. **2**(2): p. 83-92.
16. Tuli, R., et al., *Characterization of multipotential mesenchymal progenitor cells derived from human trabecular bone*. Stem cells, 2003. **21**(6): p. 681-693.
17. Hiraoka, K., et al., *Mesenchymal progenitor cells in adult human articular cartilage*. Biorheology, 2006. **43**(3, 4): p. 447-454.
18. Zuk, P.A., et al., *Human adipose tissue is a source of multipotent stem cells*. Molecular biology of the cell, 2002. **13**(12): p. 4279-4295.
19. De Bari, C., et al., *Multipotent mesenchymal stem cells from adult human synovial membrane*. Arthritis & Rheumatism, 2001. **44**(8): p. 1928-1942.
20. Tondreau, T., et al., *Mesenchymal stem cells derived from CD133-positive cells in mobilized peripheral blood and cord blood: proliferation, Oct4 expression, and plasticity*. Stem cells, 2005. **23**(8): p. 1105-1112.
21. Sarugaser, R., et al., *Human umbilical cord perivascular (HUCPV) cells: a source of mesenchymal progenitors*. Stem cells, 2005. **23**(2): p. 220-229.
22. Lee, O.K., et al., *Isolation of multipotent mesenchymal stem cells from umbilical cord blood*. Blood, 2004. **103**(5): p. 1669-1675.
23. In't Anker, P.S., et al., *Isolation of mesenchymal stem cells of fetal or maternal origin from human placenta*. Stem cells, 2004. **22**(7): p. 1338-1345.
24. Schofield, R., *The relationship between the spleen colony-forming cell and the haemopoietic stem cell*. Blood cells, 1978. **4**(1-2): p. 7-25.
25. Li, L. and T. Xie, *Stem cell niche: structure and function*. Annu. Rev. Cell Dev. Biol., 2005. **21**: p. 605-631.

26. Méndez-Ferrer, S., et al., *Mesenchymal and haematopoietic stem cells form a unique bone marrow niche*. Nature, 2010. **466**(7308): p. 829.
27. Brizzi, M.F., G. Tarone, and P. Defilippi, *Extracellular matrix, integrins, and growth factors as tailors of the stem cell niche*. Current opinion in cell biology, 2012. **24**(5): p. 645-651.
28. Scadden, D.T., *Nice neighborhood: emerging concepts of the stem cell niche*. Cell, 2014. **157**(1): p. 41-50.
29. Herrmann, M. and F. Jakob, *Bone marrow niches for skeletal progenitor cells and their inhabitants in health and disease*. Current stem cell research & therapy, 2019. **14**(4): p. 305-319.
30. Grzesik, W.J. and P.G. Robey, *Bone matrix RGD glycoproteins: immunolocalization and interaction with human primary osteoblastic bone cells in vitro*. Journal of Bone and Mineral Research, 1994. **9**(4): p. 487-496.
31. Lin, X., et al., *The bone extracellular matrix in bone formation and regeneration*. Frontiers in Pharmacology, 2020. **11**.
32. Solheim, E., *Growth factors in bone*. International orthopaedics, 1998. **22**(6): p. 410-416.
33. Luo, J., et al., *TGF β /BMP Type I Receptors ALK1 and ALK2 Are Essential for BMP9-induced Osteogenic Signaling in Mesenchymal Stem Cells [S]*. Journal of Biological Chemistry, 2010. **285**(38): p. 29588-29598.
34. Purmessur, D., et al., *Notochordal conditioned media from tissue increases proteoglycan accumulation and promotes a healthy nucleus pulposus phenotype in human mesenchymal stem cells*. Arthritis research & therapy, 2011. **13**(3): p. 1-13.
35. Phillips, J.E., et al., *Human mesenchymal stem cell differentiation on self-assembled monolayers presenting different surface chemistries*. Acta biomaterialia, 2010. **6**(1): p. 12-20.
36. Rojo, L., et al., *Self-assembled monolayers of alendronate on Ti6Al4V alloy surfaces enhance osteogenesis in mesenchymal stem cells*. Scientific reports, 2016. **6**: p. 30548.
37. Baker, B.M. and C.S. Chen, *Deconstructing the third dimension—how 3D culture microenvironments alter cellular cues*. Journal of cell science, 2012. **125**(13): p. 3015-3024.
38. Duval, K., et al., *Modeling physiological events in 2D vs. 3D cell culture*. Physiology, 2017. **32**(4): p. 266-277.
39. Qu, H., et al., *Biomaterials for bone tissue engineering scaffolds: a review*. RSC advances, 2019. **9**(45): p. 26252-26262.
40. Wubneh, A., et al., *Current state of fabrication technologies and materials for bone tissue engineering*. Acta Biomaterialia, 2018. **80**: p. 1-30.
41. Gunatillake, P.A., R. Adhikari, and N. Gadegaard, *Biodegradable synthetic polymers for tissue engineering*. Eur Cell Mater, 2003. **5**(1): p. 1-16.
42. Jing, Z., et al., *The role of natural polymers in bone tissue engineering*. Journal of Controlled Release, 2021.
43. Gilbert, T.W., T.L. Sellaro, and S.F. Badylak, *Decellularization of tissues and organs*. Biomaterials, 2006. **27**(19): p. 3675-3683.
44. Hussey, G.S., J.L. Dziki, and S.F. Badylak, *Extracellular matrix-based materials for regenerative medicine*. Nature Reviews Materials, 2018. **3**(7): p. 159-173.
45. Crapo, P.M., T.W. Gilbert, and S.F. Badylak, *An overview of tissue and whole organ decellularization processes*. Biomaterials, 2011. **32**(12): p. 3233-3243.
46. Badylak, S.F. and T.W. Gilbert. *Immune response to biologic scaffold materials*. in *Seminars in immunology*. 2008. Elsevier.
47. Murphy, M.B., K. Moncivais, and A.I. Caplan, *Mesenchymal stem cells: environmentally responsive therapeutics for regenerative medicine*. Experimental & molecular medicine, 2013. **45**(11): p. e54-e54.
48. Raicevic, G., et al., *The source of human mesenchymal stromal cells influences their TLR profile as well as their functional properties*. Cellular immunology, 2011. **270**(2): p. 207-216.
49. Guimarães-Camboa, N., et al., *Pericytes of multiple organs do not behave as mesenchymal stem cells in vivo*. Cell stem cell, 2017. **20**(3): p. 345-359. e5.
50. Bianco, P., P.G. Robey, and P.J. Simmons, *Mesenchymal stem cells: revisiting history, concepts, and assays*. Cell stem cell, 2008. **2**(4): p. 313-319.

51. Hass, R., et al., *Different populations and sources of human mesenchymal stem cells (MSC): a comparison of adult and neonatal tissue-derived MSC*. Cell Communication and Signaling, 2011. **9**(1): p. 12.
52. Sacchetti, B., et al., *No identical “mesenchymal stem cells” at different times and sites: human committed progenitors of distinct origin and differentiation potential are incorporated as adventitial cells in microvessels*. Stem cell reports, 2016. **6**(6): p. 897-913.
53. Bara, J.J., et al., *Concise review: Bone marrow-derived mesenchymal stem cells change phenotype following in vitro culture: implications for basic research and the clinic*. Stem cells, 2014. **32**(7): p. 1713-1723.
54. Lutolf, M. and J. Hubbell, *Synthetic biomaterials as instructive extracellular microenvironments for morphogenesis in tissue engineering*. Nature biotechnology, 2005. **23**(1): p. 47.
55. Yeatts, A.B. and J.P. Fisher, *Bone tissue engineering bioreactors: dynamic culture and the influence of shear stress*. Bone, 2011. **48**(2): p. 171-181.
56. Vetsch, J.R., R. Müller, and S. Hofmann, *The evolution of simulation techniques for dynamic bone tissue engineering in bioreactors*. Journal of tissue engineering and regenerative medicine, 2015. **9**(8): p. 903-917.
57. Prewitz, M.C., et al., *Tightly anchored tissue-mimetic matrices as instructive stem cell microenvironments*. Nature methods, 2013. **10**(8): p. 788-794.
58. Marinkovic, M., et al., *One size does not fit all: developing a cell-specific niche for in vitro study of cell behavior*. Matrix Biology, 2016. **52**: p. 426-441.
59. Rico-Llanos, G.A., et al., *Collagen type I Biomaterials as scaffolds for bone tissue engineering*. Polymers, 2021. **13**(4): p. 599.
60. Stein, G.S. and J.B. Lian, *Molecular mechanisms mediating proliferation/differentiation interrelationships during progressive development of the osteoblast phenotype*. Endocrine reviews, 1993. **14**(4): p. 424-442.
61. McBeath, R., et al., *Cell shape, cytoskeletal tension, and RhoA regulate stem cell lineage commitment*. Developmental cell, 2004. **6**(4): p. 483-495.
62. Rubert, M., et al., *Scaffold pore geometry influences bone-like tissue formation in dynamic cell culture conditions*. BioRxiv, 2020.
63. van Tol, A.F., et al., *The mechanoresponse of bone is closely related to the osteocyte lacunocanalicular network architecture*. Proceedings of the National Academy of Sciences, 2020. **117**(51): p. 32251-32259.
64. Guimarães, C.F., et al., *The stiffness of living tissues and its implications for tissue engineering*. Nature Reviews Materials, 2020. **5**(5): p. 351-370.
65. Oftadeh, R., et al., *Biomechanics and mechanobiology of trabecular bone: a review*. Journal of biomechanical engineering, 2015. **137**(1): p. 010802.
66. Gerardo, H., et al., *Soft culture substrates favor stem-like cellular phenotype and facilitate reprogramming of human mesenchymal stem/stromal cells (hMSCs) through mechanotransduction*. Scientific reports, 2019. **9**(1): p. 1-18.
67. Sugiyama, T., et al., *Maintenance of the hematopoietic stem cell pool by CXCL12-CXCR4 chemokine signaling in bone marrow stromal cell niches*. Immunity, 2006. **25**(6): p. 977-988.
68. Jahnen-Dechent, W., et al., *Fetuin-A regulation of calcified matrix metabolism*. Circulation research, 2011. **108**(12): p. 1494-1509.
69. Brylka, L. and W. Jahnen-Dechent, *The role of fetuin-A in physiological and pathological mineralization*. Calcified tissue international, 2013. **93**(4): p. 355-364.
70. Behnam, K., et al., *BMP binding peptide: a BMP-2 enhancing factor deduced from the sequence of native bovine bone morphogenetic protein/non-collagenous protein*. Journal of orthopaedic research, 2005. **23**(1): p. 175-180.
71. Urist, M.R., *Bone: formation by autoinduction*. Science, 1965. **150**(3698): p. 893-899.
72. Samavedi, S., A.R. Whittington, and A.S. Goldstein, *Calcium phosphate ceramics in bone tissue engineering: a review of properties and their influence on cell behavior*. Acta biomaterialia, 2013. **9**(9): p. 8037-8045.
73. Zhang, L. and T.J. Webster, *Nanotechnology and nanomaterials: promises for improved tissue regeneration*. Nano today, 2009. **4**(1): p. 66-80.

74. Yeatts, A.B., D.T. Choquette, and J.P. Fisher, *Bioreactors to influence stem cell fate: augmentation of mesenchymal stem cell signaling pathways via dynamic culture systems*. Biochimica et Biophysica Acta (BBA)-General Subjects, 2013. **1830**(2): p. 2470-2480.
75. Arora, S., et al., *Bio-mimicking Shear Stress Environments for Enhancing Mesenchymal Stem Cell Differentiation*. Current stem cell research & therapy, 2020. **15**(5): p. 414-427.
76. Melke, J., et al., *Localisation of mineralised tissue in a complex spinner flask environment correlates with predicted wall shear stress level localisation*. Eur Cells Mater, 2018. **36**: p. 57-68.
77. Heckman, C.A. and H. Plummer III, *Filopodia as sensors*. Cellular signalling, 2013. **25**(11): p. 2298-2311.
78. Kelly, D.J. and C.R. Jacobs, *The role of mechanical signals in regulating chondrogenesis and osteogenesis of mesenchymal stem cells*. Birth Defects Research Part C: Embryo Today: Reviews, 2010. **90**(1): p. 75-85.
79. De Girolamo, L., et al., *Human adipose-derived stem cells as future tools in tissue regeneration: osteogenic differentiation and cell-scaffold interaction*. The International journal of artificial organs, 2008. **31**(6): p. 467-479.
80. Sittichokechaiwut, A., et al., *Short bouts of mechanical loading are as effective as dexamethasone at inducing matrix production by human bone marrow mesenchymal stem cell*. Eur Cell Mater, 2010. **20**(4).
81. Morris, H., et al., *Mechanisms of fluid-flow-induced matrix production in bone tissue engineering*. Proceedings of the Institution of Mechanical Engineers, Part H: Journal of Engineering in Medicine, 2010. **224**(12): p. 1509-1521.
82. Terai, K., et al., *Role of osteopontin in bone remodeling caused by mechanical stress*. Journal of Bone and Mineral Research, 1999. **14**(6): p. 839-849.
83. Hanssen, E., B. Reinboth, and M.A. Gibson, *Covalent and non-covalent interactions of β 1-glycanase with collagen VI: β 1-glycanase is covalently attached to the amino-terminal region of collagen VI in tissue microfibrils*. Journal of Biological Chemistry, 2003. **278**(27): p. 24334-24341.
84. Izu, Y., et al., *Collagens VI and XII form complexes mediating osteoblast interactions during osteogenesis*. Cell and tissue research, 2016. **364**(3): p. 623-635.
85. Wolff, J., *Das gesetz der transformation der knochen*. DMW-Deutsche Medizinische Wochenschrift, 1893. **19**(47): p. 1222-1224.
86. Rubin, C.T. and L.E. Lanyon, *Regulation of bone mass by mechanical strain magnitude*. Calcified tissue international, 1985. **37**(4): p. 411-417.
87. Hsieh, Y.F. and C.H. Turner, *Effects of loading frequency on mechanically induced bone formation*. Journal of Bone and Mineral Research, 2001. **16**(5): p. 918-924.
88. Kumar, R., et al., *Canalicular fluid flow induced by loading waveforms: A comparative analysis*. Journal of theoretical biology, 2019. **471**: p. 59-73.
89. Cullen, D., R. Smith, and M. Akhter, *Bone-loading response varies with strain magnitude and cycle number*. Journal of applied physiology, 2001. **91**(5): p. 1971-1976.
90. Robling, A.G., D.B. Burr, and C.H. Turner, *Recovery periods restore mechanosensitivity to dynamically loaded bone*. Journal of Experimental Biology, 2001. **204**(19): p. 3389-3399.
91. Tomchuck, S.L., et al., *Toll-like receptors on human mesenchymal stem cells drive their migration and immunomodulating responses*. Stem cells, 2008. **26**(1): p. 99-107.
92. Dumitru, C.A., et al., *Stimulation of mesenchymal stromal cells (MSCs) via TLR3 reveals a novel mechanism of autocrine priming*. The FASEB Journal, 2014. **28**(9): p. 3856-3866.
93. de Witte, S.F., et al., *Cytokine treatment optimises the immunotherapeutic effects of umbilical cord-derived MSC for treatment of inflammatory liver disease*. Stem cell research & therapy, 2017. **8**(1): p. 1-12.
94. Jalowiec, J.M., et al., *An in vitro investigation of platelet-rich plasma-gel as a cell and growth factor delivery vehicle for tissue engineering*. Tissue Engineering Part C: Methods, 2016. **22**(1): p. 49-58.
95. Masuki, H., et al., *Growth factor and pro-inflammatory cytokine contents in platelet-rich plasma (PRP), plasma rich in growth factors (PRGF), advanced platelet-rich fibrin (A-PRF), and concentrated growth factors (CGF)*. International journal of implant dentistry, 2016. **2**(1): p. 1-6.

96. Verrier, S., et al., *Platelet-released supernatant induces osteoblastic differentiation of human mesenchymal stem cells: potential role of BMP-2*. Eur Cell Mater, 2010. **20**: p. 403-414.
97. Jing, D., et al., *Hematopoietic stem cells in co-culture with mesenchymal stromal cells-modeling the niche compartments in vitro*. haematologica, 2010. **95**(4): p. 542.
98. Lee, J.Y. and S.-H. Hong, *Hematopoietic stem cells and their roles in tissue regeneration*. International journal of stem cells, 2020. **13**(1): p. 1.
99. Wohrer, S., et al., *Distinct stromal cell factor combinations can separately control hematopoietic stem cell survival, proliferation, and self-renewal*. Cell reports, 2014. **7**(6): p. 1956-1967.
100. Crisan, M. and E. Dzierzak, *The many faces of hematopoietic stem cell heterogeneity*. Development, 2016. **143**(24): p. 4571-4581.
101. Jung, Y., et al., *Hematopoietic stem cells regulate mesenchymal stromal cell induction into osteoblasts thereby participating in the formation of the stem cell niche*. Stem cells, 2008. **26**(8): p. 2042-2051.
102. Hammoud, M., et al., *Combination of low O₂ concentration and mesenchymal stromal cells during culture of cord blood CD34⁺ cells improves the maintenance and proliferative capacity of hematopoietic stem cells*. Journal of cellular physiology, 2012. **227**(6): p. 2750-2758.
103. Chen, X., et al., *Osteoblast–osteoclast interactions*. Connective tissue research, 2018. **59**(2): p. 99-107.
104. Glass II, D.A., et al., *Canonical Wnt signaling in differentiated osteoblasts controls osteoclast differentiation*. Developmental cell, 2005. **8**(5): p. 751-764.
105. Wang, L., et al., *Osteoblast-induced osteoclast apoptosis by fas ligand/FAS pathway is required for maintenance of bone mass*. Cell Death & Differentiation, 2015. **22**(10): p. 1654-1664.
106. Matsuoka, K., et al., *Osteoclast-derived complement component 3a stimulates osteoblast differentiation*. Journal of Bone and Mineral Research, 2014. **29**(7): p. 1522-1530.
107. Tamma, R. and A. Zallone, *Osteoblast and osteoclast crosstalks: from OAF to Ephrin*. Inflammation & Allergy-Drug Targets (Formerly Current Drug Targets-Inflammation & Allergy)(Discontinued), 2012. **11**(3): p. 196-200.
108. Böhrnsen, F. and H. Schliephake, *Supportive angiogenic and osteogenic differentiation of mesenchymal stromal cells and endothelial cells in monolayer and co-cultures*. International journal of oral science, 2016. **8**(4): p. 223.
109. Loibl, M., et al., *Direct cell-cell contact between mesenchymal stem cells and endothelial progenitor cells induces a pericyte-like phenotype in vitro*. BioMed research international, 2014. **2014**.
110. Duttonhoefer, F., et al., *Endothelial progenitor cell fraction contained in bone marrow-derived mesenchymal stem cell populations impairs osteogenic differentiation*. BioMed research international, 2015. **2015**.
111. Herrmann, M., et al., *CD34/CD133 enriched bone marrow progenitor cells promote neovascularization of tissue engineered constructs in vivo*. Stem cell research, 2014. **13**(3): p. 465-477.
112. Itkin, T., et al., *Distinct bone marrow blood vessels differentially regulate haematopoiesis*. Nature, 2016. **532**(7599): p. 323.
113. Lu, P., V.M. Weaver, and Z. Werb, *The extracellular matrix: a dynamic niche in cancer progression*. J Cell Biol, 2012. **196**(4): p. 395-406.
114. Doron, B., M. Handu, and P. Kurre, *Concise Review: Adaptation of the Bone Marrow Stroma in Hematopoietic Malignancies: Current Concepts and Models*. Stem Cells, 2018. **36**(3): p. 304-312.
115. Amend, S.R., et al., *Ecological paradigms to understand the dynamics of metastasis*. Cancer letters, 2016. **380**(1): p. 237-242.
116. Hashimoto, K., et al., *Cancer-secreted hsa-miR-940 induces an osteoblastic phenotype in the bone metastatic microenvironment via targeting ARHGAP1 and FAM134A*. Proceedings of the National Academy of Sciences, 2018: p. 2204-2209.
117. de la Guardia, R.D., et al., *Detailed characterization of mesenchymal stem/stromal cells from a large cohort of AML patients demonstrates a definitive link to treatment outcomes*. Stem cell reports, 2017. **8**(6): p. 1573-1586.
118. Schroeder, T., et al., *Mesenchymal stromal cells in myeloid malignancies*. Blood research, 2016. **51**(4): p. 225-232.

119. Brahimi-Horn, M.C., J. Chiche, and J. Pouyssegur, *Hypoxia and cancer*. Journal of molecular medicine, 2007. **85**(12): p. 1301-1307.
120. Vaupel, P. and A. Mayer, *Hypoxia in cancer: significance and impact on clinical outcome*. Cancer and Metastasis Reviews, 2007. **26**(2): p. 225-239.
121. Keith, B. and M.C. Simon, *Hypoxia-inducible factors, stem cells, and cancer*. Cell, 2007. **129**(3): p. 465-472.
122. Ambrosi, T.H., et al., *Adipocyte accumulation in the bone marrow during obesity and aging impairs stem cell-based hematopoietic and bone regeneration*. Cell stem cell, 2017. **20**(6): p. 771-784. e6.
123. Watson, E.C. and R.H. Adams, *Biology of Bone: The Vasculature of the Skeletal System*. Cold Spring Harbor perspectives in medicine, 2017: p. a031559.

APPENDIX A

Affidavit

I hereby confirm that my thesis entitled “Modelling of Mesenchymal Stromal Cells Interactions within the Skeletal Niche” is the result of my own work. I did not receive any help or support from commercial consultants. All sources and/or materials applied are listed and specified in the thesis. Furthermore, I confirm that this thesis has not been submitted as part of another examination process neither in identical nor in similar form.

Wuerzburg, 22.11.2021

Place, date

Signature

Eidesstattliche Erklärung

Hiermit erkläre ich an Eides statt, die Dissertation “Modellierung der Interaktionen von Mesenchymalen Stromazellen in der skelettalen Nische” eigenständig, d.h. insbesondere selbständig und ohne Hilfe eines kommerziellen Promotionsberaters, angefertigt und keine anderen als die von mir angegebenen Quellen und Hilfsmittel verwendet zu haben. Ich erkläre außerdem, dass die Dissertation weder in gleicher noch in ähnlicher Form bereits in einem anderen Prüfungsverfahren vorgelegen hat.

Würzburg, 22.11.2021

Ort, Datum

Unterschrift

APPENDIX B

List of publications and authors contributions

Statement of individual author contributions and of legal second publication rights

Publication 1 (review article): <u>Pereira AR</u> , Trivanović D, Herrmann M. Approaches to mimic the complexity of the skeletal mesenchymal stem/stromal cell niche <i>in vitro</i> . European cells & materials. 2019;37:88-112.				
Participated in	Author Initials, Responsibility decreasing from left to right			
Study Design Methods Development	AR Pereira	M Herrmann		
Data Collection	N/a			
Data Analysis and Interpretation	N/a			
Manuscript Writing Writing of Introduction Writing of Materials & Methods Writing of Discussion Writing of First Draft	AR Pereira	D Trivanović		

Explanations: Peer-reviewed review article (IF: 3.942).

Publication 2 (protocol article): <u>Pereira AR</u> , Rudert M, Herrmann M. Decellularized human bone as a 3D model to study skeletal progenitor cells in a natural environment. Methods in cell biology. 2020;157:123-41.				
Participated in	Author Initials, Responsibility decreasing from left to right			
Study Design Methods Development	AR Pereira	M Herrmann		
Data Collection	AR Pereira			
Data Analysis and Interpretation	AR Pereira	M Herrmann		
Manuscript Writing Writing of Introduction Writing of Materials & Methods Writing of Discussion Writing of First Draft	AR Pereira			

Explanations: Peer-reviewed chapter book based on method/protocol article structure.

Publication 3 (original research article): <u>Pereira AR</u> , Trivanović D, Stahlhut P, Weissenberger M, Groll J, Herrmann M. Preservation of the naïve features of mesenchymal stromal cells <i>in vitro</i> : comparison of cell- and bone-derived decellularized extracellular matrix. Journal of Tissue Engineering. 2021 (submitted, in revision).				
Participated in	Author Initials, Responsibility decreasing from left to right			
Study Design Methods Development	AR Pereira	M Herrmann		
Data Collection	AR Pereira	P Stahlhut		

Data Analysis and Interpretation	AR Pereira	M Herrmann	D Trivanović	
Manuscript Writing Writing of Introduction Writing of Materials & Methods Writing of Discussion Writing of First Draft	AR Pereira			

Explanations: Investigation paper submitted to peer reviewed journal (IF: 7.813).

Publication 4 (original research article): Ramírez-Rodríguez GB, <u>Pereira AR</u> , Herrmann M, Hansmann J, Delgado-López JM, Sprio S, Tampieri A, Sandri M. Biomimetic Mineralization Promotes Viability and Differentiation of Human Mesenchymal Stem Cells in a Perfusion Bioreactor. International journal of molecular sciences. 2021;22(3):1447.				
Participated in	Author Initials, Responsibility decreasing from left to right			
Study Design Methods Development	GB R-Rodriguez	AR Pereira	JM D- López	M Herrmann
Data Collection	AR Pereira	GB R-Rodriguez		
Data Analysis and Interpretation	AR Pereira	GB R-Rodriguez	M Herrmann	JM D- López
Manuscript Writing Writing of Introduction Writing of Materials & Methods Writing of Discussion Writing of First Draft	GB R-Rodriguez	AR Pereira		

Explanations: Peer reviewed investigation paper, shared first-coauthorship (IF: 5.923). The study resulted from a collaboration partnership between material-scientist, GB R-Rodriguez and associated laboratories, who synthesized and characterized the new material, and our research group who was responsible for performing all cell-related experiments and respective manuscript preparation. All sections were well-defined divided between GB R-Rodriguez (Fig.1-3) and AR Pereira (Fig.4-7) work.

Publication 5 (original research article): <u>Pereira AR</u> , Lipphaus A, Ergin M, Salehi S, Gehweiler D, Rudert M, Hansmann J, Herrmann M. Modeling of the Human Bone Environment: Mechanical Stimuli Guide Mesenchymal Stem Cell–Extracellular Matrix Interactions. Materials. 2021;14(16):4431.				
Participated in	Author Initials, Responsibility decreasing from left to right			
Study Design Methods Development	AR Pereira	M Herrmann		
Data Collection	AR Pereira	A Lipphaus	S Salehi	D Gehweiler
Data Analysis and Interpretation	AR Pereira	A Lipphaus	M Herrmann	
Manuscript Writing Writing of Introduction Writing of Materials & Methods Writing of Discussion Writing of First Draft	AR Pereira	A Lipphaus		

Explanations: Peer reviewed investigation paper (IF: 3.623).

The doctoral researcher confirms that she/he has obtained permission from both the publishers and the co-authors for legal second publication.

The doctoral researcher and the primary supervisor confirm the correctness of the above-mentioned assessment.

Ana Rita Oliveira Alves Pereira 22.11.2021 Wuerzburg

Doctoral Researcher's Name Date Place Signature

Dr. Marietta Herrmann 22.11.2021 Wuerzburg



Primary Supervisor's Name Date Place Signature

Statement of individual author contributions to figures/tables/chapters included in the manuscripts

Publication 1 (review article): Pereira AR, Trivanović D, Herrmann M. Approaches to mimic the complexity of the skeletal mesenchymal stem/stromal cell niche *in vitro*. European cells & materials. 2019;37:88-112.

Figure	Author Initials, Responsibility decreasing from left to right			
Figure 1	AR Pereira	M Herrmann	D Trivanović	
Table 1	AR Pereira	M Herrmann		
Figure 2	AR Pereira	M Herrmann		

Publication 2 (protocol article): Pereira AR, Rudert M, Herrmann M. Decellularized human bone as a 3D model to study skeletal progenitor cells in a natural environment. Methods in cell biology. 2020;157:123-41.

Figure	Author Initials, Responsibility decreasing from left to right			
Figure 1	AR Pereira	M Herrmann		
Figure 2	AR Pereira	M Herrmann		
Figure 3	AR Pereira	M Herrmann		
Figure 4	AR Pereira	M Herrmann		
Figure 5	AR Pereira	M Herrmann		
Figure 6	AR Pereira	M Herrmann		
Table TS	AR Pereira	M Herrmann		

Publication 3 (original research article): Pereira AR, Trivanović D, Stahlhut P, Weissenberger M, Groll J, Herrmann M. Preservation of the naïve features of mesenchymal stromal cells *in vitro*: comparison of cell- and bone-derived decellularized extracellular matrix. Journal of Tissue Engineering. 2021 (submitted, in revision).

Figure	Author Initials, Responsibility decreasing from left to right			
Figure 1	AR Pereira	M Herrmann		
Figure 2	AR Pereira	M Herrmann		
Figure 3	AR Pereira	M Herrmann		
Figure 4	AR Pereira	M Herrmann		
Figure 5	AR Pereira	M Herrmann		
Figure 6	AR Pereira	M Herrmann		
Figure S1	AR Pereira	M Herrmann		

Publication 4 (original research article): Ramírez-Rodríguez GB, Pereira AR, Herrmann M, Hansmann J, Delgado-López JM, Sprio S, Tampieri A, Sandri M. Biomimetic Mineralization Promotes Viability and Differentiation of Human Mesenchymal Stem Cells in a Perfusion Bioreactor. International journal of molecular sciences. 2021;22(3):1447.

Figure	Author Initials, Responsibility decreasing from left to right			
Figure 1	GB R-Rodríguez	AR Pereira	JM D-López	
Figure 2	GB R-Rodríguez	AR Pereira	JM D-López	
Figure 3	GB R-Rodríguez	AR Pereira	JM D-López	
Figure 4	AR Pereira	GB R-Rodríguez	M Herrmann	
Figure 5	AR Pereira	GB R-Rodríguez	M Herrmann	
Figure 6	AR Pereira	GB R-Rodríguez	M Herrmann	
Figure 7	AR Pereira	GB R-Rodríguez	M Herrmann	J Hansmann

Publication 5 (original research article): Pereira AR, Lipphaus A, Ergin M, Salehi S, Gehweiler D, Rudert M, Hansmann J, Herrmann M. Modeling of the Human Bone Environment: Mechanical Stimuli Guide Mesenchymal Stem Cell-Extracellular Matrix Interactions. Materials. 2021;14(16):4431.

Figure	Author Initials, Responsibility decreasing from left to right			
Figure 1	AR Pereira	M Herrmann	D Gehweiler	
Figure 2	A Lipphaus	AR Pereira	M Herrmann	
Figure 3	AR Pereira	M Herrmann		
Figure 4	AR Pereira	M Herrmann		
Figure 5	AR Pereira	M Herrmann		
Figure 6	AR Pereira	M Herrmann	S Salehi	
Figure 7	AR Pereira	M Herrmann		
Figure S1	AR Pereira	M Herrmann		
Table S1	AR Pereira	M Herrmann		

I also confirm my primary supervisor's acceptance.

Ana Rita Oliveira Alves Pereira

22.11.2021

Wuerzburg

Doctoral Researcher's Name

Date

Place

Signature

APPENDIX C
Curriculum Vitae

